Enhancing Jamming Resilience in GNSS-based Localization for Safety-Critical Land Transportation : Towards an Optimized Mitigation Approach Focusing User-Requirements

Syed Ali Kazim

Université Gustave Eiffel

Ecole Doctorale MADIS 631

Thèse de Doctorat

en

Traitement du Signal et des Images

par

Syed Ali KAZIM

Thèse présentée et soutenue le 24 juin 2024

Enhancing Jamming Resilience in GNSS-based Localization for Safety-Critical Land Transportation: Towards an Optimized Mitigation Approach Focusing User Requirements

Amélioration de la résilience au brouillage d'une solution GNSS dédiée à la localisation des systèmes de transport terrestre critiques: Vers une approche optimisée de mitigation centrée sur les besoins utilisateurs

---

Members du Jury

Rapporteurs

Pr. Heidi KUSNIEMMI	Finnish Geospatial Research Institute (FGI), NLS Director, Digital Economy, University of Vaasa, Finland
Pr. Nel SAMAMA	Télécom SudParis, Institut Polytechnique de Paris, France

Examinateurs

Pr. Audrey GIREMUS	Université de Bordeaux, France
Dr. Paul THEVENON	Ecole Nationale de l'Aviation Civile (ENAC), Toulouse, France
Dr. Ni ZHU	AME/GEOLOC, Université Gustave Eiffel, Nantes, France

Directrice de thèse

Dr. Juliette MARAIS	COSYS/LEOST, Université Gustave Eiffel, Villeneuve d'Ascq, France

Acknowledgment

This doctoral study was carried out at LEOST (Laboratoire Électronique, Ondes et Signaux pour les Transports) on the Villeneuve d'Ascq campus of Université Gustave Eiffel. The research was conducted as part of the LOCSP project (No. 2019-CE22-0011), funded by the French National Research Agency (ANR).

The doctoral experience has been both challenging and rewarding, made possible through the invaluable support and mentorship of many individuals throughout the process.

I am deeply grateful to my supervisor, Dr. Juliette Marais, for her unwavering confidence in my abilities. Your continuous support and encouragement have been invaluable in shaping this work. I am especially grateful for your dedication and efforts in organizing the manuscript and suggesting thoughtful improvements.

I express my thanks to the members of my thesis committee, in particular Pr. Heidi KUSNIEMMI and Pr. Nel SAMAMA for their willingness to review my dissertation. I am deeply honored to acknowledge other committee members, including Pr. Audrey Giremus, Dr. Paul Thevenon, and Dr. Ni Zhu for their invaluable feedback and expertise, which have opened avenues for promising future research directions.

I extend my sincere gratitude to Mr. Yann COCHERIL, the director of LEOST, whose invaluable support and readiness to provide both technical and administrative assistance has been crucial to the smooth progression of this work.

To my parents, I am in immense debt of gratitude. Your unconditional love, support, and belief in me have been my strength throughout this journey. I also thank my wife, Hina Zehra, for her patience, understanding, and continuous support during the challenging times of this process. Additionally, I also acknowledge my children, Daniya Zehra, Muhammad Ibrahim, and Zoha Zehra, for being a delightful and much needed source of joy throughout this incredible journey.

Syed Ali Kazim
July 15th, 2024

Abstract

The transportation sector is undergoing a comprehensive transformation, driven by technological advancements and a growing emphasis on eco-friendly practices. Notably, this paradigm shift is more evident in road and rail transport, where large-scale initiatives, such as autonomous cars and trains are at the forefront. These groundbreaking developments not only reshape the transport industry but also forecast a myriad of socio-economic opportunities on the horizon.

In response to this transformative landscape, numerous scientific initiatives have been launched at both the European and national levels. One such initiative is the LocSP project, which is funded by the French National Research Agency. The project aims to contribute to the development of safe and precise localization solutions specifically designed for safety-critical applications. LocSP addresses several challenges through a multi-level approach and investigates collaborative, multi-sensor, and resilient solutions to address sensor measurement faults.

The research presented in this thesis places a particular emphasis on the resilience of the Global Navigation Satellite System (GNSS) against both intentional and non-intentional radiofrequency interference. It emphasizes on the robustness and reliability of location-based technologies, especially in safety-critical applications. Indeed, satellite signals are vulnerable to various disturbances, as these signals become very weak because of the large travel distance between the satellite and the receiver. One major threat to GNSS receiver is radio frequency interference originating from man-made devices particularly Personal Privacy Devices (PPDs) also known as jammers. These devices can potentially induce severe disturbances, in which a strong jammer can even completely block the GNSS signal.

The existing literature proposes various techniques for the detection and mitigation of jamming signals. However, the performance of these techniques is often evaluated from a signal perspective. Recently, some studies assessed the positioning accuracy following the mitigation process which is an important parameter for performance assessment, especially for users involved in non-safety critical applications.

In this work, we initially evaluate the performance of three techniques: Karhunen Loéve Transform (KLT), Adaptive Notch Filter (ANF) and Wavelet Packet Decomposition (WPD) representing different families of methods, particularly focusing on the key performance indicators associated with safety-critical applications.

Building on observed results during the state-of-the-art implementation phase, we propose a parameter optimization methodology for ANF. This optimization aims to suppress a certain class of jammers, specifically linear chirps, and to evaluate the impact of the optimal parameters on KPIs such as accuracy, availability and safety.

The contribution of this work lies in providing a comprehensive understanding of the phenomenon of jamming in safety-critical applications. It lays the groundwork for a targeted, multi-channel, real-time implementation of jamming detection and mitigation. The proposed system aims to continuously detect, classify and characterize various jamming situations, adapting to multiple jammer classes, multiple jamming sources, and dynamic power levels.

Résumé

Le secteur des transports est en pleine transformation, porté par les avancées technologiques et le besoin croissant de développer des pratiques écologiques. Ce changement de paradigme est notamment visible dans les domaines des transports routiers et ferroviaires, où les initiatives à grande échelle telles que le développement de voitures et de trains autonomes s'affichent au premier plan. Ces développements révolutionnaires non seulement remodèlent l'industrie des transports, mais ouvrent également une myriade d'opportunités socio-économiques. En réponse à ce contexte en transformation, de nombreuses initiatives scientifiques ont été lancées à la fois au niveau européen et national. L'une de ces initiatives est le projet LOCSP financé par l'Agence Nationale de Recherche française. Le projet entend contribuer au développement de solutions de localisation sûres et précises répondant au besoin particulier des applications à caractère sécuritaire. LOCSP adresse plusieurs défis avec une approche multi-niveaux et porte sur les solutions collaboratives, multi-capteurs et résilientes aux défaillances des capteurs. Les travaux présentés dans cette thèse portent en particulier sur la résilience des GNSS aux interférences électromagnétiques intentionnelles et non intentionnelles et insistent sur la robustesse et la fiabilité des solutions de localisation dans les applications critiques en matière de sécurité. Les signaux satellitaires sont vulnérables aux perturbations parce qu'ils sont reçus avec une puissance très faible après la longue distance parcourue depuis l'émission du signal par le satellite. Une menace majeure pour les récepteurs GNSS est l'interférence émise par des dispositifs artificiels comme les brouilleurs GNSS. Ces équipements peuvent induire des perturbations sévères et même complètement bloquer la réception des signaux GNSS dans son périmètre. La littérature existante propose diverses techniques pour la détection et la réduction des signaux brouilleurs. Les performances de ces techniques sont cependant souvent évaluées au niveau du signal. Quelques études ont récemment étudié la précision de la localisation après mitigation. Dans ce travail, nous évaluons d'abord les performances de trois techniques : Karhunen Loéve Transform (KLT), Adaptive Notch Filter (ANF) et Wavelet Packet Decomposition (WPD) qui représentent différentes familles de méthodes, en étudiant en particulier les indicateurs de performances associés aux applications sécuritaires. A partir des résultats observés pendant la phase d'implémentation de l'état de l'art, nous proposons une méthodologie d'optimisation des paramètres pour l'ANF. Cette optimisation est réalisée pour les brouilleurs de type chirp linéaire et montre qu'un paramétrage optimal influe sur les critères de performances tels que la précision, la disponibilité et la sécurité. Ce travail contribue à offrir une compréhension approfondie du phénomène de brouillage dans les applications critiques. Il pose les bases pour l'implémentation ciblée multi-canaux, temps réel d'une solution de détection et de réduction des brouillages. Le système proposé vise à détecter, classer et caractériser en continu différentes situations de brouillage, à s'adapter à de multiples classes de brouilleurs, sources et niveaux de puissance.

Contents

List of Figures

List of Tables

Acronyms

ADC Analog to Digital Converter. 14, 15, 38, 39, 43

AGC Automatic Gain Control. 38, 39, 41, 43

AIM+ Advanced Interference Mitigation. 4, 55, 62

AIS Automatic Identification System. 33

AL Alert Limit. 25–28, 54, 81

AltBOC Alternative Binary Offset Carrier. 12

AM Amplitude Modulation. 35

ANF Adaptive Notch Filter. , 4–6, 43, 44, 47, 52, 54, 55, 65, 71, 75, 77–79, 81, 83–89, 91, 93, 94, 96–98, 100–104, 106, 109, 111, 112, 115, 116, 118–120

ANFA Adaptive all-pass Notch Filter. 44

ANR Agence Nationale de la Recherche. 2

APL Along-Track Protection Level. 27

AR Auto-Regressive. 41, 76, 77

ARAIM Advanced RAIM. 26

ATC Adaptive Tightly Coupled. 42

BAM Bordered Autocorrelation Method. 48

BDS BeiDou Navigation Satellite System. 9

BOC Binary Offset Carrier. 12

BPSK Binary Phase Shift Keying. 12

CAF Cross Ambiguity Function. 15, 16, 67, 116, 119

CDF Cumulative Distribution Function. 25

CDMA Code Division Multiple Access. 11

CNN Convolution Neural Network. 39, 41, 120

CNO Carrier-to-Noise ratio. 23, 24, 34, 39, 41, 42, 54, 55, 57, 58, 61, 68–70, 79–85, 96, 98, 99, 111–116

COTS Commercial Off-The-Shelf. 3, 55, 56, 61, 62, 85

CPSD Cross-Power Spectral Density. 102, 103, 116

CWI Continuous Wave Interference. 31, 35, 44, 45

DFT Discrete Fourier Transform. 44, 45

DLL Delay Lock Loop. 16, 79

DME Distance Measuring Equipment. 31, 34, 37, 39, 43, 50

DOP Dilution of Precision. 19, 20

DTFT Discrete Time Fourier Transform. 39, 49

DVB-T Digital Video Broadcast Terrestrial. 31, 34

DWPD Discrete Wavelet Packet Decomposition. 71

DWT Discrete Wavelet Transform. 46, 71

ECEF Earth-Centered Earth-Fixed. 21

ERA European Union Agency for Railways. 2

ERAIM Extended RAIM. 26

ERJU Europe's Rail Joint Undertaking. 2

ERTMS European Rail Trafic Management System. 1, 2

EUSPA European Union Agency for the Space Programme. 2

FD Fault Detection. 26

FDMA Frequency Division Multiple Access. 11

FE Fault Exclusion. 26, 28

FIR Finite Impulse Response. 49

FLL Frequency Lock Loop. 44

FM Frequency Modulation. 35, 36

FMCW Frequency Modulated Continuous Wave. 75

FPD Frequency-Domain Power Detector. 39, 40

GBAS Ground-based Augmentation System. 18

GDOP Geometric Dilution of Precision. 20

GLONASS GLObal Navigation Satellite System. 9, 11, 34

GMPR Generalized Multivariate Polynomial Regression. 91

GNSS Global Navigation Satellite System. i, viii, , 1, 2, 4, 5, 8–10, 12–17, 19–21, 24, 29–35, 37–40, 42–44, 48, 50–52, 56, 66, 77, 79, 80, 87, 93, 94, 107, 111, 118, 120

GoF Goodness of Fit. 40

GPS Global Positioning System. 8–11, 32–34, 39, 56, 61, 62, 66, 78, 89, 96

HDOP Horizontal Dilution of Precision. 20

HMI Hazardous Misleading Information. 4, 28, 55, 58, 69, 82–86, 88, 100–102, 113–117, 119

HPE Horizontal Protection Error. 25, 27, 28, 54, 81, 100, 113, 114

HPL Horizontal Protection Level. 5, 27, 28, 54, 61, 81

IDFT Inverse Discrete Fourier Transform. 44

IIR Infinite Impulse Response. 44, 76

IMU inertial measurement unit. 121

INS Inertial Navigation System. 19, 42

JSR Jammer-to-Signal Ratio. 93

KF Kalman Filter. 21

KLT Karhunen Loéve Transform. , 4, 5, 43, 48, 52, 54, 55, 65–69, 71, 86–88, 118

KNN K-Nearest Neighbor. 42

KPIs Key Performance Indicators. , 3, 5, 8, 24, 27, 28, 54, 55, 66, 69, 71, 77, 84, 87, 88, 96, 98–100, 111, 113, 118

LMS Least Mean Square. 76, 77

LNA Low-Noise Amplifier. 15

LocSP Localisation Safe and Precise. 2, 5

LOS Line-Of-Sight. 24

LS Least Square. 8, 16, 21, 23, 27, 42

MA Moving Average. 76

MAD Mean Absolute Deviation. 102, 103, 116

MBOC Multiplexed Binary Offset Carrier. 12

MCAR Multi-Correlator with Auto-Regressive Modeling. 41

MCS Master Control Station. 9

MEO Medium Earth Orbit. 10

MFMC Multi-Frequency and Multi-Constellation. 42

ML Machine Learning. 41, 42, 107

MLP Multilayer Perceptron. 108, 109, 116, 119

MMSE Minimum Mean Square Error. 50

MPR Multivariate Polynomial Regression. 6, 88, 91, 95, 116, 119

MSINR Maximum Signal to Interference Ratio. 50

MVDR Mean Variance Distortion Response. 50

NavIC Navigation with Indian Constellation. 9

NBI Narrowband Interference. 31, 44

NLOS Non-Line-Of-Sight. 18, 19, 24

OFDM Orthogonal Frequency Division Multiplex. 34

PB Pulse Blanking. 43

PDF Probability Density Function. 38, 40

PDOP Position Dilution of Precision. 20

PE Position Error. 26, 28

PF Particle Filter. 21

PL Protection Level. 25–28, 61

PLD Power Law Detector. 39

PLL Phase Lock Loop. 16, 79

PNT Position Navigation and Timing. 8, 17

PPDs Personal Privacy Devices. , 31–33

PRN Pseudorandom Noise. 10, 11, 15, 16, 37, 68

PSD Power Spectral Density. 36, 37, 39, 40

PSNR Peak Signal-to-Noise Ratio. 102, 103, 116

PVT Position Velocity Timing. 20, 25

QMF Quadrature Mirror Filter. 72

QZSS Quasi-Zenith Satellite System. 9

RAIM Receiver Autonomous Integrity Monitoring. 8, 26

RFI Radio Frequency Interference. 30, 32

RHCP Right-Hand Circularly Polarized. 15

RMSE Root Mean Square Error. 91, 93, 94, 102, 104, 116, 119

RNN Recurrent Neural Network. 120

RRAIM Relative RAIM. 26

RTK Real-Time Kinematics. 19, 34

SBAS Satellite-based Augmentation System. 18

SFAP Space-Frequency Adaptive Processing. 43, 49, 50

SNR Signal-to-Noise Ratio. 45

STAP Space-Time Adaptive Processing. 43, 49, 50

STFT Short Time Fourier Transform. 43, 45–47

SV Space Vehicle. 17

SVM Support Vector Machine. 39, 41

TACAN Tactical Air Navigation System. 31, 34, 43, 50

TDOP Time Dilution of Precision. 20

TF Time-Frequency. 45, 46

TMBOC Time Multiplexed Binary Offset Carrier. 12, 13

TPD Time-Domain Power Detector. 39

TTA Time to Alert. 25, 28

TWSVM Twin Support Vector Machine. 41, 42

UNIFE Union des Industries Ferroviaires Européennes. 2

USRP Universal Software Radio Peripheral. 56, 63, 97

VDOP Vertical Dilution of Precision. 20

VPE Vertical Protection Error. 25

VPL Vertical Protection Level. 27

WBI Wideband Interference. 31, 61

WLS Weighted Least Square. 5, 8, 23, 69, 81, 99, 113

WPD Wavelet Packet Decomposition. iv, , 4, 5, 47, 52, 54, 55, 65, 73–75, 78–80, 83–88, 118, 119

WT Wavelet Transform. 43, 46, 73

WVD Wigner-Ville Distribution. 43, 45, 46

XPL Cross-Track Protection Level. 27

Chapter 1

GNSS - Pioneering a New Era in Rail Sector Innovation

Global Navigation Satellite System (GNSS) originally designed for military and civil aviation has undergone a profound transformative market evolution, marked by continuous growth in numerous other applications over the years. Indeed, the elimination of selective availability in the year 2000 tends to be a pivotal turning point that led to a significant performance enhancement of GNSS signals intended for civilian and commercial users. The strategic move to discontinue deliberate signal degradation paved the way for the widespread adoption of GNSS in various sectors such as transportation, agriculture, surveying, and geolocation-based services. This market expansion has a substantial socio-economic impact, where GNSS plays a crucial role in optimizing operations, increasing efficiency, enhancing safety, fostering innovation, and promoting environmental sustainability across diverse industries.

Similarly, the railway industry, which is traditionally reliant on established technologies, has undergone a paradigm shift with the emergence of GNSS as a game-changer technology to fundamentally reshape transportation infrastructure and operational practices.

1.1 Integrating GNSS in Europe's Railway Infrastructure

The European railway industry is undertaking significant modernization initiatives, manifested by the adoption of advanced technologies and improved operational practices. Some of the key initiatives include the implementation of the European Rail Trafic Management System (ERTMS) for standardized signaling, an emphasis on digitalization and automation, the expansion of high-speed rail networks, innovation in energy-efficient rolling stock, improvement in cross-border connectivity, and substantial investments in research and development that reflect a comprehensive approach of the industry. Among these revolutionizing efforts, the integration of GNSS stands out as more than just a technological resource but rather emerges as a transformative force that interconnects various dimensions of progress and resilience. It contributes profoundly to the advancement of the industry by facilitating the implementation of innovative concepts such as virtual coupling or moving blocks.

Currently, the integration of GNSS within the European railway sector aligns with the overarching objectives of promoting eco-friendly mobility. It serves as a technological foundation that not only facilitates precise localization but also optimizes resource alloca-

tion and enhances route planning. This multifaceted integration contributes substantially to the steadfast commitment of the railway industry to sustainability, portraying GNSS as a key facilitator for the advancement of environmentally sustainable practices within the railway ecosystem.

1.2 Main Stakeholders and Steering Forces in the European Railway Sector

In the network of the European rail industry, various entities collaborate and contribute to shaping the prospects of the railway sector. A nexus of collaboration emerges within the framework of Europe's Rail Joint Undertaking (ERJU) where the indispensable role of UNIFE (Union des Industries Ferroviaires Européennes - European Rail Industry Association) comes to the forefront. UNIFE representing the European rail supply industry, collaborates closely with other stakeholders, organized under the ERTMS user group association, to align technological advancements with industry requirements. The association's role is important in proposing a standardized integration of GNSS technologies into the European rail supply chain, ultimately contributing to the competitiveness and efficiency of the European rail industry on a global scale.

The regulatory oversight governed by the European Union Agency for Railways (ERA) plays a pivotal role in ensuring the standardization and integration of GNSS technology into the European rail network. As a railway regulatory authority in the European Union, ERA is responsible for managing the development of a comprehensive regulatory framework. This involves defining standards, technical specifications and safety requirements essential for the effective implementation of GNSS-based systems across European rail infrastructure.

The European Union Agency for the Space Programme (EUSPA) is a central player in advancing the integration of GNSS technology within the European rail sector. EUSPA's contributions are instrumental in propelling the technological advancements essential for a contemporary and efficient European rail system. To achieve this objective, the agency actively supports research and development initiatives, promotes innovation, and oversees the operational aspects of GNSS constellations, contributing to the enhancement of GNSS capabilities in rail applications. EUSPA in collaboration with other stakeholders has devised a roadmap that serves as a guiding framework for the systematic incorporation of GNSS technology, supported by continuous technological developments. Initiatives such as CLUG (Certifiable Localisation Unit with GNSS in the railway environment), Helmet, and Railgap converging efforts for the development of satellite-based localization for railway signaling, based on the core principle of failsafe train positioning within the broader framework of Shift2Rail.

1.3 LocSP project contribution – development of Fail-Safe Solutions

In France, the University Gustave Eiffel (formerly Ifsttar) is a key contributor in numerous EUSPA projects. To develop complementary research activities, the LocSP project, developed in collaboration with CRISTAL and M3Systems, has received funding through ANR program. The project with broader objectives concentrated on advancing technologies in road and rail transport systems, with a specific emphasis on onboard technologies essential for the modernization of land transport and the widespread adoption of connected

and autonomous transportation modes. The research conducted has made significant contributions, particularly in two specific areas:

- The first area focuses on hybrid and collaborative fault-tolerant solutions to ensure safe autonomous navigation. This involves the development of a framework for fault detection and exclusion in collaborative localization for vehicle fleets equipped with multi-sensor hybrid solutions.

- The second area, particularly the significant contribution of this Ph.D. thesis, involves developing methods to detect and mitigate electromagnetic interference commonly known as jamming. This study aims to explore different families of detection and mitigation approaches and evaluate their impact on the positioning of Key Performance Indicators (KPIs) such as accuracy, availability and safety.

In the earlier discussion, we provided an overview of the research context, highlighting our focus on land transportation, with a particular focus on railway application. The LEOST team, of which we are a part, is actively engaged in several European and French innovative projects associated with railway applications. However, the complexity involved in obtaining raw signal level data from the railway partners has prompted us to change the approach, opting to carry out research activities using static data recorded from the roof top of our laboratory. For this purpose, we have employed the Record and Reply system provided by the M3System and a customizable jamming system developed in our laboratory, this will be detailed in Chapter 4. The use of static data has enabled the development of the proposed contributions as a proof of concept, which could later be implemented without encountering expected restrictions on kinematic data obtained from road or railway campaigns.

In the following section, we will present the research objectives and provide a concise summary of the main contributions and publications originating from our work.

1.4 Novel insights and contributions on jamming countermeasures and implications on the Key Performance Indicators (KPIs)

This thesis significantly contributes by offering valuable insight into the challenges posed by jamming and the corresponding countermeasures for safety-critical applications. In this regard, the existing literature predominantly evaluates the effectiveness of jamming countermeasures at the intermediate level of the receiver processing chain [1][2][3][4][5], with very limited studies assessing the impact at the user level focusing solely on positioning accuracy [6][7]. The present research is dedicated to analyzing the impact of jamming and mitigation effectiveness at multiple processing stages, with a particular emphasis on evaluating positioning Key Performance Indicators (KPIs) to meet the user requirements. Notably, this aspect has not been taken into consideration in the existing literature. In this context, the summary of contributions published in reputable proceedings is as follows:

- In our initial investigation, we aimed to evaluate the importance of addressing jamming concerns, particularly from a safety-critical perspective. We conducted a preliminary investigation on the capabilities of an inbuilt jamming defense mechanism by a top-notch Commercial Off-The-Shelf (COTS) receiver available in the market.

Specifically, we focused on the utilization of the Advanced Interference Mitigation (AIM+) module provided by the Septentio receiver with the ASTRx4 receiver. Note that this study has been conducted on the basis of our best understanding of the mitigation function and has been tested for a limited number of interference scenarios under investigation. Our findings reveal that the Septentrio receiver undoubtedly performed exceptionally well in significantly improving the positioning accuracy with no HMI instances following the activation of the AIM+ module. However, the mitigation has consequently impacted the estimation of the protection level, leading to a considerable increase in unavailable instances in the Stanford diagram due to excessive overbounding of the position errors.

Conference: Kazim, S. A., Tmazirte, N. A., Marais, J., & Tsaturyan, A. (2022, January). **On the impact of jamming on Horizontal Protection Level and Integrity Assessment for Terrestrial Localization**. In Proceedings of the 2022 International Technical Meeting of The Institute of Navigation (ION ITM 2022) (pp. 1343-1357).

- Because of these initial outcomes, we went ahead with the investigation with the primary objective of enhancing the mitigation performance on the Stanford diagram. This involved maximizing the operational availability of the localization system while prioritizing safety concerns. In this context, we conducted a literature review and implemented existing mitigation solutions belonging to different families in a GNSS software receiver. These techniques include Adaptive Notch Filter (ANF), Wavelet Packet Decomposition (WPD) and Karhunen Loéve Transform (KLT), specifically addressing the chirp and frequency hopping interference.

  Conference: Kazim, S. A., Marais, J., & Tmazirte, N. A. (2022, September). **Interferences in Safety Critical Land Transport Application: Notch Filtering vs Wavelet Transform, an Experimental Analysis.** In Proceedings of the 35th International Technical Meeting of the Satellite Division of The Institute of Navigation (ION GNSS+ 2022) (pp. 3743-3757).

  Conference: Marais, J., Kazim, S. A., El Mawas, Z., El Najjar, M. E. B., & Skelton, J. (2023). **Contributions to the development of safe and accurate localisation solutions: The LOCSP project.** Transportation Research Procedia, 72, 391-398.

- The implemented techniques proved highly effective in restoring performance to a level very close to the nominal case. However, when dealing with the chirp scenario, these methods fell short of achieving similar performance to that observed in the previous case. Although the mitigation process successfully eliminated hazardous instances, it also led to a notable increase in the number of unavailable points on the Stanford diagram. To address this drawback, the next phase of the study contributes to the optimal parameterization of the ANF, tailoring it specifically for the chirp signal. We will see that the performance of ANF is significantly enhanced after the utilization of near-optimal parameters.

  Conference: Kazim, S. A., Marais, J., & Tmazirte, N. A. (2023, September). **On the parameterization of single pole adaptive notch filter against wide range of linear chirp interference.** In Proceedings of the 36th International Technical

Meeting of the Satellite Division of The Institute of Navigation (ION GNSS+ 2023) (pp. 3861-3877).

Journal: Kazim, S. A., Marais, J., & Tmazirte, N. A. **An End User-Focused Innovative Defense Against Chirp Jammers: Neural Network-Aided Adaptive Notch Filter in Safety-Critical Land Transportation.** Transportation research part C: emerging technologies, (under submission).

1.5 Organization and Structure of the Dissertation

This manuscript has been structured to facilitate the presentation of the global proposed approach, gradually introducing the various prerequisites and contributions outlined above. While the thesis work spanned three years and was more extensive, I would like to emphasize that this manuscript has been designed to provide a cohesive, informative, and contributory narrative. Some borderline contributions and additional developments are not addressed in this dissertation. It is organized into six chapters, with key content described in Figure 1.1. The following provides a summary of each chapter:

- **Chapter 1** provides the general context on the transformative impact of the Global Navigation Satellite System (GNSS) in the railway sector. It briefly introduces the objectives of the LocSP project under which this Ph.D. research work is conducted. Subsequently, the chapter offers a summary of contributions related to jamming countermeasures and their implications for safety-critical applications. The chapter concludes by summarizing key points and presenting the organizational structure, offering readers a comprehensive roadmap for the subsequent discussions in the dissertation.

- **Chapter 2** covers the essential concepts relevant to GNSS, offering a brief discussion of the main signal processing block within the receiver processing chain and introducing the vulnerabilities associated with GNSS. In addition, it dives into core concepts and algorithms, including the Weighted Least Square (WLS) estimator, weighting models, and the computation of Horizontal Protection Level (HPL) estimation. To facilitate performance evaluation, the chapter initially provides definitions for Key Performance Indicators (KPIs), a discussion on trade-offs, and introduces Stanford diagrams as a tool for assessing performance.

- **Chapter 3** redirects the focus to the issue of jamming techniques and corresponding countermeasure techniques. In this chapter, various jamming incidents from around the world are reported, which encompass different types of interference. Additionally, the chapter outlines diverse signal categories and classifications. In addition, it provides an overview of state-of-the-art interference countermeasures, with a particular emphasis on techniques for detection, classification, and mitigation.

- **Chapter 4** turns attention towards the implementation of jamming countermeasures. Initially, the chapter begins with a preliminary study on the resilience of the COTS receiver, particularly focusing on their applicability in safety-critical applications. Following this, the implementation phase introduces and examines three interference mitigation techniques: Adaptive Notch Filter (ANF), Wavelet Packet Decomposition (WPD) and Karhunen Loéve Transform (KLT) against chirp and frequency hopping signals. At the end of each study conducted in the implementation phase, the results are analyzed and discussed.

- **Chapter 5** contributes to the parameterization of a single pole ANF against a wide range of linear chirp interference. The chapter starts with the problem statement and discusses the role of characteristic parameters and tuning. Subsequently, two approaches are explored in this context. The first approach involves parameter modeling using Multivariate Polynomial Regression (MPR) with signal-level labelization. Finally, the second approach involves ANF parameterization using a neural network, with labelization performed at the acquisition level. The chapter concludes with a detailed analysis and discussion of the results.

- **Chapter 6** proposes an exhaustive concluding section and offers perspectives for the dissertation. It commences with a recap of the dissertation's structure and the topics covered throughout different chapters, with a primary focus on highlighting the main limitations identified in Chapter 4 and addressing them as scientific challenges in Chapter 5. The conclusion of the chapter introduces a discussion on the limitations of the proposed solution and presents a panel of potential improvements. This includes a targeted concept of a global, multi-channel, real-time implemented jamming detection and mitigation strategy. This foreseen strategy will be designed to continuously detect, classify, and characterize various jamming situations, accommodating multiple classes, diverse jamming sources, and dynamic power levels. Essentially, it synthesizes key findings and provides a roadmap for future research directions to improve resilience to jamming.

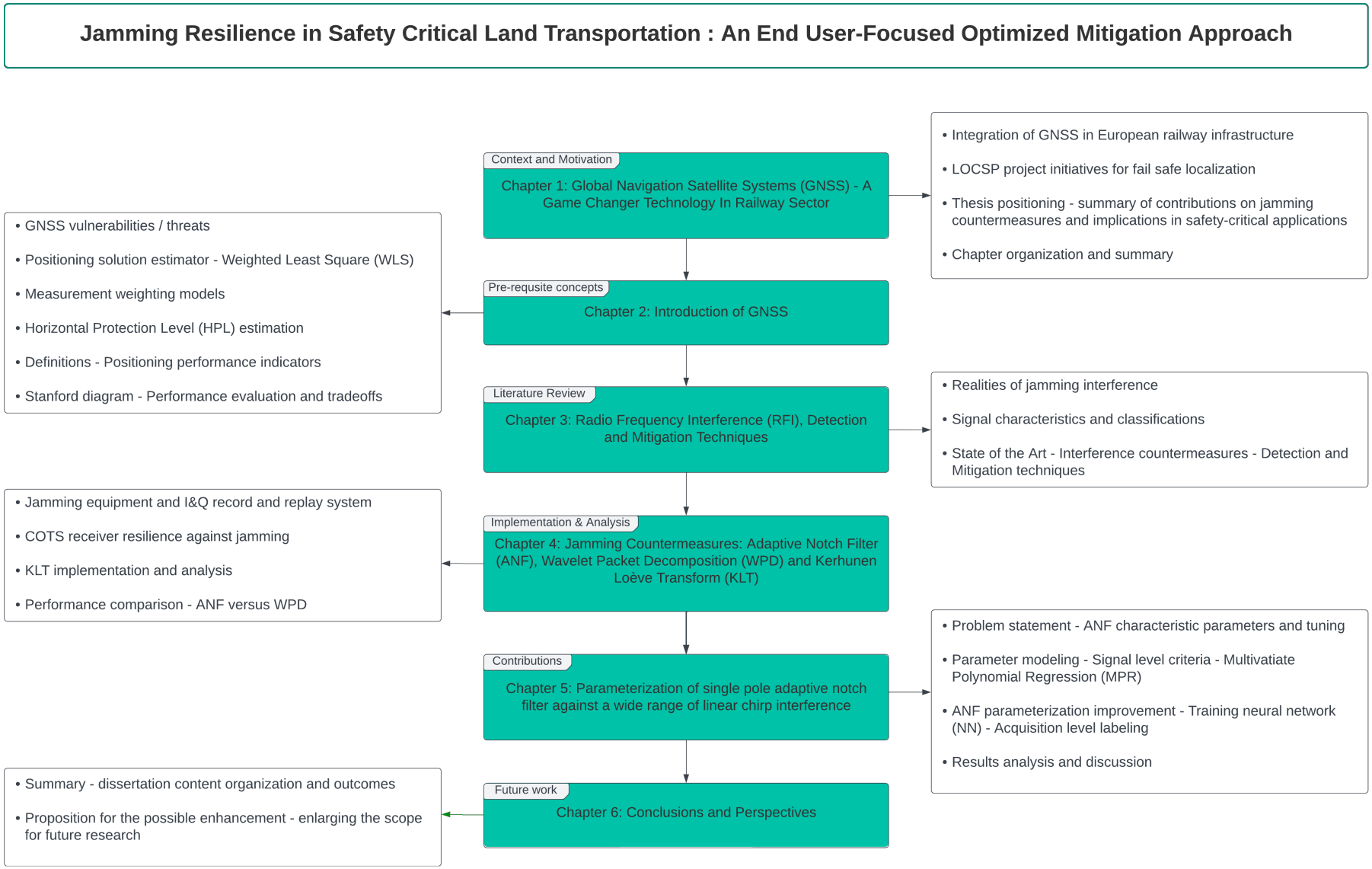

Figure 1.1: Summary outline of the chapter structures and organization

Chapter 2

Introduction of the Global Navigation Satellite Systems

2.1 Introduction

Positioning and navigation have become essential requirements in various applications, including mass-market navigation, public transport services, and vehicle guidance, wherein the Global Navigation Satellite System (GNSS) serves a pivotal role in modern technology. This first chapter provides a brief introduction to important concepts and the underlying principles of GNSS, with a particular emphasis on safety-critical applications. This chapter lays the groundwork for the subsequent sections of the manuscript.

The chapter is organized as follows: Section 2.2 presents a concise insight into the various segments of GNSS, outlining important aspects, while Section 2.3 explains the principle of triangulation to understand how the position is estimated. In Section 2.4 we go through some of the important components in the receiver processing chain. In Section 2.5, the vulnerabilities inherent to GNSS are discussed, addressing common sources of errors that can impact system accuracy and reliability. Section 2.6 focuses on the navigation block ending the chain with an introduction to the pseudorange measurement model and an explanation of the Least Square (LS) solution with specific attention given to the Weighted Least Square (WLS) estimator. Classical weighting models for estimating measurement uncertainties are also presented. Section 2.7 is dedicated to exploring GNSS in the context of safety-critical applications. This section initiates the discussion with the definitions of Key Performance Indicators (KPIs) including accuracy, continuity, availability, and integrity (or safety). The concept of Receiver Autonomous Integrity Monitoring (RAIM) is then presented, offering insights into how localization systems ensure the integrity of the solution. Additionally, it also introduces an innovation-based method for calculating the protection level. Furthermore, it concludes with a discussion on KPIs evaluation using the Stanford diagram, presenting a tradeoff between safety and availability, which is a critical consideration to ensure the effectiveness of the system in safety-critical applications.

2.2 An Overview of GNSS Segments

The Global Navigation Satellite System (GNSS) is a satellite-based system that offers Position Navigation and Timing (PNT) services. The acronym 'GNSS' is used to describe the collection of satellite positioning systems, also known as 'constellations', that have been developed by several countries to deliver regional or worldwide PNT services to their users. The main systems include the US - Global Positioning System (GPS), the European

- GALILEO, the Russian - GLObal Navigation Satellite System (GLONASS), the BeiDou Navigation Satellite System (BDS), the Japanese - Quasi-Zenith Satellite System (QZSS) and Indian - Navigation with Indian Constellation (NavIC). Each GNSS constellation consists of three main components referred to as 'segments': the space segment, the control segment and the user segment, as illustrated in Figure 2.1.

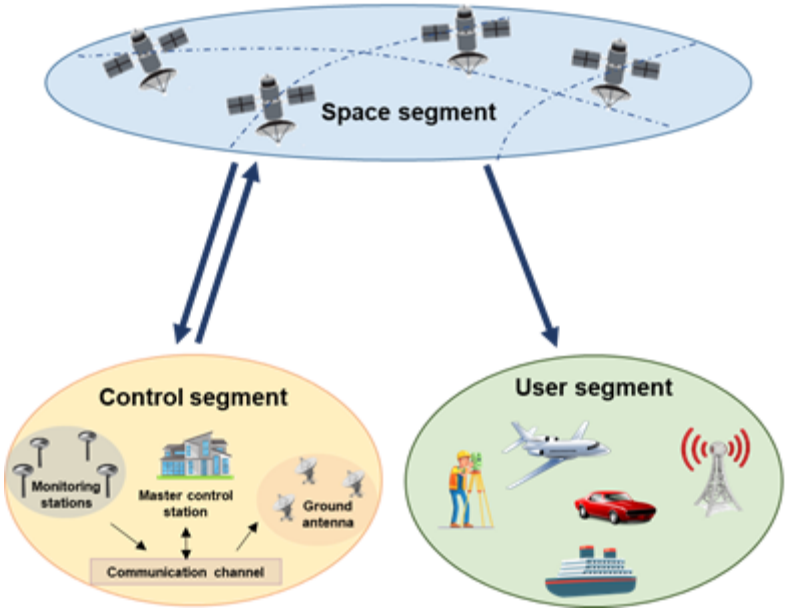

Figure 2.1: GNSS segments

2.2.1 Control Segment

The ground control segment is comprised of a network of ground antennas, monitoring stations and the Master Control Station (MCS), which collectively manages the entire navigation system. Figure 2.2 provides the geographical locations of GPS ground segment installations worldwide. The monitoring stations are strategically situated across large geographic areas to continuously monitor the signals broadcasted by the satellites. This signal monitoring facilitates the observation of satellite altitude, position, speed and overall health. The data gathered from these stations are subsequently transmitted to the MCS, which is responsible for several key tasks:

- Maintaining GPS time.
- Monitoring satellite orbits and issuing maneuvering commands for orbit adjustments.
- Ensuring satellite health.
- Updating satellite navigation messages.
- Performing other control maneuvers in the event of failures

The ground antennas serve the purpose of sending commands and updated navigation data back to the satellites. In this manner, the satellites can receive important updates regarding their health status, clock alignment, ephemeris and almanac information.

The regional satellite systems are designed to offer services within specific geographic regions. So, in the next discussion, we will describe the key characteristics of four satellite systems that offer coverage on a worldwide scale.

Figure 2.2: Geographical location of GPS ground segment installations *(source: www.gps.gov)*

2.2.2 Space Segment

The GNSS satellites are placed in precise orbits to ensure complete and uninterrupted coverage, thus making it possible for the users to benefit from the services almost everywhere on the Earth's surface. The most common orbit for GNSS is the Medium Earth Orbit (MEO) where, for instance, the GPS satellites orbit the Earth at an altitude of approximately 20200 kilometers, each having an orbital period (i.e. the time duration that satellite takes to complete its orbit) of roughly 12 hours. The GPS is committed to maintaining a constellation of 24 satellites, ensuring 95% coverage all the time. Table 2.1 provides orbital parameters for the most commonly used GNSS constellations.

Table 2.1: Orbital parameters of most common GNSS constellations

	GPS	**GALILEO**	**GLONASS**	**BeiDou**
Orbital Altitude	20200 km	23222 km	19100 km	21528 km
Operational Satellites	24	27	24	27
No of orbital planes	6	3	3	3 (MEO)
Orbital period	11h 58m	14h 4m	11h 15m	12h 53m
Orbital inclination	55°	56°	64.8°	55° (MEO)

The GNSS satellites continuously broadcast radio signals at different frequencies within the lower L-band (1164 - 1300 MHz) and the upper L-band (1559 - 1606 MHz), as illustrated in Figure 2.3. Each signal is composed of different components, for instance, the GPS L1 signal is composed of a carrier wave, navigation message, Pseudorandom Noise (PRN) code and data modulation, as shown in Figure 2.4. These characteristics are defined as follows:

- **Carrier Wave:** The 'carrier' wave is usually a sinusoidal waveform modulated with an information-bearing (or message) signal. It facilitates the transmission of information as an electromagnetic wave over a longer distance. These carrier waves generally possess a higher frequency compared to the message signal. In the GNSS, various constellations transmit multiple signals at distinct carrier frequencies, for

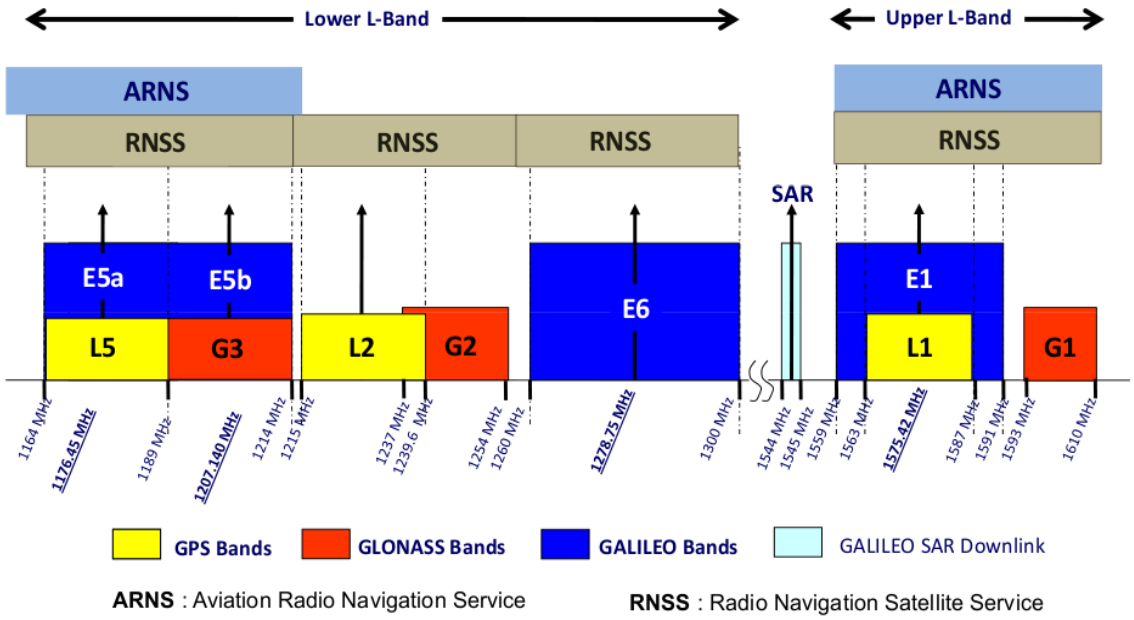

Figure 2.3: GNSS constellations band occupancy *(source: Navipedia)*

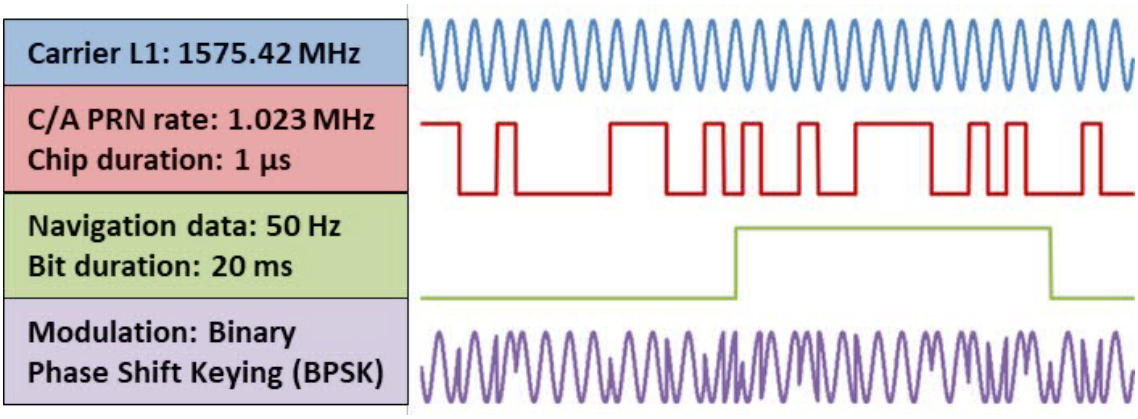

Figure 2.4: GPS L1 signal composition; carrier, ranging code and navigation data

instance, the GPS transmission frequencies include L1 - 1575.42 MHz, L2 - 1227.6 MHz and L5 - 1176.45 MHz.

- **Pseudorandom Noise (PRN) codes**: It consists of sequences comprised of 0s and 1s, which enables the user to calculate the signal travel duration between the satellite and the receiver. These binary sequences are also referred to as Pseudorandom Noise sequences or PRN codes. These distinctive binary sequences, assigned to each satellite, serve as a digital footprint that enables receivers to distinguish signals from different satellites. These codes possess unique properties; the cross-correlation between two distinct PRN codes is minimal (ideally zero), while the auto-correlation between two identical PRN codes reaches its maximum value when the codes are aligned. This characteristic allows satellites to transmit signals using the same channel or frequency band, a mode of communication known as Code Division Multiple Access (CDMA). All the constellations, except for legacy GLONASS, which employs Frequency Division Multiple Access (FDMA) by having each satellite transmit on a distinct carrier frequency modulated with a single spreading code, employed CDMA channel coding. However, as part of their modernization plan, the GLONASS system is expected to gradually reduce its reliance on FDMA in favor of adopting CDMA signals to enhance the system's capabilities and interoperability

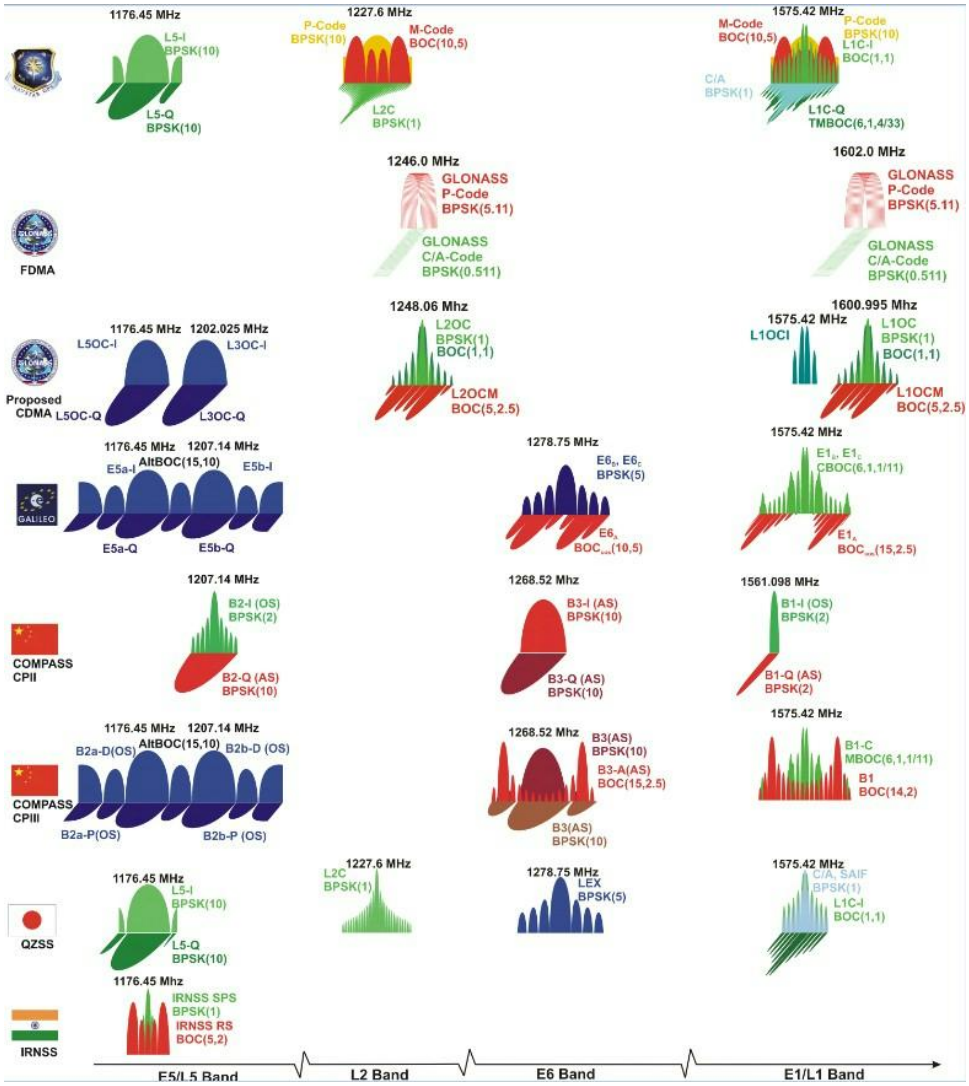

Figure 2.5: Legacy and modernized signals and Frequency bands occupancy by different GNSS systems *(source: Navipedia)*

with other satellite systems.

- **Navigation message:** It is a binary-coded data stream that contains information about satellite orbital parameters, clock corrections, and system health. The ephemeris data within the navigation message provides the satellite's orbit information, which enables the receiver to compute the position of the satellite. Additionally, the clock correction accounts for any discrepancies in the satellite onboard clock, ensuring accurate timestamping of signals.

- **Data Modulation:** It is a process of encoding digital signal information that may involve modulating parameters such as amplitude, phase, or frequency. These modulation techniques encode various types of data, including navigation messages, system status, and clock corrections into the GNSS signals. The Binary Phase Shift Keying (BPSK) is the most common modulation technique employed in GNSS. It is a form of phase modulation where the phase of the carrier signal is altered by 180 degrees in response to changes in the data signal represented by '0' and '1' bits. Other modernized modulation schemes offer higher accuracy, resistance to interference, and improved performance in challenging environments. These advanced schemes include Binary Offset Carrier (BOC), Alternative Binary Offset Carrier (AltBOC), Multiplexed Binary Offset Carrier (MBOC) and Time Multiplexed Binary Offset

Carrier (TMBOC). Figure 2.5 shows the diversity of signals and frequency bands used by different GNSS systems.

2.2.3 User Segment

The user segment encompasses a wide range of devices and applications that use GNSS signals to determine position, velocity, and time. This segment includes civilian and military users, with applications ranging from consumer devices to specialized devices for agriculture, surveying, and navigation.

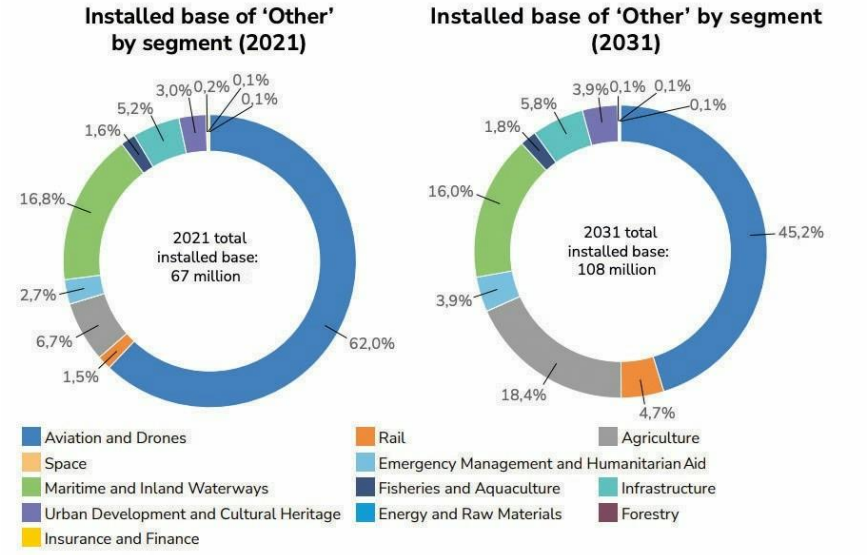

Figure 2.6: Growth expected by 2031 *(source: EUSPA market report 2022)*

The user segment has experienced significant growth, supporting location-based services, precise positioning and timing for military operations, precision agriculture techniques, accurate mapping and geodetic measurements for surveyors and geologists. The potential applications of GNSS continue to expand with emerging technologies like autonomous vehicles, drones, and smart cities. As the adoption of GNSS continues to diversify and expand, this technology remains a critical component in our modern technological landscape, with the anticipated growth by the year 2031 visually represented in Figure 2.6.

2.3 Navigating with Satellites: The Trilateration Approach

Trilateration serves as a fundamental principle within a satellite-based positioning system, primarily aimed at determining the location of an object on the Earth's surface. This method relies on the measurement of distances between the receiver and the satellites in space. Satellite signals transmit information about their position and transmission time. The receiver collects signals from a minimum of three satellites and analyzes the signal propagation time to determine the distance between the receiver and each satellite. By multiplying the travel time by the speed of light, the receiver can estimate the distances. In trilateration, the spheres are considered around each satellite with a radius equal to the receiver's estimated distances and it estimates the intersection point of these spheres to locate itself.

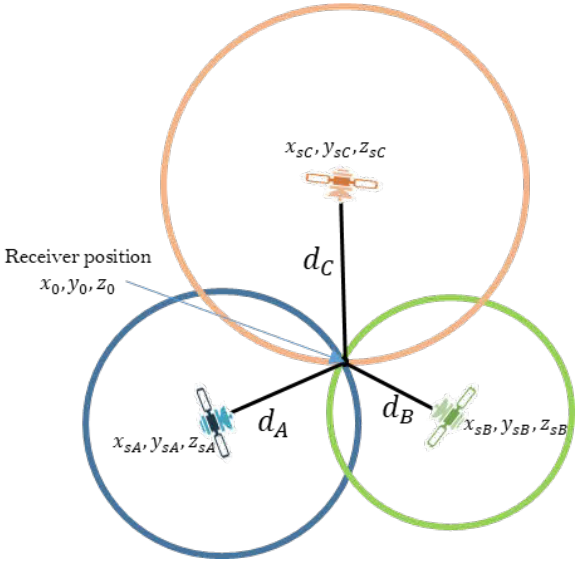

Figure 2.7: Trilateration principle with three GNSS satellites

Figure 2.7 illustrates the trilateration method, projecting the positions of the satellites in a two-dimensional plane. For satellite A, the receiver may be located at any point in the circle, with the satellite at the center of the circle, and d_c represents the distance between the satellite and the receiver. With the inclusion of two more distance measurements from satellites B and C, the receiver can pinpoint its position at the intersection point of the three circles.

2.4 GNSS Receiver Main Blocks

A GNSS receiver consists of several essential blocks that are responsible for capturing, processing and analyzing the signals from satellite constellations to provide position, navigation and timing (PNT) information to the user. The functional scheme of some important blocks of the receiver includes the antenna, front-end, Analog to Digital Converter (ADC), acquisition, tracking, and navigation blocks as illustrated in Figure 2.8.

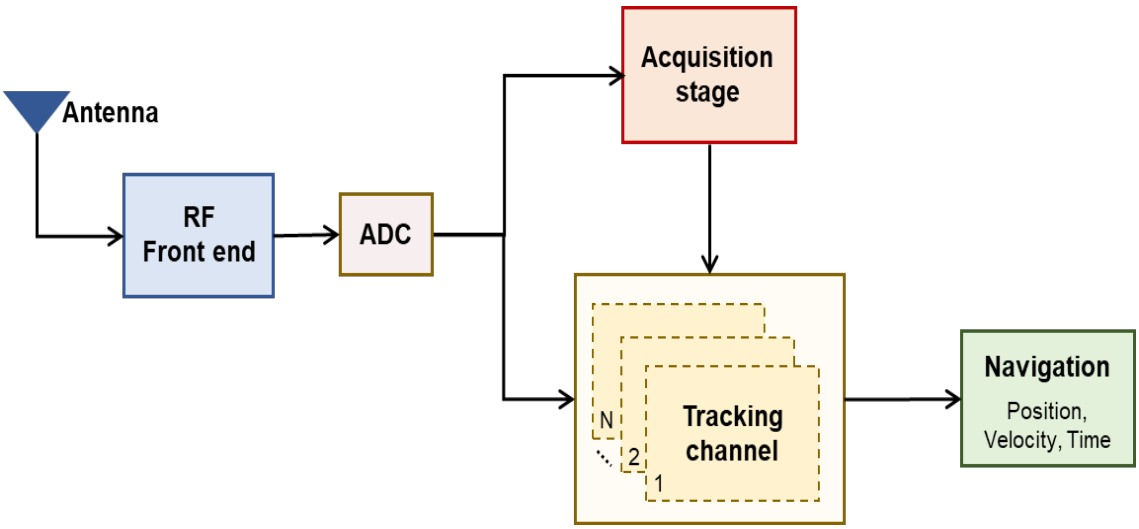

Figure 2.8: Some main functional blocks in the GNSS receiver processing chain

- **Antenna Unit:** It is the initial element of the receiver chain that is responsible for receiving satellite signals, which are often weak by the time they reach the receiver.

These signals are then amplified for further processing. Generally, the antenna filters out unwanted noise and interference, ensuring that only the relevant signals are passed on to the subsequent stages of the receiver. In the context of GNSS, antennas with Right-Hand Circularly Polarized (RHCP) are employed. They are preferred due to their high efficiency in capturing GNSS signals, which are usually RHCP. The choice of antenna type varies depending on the specific application and requirements, with various designs such as patch antennas, helical antennas and others.

- **Radio Frequency Front-End:** The signal captured by the antenna passes through the receiver front-end, which includes various components such as Low-Noise Amplifier (LNA) that amplify exceedingly weak signals coming from the satellites, a bandpass filter to limit the signal bandwidth to the desired level and a frequency downconverter responsible for transforming the signal to an intermediate frequency (IF) or directly to the baseband.
- **Analog to Digital Converter (ADC):** The ADC transforms the continuous analog signal coming from the RF front-end into discrete digital form. This conversion is accomplished by employing a two-step procedure involving sampling and quantization. The sampling process captures the analog signal at discrete time intervals, resulting in a sequence of data points that represent the signal amplitude. Subsequently, the quantization process assigns numerical values to these data points, extracting a representative discrete signal from the continuous analog signals.
- **Acquisition Unit:** The purpose of the acquisition block is to determine the presence of all the satellites within the receiver view. This process involves evaluating a 2-D correlation function known as the Cross Ambiguity Function (CAF). An extensive search is performed to determine the presence of the satellite signals and determine signal parameters such as the code phase offset and doppler frequency shift of the satellites. Once these parameters are acquired, they are used to initialize the delay and the phase tracking loop, thus enabling the receiver to synchronize with the satellite signal during the tracking phase. The evaluation of CAF involves comparing the received signal with all the possible locally generated PRN codes for different code and doppler values.

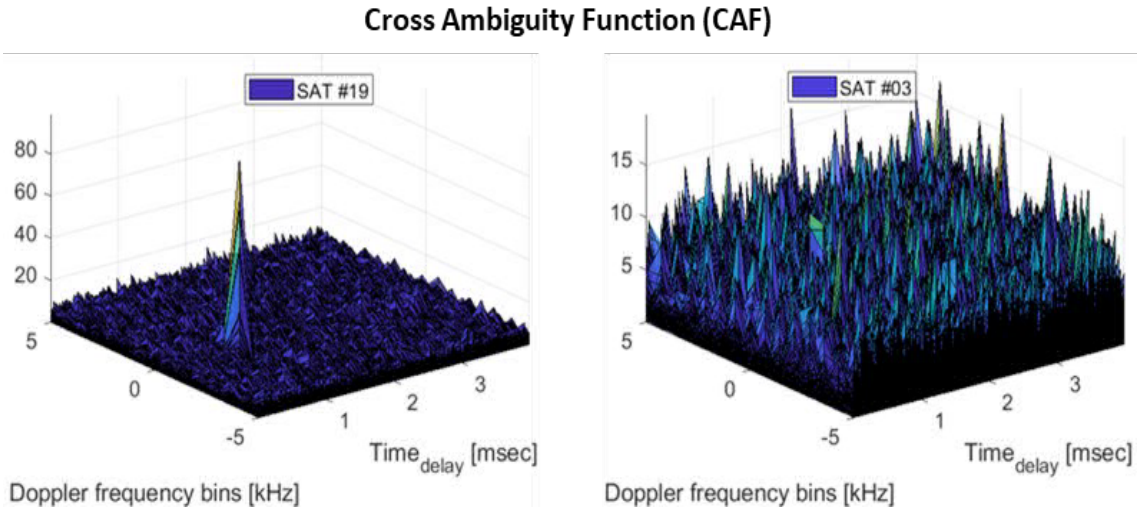

Figure 2.9: Cross Ambiguity Function of Galileo Satellites

The detection process involves comparing the correlation peak with a predetermined threshold. A distinct peak is expected to appear when the received signal code is

aligned with the locally generated PRN code. This indicates the presence of the satellite signal and provides an approximate estimate of the code delay and doppler shift. In contrast, if the satellite is not present, no peak will emerge, and CAF will only contain the correlation noise. Figure 2.9 shows the acquisition instances for two Galileo satellites. On the left, the distinct correlation peak for PRN#19 signifies the presence of the satellite, while on the right, the correlation for PRN#03 merely appears as noise, indicating that the signal from this particular satellite is not received.

- **Tracking Unit:** The next process involves continuous tracking of the satellite signals. The tracking unit's primary role is to further refine the signal parameters, namely the code and the doppler phase. It is achieved through the Phase Lock Loop (PLL) and Delay Lock Loop (DLL). The DLL helps to maintain synchronization with the satellite PRN code phase, while the PLL focuses on maintaining phase and frequency synchronization with the carrier signal. At each instance, the tracking loop provides fresh values of code and doppler phase to remove code and doppler from the received signal, as shown in Figure 2.10.

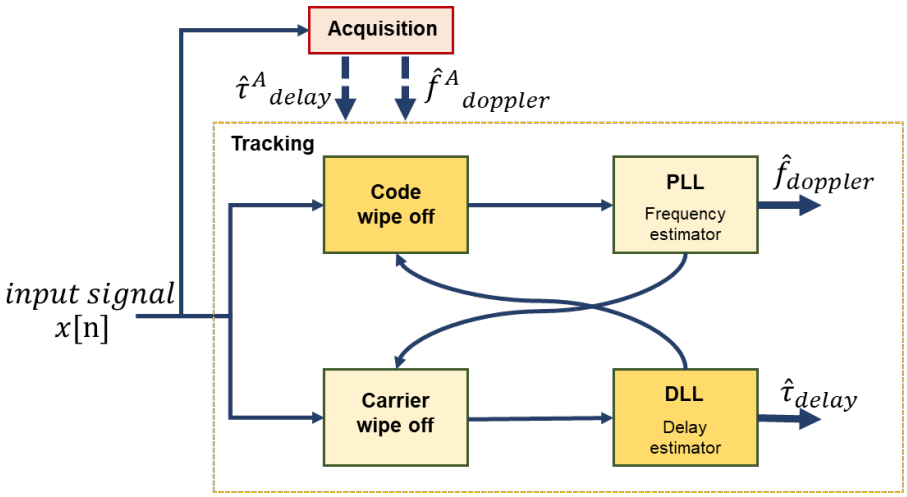

Figure 2.10: Tracking system functional view

- **Navigation Unit:** Once the GNSS signals have been acquired and tracked, the navigation unit uses them to derive meaningful navigation solutions. Using the triangulation method, the location of the receiver is determined. Subsequently, the initial estimate obtained from triangulation is further refined by a position estimator, such as the Least Square (LS) solution, by minimizing the discrepancies between the observed GNSS measurements (distances from the receiver to satellites) and the predicted values based on the estimated position. The LS estimator will be detailed in Section 2.6.

As we have presented the various segments and components of GNSS, it is increasingly important to consider the various vulnerabilities that are associated with this system. These vulnerabilities, often arising from a combination of technical limitations, system flaws and ever-evolving cybersecurity threats, present significant challenges that can potentially compromise the performance of the system. In the following section, we will explore some of the key vulnerabilities and threats associated with GNSS and examine the strategies and technologies employed to address them.

2.5 GNSS Vulnerabilities and Error Factors

The reliance on GNSS continuously expands in various applications and correspondingly, the awareness of its vulnerabilities and potential sources of errors. The GNSS signals are highly vulnerable to numerous threats due to the low power level, introducing errors in the PNT estimation. These vulnerabilities originate from various sources, as shown in Figure 2.11 while considering their occurrence. These errors originate at the satellite level, errors arising from signal propagation in the atmosphere, and errors resulting from the presence of local effects at the user segment.

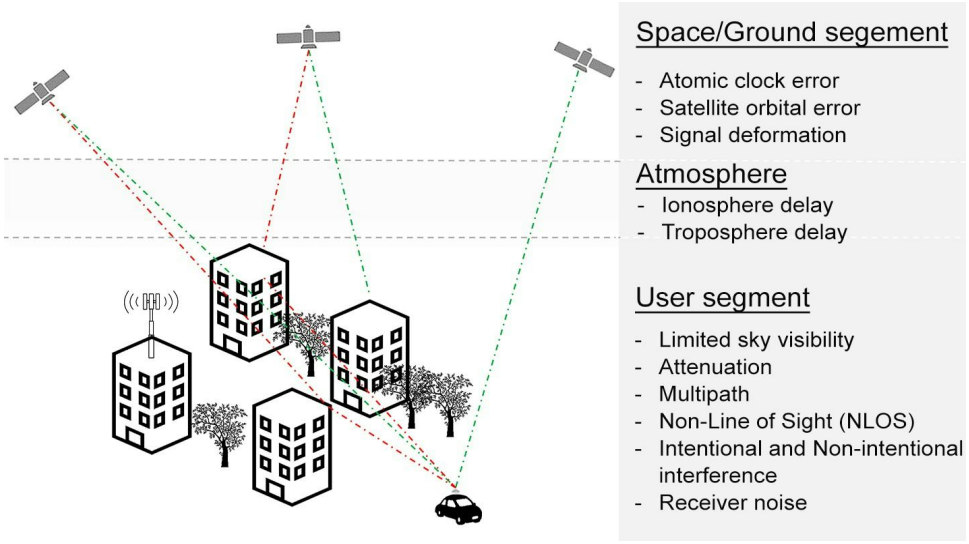

Figure 2.11: An example of typical GNSS error sources at three different levels, with their occurrence

- **Satellite level errors**: ephemeris and clock errors are primarily the two types of errors originating from Space Vehicles (SVs). The ephemeris contains information about the orbital coordinates of the satellite. The responsibility of the ground segment lies in continually monitoring the orbital parameters using past observations to ensure the decimation of up-to-date information broadcast to the user through the navigation message. However, the prediction accuracy degrades over time, especially in the event of unforeseen circumstances in space that might cause deviations in the satellite trajectory, resulting in errors in the estimated position. Additionally, GNSS satellites are equipped with highly stable onboard clocks, often using technologies like cesium and rubidium. Nevertheless, these onboard clocks are not completely faultless, typically having an error of about 8.64 to 17.28 nanoseconds per day, which corresponds to a ranging error of 2.59 m to 5.18 m. Similarly to the ephemeris data, control stations closely monitor clock drift and clock correction parameters to regularly update this information in the navigation message to account for these errors.

- **Atmospheric level errors**: The atmospheric level errors represent a significant source of inaccuracies in the GNSS. These errors are primarily associated with the passage of the satellite signal through the Earth's atmosphere. The atmospheric conditions, particularly the ionosphere and the troposphere, introduce delays and distortions in the GNSS signals. The *ionosphere*, which is the uppermost layer of the atmosphere, extends from 50 km to 1000 km or even beyond. It is formed when the sun's radiations interact with the gas molecules and the atoms, leading to

ionization. This process allows electrons to break free from their respective atom or molecule. These free-charged particles act as a dispersive medium for the signal propagation, causing radio signals to bend and altering their speed of propagation. The electron density in the ionosphere varies with the altitude and time, being denser and more extended during the day due to solar radiation. Generally, the low-elevation satellites experience greater ionospheric delays compared to the satellites at the zenith. The typical delay can range between 3 m to 45 m, but can be minimized using various techniques such as the application of empirical models like Klobuchar [8] and NeQuick [9]. These models utilize coefficients broadcasted in the navigation message, allowing for the removal of up to 50 - 70% of the errors. Since the ionospheric delay is dependent on the frequency, the error can also be reduced by estimating the delay using an ionosphere-free linear combination. Additionally, regional networks also correct the ionospheric delay, with options like the Satellite-based Augmentation System (SBAS) or Ground-based Augmentation System (GBAS). The *troposphere*, on the other hand, is the lower part of the atmosphere extending up to 50 km from the Earth's surface. Within the region, it serves as a non-dispersive medium for radio frequencies below 15 GHz. The tropospheric delay results from a combination of factors, including humidity, temperature and pressure. This delay is typically divided into two components: the hydrostatic delay, associated with the dry atmospheric content comprising gases and particles, which make up approximately 90% of the total tropospheric delay. Empirical models such as Saastamoinen [10] and Hopfield [11] are commonly utilized for the estimation of the dry delay component. The wet component, on the other hand, arises from the presence of water vapor suspended in the atmosphere and is notably very challenging to predict due to its high variability, posing limitations on achieving millimeter-level accuracy. The typical variation in the tropospheric delay ranges from 2.3m at the zenith (when the satellite is directly overhead) to approximately 20 to 28m at an elevation of 5 degrees.

- **User level errors:** These errors are induced by 'local' events or phenomena which usually originate from the vicinity of the receiver antenna. The errors are mainly due to the signal interaction with obstacles like buildings, trees or any other obstacles causing signal scattering, reflections and diffraction which can give rise to phenomena such as multipath, masking or shadowing. *Multipath* error occurs when signals reflect off from the surfaces or objects before reaching the receiver antenna. This can lead to signal interference and distortions, affecting the accuracy of the position estimation. Conversely, *Non-Line-Of-Sight(NLOS)* conditions arise when there is no direct line of sight between the transmitter and receiver, typically due to obstructions or signal blockage.

  Intensive research has been and is still being conducted on the identification and mitigation of multipath and NLOS errors, particularly in the urban environment where the challenges are prevalent. Researchers have explored a wide range of techniques and strategies to comprehensively address these concerns. These investigations encompassed diverse innovative approaches, such as the development of advanced antenna designs aimed at minimizing multipath effects [12][13][14], Moreover, receiver-based correlator designs have been explored to enhance signal tracking in the presence of reflections and obstructions [15][16], Weighting models have been developed to consider the uncertainty associated with measurements in the positioning solution [17][18].

  In addition to these strategies, there has been significant attention given to the multi-constellation solution that leverages signals from multiple satellite systems to

increase robustness in challenging environments [19][20]. An extensive environment modeling [21][22][23][24][25] has been undertaken to predict behavior under various urban conditions. Furthermore, the integration of GNSS with the Inertial Navigation System (INS) [26] has been explored to increase the robustness, offering seamless positioning, particularly during short NLOS intervals. A more sophisticated system, such as hybridization with fisheye cameras [27], has also been investigated to provide visual context to aid in the detection of signal blockage. More complex techniques, such as Ray Tracing and shadow matching [28][29] have been developed to model the signal paths and identify possible obstructions or multipath sources. Moreover, consistency-checking algorithms have been devised to detect and filter out measurement outliers [17][30][31].

Another form of signal interaction can occur with signals originating from 'artificial' sources or man-made devices and disrupting the useful signal, commonly referred to as interference. Radiofrequency interference can be broadly classified into two main categories: intentional and non-international interference. *Intentional interference* includes jamming, spoofing and meaconing. *Jamming* refers to the deliberate transmission of malicious signals within the GNSS frequency band to obscure useful signals by introducing noise, thereby impeding the receiver's ability to acquire satellite signals. On the other hand, *Spoofing* involves the transmission of synthetic GNSS-like signals, compelling the receiver to provide false position information. *Meaconing* closely resembles spoofing as it involves rebroadcasting of authentic GNSS signal by the radio transmitter.

The second form of interference is *non-intentional interference*, which can be further categorized into in-band or out-band interference. *In-band interference* occurs when different systems share the same frequency band for transmission, while *out-band interference* is caused by systems transmitting close to the frequency band of interest, often caused by harmonics or intermodulation products. The issues related to interference, their impact and potential mitigation strategies will be discussed more in detail in Chapter 3.

Receiver clock error, which is another important factor affecting the accuracy of satellite-based positioning technologies, emerges from discrepancies between the highly accurate atomic clocks onboard satellites and less accurate clocks within receivers. Since GNSS systems rely on accurate measurement of the signal travel time or determining the position, even minor errors in the receiver's clock can lead to substantial inaccuracies. For example, only nanosecond discrepancy can result in positioning errors of 30 cm. To address this issue, the receivers employ techniques such as multi-satellite time synchronization to estimate and compensate for clock biases. Additionally, differential correction services like Real-Time Kinematics (RTK) offer real-time corrections to further enhance positioning accuracy by rectifying receiver clock errors.

The *Dilution of Precision (DOP)* is another important parameter that influences the positioning accuracy. It serves as an indicator of the geometric arrangement of satellites relative to the receiver view. This parameter does not directly correlate with the measurement condition but acts as an indicator to quantify the geometric coverage. For instance, evenly distributed satellites around the receiver lead to a lower DOP value, thereby yielding high positioning accuracy. On the contrary, an inadequate configuration with satellites closely spaced in a small region, leads to an increased value, causing higher inaccuracy in the position estimation. The effects of satellite geometry and the dispersion of positioning uncertainty are illustrated in Figure 2.12. The uncertainties are evaluated using various DOP factors. The

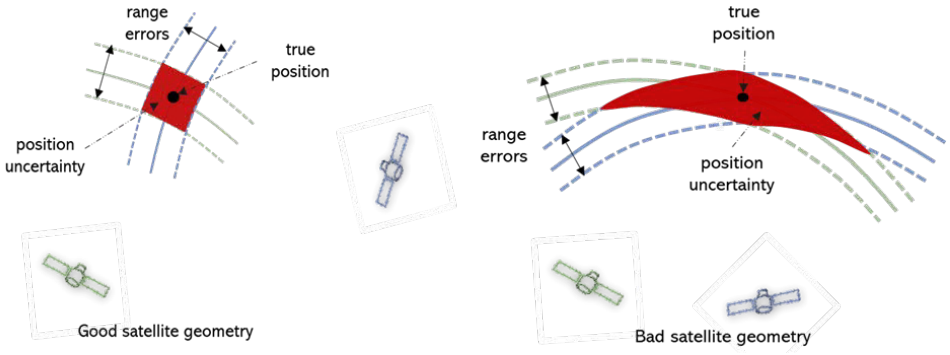

Figure 2.12: 2D illustration of relative geometry and dilution of precision a) geometry with smaller DOP (left) and b) geometry with larger DOP (right) GNSS Measurement Model and PVT estimation

Horizontal Dilution of Precision (HDOP) and Vertical Dilution of Precision (VDOP) represent uncertainties along horizontal and vertical components, respectively. By combining VDOP and HDOP, a Position Dilution of Precision (PDOP) is obtained, which provides an overall measure of position solution uncertainty. Additionally, the DOP factor also includes Time Dilution of Precision (TDOP), which characterizes the uncertainty associated with the timing information. Finally, Geometric Dilution of Precision (GDOP), which is the combination of all the uncertainty previously mentioned components. The PDOP, TDOP and GDOP are expressed as follows:

$$PDOP = \sqrt{\sigma^2{}_x + \sigma^2{}_y + \sigma^2{}_y} \tag{2.1}$$

$$TDOP = \sqrt{\sigma^2{}_t} \tag{2.2}$$

$$GDOP = \sqrt{\mathrm{PDOP}^2 + \ \mathrm{TDOP}^2} \tag{2.3}$$

where σ_x, σ_y and σ_z are the uncertainties of x, y and z position components.

We have explored various sources of errors within the GNSS measurements. In the following section, we will introduce the measurement model, which accounts for both systematic and random errors in the estimation of the Position Velocity Timing (PVT) solution.

2.6 GNSS Measurement Model and PVT Estimation

The GNSS receiver provides pseudorange and carrier measurements to estimate the distance between satellites and a receiver, as explained in Section 2.4. The pseudorange measurements are determined by calculating the signal travel time from the satellites to the receiver. This involves comparing the signal transmission time from the satellite to the signal reception time at the receiver, obtained through the phase delay between the received and locally generated code signals. Multiplying the time difference by the speed of light yields the pseudorange estimate, providing meter-level accuracy. The pseudorange measurements are relatively easy to obtain and offer meter-level accuracy. However, pseudorange measurements are susceptible to errors like clock inaccuracies, atmospheric delays, and multipath interference, limiting their effectiveness in highly accurate applications.

In contrast, distance estimation from carrier measurements offers enhanced accuracy but is more complex than code measurements. The carrier measurements rely on the phase difference between the carrier frequency of the received signal and the locally generated carrier signal. To obtain carrier measurements, receivers need to continuously track the carrier frequency without any interruption or cycle slip. Moreover, the carrier measurements are ambiguous, meaning that they are uncertain by an unknown integer number of wavelengths (λN). Resolving these ambiguities requires specialized techniques, such as double-difference carrier measurements between sets of satellites and sets of receivers. The primary advantage of carrier measurements lies in their reduced susceptibility to common mode errors, making them suitable for high-precision applications. Both the pseudorange and carrier measurements for the jth satellite can be mathematically modeled as:

$$\rho_j = r_j + c\left(\delta t_u - \delta t_j\right) + I_{\rho_j} + T_{\rho_j} + \mathcal{M}_{\rho_j} + n_{\rho_j} \tag{2.4}$$

$$\phi_j = r_j + c\left(\delta t_u - \delta t_j\right) + I_{\phi_j} + T_{\phi_j} + \mathcal{M}_{\phi_j} + \lambda_j N_j + n_{\phi_j} \tag{2.5}$$

where r_j is the true geometric distance between the satellite and the receiver,

δt_u is the receiver time difference from the system time.

δt_j represents the satellite time difference from the system time.

λ_j and N_j represent the carrier wavelength and the phase ambiguity,

I_{ρ_j} and I_{ϕ_j} is ionospheric propagation delay residual on code and carrier measurements,

T_{ρ_j} and $T_{\phi_j}$is the tropospheric propagation delay residual on code and carrier measurements,

$\mathcal{M}_{\rho_j}$ and $\mathcal{M}_{\phi_j}$ represent the multipath error on code and carrier measurements,

n_{ρ_j} and n_{ϕ_j} accounts for the noise in the code and carrier measurements.

The aforementioned measurement models serve as the basis for understanding the process of acquiring and representing GNSS data. Now, we turn our attention to a discussion on position estimators, which are derived from these measurements. Our primary emphasis will be on pseudorange measurements, which are not only relatively easier to obtain but also widely adopted for position estimation. Carrier measurements are considered beyond the scope of this study. In terms of computing the navigation solution, there exist various estimators, including the Kalman Filter (KF) [32][33], Particle Filter (PF) [34][35], and Least Square (LS) [36]. In the next section, we will introduce the LS estimator, focusing on its weighted variant.

2.6.1 Position Estimator Least Square (LS) Solution

The Least Square (LS) estimator is the conventional method that aims to minimize the sum of the squared difference between the observed and computed pseudorange measurements. In contrast to the KF, the LS is a snapshot (non-recursive) estimator that provides point position solutions without considering the dynamics of the system. The measurement model, as described in Eq.2.4, can be expressed in a simplified manner to represent the actual geometric distance between the jth satellite and the user receiver in the Earth-Centered Earth-Fixed (ECEF) coordinate system:

$$\rho_j = \sqrt{\left(x_j - x_u\right)^2 + \left(y_j - y_u\right)^2 + \left(z_j - z_u\right)^2} + c\left(\delta t_u - \delta t_j\right) + noise \tag{2.6}$$

The satellite position $(x_j,\ y_j, z_j)$ and δt_j, representing the satellite clock bias, can be derived from the navigation data. In the pseudorange model, there are four unknown variables: the user position $(x_u,\ y_u, z_u)$ and the receiver clock bias δt_u. Expressing a

pseudorange observation within the measurement model, which accounts for four unknown variables, a noise-free pseudorange observation can be rewritten as:

$$\rho_j = \sqrt{(x_j - x_u)^2 + (y_j - y_u)^2 + (z_j - z_u)^2} + c.\mathrm{b}_u \tag{2.7}$$

Here, b_u denotes the receiver clock offset relative to the system time. Since Eq. 2.7 is a nonlinear function, the initial step involves linearizing this function to estimate the solution. To achieve a 1st-order approximation with Taylor expansion with respect to the current estimate, the linearized equation is given as:

$$\rho_j = f\left(x_u\ ,\ y_u\ ,\ z_u\ , b_u\right) = \ f\left(\widehat{x}_u + \Delta x_u\ ,\ \widehat{y}_u + \Delta y_u\ ,\ \widehat{z}_u + \Delta z_u\ , \widehat{t}_u + \ \Delta t_u\right) \tag{2.8}$$

$$\begin{aligned} &= f(\widehat{x}_u, \widehat{y}_u, \widehat{z}_u, b_u) + \frac{\delta f(\widehat{x}_u, \widehat{y}_u, \widehat{z}_u, b_u)}{\delta \widehat{x}_u}\Delta x_u + \frac{\delta f(\widehat{x}_u, \widehat{y}_u, \widehat{z}_u, b_u)}{\delta \widehat{y}_u}\Delta y_u \\ &\quad + \frac{\delta f(\widehat{x}_u, \widehat{y}_u, \widehat{z}_u, b_u)}{\delta \widehat{z}_u}\Delta z_u + \frac{\delta f(\widehat{x}_u, \widehat{y}_u, \widehat{z}_u, b_u)}{\delta \widehat{t_u}}\Delta t_u \end{aligned} \tag{2.9}$$

$$= \widehat{\rho}_j - \frac{x_j - \widehat{x}_u}{\widehat{r}_j}\Delta x_u - \frac{y_j - \widehat{y}_u}{\widehat{r}_j}\Delta y_u - \frac{z_j - \widehat{z}_u}{\widehat{r}_j}\Delta z_u + c\Delta t_u \tag{2.10}$$

Here, $(\widehat{x}_u,\ \widehat{y}_u, \widehat{z}_u)$ represent position coordinates of the linearization point, $\widehat{\rho}_j$ signifies the computed pseudorange from the last iteration and $\widehat{r}_j$ denotes the distance between the satellite and the linearization point, as follows:

$$\widehat{r}_j = \sqrt{(x_j - \widehat{x}_u)^2 + (y_j - \widehat{y}_u)^2 + (z_j - \widehat{z}_u)^2} \tag{2.11}$$

$$a_{\mathrm{xj}} = \frac{x_j\ -\ \widehat{x}_u}{\widehat{r}_j},\ a_{\mathrm{yj}} = \ \frac{y_j\ -\ \widehat{y}_u}{\widehat{r}_j},\ a_{\mathrm{yj}} = \ \frac{z_j - \widehat{z}_u}{\widehat{r}_j} \tag{2.12}$$

The measurement residual is determined by calculating the difference between the observed and estimated measurements:

$$\Delta\rho_j = \ \widehat{\rho}_j - \rho_j = \ a_{\mathrm{xj}}\Delta x_u + a_{\mathrm{yj}}\Delta y_u + a_{\mathrm{zj}}\Delta z_u - c\Delta t_u \tag{2.13}$$

The system consisting of m equations can be expressed in matrix form as follows:

$$\begin{bmatrix} \Delta\rho_1 \\ \Delta\rho_2 \\ \Delta\rho_3 \\ \Delta\rho_4 \\ \vdots \\ \Delta\rho_m \end{bmatrix} = \begin{bmatrix} a_{x1} & a_{y1} & a_{z1} & 1 \\ a_{x2} & a_{y2} & a_{z2} & 1 \\ a_{x3} & a_{y3} & a_{z3} & 1 \\ a_{x4} & a_{y4} & a_{z4} & 1 \\ \vdots & \vdots & \vdots & \vdots \\ a_{xm} & a_{ym} & a_{zm} & 1 \end{bmatrix} \begin{bmatrix} \Delta x_u \\ \Delta y_u \\ \Delta z_u \\ -c\Delta t_u \end{bmatrix}$$

Eq.2.11 can be written in vector form as:

$$\Delta\rho = \ H \times \Delta X + r \tag{2.14}$$

where $\Delta\rho$ represents the residual vector, which is the difference between the measured and the predicted pseudorange. The designed matrix is denoted as H, ΔX represents the error state vector and r accounts for the measurement error vector. Applying the linearized equation, the computed residuals can be expressed as follows:

$$\widehat{r} = \ \Delta\widehat{\rho} - H \times \Delta\widehat{X} \tag{2.15}$$

The LS solution can be determined iteratively by adjusting $\Delta\widehat{X}$ until the norm of the residual vector is minimized, as expressed by the following equation:

$$R_{\mathrm{SE}} = \hat{r}^T \hat{r} \tag{2.16}$$

The LS solution of ΔX is:

$$\Delta\widehat{X}_{\mathrm{LS}} = \left[H^T H\right]^{-1} H^T \times \Delta\rho \tag{2.17}$$

In our discussion, we introduced the LS estimator, which assumes equal importance for all measurements, regardless of their inherent quality. Nevertheless, in reality, measurements come with a varying degree of uncertainty. To address this, the Weighted Least Square (WLS) approach is adopted, which assigns weights to individual measurements to accommodate their variances or uncertainties. In the next section, we will go through different weighting schemes used in the WLS solution to enhance the accuracy and reliability of position estimation.

2.6.2 Weighted Least Square (WLS) Estimator: Measurement Weighting Schemes

The Weighted Least Square (WLS) method introduces the concept of assigning varying levels of confidence to the observations, emphasizing the importance of measurements relative to their accuracy and reliability. Under this approach, the measurements with higher variance get lower weightage, resulting in a reduced influence on the position estimation. Conversely, measurements with smaller error variances are given higher weightage, allowing them to contribute significantly to the estimation process. The WLS solution of Eq.2.15 is given as:

$$\Delta\widehat{X}_{\mathrm{WLS}} = \left[H^T \ \mathrm{W} \ \mathrm{H}\right]^{-1} H^T \ W \times \Delta\rho \tag{2.18}$$

$$W = \begin{pmatrix} \frac{1}{\sigma_1^2} & \cdots & 0 \\ \vdots & \ddots & \vdots \\ 0 & \cdots & \frac{1}{\sigma_m^2} \end{pmatrix}$$

Here, W represents the weighting matrix, defined as the reciprocal of the measurement variance. The literature has explored various weighting models, with one of the most common is the sine-elevation model, as proposed in [37][38]. The variance computed using the sine-elevation model is given as:

$$\sigma_k^2 = \frac{1}{\sin(\vartheta_k)^2} \tag{2.19}$$

where ϑ_k represents the elevation angle of the kth satellite. The variance model based on elevation angle considers that satellites at lower elevations are more susceptible to higher error variances compared to those at higher elevations. Consequently, the weighting scheme assigns less significance to measurements obtained from satellites at lower elevations in the position estimation process. Notably, the authors in [39] introduced Carrier-to-Noise ratio (CNO) into the variance model, which serves as a metric indicating the quality of the received signal. Expanding on this concept, the authors in [40][41] extended CNO weighting strategy and introduced the sigma-ϵ and sigma-Δ models. Furthermore, the author in [18] has put forth a generic formula for sigma-ϵ, designed to be compatible with various types of receivers. The variance computed from the CNO measurement is given as:

$$\sigma_k^2 = a + b\ 10^{\frac{-\mathrm{CNO}_k}{10}} \tag{2.20}$$

where $a(m^2)$ and $b(m^2\mathrm{Hz})$ represent parameters that are dependent on the receiver, antenna and frequency. In [42], a hybrid model is presented that considers both the CNO and satellite elevation in the variance estimation.

$$\sigma_k^2 = k\frac{10^{\frac{-CNO_k}{10}}}{\sin(\vartheta_k)^2} \tag{2.21}$$

Here, the parameter k serves as the LOS/NLOS indicator, where $k = 1$ denotes the LOS signal, and $k = 0.5$ indicates NLOS signals. The weighting models described above take advantage of the knowledge of the elevation and/or the CNO to estimate the variance of GNSS observations. These approaches have led to a significant enhancement in positioning accuracy compared to assigning the same variance to all the observations.

With the completion of the discussion up to this point, we have acquired a comprehensive understanding of various signal processing stages leading to the determination of a navigation solution. Building on the insights presented earlier, we are now in the final phase of our exploration of this chapter. The following section will shift the emphasis toward the evaluation of the KPIs, particularly in the context of safety-critical applications.

2.7 Positioning Performance Concerning Safety Critical Applications

The concern about positioning errors remains an everlasting issue in many situations due to their unpredictable nature and varying magnitudes, especially those arising from local threats, as detailed in Section 2.5. In safety-critical applications, exceeding these errors beyond specified limits can have dire consequences, potentially leading to accidents causing harm to individuals and substantial damages. In this context, simply quantifying accuracy by assessing errors within a standard confidence interval around 95% percentile is not sufficient. Instead, what emerges as truly essential is the statistical estimation of the error bounds to account for errors even with exceptionally low probabilities, thereby ensuring the safety of operations. With this in mind, we will now introduce various Key Performance Indicators (KPIs) related to safety-critical applications.

2.7.1 Positioning Performance Indicators

The performance of the Global Navigation Satellite System (GNSS) is fundamentally characterized by four key indicators, each of which plays a crucial role in ensuring the system's reliability and effectiveness. These performance indicators include accuracy, integrity, continuity and availability. The definitions of these parameters are as follows:

Accuracy: The term 'accuracy' is most often used to describe the overall performance of the system, but when it comes to real-time operations, measuring accuracy can be very challenging because true position information is not available. Accuracy is best evaluated in a post-processing context where the position estimate can be compared to the true position with a predefined confidence interval. *Accuracy is a degree of compliance between the true position and the estimated position at any given instance of time with a predefined confidence interval.*

In some applications, such as the railway, where the movement of a train is confined on a fixed track on the ground, it is more relevant to describe accuracy in terms of Horizontal Protection Error (HPE), while Vertical Protection Error (VPE) is less relevant. HPE is determined by calculating the error between the reference (or ground truth) position and the estimated position provided by the system. It is expressed as follows:

$$\text{HPE} = \sqrt{(x_{\text{ref}} - x_{\text{est}})^2 - (y_{\text{ref}} - y_{\text{est}})^2} \tag{2.22}$$

Here, x_{ref} and y_{ref} represent the coordinated reference position, while x_{est} and y_{est} represent the estimated position coordinated. Accuracy is often quantified using the Cumulative Distribution Function (CDF) of the position error, indicating a certain percentage of time the system can provide accurate Position Velocity Timing (PVT) information.

Integrity: The term 'integrity' serves as an indicator of the trustworthiness of the information provided by the navigation system. In an alternative definition, integrity is the system's ability to issue a warning to the users within a specified Time to Alert (TTA) when it is not advisable to use the system for navigation. The primary concerns arise from the potential errors that are large enough to exceed the acceptable limit, referred to as the Alert Limit (AL), which is dependent on the application requirements. During the online phase of operation, the position error remains unknown, making it essential to determine a statistical bound of position error called the Protection Level (PL). The PL is computed from the uncertainties in the measurement and serves to ensure with a high probability, that the true position (unknown) is constrained within this interval. The integrity of the system is considered at risk when the user-computed PL exceeds the AL. In such a situation, preserving integrity requires generating an alert to inform the user about the system's state, potentially leading to the termination of operation. Alternatively, an integrity loss occurs when the system error state goes undetected, posing a risk of a potential accident if the system state is not restored to normal condition within a given time frame, or TTA. This particular situation undermines the system's safety, which will be further elaborated in Section 2.74.

Continuity: The term 'continuity' refers to the system's ability to operate without interruptions, even during signal interruptions caused by obstructions such as buildings. It represents the probability that the specified system performance will be maintained for a certain duration of a phase, presuming that the system was available at the beginning of that phase operation. Alternatively, continuity risk quantifies the likelihood of an unexpected loss of navigation service during an operation, which might require to termination of the operation for the safety of the system. The continuity risk requirement is typically expressed as the maximum tolerable probability of a disruption in the system's continuous operations.

Availability: The term 'availability' is a measure of the operational utility of the navigation service. In simpler terms, it represents the probability over a certain period that all the requirements (such as accuracy, continuity and integrity) of a given operation are achieved simultaneously, so the operation can be conducted safely and efficiently. The availability requirements may differ depending on the specific mode of operation. For instance, in aviation, different availability standards are established for the en-route, approach and arrival phases.

In another definition, it is characterized as the maximum time interval between service outages, often referred to as Operational availability. A positioning system can provide a solution while ensuring that the position error (PE) is within the confidence interval or the protection level (PL) and that the PL remains below the alarm limit (AL). Operation

availability can be expressed as follows:

$$A(T) = 100 \left(\frac{1}{T} \sum_{t=0}^{T} a(t) \right) \tag{2.23}$$

Here, $a(t)$ represents a set of points during which the positioning system maintained 'normal operation' (i.e. PE < PL < AL) over the time interval T.

2.7.2 Receiver Autonomous Integrity Monitoring (RAIM)

Receiver Autonomous Integrity Monitoring (RAIM) is a concept that was initially developed for aeronautical applications, aimed at self-evaluating the trustworthiness of the navigation solution provided by the positioning engine [43]. Its primary purpose is to provide the user with timely alerts in situations when the system exceeds the specified tolerable level. Integrity monitoring schemes are built on two important steps: the estimation process and the fault detection mechanism. The estimation algorithm typically merges the noisy measurements to provide state estimation and its associated uncertainty, given by the state covariance matrix. In the Fault Detection (FD) step, the estimated residual(s) is compared with the predefined threshold(s) to identify the occurrence of the fault(s). In many architectures, this process can also incorporate the Fault Exclusion (FE) algorithm that is designed to isolate the flagged measurements to correct the state estimation errors.
Another important aspect of the integrity monitoring framework is the Protection Level (PL) evaluation which establishes the boundaries around the state estimation. PL estimation takes into account the combined effects of both the estimation process and the uncertainty associated with the measurements. Generally, a conservative policy is applied, accounting uncertainty for the worst case (measurement) to ensure integrity. Nonetheless, such a conservative policy poses a continuity risk, potentially resulting in the unavailability of the position solution when PL exceeds the AL. For this reason, in many studies, FE mechanism is applied to remove the erroneous measurement to improve continuity. Despite the existence of numerous integrity monitoring approaches, in literature, these algorithms can be broadly classified into snapshot and sequential methods. The ***snapshot methods*** rely on the error metric that only uses information about the present state, typically derived from the residuals of the least square estimator or the estimation from the redundant information provided by the sensor. On the contrary, the ***sequential methods***, also referred to as the recursive methods, incorporate errors derived from the present and previous state information. It is generally implemented with a test statistic based on innovation from a Kalman filter.

Presently, since the initial conception, the integrity monitoring algorithms have significantly evolved, offering improved performance in challenging environments, particularly associated with terrestrial applications such as urban canyons and dense foliage. RAIM implementation comes in various forms, offering different approaches to enhance the reliability of navigation solutions. In the earlier version, the standard RAIM [44] is limited to a single satellite constellation and supports only single-frequency signals. Some of these shortcomings are addressed by the Advanced RAIM (ARAIM) [45] [46], which incorporates multiple-fault detection, dual frequency and multi-constellation GNSS signals. Furthermore, the Relative RAIM (RRAIM) [47] [48] includes time differential carrier phase measurements to enhance service availability. The Extended RAIM (ERAIM) [49] [50] enables the integration of INS and GNSS measurements in the integrity monitoring framework, which is generally based on the EKF filter.

In the earlier discussion, we offered a broader view of integrity monitoring. For a deeper exploration of this subject, readers are encouraged to refer to [51] and [52]. Within the

context of this Ph.D. study, we will examine positioning KPIs that rely on the computation of PL and the mathematical expression will be presented in the following section.

2.7.3 Horizontal Protection Level (HPL) Estimation

Protection Level (PL) is a statistical boundary that shall ensure with a very high probability that the true position error remains within the specified limits. This is essential to guarantee that the probability of positioning error exceeding these limits is kept below or equal to a target integrity risk. Integrity is typically realized through the utilization of the Horizontal Protection Level (HPL) and Vertical Protection Level (VPL). In contrast, in rail or road applications, where vehicles typically move along predefined paths, the HPL is further decomposed into Cross-Track Protection Level (XPL) and Along-Track Protection Level (APL). Various methodologies have been proposed in the literature for calculating HPL which can be found in [53] and [54]. In our approach, we adopted HPL computation based on HslopeMax as presented in [53], which is given as:

$$\mathrm{HPL} = max_i \left(H\mathrm{slope}_i \times \sigma_i \right) \times \sqrt{\mathrm{NSSE}} + K(P_{\mathrm{md}}) \times d_{\mathrm{major}} \tag{2.24}$$

Here, the LS residual based Hslope_i represents the sensibility of the Horizontal Protection Error (HPE) to the bias of the ith satellite. It can be expressed as:

$$\mathrm{Hslope}_i = \sqrt{\frac{\left(H^+_{N,i}\right)^2 + \left(H^+_{E,i}\right)^2}{S_{\mathrm{ii}}}} \tag{2.25}$$

and, the normalized sum of squared error (NSSE) can be written as:

$$NSSE = \widehat{r}^{\,T} \Sigma^{-1} \widehat{r} \tag{2.26}$$

with $H^+ = (H^T W H)^{-1} H^T W$ and $S = I - HH^+$, the parameter σ_i represents the standard deviation of ith the measurement, $\widehat{r}$ represents the residual vector, which is the difference between the measurements and their prediction, $K(P_{\mathrm{md}})$ is an inflation factor that depends on the predefined probability of missed detection and d_{major} represents the position error uncertainty along the semi-major axis of the error ellipse [55].

2.7.4 Performance Evaluation and Tradeoffs

The Stanford diagram serves as a very useful tool to explain and illustrate the concepts related to integrity, as well as their relationship to the performance evaluation of the positioning system. In the Stanford diagram, as shown in Figure 2.13, the abscissa represents the absolute Horizontal Protection Error (HPE), while the ordinate represents the Horizontal Protection Level (HPL). The diagonal line separates the samples according to the relationship between position error and protection level. The samples located above the diagonal line symbolize points wherein HPL bounds HPE, whereas the samples below the diagonal line indicate points wherein the estimated HPL has failed to bound HPE. According to the relationship between HPE, HPL and the AL, the position samples are distributed into different regions, each zone signifying a specific state of the positioning system:

- ***Nominal operation:*** It is the state in which the system is available, the HPL well bound the HPE and both remain below the AL.
- ***System unavailable:*** It is the state in which the system is unavailable, the HPL exceeds AL even though HPE is well bounded by the HPL.

- ***Misleading Operation*:** It is the state in which the system is available, both HPE and HPL are below AL, however, HPL underestimates the HPE.
- ***Misleading Information and System unavailable:*** It is the state in which the system is unavailable, the HPL failed to bound the HPE and both are greater than the AL.
- ***Hazardous Misleading Information (HMI):*** It is the state in which the system is wrongly declared available, HPE exceeds HPL but remains below the AL.

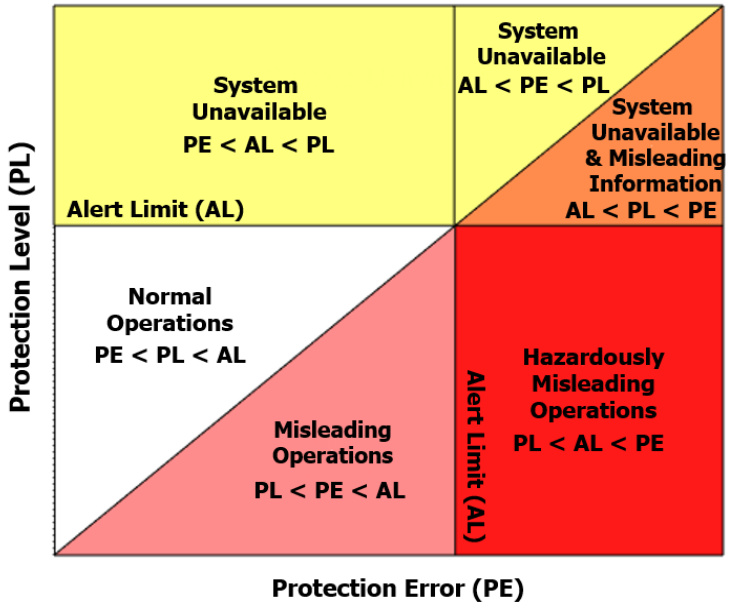

Figure 2.13: Stanford Diagram for KPIs evaluation

We introduced various notions in the earlier discussion that are established based on the logical relationship between PL, AL and PE signifying the operational states or modes of the localization function. These factors are primarily assessed when evaluating the performance of the positioning solution, especially concerning safety-critical applications. Notably, when designing the localization function for such applications, the main paradox remains the tradeoff between positioning availability and integrity of the provided solution. The integrity is violated when the system's faulty state goes undetected beyond a certain time interval given by TTA. Nevertheless, in the following discourse, we will ignore the evolution of the system state over time thus omitting the consideration of the TTA parameter in the evaluation of KPIs. Therefore, we will adopt a conservative approach where we will consider 'snapshot' integrity failure as a safety concern.
The constraint imposed by PL and AL plays crucial in safeguarding against HMI events, thereby ensuring system integrity. Nonetheless, these parameters may also influence operational availability. Adhering to stringent PL limits with a proper error characterization can ensure integrity and protection against HMI whereas an excessively cautious approach might lead to frequent unavailable instances as a result potentially compromising the functionality and practicality of the system. In either situation, the implementation of complementary measures such as Fault Exclusion and (or) sensor integration would be vital to enhance system availability while maintaining integrity. Nevertheless, it is important to clarify that these solutions are considered beyond the scope of this study.

2.8 Chapter summary

This chapter offered an insight into the foundational principles of the Global Navigation Satellite System (GNSS), with a particular focus on its significance in safety-critical applications. In the next chapter, we will present state-of-the-art interference countermeasure strategies that have been addressed in the literature.

Chapter 3

Radio Frequency Interference (RFI), Detection and Mitigation Techniques

3.1 Introduction

In the previous chapter, we outlined some key aspects of the fundamentals of the Global Navigation Satellite System (GNSS) and briefly discussed vulnerabilities associated with satellite-based positioning. In this chapter, our exclusive focus is on addressing the issue of jamming and exploring potential countermeasures to mitigate the impact of jamming interference. The purpose of this exercise is to serve multiple objectives, including becoming familiar with the topic, recognizing the importance of addressing interference concerns in GNSS, exploring existing solutions and required resources, and understanding the performance of these techniques and their limitations. Most importantly, it allows us to identify gaps in the current literature and the potential for future research avenues. To facilitate a comprehensive discussion, we have divided this chapter into two main sections. Section 3.2 delves deeply into the complexities associated with interference. In this section, we will explore various interference signals, offering insight into mathematical models of some common signals found in the literature. We will go through the sources of these signals, presenting real-world interference incidents that occur very frequently. Section 3.3 will provide a comprehensive view of the state-of-the-art interference countermeasures. We will discuss the performance and limitations of existing detection and mitigation techniques, particularly dealing with different types of interference signals.

3.2 Radio Frequency Interference (RFI)

Definition: Radio Frequency Interference (RFI) is the effect of ***unwanted energy*** *due to one or a combination of emissions, radiations, or inductions upon reception in a radio communication system, manifested by any* ***performance degradation***, ***misinterpretation***, *or* ***loss of information*** *which could be extracted in the absence of such unwanted energy* (Source: International Telecommunication Union).

The issue of Radio Frequency Interference (RFI) has undeniably become an inevitable challenge in the realm of wireless communication. This concern is steadily growing due to the exponential growth of wireless devices. The Global Navigation Satellite System (GNSS) receivers are particularly vulnerable to RFI due to their reliance on exceedingly feeble signals. The presence of interference can severely impair the performance of these receivers or even cause a complete denial of GNSS service in a specific area, especially when operating under a strong influence of interference. Although international regulations

protect the frequency bands reserved for GNSS signals, the unauthorized use of Personal Privacy Devices (PPDs), commonly known as jammers and the widespread reliance on wireless communication have increased the interference problems for GNSS devices. The interference signal can manifest in several different forms, including pulsed interference emanating from an aeronautical system such as Distance Measuring Equipment (DME) or Tactical Air Navigation System (TACAN), Continuous Wave Interference (CWI) possibly caused by the harmonics from a Digital Video Broadcast Terrestrial (DVB-T) and swept frequency CWI transmitted by PPDs like cigarette lighter jammer designed to evade vehicle tracking.

In the present discourse, it is important to note that, as briefly mentioned in Chapter 2, interference concerning the source can be classified into two main categories: intentional interference and non-intentional interference, considering the transmission intent of such an undesirable signal. The potential sources of ***unintentional interference*** are numerous and diverse, increasing at an alarming rate. These sources include systems operating within the same frequency band as GNSS, which include DME/TACAN and radio amateur systems. Additionally, there are also sources operating outside the GNSS band, such as TV transmitters [56]. The frequency allocations of different systems are shown in Figure 3.1. On the other hand, ***intentional interference*** may arise from sources with specific aims of disrupting GNSS bands, such as jamming and spoofing.

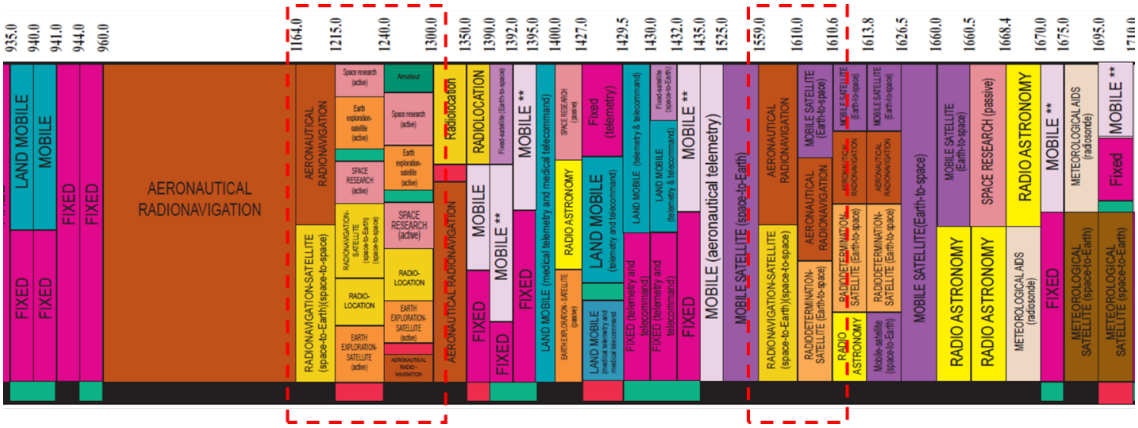

Figure 3.1: Frequency resources allocated to different wireless systems with highlighted regions representing the frequency band for GNSS signals *(source: www.gps.gov)*

The other possible manner to classify interference is based on the spectral characteristics of the interfering signal relative to the signal characteristics of the desired signal. Interference signals can be classified as in-band and out-band interference signals. To be more specific, ***in-band interference*** refers to an interfering signal from a source with a carrier frequency falling inside the GNSS frequency band ($f_{\text{GNSS}} - \frac{B_{\text{GNSS}}}{2} < f_i < f_{\text{GNSS}} + \frac{B_{\text{GNSS}}}{2}$). On the other hand, ***out-band interference*** refers to an interfering signal from a source with carrier frequency located near the GNSS frequency band $\left(f_i < f_{\text{GNSS}} - \frac{B_{\text{GNSS}}}{2} \text{ or } f_i > f_{\text{GNSS}} + \frac{B_{\text{GNSS}}}{2} \right)$. Furthermore, while considering the relative bandwidth (or spectral width) with the GNSS signal, interference can be generally classified further into narrowband and wideband interference. ***Narrowband Interference (NBI)*** refers to the interfering source with a significantly smaller spectral width compared to the GNSS signal ($B_i \ll B_{\text{GNSS}}$). Conversely, ***Wideband Interference (WBI)*** refers to the source of the interference with spectral width very much comparable to the GNSS signal ($B_i \approx B_{\text{GNSS}}$).

3.2.1 The Realities of Interference: A Matter of Concern

Over the past decade, the threat of radio frequency interference has experienced a persistent and exponential surge, a trend that has been undeniably supported in numerous reports. For instance, The Guardian, a prominent media outlet, published a comprehensive report on February 13, 2013, featuring expert opinion. The report highlighted the substantial risks posed by thousands of individuals using GPS jammers on UK roads. These devices are capable of effectively disrupting systems designed for tracking stolen vehicles or monitoring the movements of truck and taxi drivers who work prolonged hours, thereby augmenting challenges for law enforcement agencies *(Source: Thousands Using GPS Jammers on UK Roads Pose Risks, Say Experts, 2013)*.
Similarly, in March 2021, a seminar organized by EUROCONTROL unveiled findings indicating a distressing 2000% increase in the number of incidents of GNSS RFI within just three years, as data collected from voluntary incident reporting (*Source: EUROCONTROL Stakeholder Forum on GNSS, 2023*).
In February 2023, the European Union Aviation Safety Agency (EASA) issued a safety information bulletin, highlighting a significant rise in interference incidents caused by jamming and/or spoofing, with particular emphasis on areas near the conflict zones. These incidents have been observed in the Eastern Mediterranean, Baltic Sea, and Arctic regions (*Source: GNSS Outage Leading to Navigation / Surveillance Degradation EASA Community, 2023).*

Personal Privacy Devices (PPDs)

Personal Privacy Devices (PPDs) also known as jammers, serve a specific purpose to disrupt GNSS coverage. These devices are typically used to evade tracking by fleet management or to bypass toll collection. The interference signal generated from these devices not only affects their intended target but also has a collateral impact on all the users in the vicinity. Figure 3.2 depicts some of the very commonly used jamming devices, which are designed not only to block the GNSS signal but they can also interfere with other radio signals such as WiFi, cellular networks and others. Even though the use of such devices is prohibited in many countries, their possession may not necessarily be illegal. Moreover, these devices are readily available in the online market at the cost of a few tens of dollars.

Figure 3.2: Common jamming devices available in the online market

In the year 2010, the airport administration in Newark, located in the state of New Jersey, experienced sporadic disruptions in their air traffic control system due to the

installation of Personal Privacy Devices (PPDs) on the trucks. The jamming device is often used to conceal the truck's location, thereby evading being tracked by the fleet management authority. However, in August of 2013 same incident gained public attention when the Federal Communications Commission imposed a hefty fine of nearly $32,000 on a Readington man for interfering with flight operations. An investigation revealed that the truck driver had installed a GPS jamming device in his pickup truck to hide from his company, unintendedly disrupting Newark Liberty International Airport's satellite-based tracking system. Regrettably, such incidents are not the first of their kind and undoubtedly not the last, given that such devices are frequently employed for many other reasons, often without users realizing the potential consequences or dangers to those in the vicinity (*N.J. Man Fined $32K for Illegal GPS Device That Disrupted Newark Airport System, 2013*).

In August of 2017, another jamming incident was reported in Nantes, France, when a resident of La Rochelle left a GPS jammer switched on in his car parked at Nantes Atlantique Airport. This led to severe disruption in flight operations, causing delays to multiple flights. The jammer was eventually located and disabled (*Forgotten' GPS Jammer Costs Motorist €2,000, 2023*). The use of privacy devices is on the rise which is expected to challenge any emerging satellite-based services, such as "pay as you drive" insurance or road toll collection, as individuals attempt to reduce their payments or evade road tolls. The issue of jamming must be promptly addressed to guarantee the durability of these imminent services.

Repeaters and Pseudolites

The repeaters and pseudolites are essentially employed for augmenting GNSS coverage in areas where signals might be obstructed such as inside buildings or mines. GNSS repeaters are designed to rebroadcast the received signal after the amplification. On the other hand, pseudolites are ground-based systems that generate ranging signals similar to those transmitted by satellites. Nevertheless, these systems must operate under strictly controlled conditions because any malfunction can lead to interference with satellite signals, thereby potentially disrupting GNSS services in certain areas. In a specific instance, an interference event in Hanover, Germany, in 2012 disturbed flight operations during the takeoff, landing, and taxi-in of the airplanes due to malfunctioning of the GNSS repeater in the airport's hanger. Subsequently, the repeater's operation was suspended and it was discovered that an issue occurred from the repeater transmitting at a power higher than the recommended level, causing signal leakage beyond the hanger and affecting GNSS services.

Conceptually, repeater and pseudolite systems with deceptive intent are equivalent to meaconing and spoofing systems. In March 2020, an incident involving circle-style GPS spoofing was reported in Tehran, Iran. According to the user statement, *"Some of GPS devices received fake signal and show the fake valid location. Yesterday I test a device, it can get signal and give real position. After 10 minutes the device show moving around a big circle in Tehran by 35 km/h speed. I can't fix this problem by restarting the device" source: (GPS Circle Spoofing Discovered in Iran - GPS World, 2023).* A similar incident was reported at the port of Shanghai, China, in July 2019, when the captain of Manukai, an American container ship, observed unusual events on his Automatic Identification System (AIS) display. He observed a nearby vessel seemingly moving back and forth at the dock. Upon viewing this with binoculars, it became evident that the vessel had remained stationary at the dock the entire time. Later, the captain's vessel also encountered strange events while approaching the berth, rendering the primary system and the backup satellite-based systems, incapable of providing the vessel's position.

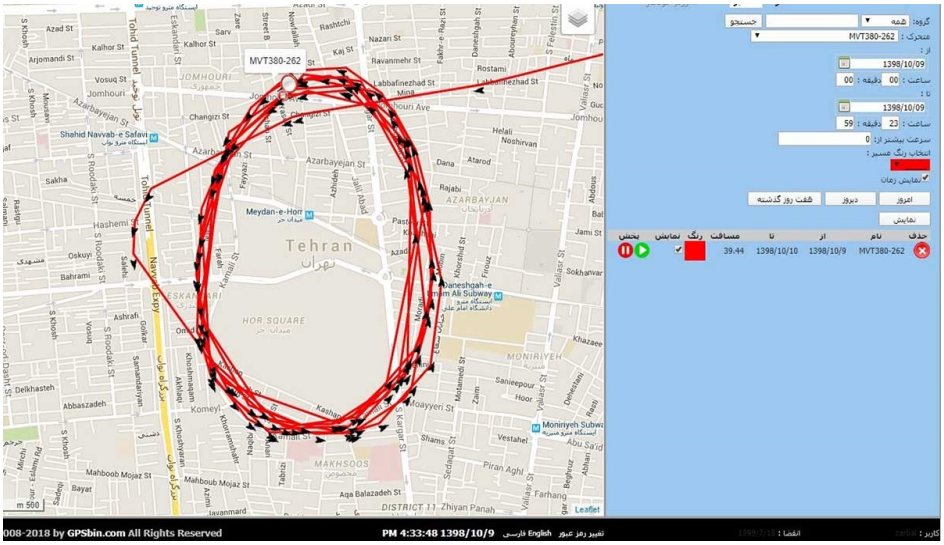

Figure 3.3: Circle-style spoofing observed in Tehran, Iran (Source: Dana Goward)

Television transmission

The Digital Video Broadcast Terrestrial (DVB-T), is a widely adopted standard for terrestrial TV transmissions worldwide. It efficiently utilizes the radio spectrum by broadcasting multiple channels simultaneously in a single transmission using the Orthogonal Frequency Division Multiplex (OFDM) modulation. However, it has been identified as a potential source of out-band interference, mainly due to electronic component malfunctions that generate signal harmonics or intermodulation products. In April 2006, spurious emissions from TV transmitters employing the DVB-T standard were detected in Torino, Italy. This specific instance was considered a likely cause of degradation in the vicinity of the transmitter.

Distance Measuring Equipment (DME)

The GNSS shares its frequency band with other wireless systems that transmit signals in the same frequency band, making them the potential source of interference. One such instance is the aeronautical systems Distance Measuring Equipment (DME) and its military version Tactical Air Navigation System (TACAN), which both operate in the frequency range of 960 MHz to 1215 MHz. These systems are critical for air navigation and guidance as they provide range measurements between the aircraft and the ground station. However, these systems transmit strong pulsed signals that can potentially interfere with Galileo E5 and GPS L5 signals. An incident from 1995 serves as an example, where a DME transmitter at the Edinburg airport in Germany caused a Carrier-to-Noise ratio (CNO) degradation [57].

Radio/TV Amateur

The radio/TV amateur, with a reserved frequency band from 1240 MHz to 1300 MHz for the transmission, is another source of in-band interference. An instance of this particular interference was observed in the harbor of Ostend, Belgium. The equipment with RTK functionality routinely experienced service interruptions for several hours, nearly at the same time of the day. This interference signal had a significant impact on GLONASS and the GPS L2 band, disrupting the precision work that relied on dual frequency measure-

ments. Subsequent analysis revealed that a local amateur television transmitter installed on a lighthouse was a source of this interference. Whenever the owner used to turn on the system after returning from work, the equipment used at a construction site was observed to lose RTK functionality (Source: GNSS interference whitepaper by Septentrio).

Table 3.1: Some typical sources of interference and their signal characteristics

Source	Modulation	Bandwidth	Purpose of intend
Local Oscillator (LO) spur leakage	CW	Narrow	Unintentional
Harmonics from radio broadcast	AM/FM	Narrow, Moderate	Unintentional
Radar system, Distance Measuring Equipment (DME) and Tactical Air Navigation (TACAN)	Pulse	Wide	Unintentional
TV broadcasting, microwave links, and Spread Spectrum Communication	AM/FM	Wide	Unintentional
Personal Privacy Devices (PPDs)	CW/Chirp /Pulse	Narrow Moderate Wide	Intentional
GNSS repeater, Pseudolites, Spoofer, Intera-System Interferences	Matched Spectrum	Wide	Unintentional Intentional
Inter-System Interferences	Other GNSS Spectrum	Wide	Unintentional

Several potential sources of interference and specific incidents have been presented, although not exhaustively; more examples of interference incidents can be found in [58][59]. It is noteworthy that the impact of interference signals emanating from different sources can vary depending on the specific GNSS receiver in use. The degradation in receiver performance depends on the type of interference, the signal power level, and the receiver's inherent capability to withstand such a signal. Table 3.1, summarizes these examples by listing potential sources of interference signals and their key signal characteristics.

3.2.2 Interference Signal Classification: What You Need to Know

Interference signals can be classified based on their signal characteristics, including bandwidth, carrier frequency and modulation. For personal privacy devices, a study in [60][61] proposed four categories of jammers, from class I to class IV, depending on the signal characteristics and complexity. Additionally, a fifth category is introduced in [59] to encompass all signals not belonging to classes I to IV. To maintain coherence, we have adopted a similar classification for interference signals, which is as follows:

Class I - Continuous Wave Interference (CWI): This group represents the most basic form of a jamming signal, which includes sinusoidal waveform(s) with a bandwidth of up to 100 kHz. Continuous Wave Interference (CWI) includes both single-tone and multi-tone with Amplitude Modulation (AM) and Frequency Modulation (FM) signals. The general mathematical model of AM interference is given as:

$$i(t) = \sum_{k=1}^{N} \sqrt{P_{I_k}} \exp\left(j2\pi f_{I_k} t \; + \; \vartheta_{I_k}\right) \tag{3.1}$$

Here, N denotes the number of tones (e.g., N = 1 indicates a monotone signal), P_I is the power of the interference signal, while f_I and ϑ_I represent the frequency and phase of the

respective tone. Figures 3.4 (a) and (b) display the Power Spectral Density (PSD) and spectrogram of the AM signal centered at 10 kHz. The generic form of an FM signal can be expressed as:

$$i(t) = \sum_{k=1}^{N} \sqrt{P_{I_k}} \exp\left(j\left(2\pi f_{I_k} t \; + \; \beta_k \sin\left(2\pi f_{I_k} t\right)\right)\right) \tag{3.2}$$

where N signifies the number of tones of interference signal with power P_I, frequency f_I, and modulation index β_k of the tone. Figures 3.4 (c) and (d) illustrate the PSD and spectrogram of the FM signal with modulation index ($\beta = 1$), centered around 100 kHz.

Class II - Single Sawtooth Chirp Interference: This group involves a linear chirp signal, where the frequency is modulated linearly over time. The mathematical model of linear chirp interference is given as:

$$i(t) = \sqrt{P_I} \; e^{(j \; (f_{\text{inst}}(t) \; + \; \theta_I)} \tag{3.3}$$

where P_I represents the power, θ_J is the initial phase, t denotes the time instance, and $f_{\text{inst}}(t)$ is the instantaneous frequency of the jamming signal over the time. The instantaneous frequency is written as:

$$f_{\text{inst}}(t) = 2\pi f_I t + \pi b \frac{(f_{max} - f_{min})}{T_{\text{sweep}}} \; t^2 \tag{3.4}$$

In Eq 3.4, f_I denotes the starting frequency, b represents the sweeping direction, which can be either upward ($b = +1$) or downward ($b = -1$), T_{sweep} is the sweep period, and $f_{\text{min}} - f_{\text{max}}$ is the sweep bandwidth, where f_{min} and f_{max} represent the minimum and maximum frequencies, respectively. Figures 3.4 (i) and (j) illustrate the Power Spectral Density (PSD) and spectrogram of a single chirp signal characterized by a 7.5 MHz bandwidth and a 10 µsec sweep period in the downward direction.

Class III - Multi-Sawtooth Chirp Interference: It is simply the combination of multiple single chirp signals. Following Eq. 3.3, multi-sawtooth chirp can be expressed as the weighted sum of various chirp signals:

$$i(t) = \sum_{k=1}^{N} \sqrt{P_{I_k}} \; e^{(j \; (2\pi f_{I_k} t + \; \pi b_k \; \frac{\left(f_{\max_k} - \; f_{\min_k}\right)}{T_{\text{sweep}_k}} \; t^2 \; + \; \theta_{I_k})} \tag{3.5}$$

here, P_I represents the signal power, θ_I denotes the initial phase, f_I is the starting frequency, b is the sweeping direction, which can be either in the upward direction ($b = +1$) or downward direction ($b = -1$), T_{sweep} is the sweep period and $f_{\text{min}} - f_{\text{max}}$ is the sweep bandwidth with f_{min} and f_{max} is the minimum and the maximum frequency of the N-th chirp signal. Figures 3.4 (k) and (l) show the PSD and spectrogram of a dual chirp signal. The first chirp signal is characterized by a 7 MHz bandwidth and a 30 µsec sweep period in the upward direction, and the second chirp signal has a 3 MHz bandwidth and a 20 µsec sweep period in the downward direction.

Class IV - Chirp signals with frequency burst: This particular group resembles the previously discussed classes II and III in its basic composition. It is characterized by the presence of chirp signals with frequency bursts, where bursts are used to broaden the range of frequencies affected by the jammer.

Class V - Other kinds of interference signals: This group includes signals that are not classified from classes I to IV. A prominent example of such signals is the pulsed

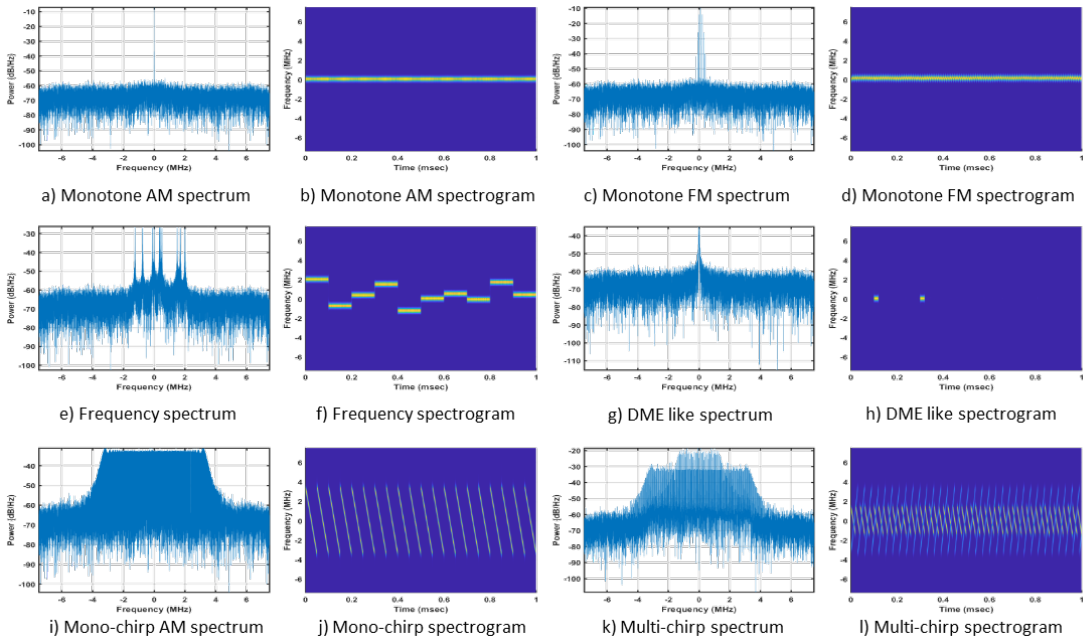

Figure 3.4: Power spectrum and spectrogram of GPS signal with common examples of jamming signal at the baseband

signal, which is typically associated with radar systems. These signals are active only during the repetitive period for a short time interval called a duty cycle. The mathematical representation of a pulsed signal is given as:

$$i(t) = \sqrt{P_I}\; p_\tau(t) \otimes \sum_{k=1}^{N} \delta\left(t - \frac{1}{f_{r_k}}\right) \sqrt{P_{I_k}}\; e^{(j\ (2\pi f_{I_k} t))} \tag{3.6}$$

where P_I is the power, $p_\tau(t)$ is the rectangular pulse with τ representing the pulse width and f_r is the pulse repetition frequency, $\otimes$ is the convolution operator, $\delta(t)$ is the Dirac function and N is the number of pulses. Figures 3.4 (g) and (h) illustrate the PSD and spectrogram of a DME-like signal with two distinct pulses of 20 µsec duration appearing in the time-frequency plot at 100 µsec and 300 µsec.

3.3 Interference Detection and Mitigation Techniques: A Comprehensive view of the State-of-the-art countermeasures

The Global Navigation Satellite System (GNSS) uses a spread spectrum technique that makes it more resilient to narrowband interference. This technique employs Pseudorandom Noise (PRN) codes to modulate signals, which spreads the signal power across a wide frequency band. The spread spectrum nature effectively reduces signal susceptibility to narrowband interference, although stronger interference (whether intentional or unintentional) can still present challenges for GNSS signals. Interference can introduce noise and distortions into the useful signal, and in severe cases, it can make it difficult for the receiver to acquire and track satellite signals. The impact of an interference signal could vary depending on various factors, such as the type of interfering signal, the strength of the interference, the proximity of the source, and the operating environment around the receiver. For instance, moderate interference can cause minor disruptions or temporary signal degradation that can be managed during signal processing, whereas strong inter-

ference can lead to more severe consequences such as loss of quality, reduced accuracy in positioning, or even a complete loss of signal lock. Under such circumstances, addressing the impact of the interfering signal becomes important to ensure the uninterrupted usage of GNSS services. Various countermeasures can be possible depending on the specific requirements. For instance, in certain cases, a simple warning alert can be sufficient, providing timely caution to permit proactive actions such as a pilot relying more on visual sight during the landing phase to avert any potential emergency. However, in some cases, further action may be necessary to effectively manage and mitigate interference challenges. Recently, a comprehensive survey has been published on the GNSS interference management solutions [59], which presented a 4-level framework. This framework includes techniques (or strategies) for the detection, classification, mitigation, and localization of the interfering source, offering valuable insights for addressing GNSS interference issues.

This section offers a comprehensive overview of the present state-of-the-art methodologies used for the detection and mitigation of interference signals. The techniques are implemented at various signal processing stages of the receiver chain, including strategies employed at the front-end level, pre-correlation level, post-correlation level, and navigation level, as shown in Figure 3.5. In the following section, we will explore some common techniques for both detection and mitigation of interference.

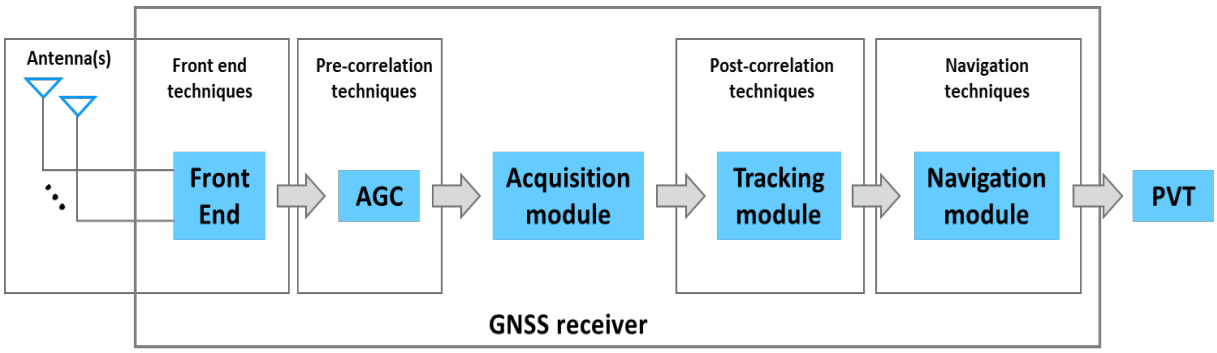

Figure 3.5: GNSS receiver processing chain with several possibilities of implementing interference countermeasures

3.3.1 Detection methods

In the current context, the term 'detection' refers to the process of determining the presence or absence of a specific signal. It is used in a similar sense as the detection theory to establish a null and alternative hypothesis. However, when it comes to interference detection, the distinction between detection and mitigation can sometimes not be possible, especially when a given approach can be employed for multiple purposes. For instance, antenna array processing can be utilized for the detection, mitigation and localization of the interference source. Nonetheless, this section is dedicated solely to detection techniques, with the primary goal of identifying the presence of an interference signal without any further course of action.

A multitude of approaches for interference detection have been extensively explored in the literature. Within this discussion, we have chosen representative techniques that rely on a diverse array of observables from various stages within the receiver processing chain. These techniques include monitoring the Automatic Gain Control (AGC) response, the statistical analysis of signal samples at the output of the Analog to Digital Converter (ADC), which includes monitoring of Probability Density Function (PDF) and the application of a kurtosis detector. Furthermore, these techniques involve power monitoring

in either the time or frequency domain, enabling the identification of anomalies through power spectrum analysis using techniques like Frequency-Domain Power Detector (FPD) and the Welch method. We also explore techniques such as monitoring the correlation output and the Carrier-to-Noise ratio (CNO) observables. To enhance the interference detection capabilities, advanced machine learning approaches such as Support Vector Machine (SVM) and Convolution Neural Network (CNN) are also discussed.

3.3.1.1 Automatic Gain Control (AGC) monitoring:

Automatic Gain Control (AGC) plays an important role in the front-end components of most GNSS receivers, which serves to control and maintain a consistent signal power level. It is accomplished by adjusting the gain or amplification factor to ensure that the signal level remains within the input dynamic range of the Analog to Digital Converter (ADC) thus minimizing the quantization loss. Due to the relatively weak GNSS signals, AGC is typically configured to operate at the thermal noise level. Under normal operating conditions, the gain variation remains relatively steady since average power fluctuations are minimal and can be calibrated accordingly. However, in the presence of interference, AGC takes on the essential role of preserving the signal level within the dynamic range, thus preventing ADC saturation. It achieves this by reducing the gain in response to an unexpected increase in the power level. The response of AGC to such unexpected variations in received signal power is employed in various case studies for interference monitoring. For instance, in [62], AGC is used as a tool to assess the impact of pulsed interference, often associated with Distance Measuring Equipment (DME) systems on GNSS L1/E5 signals. The same approach has been adopted in [63][64] to detect interference within the GPS L1 band, due to harmonics originating from the TV transmitter station.

3.3.1.2 Time-Domain Power Detector (TPD)

The Time-Domain Power Detector (TPD), also referred to as the Power Law Detector (PLD) is an energy-based detection technique employed to detect the presence of interference. This straightforward approach involves monitoring the energy or power of the received signal and comparing it to the maximum expected power under nominal conditions without any interference. The TPD test statistics can be expressed as:

$$P_{\text{TPD}} = \frac{1}{N} \sum_{n=0}^{N-1} |x[n]|^{2\upsilon} \tag{3.7}$$

Here, the window size denoted by the number of samples N is used to estimate the power of the received signal $x[n]$. The parameter ν, following a power law, is a positive integer, and when $\nu = 1$, it signifies an energy-law detector. The detection process involves comparing the test statistic to a predefined threshold, with interference being detected when the test statistic exceeds the threshold value.

3.3.1.3 Frequency-Domain Power Detector (FPD)

The Frequency-Domain Power Detector (FPD) method is based on spectral analysis representing the power distribution within each frequency component of the received signal. This method is commonly referred to as Power Spectral Density (PSD) or power spectrum, which denotes the relative strength of various frequencies present in the signal. Spectral estimation is typically achieved through the Discrete Time Fourier Transform (DTFT), while the periodogram is defined as the square magnitude of the transformed signal. The FPD test statistic can be expressed as:

$$P_{\text{FPD}} = \left| \sum_{n=0}^{N-1} x[n] e^{-i\frac{2\pi}{N}\text{kn}} \right|^2 \tag{3.8}$$

Similar to the TPD, the detection process involves comparing the power spectral density of the signal with the threshold (or spectral mask) that represents the interference-free conditions.

3.3.1.4 Welch detector

Similar to the FPD, the Welch method estimates the PSD of the signal by utilizing a finite set of data points (or segments). This method involves the use of an overlapping window function to divide the signal into smaller data segments of equal length. For each window, the periodogram is estimated and then averaged together, resulting in a smoother version of the frequency spectrum. The Welch estimate of PSD is expressed as [65]:

$$P_{\text{Welch}} = \frac{1}{K} \sum_{m=0}^{K-1} \left| \sum_{n=0}^{N-1} x[n] e^{-i\frac{2\pi}{P}\text{ nk}} \right|^2 \tag{3.9}$$

Here, the variable K represents the total number of segments, and N denotes the number of samples in each observation window. During the detection process, the power spectral density of the received signal is compared to a spectral mask that represents interference-free conditions. Interference is identified when the power spectral density exceeds this predefined threshold.

3.3.1.5 Probability Distribution Function (PDF)-based detector:

The Probability Density Function (PDF) based detection involves a comparison between the distribution of the observed signal and the distribution obtained under interference-free conditions. When there is no interference, the GNSS signal can be modeled as a zero mean white Gaussian process. However, in the presence of an interference signal, this distribution deviates from the Gaussian model, which serves as a detection mechanism. The complete process involves the construction of a reference histogram, which mainly represents the discrete version of the PDF. The histogram creation requires a considerable number of samples in the absence of an interference signal, thereby verifying the *H0* condition. Similarly, a histogram is constructed from the observed signal, potentially containing an interference signal. The method evaluates the test statistic, which can be expressed as a chi-square Goodness of Fit (GoF) test given as:

$$T = \sum_{i=1}^{N} \frac{(O_i - E_i)^2}{E_i} \tag{3.10}$$

A test statistic is used to distinguish between the null hypothesis $H0$ and the alternative hypothesis $H1$. The observed histogram is denoted by O while the reference histogram is represented by E. Here, i represents the bin count indicating the number of samples in each bin. The PDF-based detection is investigated in [66] for the detection of continuous wave (CW) and chirp interferences. The results of this investigation demonstrated the effectiveness of a PDF-based detector in detecting even a low-power chirp signal, which had previously appeared indistinguishable in both the time and spectral analyses.

3.3.1.6 Kurtosis detector

Kurtosis is a statistical parameter that describes the shape and distribution of the samples in the dataset. It is computed by dividing the fourth statistical moment by the square of

the second central moment. The kurtosis of the received signal can be expressed as:

$$K = \frac{\frac{1}{N}\sum_{n=0}^{N}\left(x[n] - \mu\right)^2}{\left(\frac{1}{N}\sum_{n=0}^{N}\left(x[n] - \mu\right)^2\right)^2} \tag{3.11}$$

where N represents the number of samples, and μ is the mean value of the received signal, denoted as $x[n]$. The kurtosis value serves as a metric for assessing the non-normality of the received signal, indicating any deviation from the Gaussian distribution. In normal conditions, the kurtosis value is typically 3 [67] and this value is expected to deviate in the presence of interference signals, which serve as a basis for detection.

3.3.1.7 Carrier-to-Noise Ratio (CN0) Monitoring

The Carrier-to-Noise ratio (CNO) is an important parameter to quantify the tracking quality of the satellite signals. It is the measure of the power of the carrier signal relative to the variance of the Gaussian noise in the received signal. In the presence of interference, the CNO is significantly impacted due to an increase in the noise level within the useful signal. This behavior is exploited in many studies [68][69][70][71] where the CNO metric has been adopted for interference detection. One such study [68] applied a binary hypothesis testing approach, using a predefined threshold with a false alarm probability to detect interference. Furthermore, an effective CNO estimation is proposed in [69] for the detection, which factors out the influence of satellite elevation and receiver noise. Although CNO estimation may be influenced by other factors such as multipath and attenuation induced by foliage, it is less probable that all the satellite signals are simultaneously impacted. This condition has been exploited in [70] where CNO measurements from all the satellites are used in the detection. As an alternative approach, in [71] the AGC behavior is complemented with CNO observations in the decision rule to enhance the detection reliability.

3.3.1.8 Multi-Correlator with Auto-Regressive (MCAR) Modeling

The Multi-Correlator with Auto-Regressive Modeling (MCAR) technique is based on monitoring the correlation outputs from a multi-correlator receiver. In a multi-correlator receiver architecture, each channel is tracked using the correlation of the received signal with numerous delayed versions of the local code, providing a higher resolution for the detection. In [72][73], an Auto-Regressive (AR) approach has been applied to the output of a multi-correlator receiver for real-time detection and characterization of CW and FM jammers.

3.3.1.9 Machine Learning Algorithms (MLA)

Machine Learning (ML) algorithms are frequently employed to solve regression and classification problems, where classical binary classification can be utilized to detect the presence or absence of interference signals. The machine-assisted algorithms are primarily designed to create predictive models from the selected input features. There are several ML-based approaches recently adopted for the detection of interference [74][75][76]. For instance, in [74] it is regarded as an image recognition problem where the signal features are extracted from the black and white images representing the spectrogram of the received signal. The author analyzed Support Vector Machine (SVM) and Convolution Neural Network (CNN) approaches for the classification of various interference signals. In another approach [75], a Twin Support Vector Machine (TWSVM) method is applied to several signal features extracted from the pre-correlation and post-correlation stages,

including correlator output, CNO, and power spectrum, among others, to facilitate classification. The technique involves the creation of a TWSVM model and its solution is derived using the Least SquareTwin Support Vector Machine (LSTWSVM) algorithm, underscoring its suitability for interference monitoring applications. Furthermore, a very classical ML approach based on the K-Nearest Neighbor (KNN) is applied in [76] for classification.

3.3.2 Mitigation methods

The notion of 'mitigation' generally has a broader meaning as it refers to the techniques and methodologies that aim to minimize or eliminate the impact of unwanted signals. In the context of GNSS, the mitigation of interfering signals can be considered as the receiver's capability to retrieve to its correct state while being subject to interference, thereby reducing the influence of such unwanted signals.

One of the simplest countermeasures is switching to an alternative frequency that remains unaffected by interference. This approach is quite practical, given the availability of multiple satellite constellations transmitting signals on multiple frequencies. The concept of the frequency switching approach is explored in [77] where the endurance of a Multi-Frequency and Multi-Constellation (MFMC) receiver is analyzed. The author has developed a software receiver that leverages frequency diversity to combat single-frequency interference, resulting in improved positioning accuracy compared to single-constellation receivers. The MFMC receiver is designed to automatically select the optimal satellite signals across different frequencies from various constellations, effectively reducing the impact of interference.

Another method to counter interference involves integrating complementary information from other positioning sensors such as an Inertial Navigation System (INS). The integration of GNSS/INS can be realized through three different approaches such as loosely coupled, tightly coupled and deeply (or ultra-tightly) coupled architecture. These approaches differ in the manner in which they use information from the different sensors. For instance, in [78], a novel Adaptive Tightly Coupled (ATC) integration approach is investigated that combines the GNSS/INS integration and GNSS tracking functions into a signal estimation algorithm. By adjusting the bandwidth, the response of code and carrier tracking loops is modified, making them more suitable for moderate jamming environments as they become more resistant to noise.

Additionally, vector tracking is a promising approach that can offer limited protection against interference signals. Conventional GNSS receivers rely on individual tracking loops for each satellite in view, which operate independently. In vector tracking, signal channels are interconnected through the shared receiver state. This enables the coordinated tracking of individual channels through the receiver states. This technique is particularly advantageous when more than four satellites are visible, as shared information from multiple satellites can bolster the signal strength of the weaker ones [79].

In this discussion, the term 'mitigation' is explicitly considered from a signal processing perspective. The mitigation strategy is seen as a method that may include processes like identification and isolation, subsequently leading to the suppression of interference signals while retaining valuable content. These mitigation techniques often serve dual roles as detection and mitigation approaches, complementing the detection strategies previously presented in Section 3.3.1 The jamming mitigation countermeasures are primarily addressed in the precorrelation stage before the signal dispreading process. Since the post-correlation methods require normal signal acquisition and tracking as a precondition, they are therefore suitable for less severe interference and can provide limited protection.

The precorrelation countermeasure techniques are classified depending on the processing domain where the mitigation is applied. These techniques include time-domain Pulse Blanking (PB), adaptive frequency domain filtering with Adaptive Notch Filter (ANF), signal transformation techniques in the time-frequency domain involving Short Time Fourier Transform (STFT) and Wigner-Ville Distribution (WVD), time-scale domain filtering employing the Wavelet Transform (WT), projecting a signal in the subspace domain with Karhunen Loéve Transform (KLT), multi-antenna spatial processing for beamforming using Space-Time Adaptive Processing (STAP) and Space-Frequency Adaptive Processing (SFAP).

3.3.2.1 Time Domain Technique

Time domain techniques offer a straightforward and practical approach, making them exceptionally well-suited for real-time applications. They are particularly used for the detection of interfering signals. Moreover, these methods can be effectively employed to suppress interference that has a very sparse representation in the time domain such as pulsed interference.

3.3.2.1.1 Pulse Blanking (PB)

Pulse Blanking (PB) is a simple and yet highly effective method, particularly when dealing with unintentional pulsed interferences, such as the one transmitted by the DME or TACAN system [80][81]. This technique involves replacing the signal sample amplitude with a null value (or zero), essentially 'blanking' out any unwanted interference. In some receivers, this blanking process is typically employed while monitoring the Automatic Gain Control (AGC) response. Figure 3.6 shows the block diagram of the pulse blanker integrated within the front end of the GNSS receiver. The AGC function ensures that the signal level remains within the dynamic range ADC to minimize the quantization loss. However, in the presence of interference, it automatically reduces the gain to prevent ADC saturation. This particular behavior is used in interference monitoring and subsequently, to activate the blanking module.

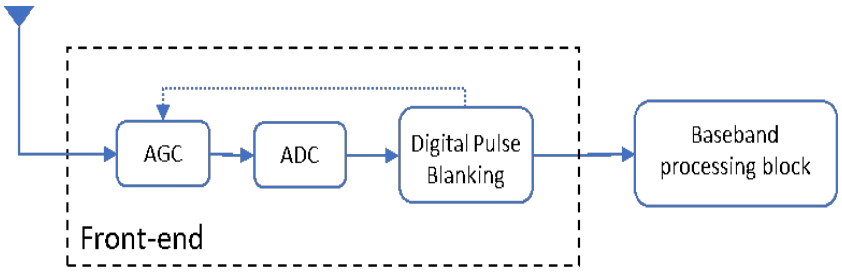

Figure 3.6: Digital Pulse blanking scheme in GNSS receiver architecture

Pulse banking proves to be a highly effective technique for the suppression of pulsed signals. However, it can become ineffective when the signal is weak. Furthermore, according to [81], the performance of pulse blanking may be compromised by the limited dynamics of AGC. This is because the amplification factor relies on the average input signal power over a certain time duration that is generally longer than the pulse itself. This situation could lead to the unnecessary removal of signals that are unaffected by interference.

3.3.2.2 Frequency domain technique

The countermeasure approaches in the frequency domain are very common when dealing with Narrowband Interference (NBI) or Continuous Wave Interference (CWI). These types of signals occupy a narrow portion of the frequency spectrum, making it possible to suppress them in the frequency domain processing by filtering out a small portion of the spectrum. This can be accomplished without affecting the useful GNSS signal. One approach for suppressing interference signals is through spectral estimation, which involves applying the Discrete Fourier Transform (DFT). The detection process involves a comparison between the spectrum of the received signal and a threshold value representing the frequency spectrum in interference-free conditions. Subsequently, the mitigation process involves either applying a spectral null or notch filtering. After the mitigation process, the time representation can be obtained by applying the Inverse Discrete Fourier Transform (IDFT). However, this method is most effective when signal characteristics remain stationary over time. If the spectral characteristics of the interfering signal change over time, such as in the case of a chirp signal, adaptive filtering methods are necessary to remove the interference signal. One strategy involves introducing a spectral null while observing the signal over a short time interval. Alternatively, a parametric frequency adaptive technique can be applied to address the dynamic changes in the interfering signal's spectral characteristics.

3.3.2.2.1 Adaptive Notch Filter (ANF)

The Adaptive Notch Filter (ANF) has gained significant attention in the research community and is regarded as a highly effective technique, particularly against the chirp signal [82][83][84][85][86][87]. It is an extension of the classical notch filter with an additional integrated adaptation unit to continuously track and attenuate the frequency of the unwanted signal, which may change over time. The transfer function of a single-pole Infinite Impulse Response (IIR) notch filter can be written as:

$$H(z) = \frac{1 - z_0[n]z^{-1}}{1 - k_\alpha z_0[n]z^{-1}} \tag{3.12}$$

Here, $k_\alpha \in [0, 1)$ represents the pole contraction factor that controls the notch bandwidth and $z_0[n]$ is the filter zero that determines the position of the notch in the complex plane. Figure 3.7 depicts the general block diagram of ANF comprising of a notch filter and an adaptation block. Two adaptive techniques are proposed in [82] and [85] namely regular ANF and FLL-based, for tracking swept-frequency signals. The FLL equivalent technique employs a Frequency Lock Loop (FLL) approach, while regular ANF architecture utilizes a stochastic gradient-based technique to estimate the frequency of the interfering signal. It continuously estimates z_0 for each sample using a least square-based iterative rule that aims to minimize energy at the output of the filter.

In literature, multiple ANF realizations have been presented. In [88], a comparative study was conducted for two structures: the second-order direct form and the lattice-based notch filters. The comparison focuses on parameters such as tracking performance, convergence speed, and output signal-to-noise ratio (SNR). The results indicated that the lattice structure with the proposed gradient algorithm outperformed the direct form in effectively suppressing the frequency hopping interference. Another study, [89], introduced an Adaptive all-pass Notch Filter (ANFA) for the suppression of CWIs. The ANFA based on an all-pass filter with Gaussian-Newton as an adaptation algorithm improved the convergence rate. In addition, a cascade ANF architecture was analyzed in [90], where multiple cascaded filters enhanced the suppression effectiveness, particularly when dealing

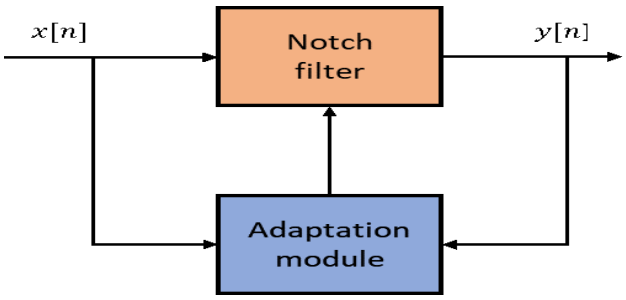

Figure 3.7: simplified block diagram of the adaptive notch filter

with two simultaneous chirp interferences. The results showed that the cascaded approach is effective when there is a sufficient power difference between the frequency-modulated continuous wave (FMCW) interferences. Otherwise, the filter could lock onto the wrong frequency, leading to significant performance degradation. Furthermore, two-pole and multipole notch filters are presented in [82] to suppress the CWIs signal. A slightly modified algorithm is proposed in [91] that first detects the presence of the interfering signal and then adjusts the amplitude parameter to maximize the SNR at the output. According to the author, this approach is capable of perfectly suppressing the frequency hopping signal, even in the presence of considerably strong interference.

3.3.2.3 Time-Frequency domain techniques

The transformation of a signal in the Time-Frequency (TF) domain provides another way to analyze signal characteristics in both the time-frequency domain. In TF representation, the resolution is constrained by the Heisenberg uncertainty principle, also known as the Gabor limit, which establishes a tradeoff between time and frequency resolution. In this method, the mitigation process requires a preliminary assessment of the TF mask (or threshold plane) under interference-free conditions for the identification of interference components, represented by coefficients exceeding the threshold value. To filter interference, one can either blank out these coefficient values or secondarily, separate the interference components to create a synthetic interference signal that can then be subtracted from the received signal. For the discussion, we have included the Short Time Fourier Transform (STFT) and the Wigner-Ville Distribution (WVD), as they are the most common methods used for characterizing the time-frequency signal.

3.3.2.3.1 Short-Time Fourier Transform (STFT)

The Short Time Fourier Transform (STFT) method is employed to analyze the time-varying frequency content of a signal using a short window function. This method involves dividing the entire signal into smaller intervals (windows) of equal intervals. Each interval is then multiplied by the window function (e.g. Hamming or Hanning windows) to minimize the spectral leakage. Subsequently, the frequency content is estimated for each segment using Discrete Fourier Transform (DFT). The STFT is mathematically represented as:

$$\text{STFT } \{x[n]\} \equiv X(m,f) = \sum_{m=n}^{N+L-1} x[n]w[n-m]e^{-j2\pi fn} \tag{3.13}$$

Here, $x[n]$ represents the received signal, $w[n]$ is the window function of length L where the signal is assumed to be stationary, and f is the frequency domain variable. The spectrogram of the signal is the representation of the normalized squared magnitude of STFT coefficients, defined as [92]:

$$\text{spectrogram}\{x[n]\} \equiv |X(m,f)|^2 \tag{3.14}$$

The balance between time and frequency resolution in the Time-Frequency (TF) analysis is inherently linked to the window size. A longer window provides more accurate frequency estimation but limited time resolution, while a shorter window provides higher time resolution but at the cost of reduced frequency resolution. Nonetheless, researchers have proposed various techniques, including those outlined in [93], to optimize the choice of the analysis window to achieve maximum TF resolution.

3.3.2.3.1.1 Wigner-Ville Distribution (WVD)

The Wigner-Ville Distribution (WVD) is classified as a quadratic time-frequency distribution, which offers an attractive alternative for representing signals in the Time-Frequency (TF) domain. This method provides a better spectral resolution without the tradeoff between time and frequency resolution, as in the STFT. The discrete-time WVD is mathematically represented as [94]:

$$W_{x,x}(m,f) = \sum_n x[m+n]x^*[m-n]e^{-j4\pi fn} \tag{3.15}$$

For a finite segment of the signal, e.q. 3.15 can be expressed as:

$$W_{x,x}(m,f) = \sum_n \text{w}[m+n]\ \text{x}[m-n]\ \text{x}^*[m-n]\ w^*[m+n]e^{-j4\pi fn} \tag{3.16}$$

Here, $w[m]$ presents the window function applied to select the finite signal $x[m]$ and $(*)$ represents the conjugate operation. WVD offers improved spectral resolution compared to STFT, however, it suffers from unwanted cross-terms resulting from various signal components [95][1]. In [1], a TF analysis based on the spectrogram and the WVD distribution method were adopted, and a peak-interpolation method was applied for the estimation of interference instantaneous frequency.

3.3.2.4 Time-Scale Domain Technique: Wavelet Transform

Wavelet Transform (WT) is a widely used signal processing technique primarily utilized for denoising applications [96][97]. Its extensive research study and application have made it a versatile tool across diverse domains, including medical imaging, audio signal processing and video coding. Wavelet analysis is highly regarded for its effectiveness in analyzing non-stationary signals, as it overcomes the limitations of other techniques. This is achieved by utilizing analytical functions that localize the signal components in both time and frequency [97][98][99], allowing a more accurate representation of the signal's characteristics. The wavelet transform overcomes the limitation of the fixed window as it analyzes the signal by using a scaled and translated version of a wavelet function, also known as the mother wavelet. There are several different families of wavelet functions each characterized by a finite duration and distinct shapes. Among the most commonly employed wavelet functions are the Symlet, Haar, Coiflet, Daubechies, and Mexican hat. The Discrete Wavelet Transform (DWT) is mathematically represented as:

$$W(j,m) = a^{-j/2}\sum_j\sum_m x[n]\ \psi\left[a^{-j}n - m\right] \tag{3.17}$$

where $a > 1$, $x[n]$ represents the received signal, $\psi[n]$ is the mother wavelet function, j is the scaling (or dilation) factor and m is the wavelet translation (or shift) index. Scaling is accomplished by utilizing compressed and stretched wavelet functions, allowing

signal analysis at different scales or equivalently with different levels of frequency resolution. Figure 3.8 illustrates the wavelet scaling effects on time-frequency resolution. A compressed wavelet function possesses a short observation window, allowing to capture of higher frequencies components with a better time resolution. On the other hand, the stretched wavelet function has a larger observation window and can capture lower frequency components, although this comes at the expense of time resolution.

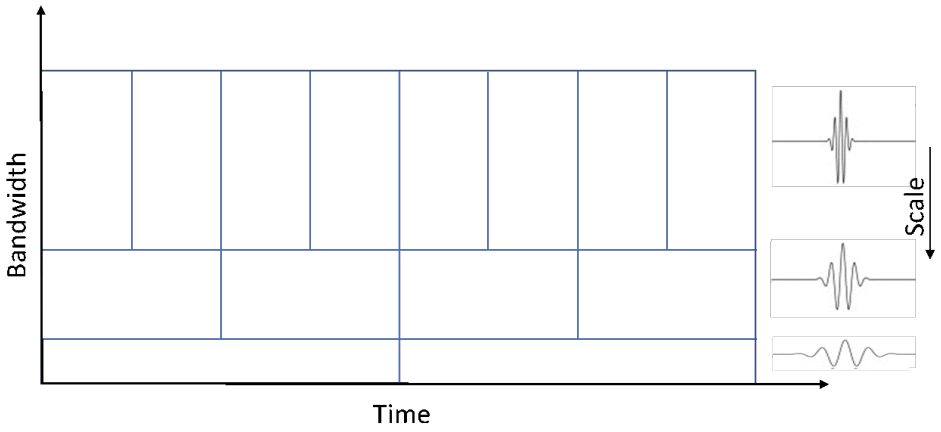

Figure 3.8: Wavelet scaling vs time-frequency resolution

The discrete wavelet transform can be implemented by employing a bank of bandpass filters, each characterized by a distinct frequency response. The process involves breaking down the discrete signal through the use of low-pass and high-pass filters, followed by subsampling. This filtering and resampling process corresponds to the scaling and translation operations in the wavelet transform. The signal decomposition is performed in multiple steps, each time the filter output is further decomposed to form tree-like structures, also called Wavelet Packet Decomposition (WPD). A more detailed implementation of WPD-based detection and mitigation will be discussed in Chapter 4.

The wavelet transform offers a way to analyze signals at multiple resolutions, effectively overcoming the limitation of a fixed window posed by Short Time Fourier Transform (STFT). However, the performance of mitigation and implementation complexity depends on the choice of the wavelet used during the analysis.

- The computational complexity increases with more decomposition stages, but this can be reduced by analyzing the signal with only orthogonal basis functions.
- The mitigation performance can be enhanced by selecting an appropriate wavelet function that maximizes the correlation with the signal under analysis.

Wavelet-based mitigation has been explored in various studies to mitigate Continuous Wave (CW) and pulse interference signals [100][101][102]. In [102] a comparative study was conducted on six different wavelet functions, namely Haar, Daubechies, Symlets, Coiflets, Biorthogonal Spline and Meyer. The result indicated that in the presented chirp scenario, the Coiflets and Meyer wavelet functions demonstrated relatively better performance compared to the other candidates. Additionally, in [100] the mitigation performance of WPD was investigated in the presence of multiple pulsed and narrowband interference scenarios. The finding suggested that the proposed approach outperformed the classical pulse blanking technique for pulsed interference. The paper [101] conducted a comparison between two interference mitigation techniques, ANF and WPD in the presence of intentional and unintentional interference. The results demonstrated that WPD offers significant performance enhancement over notch filtering in terms of acquisition, tracking and positioning metrics.

3.3.2.5 Subspace domain filtering technique: Kerhunen-Loève Transform

The Karhunen Loéve Transform (KLT) is a subspace domain technique used for signal decomposition. It is achieved by projecting a signal into a vector subspace using a set of orthogonal base functions, also referred to as eigenfunctions or eigenvectors. KLT is known for its flexibility since its base functions can be of any form, resulting in a more effective decomposition. The KLT analysis integrates both deterministic and stochastic analyses, which enable it to provide insights on both the signal and noise. The KLT decomposition of a signal $x(t)$ over a finite time interval is expressed as [103]:

$$x(t) = \sum_{n=1}^{\infty} Z_n \Phi_n(t) \tag{3.18}$$

Here, Z_n represents statistically independent scalar random variables and $\Phi_n(t)$ are the deterministic functions also called eigenvectors or eigenfunctions. The random variable Z_n is obtained by projecting the given stochastic process $x(t)$ over the corresponding eigenvector $\Phi_n(t)$ given as:

$$Z_n = \sum_{-\infty}^{+\infty} x(t)\Phi_n(t)\mathrm{dt} \tag{3.19}$$

The KLT technique offers several advantages in comparison to other transformation techniques.

- The detection performance of KLT is independent of the nature of the interfering signal, making it equally effective for both narrowband and wideband interference.
- It offers superior signal decomposition since the eigenfunctions adapt to the characteristics of the processed signal.
- KLT can analyze both the deterministic and stochastic components of the signal, resulting in better separation between the signal and the noise content in the received signal.
- KLT is capable of detecting very weak signals hidden under the noise [103].

Despite its numerous advantages, KLT has a significant drawback, primarily related to its complexity and high computational requirements. Interference mitigation using the KLT algorithm is investigated in [104][103][105]. The algorithm projects the signal onto a subspace to distinguish interference components from useful GNSS signals. To achieve this, the magnitude of eigenvectors is proposed in [104], serving as a metric to discriminate between interference and useful GNSS components. Interference was identified by examining the magnitude of eigen coefficients, which appeared to be significantly large and distinct from the coefficients observed in the absence of interference. A potentially more computationally efficient solution is proposed in [103] with the Bordered Autocorrelation Method (BAM) KLT to significantly reduce the computational complexity.

3.3.2.6 Spatial filtering with multiple antennas

The adaptive antenna or spatial filtering concept, was originally introduced in radar and communication systems. This method involves the use of an array of antenna elements arranged in a specific geometric configuration to acquire signals, thus enhancing spatial diversity in signal processing. Signals acquired from different antennas represent the time-delayed version of the received signal, which depends on the array configuration (i.e., the relative geometry between the antenna array). The output signal is a weighted sum of

the signals from various antenna elements, with these weights determined through cost function optimization. Adaptive array processing typically employs two approaches: null steering and beamforming.

Null steering relies on the principle that GNSS signals are typically submerged beneath the thermal noise floor and any signal exceeding the noise level is considered interference. It involves the continuous adjustment of weights to minimize the output energy, thus steering the antenna response away from high-power sources and creating a null in the direction of the interfering source.

Beamforming on the other hand, is a technique that employs signal steering to numerically control the radiation pattern of the antenna array to direct it towards the desired source. It is achieved by adjusting the weights in a way that maximizes signal gain in the direction of the satellite while attenuating signals originating from other directions.

In the literature, there are mainly two beamforming approaches adopted for the suppression of interference signals: Space-Time Adaptive Processing (STAP) and Space-Frequency Adaptive Processing (SFAP) [106][107][108][109][110][111].

3.3.2.6.1 Space-Frequency Adaptive Processing (SFAP)

In the SFAP system, the signal received by multiple antennas is transformed from time to frequency domain using Discrete Time Fourier Transform (DTFT). SFAP method effectively utilizes both spatial and frequency dimensions for adaptive signal processing. Figure 3.9 illustrates the block diagram for the space-frequency array processing. In SFAP the interference suppression is primarily carried out in the frequency domain, and then the signal is transformed back to the time domain using inverse transformation. A more comprehensive discussion on SFAP can be found in [108][107].

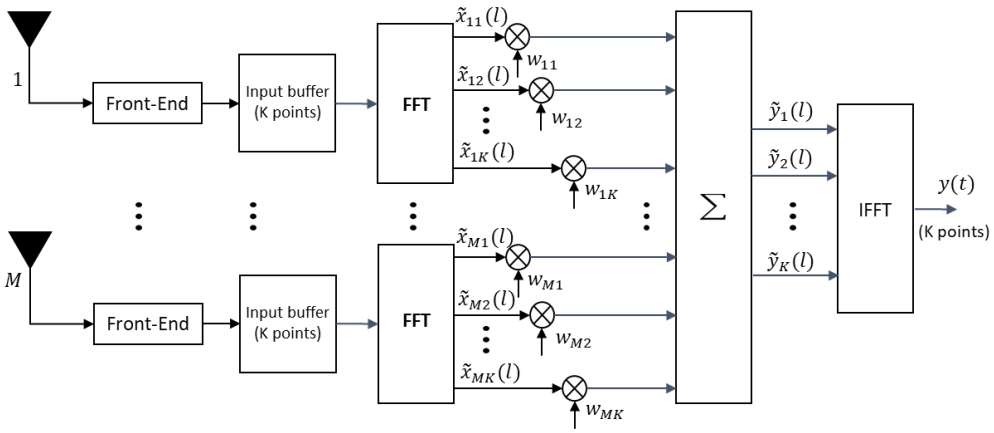

Figure 3.9: Space-frequency array processing block diagram

3.3.2.6.2 Space-Time Adaptive Processing (STAP)

The Space-Time Adaptive Processing (STAP) approach works by combining spatial and temporal information, taking advantage of the spatial diversity and temporal characteristics of the signals. The STAP architecture incorporates Finite Impulse Response (FIR) filters for temporal processing. It involves the processing of spatially acquired digital samples from the ADC in the time domain to effectively suppress interference. Figure 3.10 illustrates the block diagram of a space-time array processor with M elements and N-tap FIR filter.

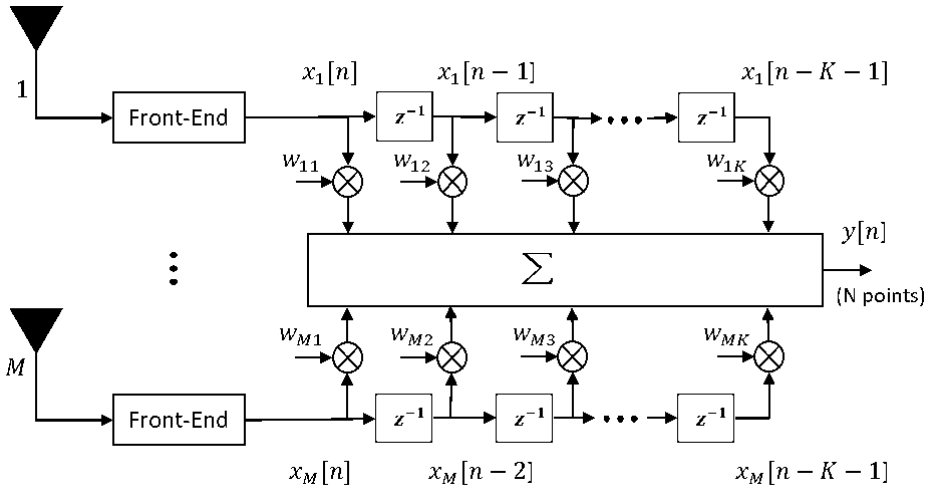

Figure 3.10: Space-time array processing block diagram

The STAP output can be mathematically expressed as [106]:

$$y[n] = \sum_{m=1}^{M} \sum_{k=1}^{K} w_{\mathrm{mk}} x_m[n-k+1] = \mathbf{W}^T \mathbf{X} \tag{3.20}$$

Here, w_{mk} represents the weight at the k-th tap of the FIR filter after the m-th antenna element, x_m is the n-th sample of the m-th array element output , $\mathbf{W}$ and $\mathbf{X}$ are the STAP weight and input vectors, given as:

$$\mathbf{W}=[w_{11},\ldots,w_{1k},\ldots,w_{M1},\ldots,w_{\mathrm{MK}}]^{\mathbf{T}} \tag{3.21}$$

$$\mathbf{X}=[x_1[n],..,x_1[n-k+1],\ldots,\ x_m[n],\ldots,x_m[n-k+1]]^T \tag{3.22}$$

Minimum Mean Square Error (MMSE) weight control algorithm is defined as:

$$\mathbf{W}_{\mathrm{opt}} = \arg\min_{w} E\left\{\left|s_{\mathrm{ref}} - \mathbf{W}^T\mathbf{X}\right|^2\right\} = \mathbf{R}^{-1}\mathbf{G}_s \tag{3.23}$$

Here, $\mathbf{R}$=E{X $\mathbf{X^H}$} represents the covariance matrix, and $\mathbf{R}$=E{X $\mathbf{X^H}$} is the cross-correlation vector between the STAP input and the reference signal. The adaptive weights are applied to enhance the gain in the satellite direction and attenuate the signal from the interfering source, having a significant impact on the formation of the beam. Several adaptive control algorithms are implemented in spatial filtering to update these weights, including Mean Variance Distortion Response (MVDR), Minimum Mean Square Error (MMSE) and Maximum Signal to Interference Ratio (MSINR). Previously, in [106], a multi-beamforming multichannel GNSS receiver was introduced, where the STAP method was examined against multiple types of interference signals. The performance of STAP improved with the increase in the number of taps but a good tradeoff between performance and complexity for the pulsed DME/TACAN interference scenario was achieved with 5 or 7 taps. Furthermore, the results obtained show that the MVDR processor with directional constraints delivered better tracking performance with minimal distortions in the useful GNSS signal. Another approach proposed in [108] addresses the challenge of concurrent narrowband and wideband jammers using SFAP. In this approach the weights of each sub-band are determined by utilizing signal representation from both the sub-band under consideration and adjacent sub-bands, resulting in substantial improvement in the performance for the suppression of multiple concurrent jammers.

3.3.3 Summary and categorization of presented techniques

In this chapter, we have presented an overview of various countermeasure methods employed for the detection and mitigation of jamming signals in GNSS. As we summarize and compare these approaches, it becomes evident that each method has its unique strengths and weaknesses. Table 3.2 provides a summary of these techniques, categorizing different techniques based on their placement in the receiver processing chain, and highlighting their computational requirements and limitations.

Table 3.2: A summary of different categories of countermeasure techniques for the detection and mitigation of jamming signals.

Receiver processing level	**Method**	**Purpose Detection** |**Mitigation**	**Computational burden**	**Limitations**	**References**
Front end	Frequency switching	☑ ☑	moderate	- Necessitates a multi-frequency receiver. - At minimum, one frequency should remain unaffected by interference.	[77]
	AGC	☑ ☐	low	- Sensitive to temperature variations - Recalibration may be necessary to maintain its effectiveness.	[62][63][64]
	Null steering CRPA	☑ ☑	high	- System complexity with multiple antennas and associated components. - Calibration and alignment issues. - Limited adaptability against various forms of interferences.	
Pre-correlation	Power spectrum (TPD, FDP and welch method)	☑ ☐	moderate	- Sensitive to observation window parameters shape and size	[65]
	ANF	☑ ☑	moderate	- Performance depends on the choice of parameters. - Filter tuning should be tailored according to jammer type.	[82][83][84] [85][86][87] [88][89][90] [91]
	PB and spectral nulling	☐ ☑	moderate	- Threshold value needs to be customized for the specific jammer type - Not suitable for chirp signals	[80][81]
	PDF	☑ ☐	moderate	- Requires a substantial number of samples to obtain a representative distribution. - Effective primarily at higher JNR.	[66]
	Kurtosis	☑ ☐	moderate	- Works only at higher JNR	[67]
	STFT	☑ ☑	low	- Fixed window size constraints on the TF resolution.	[94][93]
	WVD	☑ ☑	low	- Cross terms appear in the presence of multiple components.	[94][95][1]
	Wavelet Transform	☑ ☑	moderate	- Sensitive to the choice of basis function.	[97][98][99]

	KLT	☑ ☑	very high	- Determining the appropriate decomposition samples and the threshold can be highly challenging	[104][103][105]
	STAP/SFAP	☑ ☑	very high	- Not suitable for chirp interference.	[106][107][108] [109][110][111]
Post-correlation	CNO	☑ ☐	moderate	- Distinguishing various factors contributing to low CNO can be challenging	[68][69][70] [71]
	MCAR	☑ ☐	high	- Requires multi-correlator receiver.	[72][73]
	Machine learning algorithm (SVM, CNN and KNN)	☑ ☐	high	- Limited by interference scenario diversity presented in the training dataset.	[74][75][76]
Navigation	Vector tracking	☑ ☑	high	- Enhances overall robustness but not studied for the jamming.	[79]
	Sensor fusion	☑ ☑	high	- Limited to moderate jammers.	[78]

It is important to note that the computational complexity and limitations mentioned in the summary are drawn from the literature. However, it is vital to recognize that these findings may vary depending on the specific implementation and the scenario under investigation.

3.4 Chapter summary

This chapter, along with the previous chapter, has emphasized the significance of addressing interference in satellite-based positioning systems. The state-of-the-art mitigation techniques that have been presented in this chapter show that they are primarily based on signal processing methods that have been developed over several decades. Nevertheless, the issue of interference continues to be a hot topic in Global Navigation Satellite System (GNSS) for several reasons. These include the changing nature of the interference problem due to the widespread availability of radio devices capable of broadcasting customized and more complex signals, a variety of applications relying on GNSS with higher requirements, and the necessity for adaptable, efficient, and robust solutions.

The presented countermeasures have been purposefully selected from a range of techniques that can be categorized into different signal-processing domains. These techniques involve interference mitigation in the time domain, frequency domain, time-frequency domain, time-scale domain, subspace domain, and spatial domain. The literature has long been concerned with the performance analysis of these techniques from the signal perspective. However, recent studies have shifted their focus to assess the effectiveness of these techniques at the intermediate levels, such as satellite acquisition level and the signal-to-noise ratio of the satellites at most presenting performance analysis at the level of positioning accuracy. One of the main originality of the next chapter will be to assess the performance of the implemented techniques in the context of safety-critical applications.

We will delve further into the topic and will provide a detailed discussion on the implementation of three techniques belonging to different families, namely the Adaptive Notch Filter (ANF), Wavelet Packet Decomposition (WPD), and Karhunen Loéve Transform

(KLT), with computational complexity levels increasing from low to high respectively. We will deal with two different types of interference signals namely frequency hopping and chirp signal in our investigation. Furthermore, we will examine the effectiveness of each mitigation technique on different levels of the receiver processing stage namely acquisition, tracking and positioning, primarily presenting the key performance indicators linked to safety-critical requirements using the Stanford diagram.

Chapter 4

Implementation of Adaptive Notch Filter (ANF), Wavelet Packet Transform (WPD) and Karhunen Loève Transform (KLT)

4.1 Introduction

In Chapter 3, we presented an overview of the state-of-the-art precorrelation level countermeasures presented in the literature, mainly dealing with jamming detection and mitigation. Our main motivation for this study is to investigate the impact of jamming and evaluate the performance of mitigation techniques in the context of safety-critical land transportation applications. For this purpose, we have selected three techniques belonging to different categories with different computational requirements. These techniques include Adaptive Notch Filter (ANF), Wavelet Packet Decomposition (WPD), and Karhunen Loéve Transform (KLT). In this chapter, we will provide a comprehensive and detailed implementation, thoroughly assessing the performance of each of these techniques. Indeed, as presented in Chapter 3, the performance of the mitigation techniques has been predominantly focused on the intermediate levels involving estimation of the interference frequency, satellite acquisition, and signal tracking [1][2][3][4][5]. Recently, the authors [6][7] have taken a further step and presented mitigation performance from the end user perspective by analyzing the positioning accuracy. The originality of this chapter relies on assessing the mitigation performance across various levels of the receiver processing stages and most importantly, the evaluation of the positioning Key Performance Indicators (KPIs) associated with safety-critical applications, which has not been previously undertaken in the literature.

We will employ the Stanford diagram, previously introduced in Chapter 2 as a visualization tool to assess and compare the KPIs such as accuracy, availability, and safety of the localization system. The Stanford diagram is established directly by comparing the Horizontal Protection Error (HPE), the Horizontal Protection Level (HPL), and the Alert Limit (AL) defined specifically to meet the application requirements. HPL, which serves the purpose of bounding the position errors, is determined using three well-established measurement weighting models, namely elevation, Carrier-to-Noise ratio (CNO), and the hybrid model (which is the product of CNO and elevation), as introduced in Section 2.6.2. It is important to acknowledge that the term 'safety' has a very broad meaning and is much more complex to define at this level. Ensuring safety requires complementary measures, redundant systems, and subsystems (or functions) as means to provide robust

solutions while having the capability of handling the 'faults' that could lead to imminent danger or fatal accidents. For simplicity, in our discussion, the term safety will be used to associate 'potential' risk with the localization system in the case of unbounded position errors that represent HMIs in the Stanford diagram.

The CNO metric has been extensively examined and analyzed in various research studies, wherein a drop of CNO across each channel is regarded as an indication of the existence of interference. To enhance and provide an additional layer of protection, it is anticipated that including this information in the protection level estimation would be highly beneficial, especially in situations where no mitigation measures have been implemented or even if the currently employed mitigation measures are not optimally utilized. Our investigation includes well-known classical weighting models that rely on CNO and (or) elevation information to evaluate the positioning Key Performance Indicators (KPIs) on the Stanford diagram.

Furthermore, in addition to the aforementioned points, Chapter 3 also provided an overview of various types of interference signals discussed in the literature. However, in our investigation, we will specifically focus on two types of signals, namely frequency hopping and chirp interference. These two interference signals possess unique characteristics in terms of how the frequency varies over time. The two signals are expected to challenge the mitigation techniques differently. In our investigation, we will follow the same protocol to analyze the performance of the mitigation techniques against these interference signals. This will be achieved by presenting three cases; the first will be referred to as the "reference case," which will serve as a control scenario without any interference present. The second will be designated as the "interference case," employed to assess and evaluate the impact of the jamming signal. Lastly, the third will be referred to as the "mitigated case," to thoroughly analyze and assess the effectiveness of the employed interference suppression strategy.

The chapter is structured into various sections to discuss the investigations conducted across different phases. In Section 4.2, we will go through the preliminary investigation on the Advanced Interference Mitigation (AIM+) module integrated into the Septentrio receiver. Section 4.3 is dedicated to the experimental protocol, providing specific details about the tools used in the subsequent investigations detailed in this chapter. As we proceed to Section 4.4, we will explore and analyze the Karhunen Loéve Transform (KLT). Furthermore, Section 4.5 offers a comparative study between Adaptive Notch Filter (ANF) and Wavelet Packet Decomposition (WPD). Finally, in Section 5.5, we will wrap up with a comprehensive summary and conclusion of this chapter.

4.2 Interference a matter of concern: How COTS receivers are dealing with interference?

In this study, we have undertaken a preliminary investigation into the existing interference mitigation solutions available in the Commercial Off-The-Shelf (COTS) receiver. The two primary reasons for this inquiry are first to understand whether interference should genuinely be regarded as a matter of concern, especially in the context of safety-critical applications, and secondly, to assess the level of performance offered by the advanced receiver(s). This investigation has been carried out on a Septentrio receiver, which recently integrated an interference mitigation module referred to as Advanced Interference Mitigation (AIM+). The receiver manufacturer claims that the COTS module offers self-

protection against the interfering signals impinging on the GNSS spectrum. Specifically tailored to protect against both narrowband and wideband interferences, making it an attractive option for end users. In the upcoming discussion, we will assess the performance of the receiver against frequency hopping and the chirp. We will provide details of our experimental setup, a description of the interference scenario and subsequently present an analysis and discussion of the results. Lastly, we will summarize our findings from this preliminary investigation.

4.2.1 COTS receiver against frequency hopping

We conducted data acquisition using a Septentrio (AsteRx4) receiver that is connected to a PolaNT (AT1675-29S) antenna placed on the rooftop of our laboratory building. This setup allowed us to obtain a relatively clean signal from a static position. To generate a customized interference scenario, we utilized a MATLAB-based GeGnIUs tool, which has been developed in our laboratory. We specifically configured the GeGnIUs tool to transmit frequency tones through a Universal Software Radio Peripheral (USRP)-2910. The interference signal is combined with the GNSS signal using an RF combiner and then delivered to the Septentrio receiver via a wired connection. Throughout the entire thirty-minute data acquisition period, two tones are transmitted at regular intervals with a slight time delay. During these intervals, the interference source is temporarily removed, allowing the receiver to return to its normal state before the start of the next interval. Similarly, these tones continued to randomly interfere within a 6 MHz range of the GPS L1 band for the entire duration of the data acquisition. Figure 4.1 shows the jamming profile that is used for this investigation.

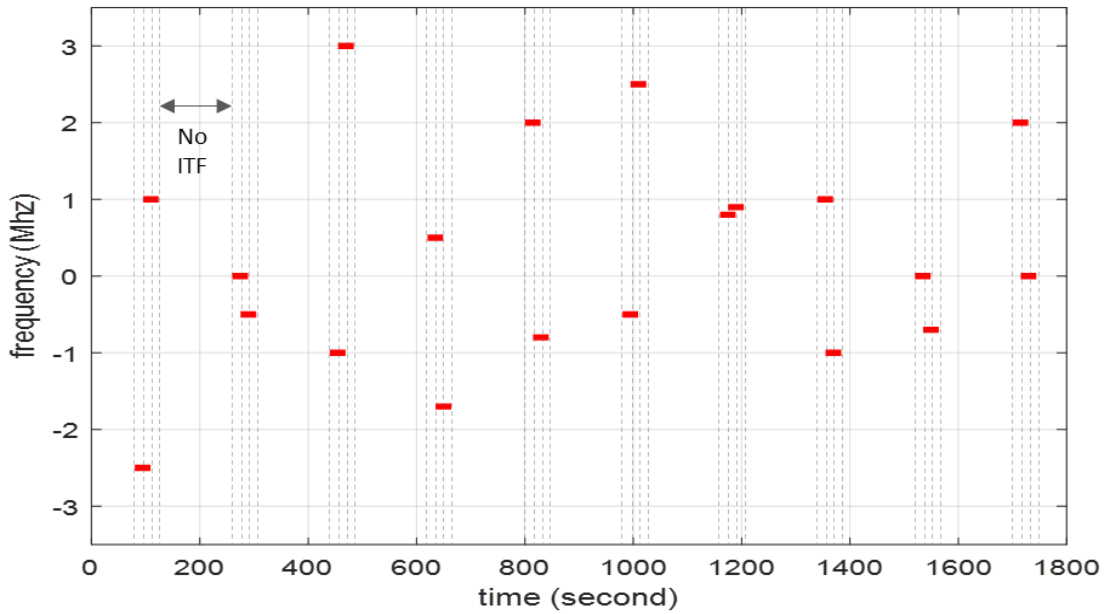

Figure 4.1: Interference profile at the baseband with frequency tones (red) hopping randomly for 30 seconds within ±3 MHz around the GPS L1 frequency. The dashed vertical lines highlight the regions with active interference.

We recorded consecutively three files, each involving the acquisition of GNSS signals: 1) in the absence of an interference signal. 2) in the presence of interference without applying any mitigation technique, and 3) after applying the inbuilt mitigation utility available in the COTS receiver. We activated two notch filters simultaneously, setting them to 'auto' mode to track independently the tones that would appear simultaneously

in the spectrum for a limited duration. Figure 4.2 shows the sky plot depicting the configuration of the visible satellites during the time of acquisition. Now, we will present the results after processing the RINEX files using open-source 'GoGPS' software [112].

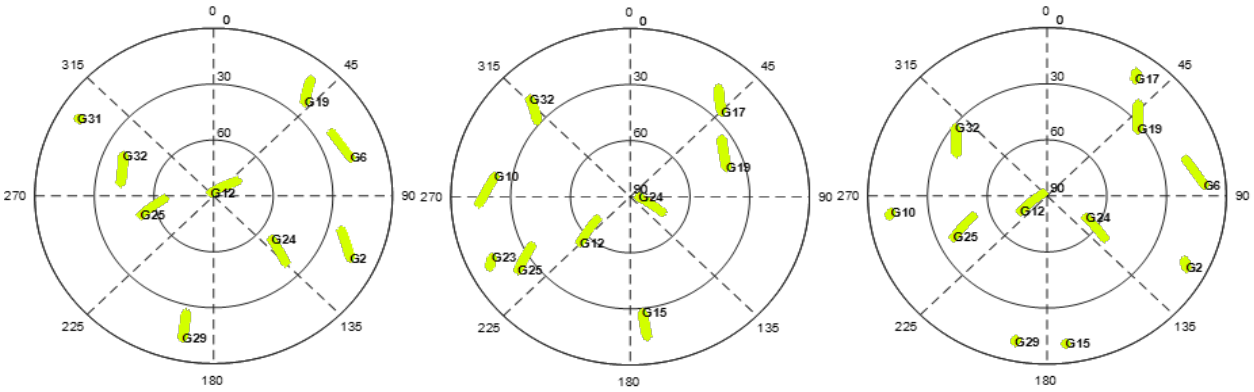

Figure 4.2: Sky plot to show satellite configuration for the three cases: Reference (Right) without interference, interference with no mitigation applied (center), and interference with active mitigation block

4.2.2 Results and Analysis

Figures 4.3 and 4.4 provide clear evidence of the considerable impact of interference on positioning accuracy, emphasizing the importance of implementing an effective mitigation strategy. By examining the Stanford diagram, it can be seen that the errors are exceedingly small in the absence of interference, which appears to be less than 2 meters. Conversely, in cases where interference is present and no mitigation measures have been applied, as expected, there is an increase in the number of points representing errors greater than 10 meters. However, after mitigation, a considerable improvement in accuracy is observed. Unexpectedly, the results show that the weighting models do not significantly affect the positioning accuracy in our case. It is very evident from Figures 4.3 and 4.4 that the choice of weighting scheme has a profound impact on the performance requirements of the localization system, particularly in the three cases that have been presented. Figure 4.3 offers a more comprehensive understanding by taking into consideration the variation of certain parameters such as CNO, elevation, and satellite visibility, which are crucial in estimating performance over time. It is important to note time analysis holds significant importance for the following reasons:

- The three cases under consideration are recorded successively within 2 hours. It is evident from the sky plot presented earlier that the configuration of the satellites has changed over time. It should be noted that the purpose of time analysis is not to draw comparisons between the different cases, as they were recorded at different times. However, it can help in analyzing the impact of weighting schemes on the protection level for each case independently.
- Both the interference case and the mitigation case will also influence the variation of the protection level, and thus, both cases need to be analyzed separately.

In Figures 4.3 and 4.4, the significance of the weighting scheme in the estimation of the protection level can be observed for all three cases. In situations where interference mitigation is not applied, the protection level estimated from the CNO-based weighting scheme closely follows the variation of the CNO measurements, as can be observed in Figure 4.4(c) and (d). Since interference has a direct impact on the CNO resulting in

normal operation, it is reduced to 81.751% with 321 unavailable points, ensuring completely safe positioning without any HMI. However, after the recovery of CNO with the mitigation technique, normal operation increases to 98.333 % with only 30 unavailable points. In general, the CNO model tends to be highly conservative whenever interference or the remnants of interference are present.

The sine-elevation model assigns a higher weight to high-elevation satellites than those at lower elevations. This model does not consider the signal quality, which is crucial in the presence of interference. Without mitigation, the sine-elevation model resulted in a higher percentage of normal operations (93.462 %) compared to the CNO model, but at the expense of 19 HMI points and 4 MI points. However, the model becomes even more conservative due to the lower availability of satellites following the mitigation process, resulting in a decrease in normal operations to 80.722 % with 347 unavailable points. The hybrid model, combining elevation and CNO models, makes it the most conservative choice among other weighting models. The results clearly show that in the case of interference without mitigation, normal operations are reduced to 74.474 % with 449 unavailable points. Similarly, in the case of interference with active mitigation, only 67.611 % of the points are in normal operations, with 583 unavailable points.

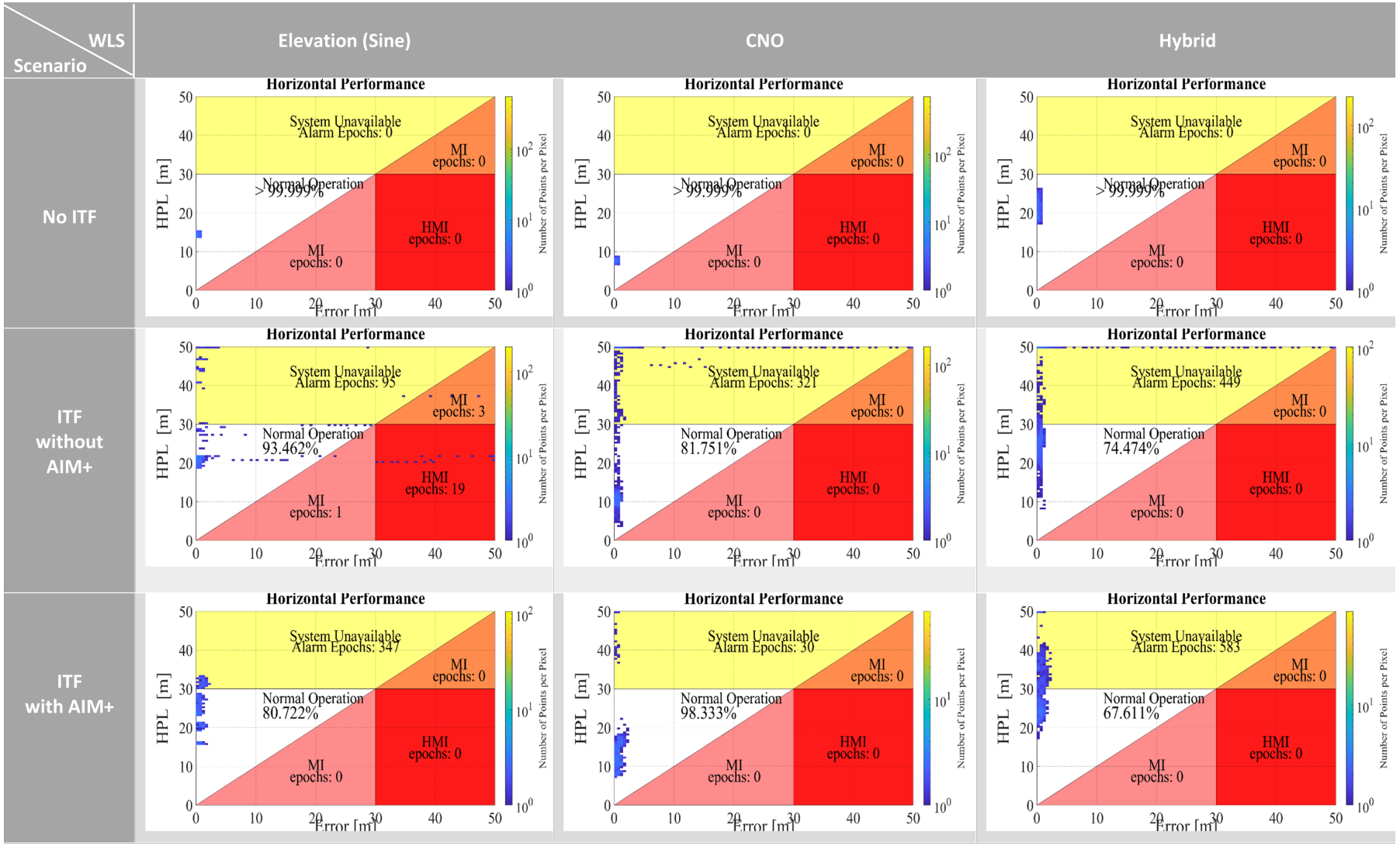

Figure 4.3: Stanford diagram of each weighting scheme representing three cases: in the absence of interference (upper row), ITF but without mitigation (middle row), and ITF and with active mitigation (lower row). Here, AIM+ provided by the Septentrio receiver is applied for mitigation.

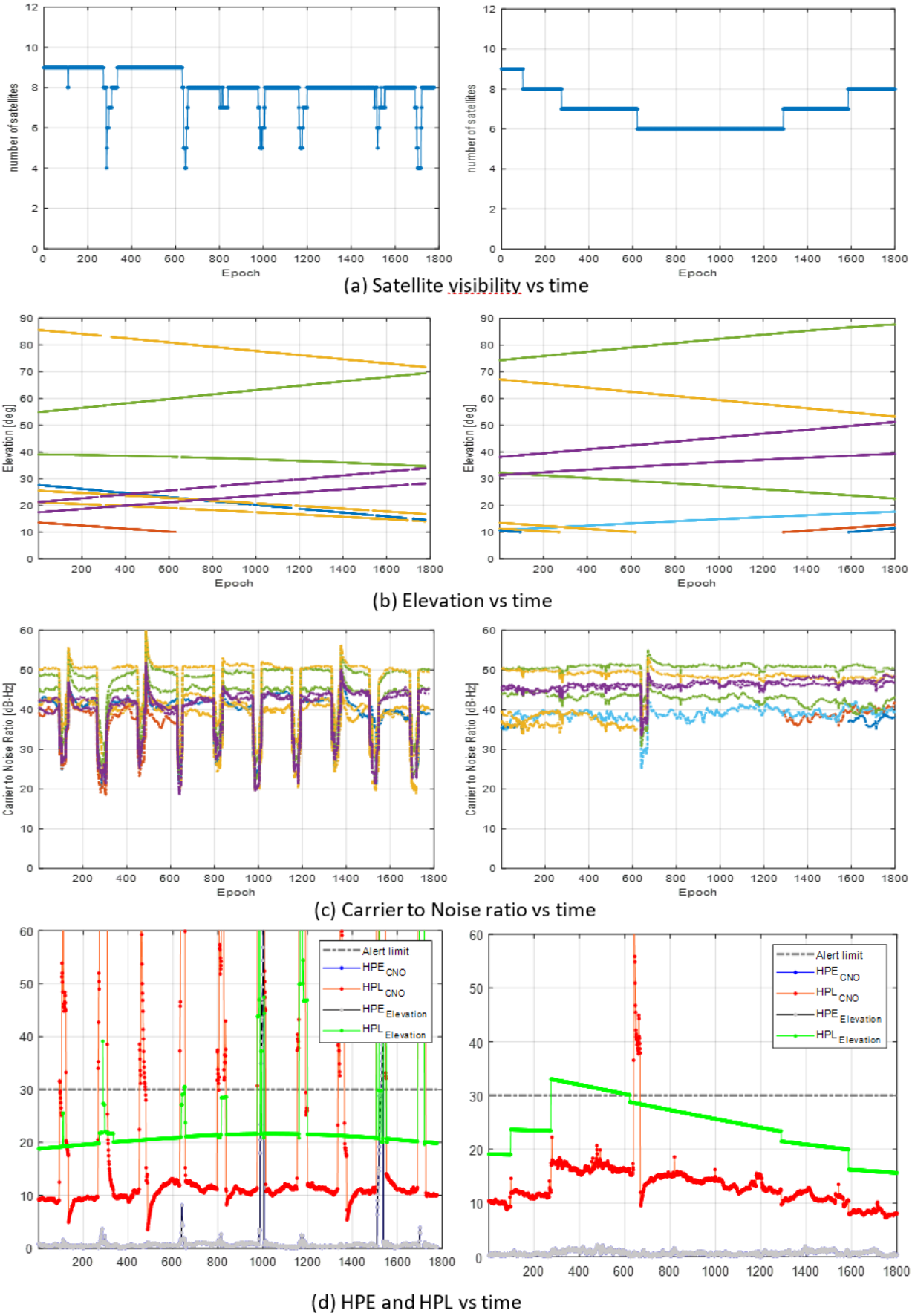

Figure 4.4: The assessment of different parameters (carrier-to-noise ratio, elevation and satellite visibility) contributes to the estimation of the HPE and HPL vs time. The interference case without mitigation (Left) and mitigated case with active AIM+ (right)

4.2.3 COTS receiver against chirp

Similarly, we have undertaken another brief study considering chirp interference, centered around the GPS L1 band with a sweeping frequency of 7 MHz in 50 μsec. Figure 4.5 shows the resultant spectrum of the jamming signal. In this particular scenario, we introduced an interference that lasted for 50 seconds and was applied at two different intervals. Throughout the first interval, the COTS module is deactivated, while during the second interval, the COTS module is activated. A Wideband Interference (WBI) mitigation is employed, as recommended by the receiver manufacturer, to counter the distortions induced by the chirp signal. We will now present the outcomes and discuss the results. Note that we will present only selective results, avoiding repetition of the exhaustive process as previously done for the frequency hopping case, highlighting the issue we specifically aim to address in this dissertation.

Figure 4.5: Power spectrum of the signal after applying chirp interference (bandwidth 5MHz, sweep rate 50 μsec, and J/N power 30 dB)

4.2.4 Results and Analysis

In this section, we will present the results of the previously introduced chirp scenario, taken from the 'SBF analyzer'. The summary of results, as illustrated in Figure 4.6 shows the impact of interference and mitigation on both Carrier-to-Noise ratio (CNO) and Horizontal Protection Level (HPL). It can be observed that the CNO has generally improved subsequently after the mitigation. However, is also evident that the mean value of the Protection Level (PL) has increased from 8.5 m to 26 m. These outcomes resemble the observations made in the frequency hopping case. Despite the receiver's ability to provide a very accurate position after the mitigation, the increase in PL has led to a considerable increase in the number of unavailable instances.

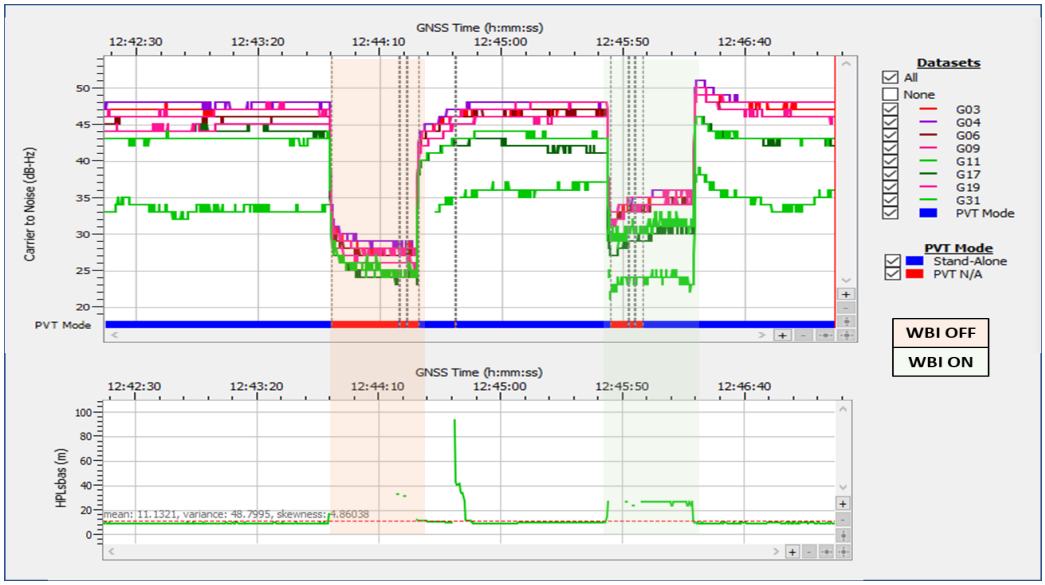

Figure 4.6: CNO of the tracked satellites (Upper panel) and Horizontal Protection Level (HPL) with highlighted regions depicting the interval with an active chirp jammer without mitigation (red) and after activation of the WBI technique in the AIM+ module.

4.2.5 Conclusion on COTS Receiver Performance

We have presented our initial findings on the existing mitigation solutions that are available in the COTS receiver. Although this study is not comprehensive, we could have explored alternative solutions offered by other receiver brands, if any exist. Since we had access to mitigation solutions provided by Septentrio receivers, we conducted this preliminary investigation on it with some realistic scenarios. Note that the purpose of this investigation was not to seek limitations of COTS, the embedded mitigation module in the receiver. Rather, it aimed to assess the performance level of the available solutions in the context of safety-critical applications. Therefore, we employed the mitigation function (tool) as a black box to conduct this investigation against frequency hopping and chirp interference. Undoubtedly, the receiver exhibited exceptional performance for the two presented cases and provided highly accurate positions following the activation of the AIM+ module. As expected, mitigation has a consequent impact on the protection level, resulting in a considerable increase in the unavailable instances. These outcomes have encouraged us to investigate further into this matter to retrieve a performance similar to the nominal situation, wherein the emphasis is on maximizing normal operations while prioritizing the safety of the localization system. This aspect will be further addressed in subsequent investigations.

4.3 Dealing with IQs: Jammer and recording system

From this point forward, our discussion will concentrate on various precorrelation-level signal processing techniques to effectively minimize the influence of the interfering signal. These techniques necessitate the processing of discrete signals, which in our case are the in-phase (I) and quadrature (Q) components, representing the real and imaginary parts of the complex baseband signal. To record the baseband signal, we have employed the Stella NGC Record and Playback (RP) software utility connected to the Universal Software Radio Peripheral (USRP 2954R) from National Instruments. The software interface of the recording tool is depicted in Figure 4.7 which is configured to record the GPS L1(1575.42 MHz) signal at a sampling rate of 15 MSamples/sec and 12 MHz bandwidth using an

8-bit quantization level.

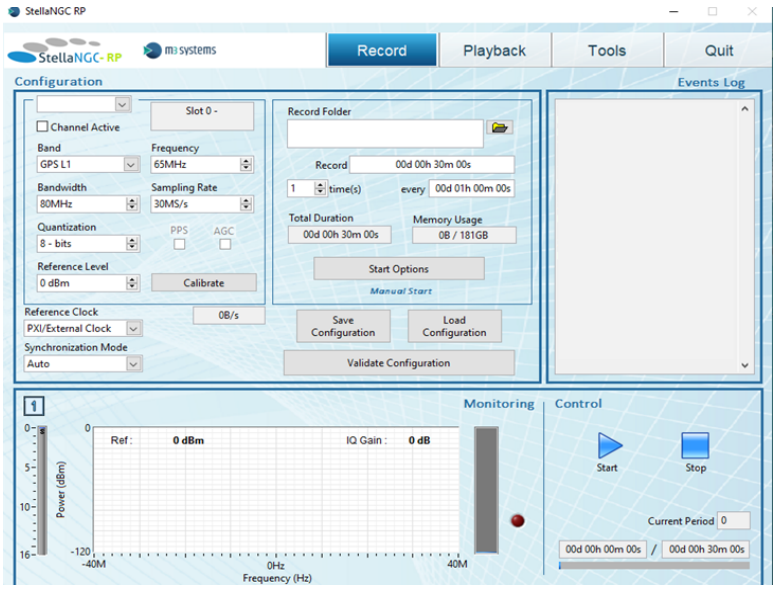

Figure 4.7: Stella NGC Record and Playback software interface for recording baseband signal.

To simulate the interference scenario, we have employed the Matlab-based software tool 'GeGNIUs' developed within our laboratory. This utility offers realistic emulation of various forms of signals, some examples of very common signals are presented in Chapter 3. Additionally, it provides the flexibility to customize the scenario according to the requirements, facilitated by another USRP 2910s for the transmission of the signal.

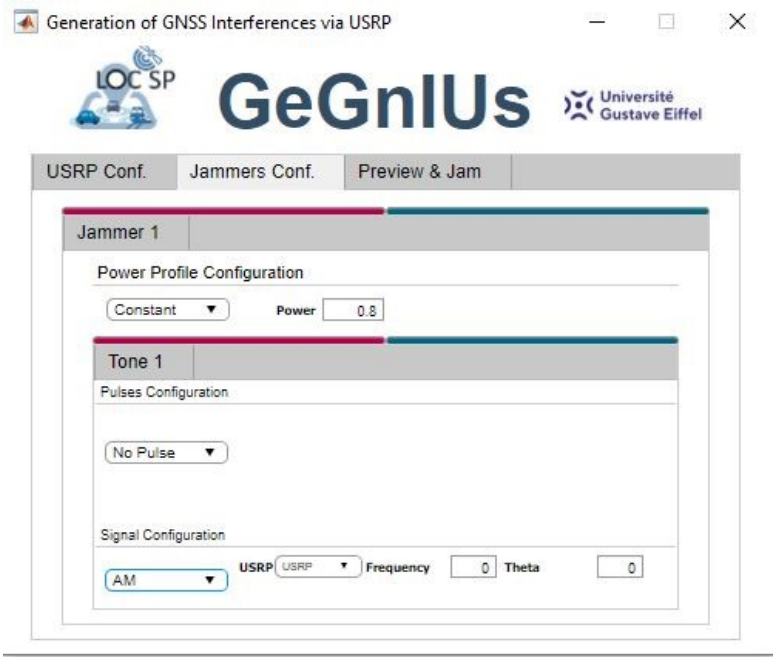

Figure 4.8: The software interface of MATLAB-based Jammer.

4.3.0.1 GNSS signal acquisition and jamming scenario

The acquisition process begins with the recording of a radio frequency signal using an Adsotech ASH11661 antenna, which is mounted on the roof of our university site. The antenna is placed in an open-sky location to receive satellite signals in the best possible conditions, thereby minimizing disturbances induced by the presence of obstacles in the

close vicinity of the antenna. The signal captured by the antenna is combined with the jamming signal through a combiner, which is delivered to the USRP dedicated to recording the signal through a wireless link. The entire acquisition setup is shown in Figure 4.9.

Figure 4.9: GNSS Signal Recording System and MATLAB-based Jammer (Left) connected to an antenna mounted on the roof of the building (Right).

We have prepared two interference scenarios with frequency hopping and linear chirp signals belonging to class I and class II categories, as previously presented in section 3.2.2. The spectrogram of these two interference signals are visually depicted in Figure 4.10, representing time-frequency evolution. The main distinguishing characteristic between the two signals is variations in the frequency pattern and dynamics of the signal. In the case of frequency hopping, the signal frequency is altered randomly and is maintained for a certain duration, whereas in linear chirp, the frequency is continuously modified in a linear pattern, resulting in a relatively higher level of signal dynamics.

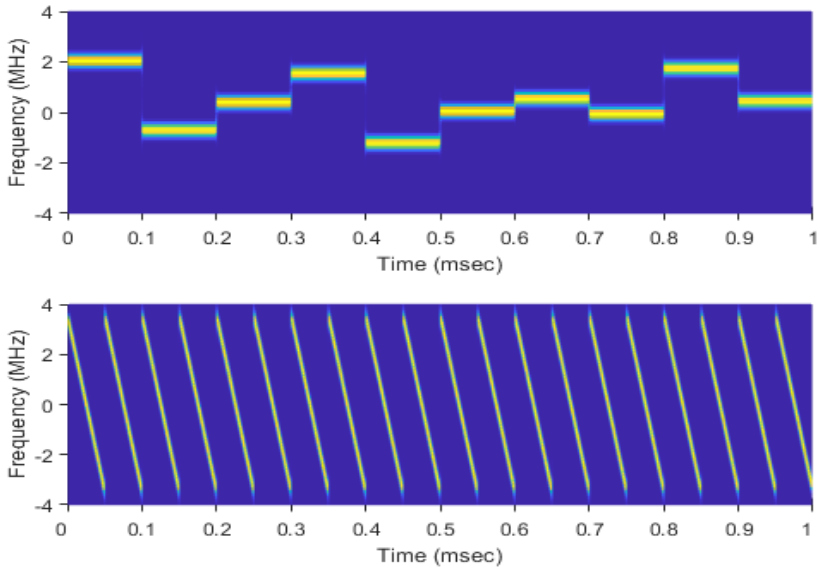

Figure 4.10: spectrogram of the frequency hopping (Upper Panel) and chirp signal (Lower Panel) at the baseband

A more detailed description of the interference used in these cases is provided in Table 4.1. We have recorded a total of eighteen IQ files, with nine files designated for each interference scenario.

To obtain various satellite configurations and visibility, signal acquisition is conducted during three distinct periods throughout the day. Each record lasted for 90 seconds, and the interference signal of 30 seconds was added approximately after 55 seconds.

Table 4.1: Signal Parameters settings for the Recording system and Interference generator

Recording system and jammer signal parameters		
Receiver configuration	Central frequency	GPS L1 (1575.42 MHz)
	Sampling frequency	15 MHz
	Bandwidth	12 MHz
	Quantization	8 bits
Frequency hopping	Frequency pattern	[2.0, -1.5, 0.7, 3, -2.5, 0.0, 1.0, -0.2, 3.4, 0.8 MHz]
	Hopping rate	100 µsec
	Hopping period	1 msec
	Duration	30 sec
Chirp	Bandwidth	7 MHz
	Chirp rate	0.14 MHz/µsec
	Sweep period	50 µsec
	Duration	30 sec

Now, we will undertake a comprehensive view of three state-of-the-art signal processing interference mitigation techniques: Adaptive Notch Filter (ANF), Wavelet Packet Decomposition (WPD), and Karhunen Loéve Transform (KLT). These interference mitigation methods belong to distinct families of techniques and possess different computational requirements, increasing from low to extreme, respectively.

4.4 Subspace domain: Kerhunen Loève Transform (KLT)

The KLT is a highly versatile technique that is applied in various fields such as image compression, feature extraction, noise reduction, and interference mitigation. It belongs to a subspace domain technique that involves the decomposition of the signal in the vector space using orthonormal (or eigen) functions that can be of any form. The projection of the received signal within the eigenfunction domain allows the identification and isolation of interference components from the noise components, which can be performed with the following steps:

- **Computation of autocorrelation**: The first step involves the computation of signal autocorrelation. The autocorrelation function measures the similarity of the received signal to the delayed version of itself, which can help to determine the underlying patterns and structure of the signal. The autocorrelation of the received signal $x[n]$ is given as:

$$R_x[n] = \mathbb{E}[x[\tau] \cdot x[\tau - n]] \tag{4.1}$$

- **Calculation of Toeplitz matrix:** The Toeplitz matrix is computed from N samples of the autocorrelation $R_x[n]$ which can be written as:

$$R_{\text{Toeplitz}} = \begin{bmatrix} Rx[0] & Rx[1] & \dots & Rx[N] \\ Rx[1] & Rx[0] & & Rx[N-1] \\ \vdots & \vdots & \ddots & \vdots \\ Rx[N] & \cdots & \cdots & Rx[0] \end{bmatrix} \tag{4.2}$$

- **Eigenvalue decomposition:** The decomposition is accomplished by determining the eigenvalues λ_i and the eigenvectors Φ_i from the Toeplitz matrix.
- **Sort eigenvectors:** The eigenvectors are arranged in descending order according to their corresponding eigenvalues. This organization arranges them in sequential order of their significance, with the most dominant (or principal) components followed by the least dominant components.
- **Interference detection:** It involves careful examination of the transformed signal components to identify the principal components that exhibit considerable deviation from the nominal (or interference-free) signal characteristics when interference is present.
- **Signal reconstruction:** The components that represent interference are subsequently eliminated, and the signal is then reconstructed through the multiplication of the coefficients with the remaining interference-free components.

Now, the steps for performing interference suppression with KLT have been presented. In 4.4.1, we will present the discussion on the implementation, applying it to the real GNSS IQ dataset. There are very limited implementation examples available in the literature where KLT has been employed as a countermeasure to suppress interference, particularly in the GNSS application. In [105], the mitigation performance is mainly presented at the signal level by comparing the frequency spectrum of the interfered and filtered signals. The authors in [113] conducted an extensive study and also analyzed the performance at the positioning accuracy level. The originality of this study is that we will analyze performance at multiple receiver processing stages, ultimately presenting the positioning KPIs for various values of k (which represents k onwards samples considered in the signal reconstruction with k as a first sample index).

4.4.1 Results and Analysis

One crucial aspect of the KLT analysis is the selection of the number of samples, which is directly related to the decomposition level to be achieved. Moreover, the selection is also dependent on the characteristics of the signal being analyzed. Increasing the number of samples could be beneficial in capturing more accurate statistical properties and relationships in the data, but it comes at the expense of longer computation time. Due to its demanding computational requirements, in the literature, the KLT method is only considered for post-processing purposes. In our analysis, we have employed KLT to suppress the frequency hopping scenario presented in section 4.3. Following some extensive testing and experimentation, we have selected 500 samples for the signal decomposition as a reasonable compromise between the achievable performance and the computation time. The eigenvalues, which are illustrated in Figure 4.11, are obtained from the KLT decomposition of both the interference-free GPS L1 signal and the interfered signal. In the absence of interference, the eigenvalues (as depicted in blue) have a very flat trend with nearly the same magnitude. However, it is evident that in the presence of interference, there are very few eigenvalues (as depicted in red) that possess relatively higher magnitudes compared to the others.

Now the question arises concerning the number of samples that should be considered to obtain the best possible separation between the interference and the clean GNSS signal components. From Figure 4.11, it is not very evident where the threshold should be set. It seems that the most suitable option would be either at the point of intersection of two lines, which is around k = 20, or somewhere between k = 40 and 50, from where the eigenvalues (as depicted in red) almost have constant magnitude. Moreover, in the

borderline case, the choice of k involves a compromise between the suppression level and preserving the useful signal components. To demonstrate the influence of k on the mitigation performance, we have selected three values with k = 20, 80, and 140.

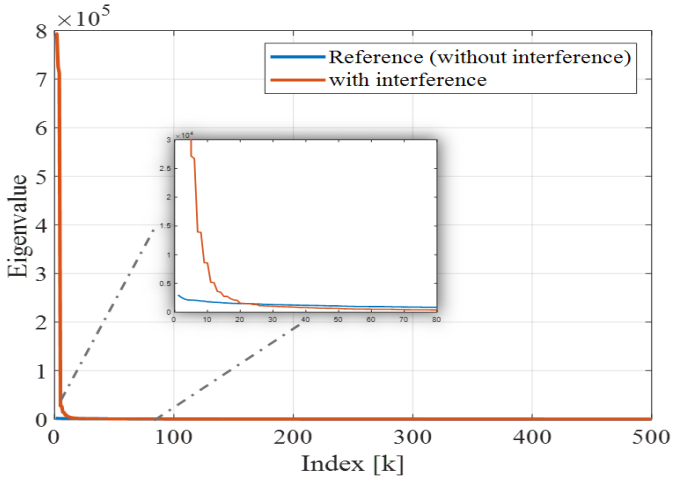

Figure 4.11: KLT decomposition of GPS L1 signal in interference-free conditions and the presence of a frequency-hopping signal.

The power spectrum, as shown in Figures 4.12a and 4.12b, presents the comparison of three cases with different values of k. The power spectrum is estimated after discarding initial k-1 components from a total of 500 during the reconstruction process. In each of the three k values, the elimination of the principal component has significantly attenuated the interference signal. It is evident that for the first choice (k = 20), the residual interference remains in the signal, while for the second choice (k = 80), the spectrum appears to be very clean. Conversely, the third choice (k = 140) seems to have excessively attenuated the useful signal.

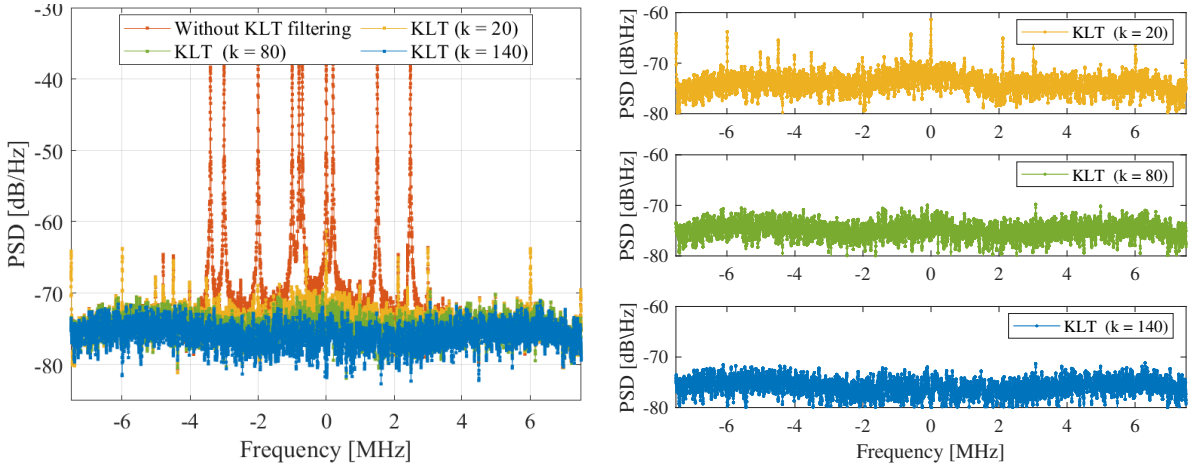

(a) (b)

Figure 4.12: Power spectrum before and after KLT filtering for k = 20, 80, and 140.

The Cross Ambiguity Function depicted in Figure 4.13 represents the signal search space associated with PRN 29. It is evident that, after the KLT mitigation, the signal peak is retrieved back in all three cases, each with a distinct value of k, as shown in Figure 4.13(c), (d), and (e). A comparison between Figure 4.13 (c) and (d) shows that when k = 20, the noise floor around the correlation peak appears to be relatively noisier than with k = 80. Furthermore, by removing more components in the case of k = 140, the

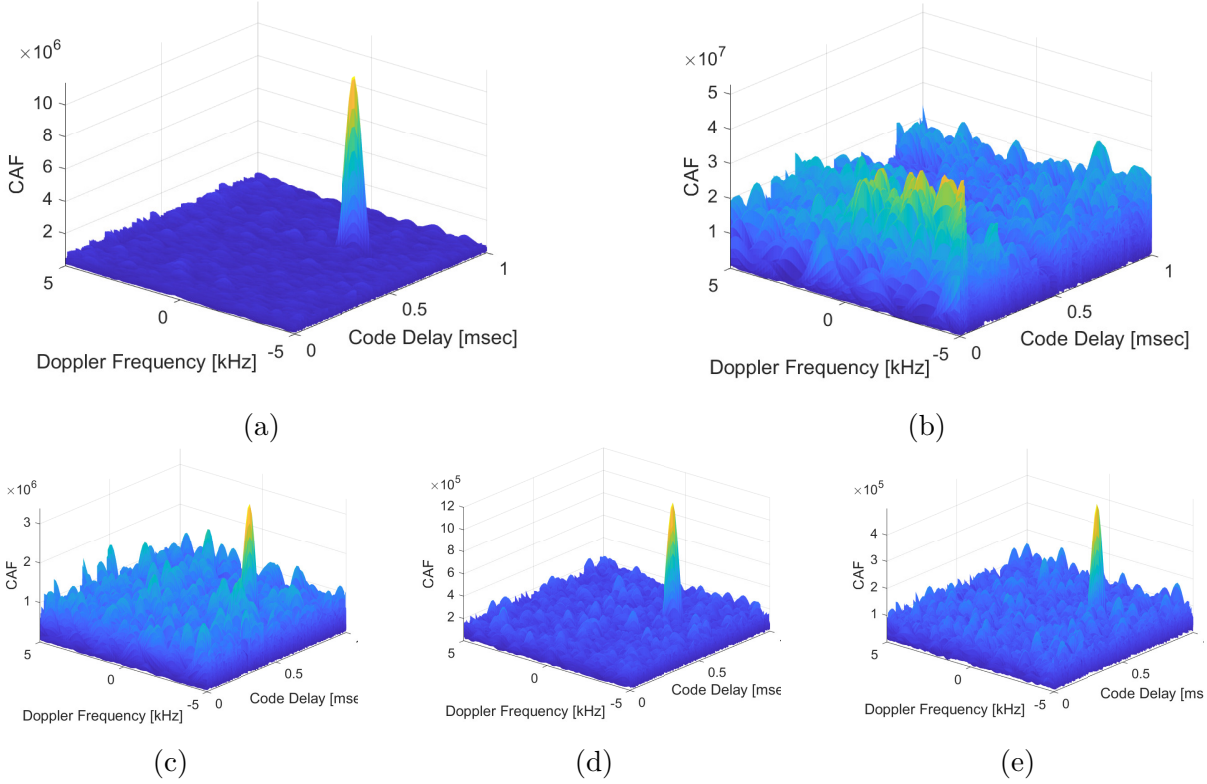

Figure 4.13: CAF representing signal search space of PRN# 29 a) nominal conditions, in the presence of interference b) before KLT mitigation and after KLT mitigation discarding k-1 components with c) k = 20, d) k = 80, and e) k = 140.

correlation peak has reduced significantly, thereby suppressing unnecessarily the useful content of the signal.

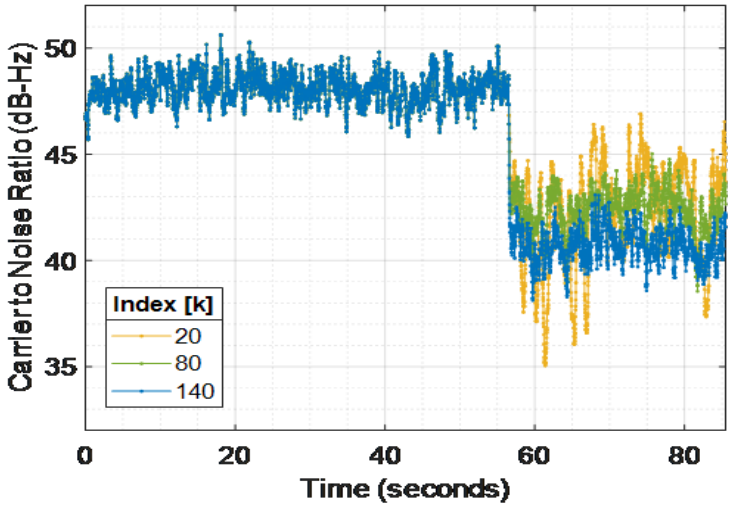

Figure 4.14: Carrier to noise ratio (CNO) of PRN 29 after KLT filtering for different values of k sample index

The Carrier-to-Noise ratio (CNO) metric, which indicates the quality of the tracked signal, is illustrated in Figure 4.14. A similar trend can be observed when comparing the CNO associated with PRN #29, considering three distinct values of k. It should be noted that in this scenario, the interference emerges at approximately 55 seconds. It is evident that with the implementation of KLT mitigation over an entire 30-second duration of jamming, the CNO shows considerable fluctuations, particularly when k is set to 20.

The CNO estimation appears to be relatively stable when k is set to 80. The removal of additional components in the case when k is set to 140 leads to a few dB drop in CNO.

Now, we will analyze Key Performance Indicators (KPIs) related to the position by presenting them on the Stanford diagram. In this particular case, to get a reasonable number of points on the Stanford diagram, we have computed the position at a rate of 100 Hz. We have considered three measurement weighting schemes: a) elevation only, b) Carrier-to-Noise ratio (CNO), and a hybrid model. These models are employed for the estimation of the Weighted Least Square (WLS) solution and also to estimate the protection level. Figure 4.15 presents the Stanford diagram for the 'reference case', including all the instances before the occurrence of interference.

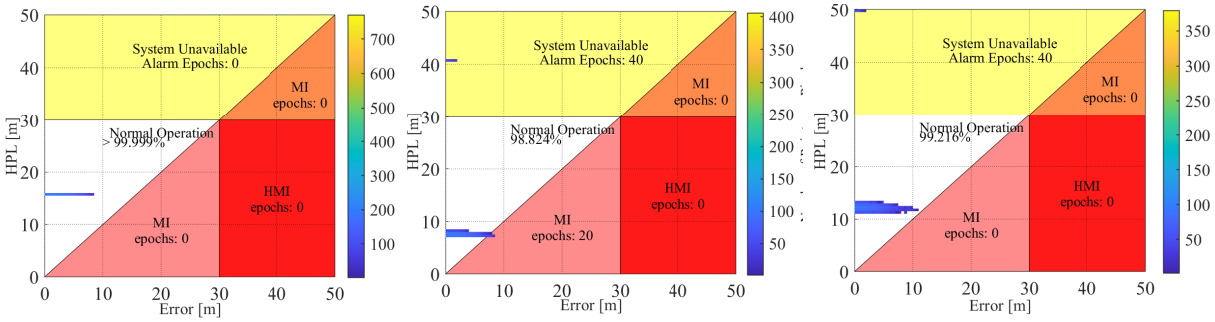

(a) (b) (c)

Figure 4.15: Stanford diagram representing nominal (interference-free) conditions with different weighting models: a) elevation (left), b) carrier-to-noise ratio CNO (middle) and c) Hybrid model (right)

In the absence of interference, the three weighting models demonstrated very similar performance, achieving approximately 99% of normal operations. The normal operation suggests the system is available, and the position errors are well-bounded. When comparing the models, it can be observed that the elevation model effectively constrained the position errors, whereas the CNO has 20 MI instances, indicating unbounded errors without any potential risk (PL < PE < AL) and 40 unavailable instances where the protection level over bounds the positioning errors and also exceeds the alert limit (PE < AL < PL). The hybrid model, on the other hand, has only 40 unavailable instances.

Figure 4.16 illustrates positioning performance in the presence of interference without the implementation of any mitigation strategy. Note that approximately 64% of the instances correspond to epochs free from interference, while the remaining 36% of instances indicate points that are subjected to interference. A considerably large number of points with position errors exceeding 30 meters show that interference significantly degrades positioning accuracy. In this case, using CNO information somehow attempts to increase the protection level, thereby making the system unavailable, although not sufficient enough to completely isolate the position points affected by interference. In all three models, the majority of interference instances are present in the HMI, representing unbounded position errors exceeding the AL. This indicates that interference, when not mitigated, poses a potential risk to the system, which could result in a fatal accident if not timely warned.

The positioning performance after the implementation of KLT-based mitigation is presented in Figure 4.17 for three distinct values of k. In each case, the application of KLT filtering seems to be very effective in improving normal operations. The importance of k, which had not been very apparent previously at the signal level, now becomes distinctly evident at the Stanford level. When k is set to 20, a portion of the dominant components is discarded, still resulting in a higher number of HMI instances due to the presence of residual interference. However, after the removal of some additional components, the mitigation technique showed significant improvement. The optimal threshold appears to be

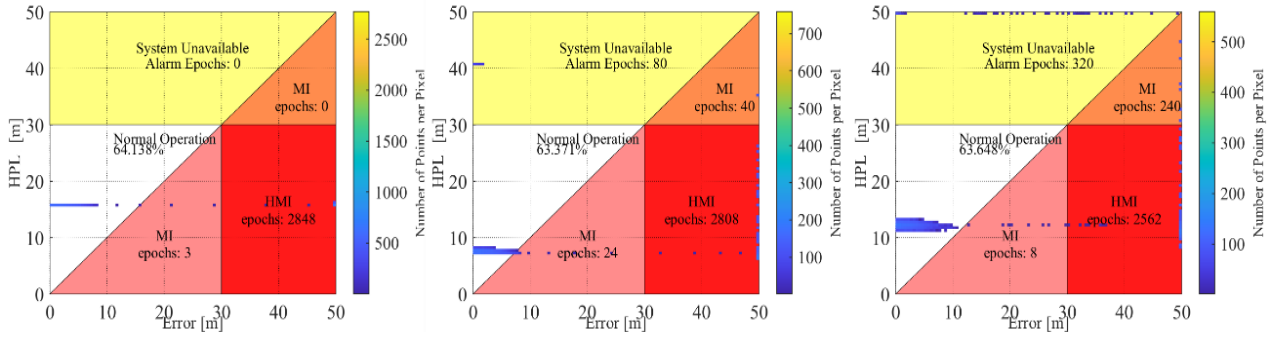

Figure 4.16: Stanford diagram representing the interference case without any mitigation countermeasure with different weighting models: elevation (left), carrier-to-noise ratio CNO (middle), and Hybrid model (right)

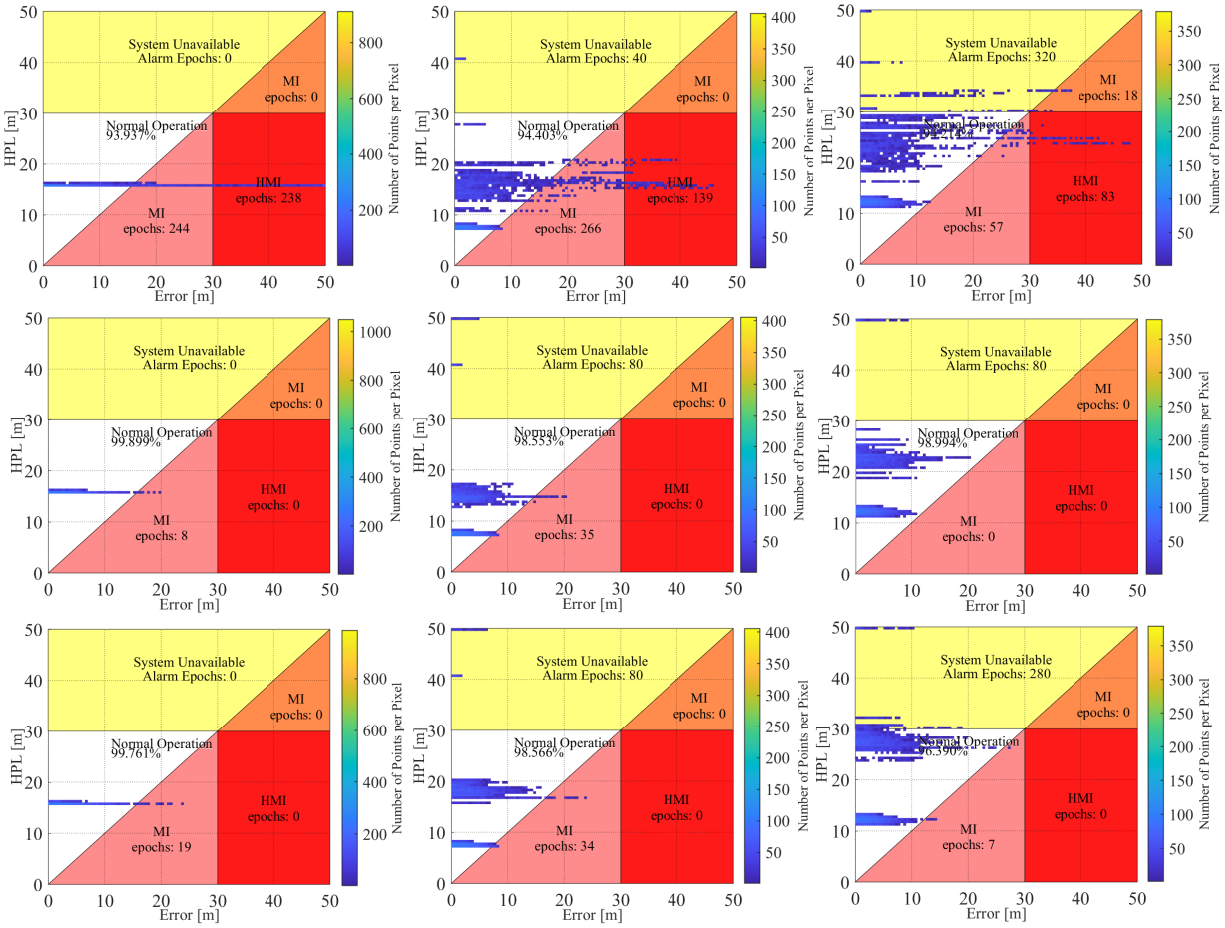

Figure 4.17: Stanford diagram after KLT mitigation for k = 20 (upper panel), 80 (middle panel), and 140 (bottom panel) with different weighting models: elevation (left), carrier-to-noise ratio CNO (middle), and Hybrid model (right)

around 80, which almost restores the performance to a level similar to the reference case. The elevation model maximizes the nominal operation ≈ 99 % with 8 MI instances. As the mitigation process leads to a decrease in CNO compared to the nominal case, its inclusion in the estimation of measurement uncertainty causes an increase in the protection level, as evidenced in CNO and the hybrid model. Further removal of additional components beyond 80 seems to attenuate the useful signal and result in a further increase in the protection level. These effects are more obvious in the case of the hybrid model, leading to an increase in the unavailability of 280 instances and 7 MI instances.

4.4.2 Conclusion on KLT Performance

The implementation of the Karhunen Loéve Transform (KLT) as an interference countermeasure has demonstrated substantial potential. It has shown very promising results against the frequency hopping signal, notable in the retrieval of the positioning Key Performance Indicators (KPIs), as observed through the Stanford diagram. Nonetheless, a significant challenge remains is the substantial computational resources associated with this technique. The process involves the selection of an appropriate number of samples for the desired decomposition level, a choice that depends on the characteristics of the signal being analyzed. Furthermore, fine-tuning the threshold value to exclude principal components representing interference signals contributes to the computational complexity. In our specific implementation, a 30-second interfered signal with a 15 MHz sampling rate required approximately 40 hours of processing time, with the available resources at our disposal. This extensive computational demand underscores the impracticality of this technique in real-world applications. Consequently, we have opted not to continue any further investigations with the KLT method within the scope of this work.

As a next step, we will present a comparative study exploring alternative solutions that offer substantially lower computational requirements. This investigation aims to identify more practical and effective mitigation solutions, with a particular emphasis on reduced computational complexity to better suit real-world applications.

4.5 Notch Filtering versus Wavelet Transform, an Experimental Analysis

In this section, we will first provide a discussion on signal analysis methodology that utilizes digital filters to implement the Discrete Wavelet Transform (DWT). This method involves the decomposition of the signal into smaller packets, the process commonly referred to as Discrete Wavelet Packet Decomposition (DWPD). The primary purpose of signal analysis methodology is to the identification of interference components that can subsequently be eliminated during the mitigation process. Following this, we will present an Adaptive Notch Filter (ANF). The technique involves the utilization of a notch filter together with an adaptation module, which serves the purpose of tracking and suppressing the interfering signal.

4.5.1 Wavelet Packet Decomposition (WPD)

The realization of Discrete Wavelet Transform (DWT) equivalent implementation can be accomplished by employing wavelet-based digital filters [3]. The process of signal decomposition is mainly realized using the frequency scaling process, which allows analysis of the frequency component of the signal at different scales, leading to a multi-resolution signal analysis. The decomposition process involves dividing the signal into low-frequency and high-frequency components after passing it through lowpass and highpass filters. These filters possess equal bandwidth, equal to half of the input signal bandwidth. The lowpass filtering corresponds to an averaging operation, which extracts the coarse approximation of the signal. On the other hand, highpass filtering corresponds to a differentiation operation, which extracts the detailed information of the signal. According to [114], the filter outputs following the first level decomposition can be mathematically expressed as:

$$y_L[n] = \sum_k x[k] \cdot g[2n - k] \tag{4.3}$$

$$y_H[n] = \sum_k x[k] \cdot h[2n - k] \tag{4.4}$$

Here, $y_L[n]$ and $y_H[n]$ denote the outputs of the lowpass and highpass filters respectively. The impulse response of the scaling (or highpass filter) and the wavelet (or lowpass filter) functions is represented by $h[n]$ and $g[n]$ respectively. The scales are altered in dyadic order, with the factor of 2 indicating the scaling operation for the first level decomposition ($2^k = 2 \mid k = 1$). The impulse response of the wavelet function $g[n]$ can be expressed in terms of the scaling function $h[n]$ as:

$$g[n] = (-1)^n h[2k + 1 - n] \tag{4.5}$$

These pair of filters, denoted as $g[n]$ and $h[n]$ constitute the Quadrature Mirror Filter (QMF) pair which implies that each filter can be represented as a mirrored version of the other filter. The filter pair can be written interchangeably by mirror reflection of each other with an additional inversion sign at the odd indices. The visual representation of the impulse response and frequency response of the 'Symlet' wavelet function is shown in Figure 4.18.

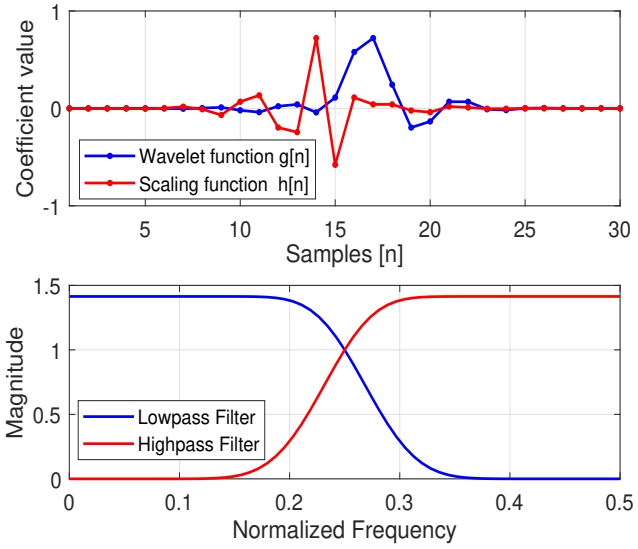

Figure 4.18: A quadrature mirror filter pairs the Symlet wavelet function (N = 15 -filter length) with impulse response (upper panel) and frequency response (lower panel).

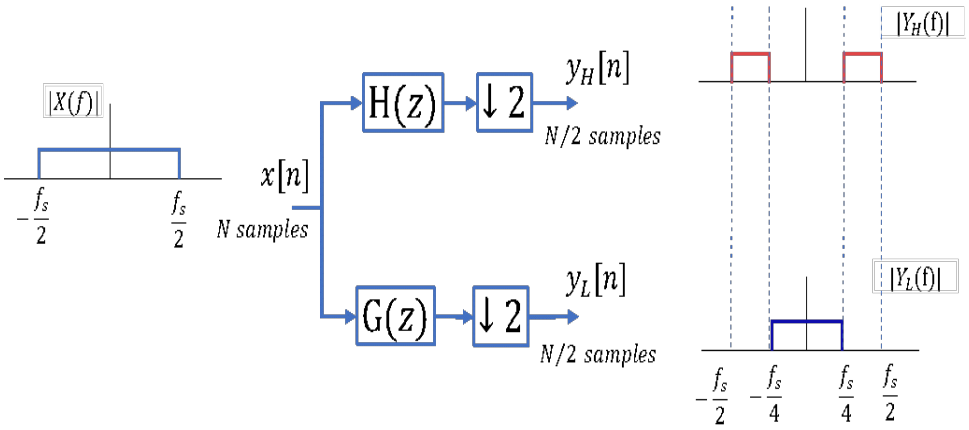

Figure 4.19: Signal decomposition with DWT using lowpass and highpass filters.

In a wavelet decomposition, the first branch consists of a pair of lowpass and highpass filters followed by a subsampling process, as illustrated in Figure 4.19. The subsampler unit downsamples the signal by a factor of 2, eliminating alternate samples from the filtered signal to reduce the sample redundancy. Consequently, the sampling interval of the output signal thereby becomes twice the input signal sampling interval, leading to a decrease in the time resolution by half while simultaneously doubling the frequency resolution (as the bandwidth is halved). The 3-level decomposition stages using the wavelet transform are illustrated in Figure 4.20. In each stage, the signal is further decomposed through the expansion of the approximation branch, wherein the same process of signal division is repeated on a different scale using a lowpass and highpass filter. This provides a multi-resolution signal analysis obtained through the processing of input signals with non-uniform filters. Figure 4.21 shows the frequency response of non-uniform filters from each decomposition level, obtained by dyadic scaling of the 'Symlet' wavelet function.

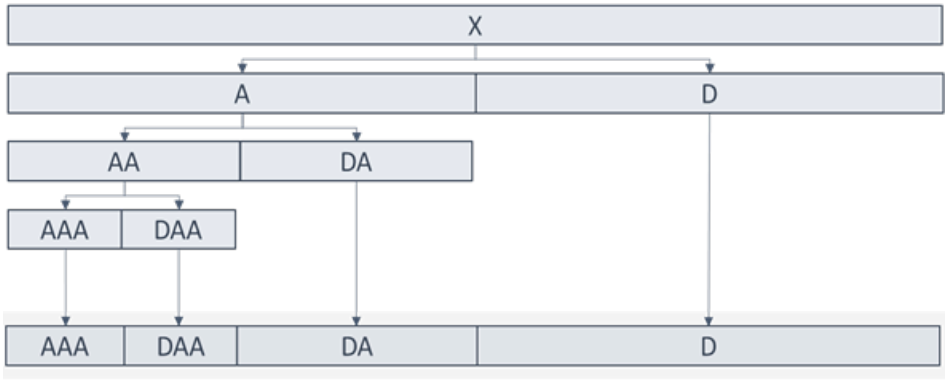

Figure 4.20: A three-level discrete wavelet decomposition (dwt); approximation (a) and detail (d) block represent the lowpass and highpass filtering and the subsampling operation

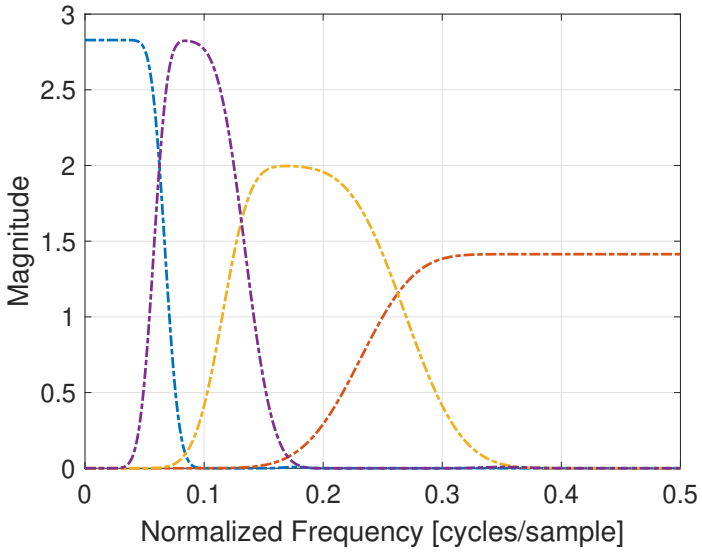

Figure 4.21: Non-uniform frequency response of 'Symlet' wavelet functions

The Wavelet Packet Decomposition (WPD) can be realized similarly to the Wavelet Transform (WT). In WPD, the detailed branch is additionally expanded, leading to the formation of a tree-like structure. This particular process gives rise to several additional wavelet packets after passing the signal through a uniform wavelet filter bank. Each decomposition stage generates 2^N wavelet packets, representing a specific portion of the input signal frequency, with N denoting the decomposition level. Figure 4.22 illustrates

a 3-level signal decomposition using WPD, where the input signal is decomposed into 8 packets in the final stage, each representing different frequency components of the signal.

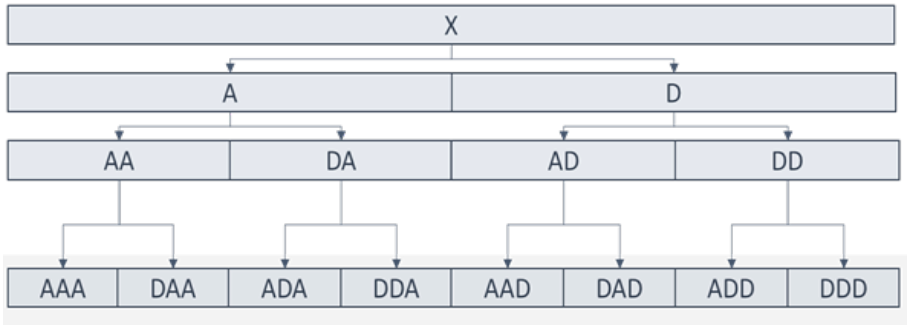

Figure 4.22: A three-level discrete Wavelet Packet Decomposition (WPD) with approximation and detail blocks representing lowpass and highpass filtering respectively, and subsampling operation

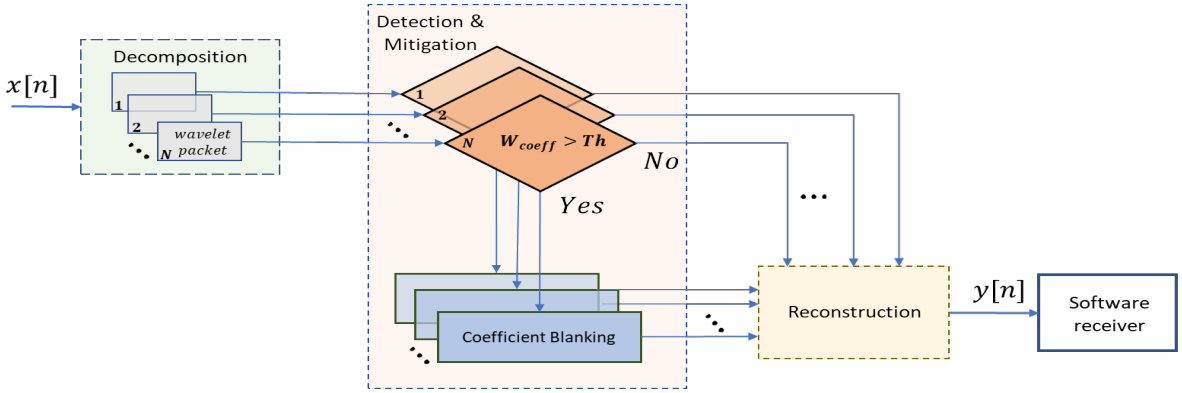

Figure 4.23: Several stages in WPD-based mitigation

The suppression of interference signal with WPD requires a four-step procedure that includes decomposition, detection, mitigation, and reconstruction. The explanation of each phase in the mitigation process, as depicted in Figure 4.23 is as follows:

Step 1: Decomposition

In the decomposition stage, the signal containing interference is passed through a uniform filter bank. This results in the decomposition of the signal into constituent frequency components, to obtain an equivalent time-scale representation. The effectiveness of the technique depends on the number of decomposition stages. A higher decomposition level is better for characterizing various frequency components present in the signal. However, it may also lead to an aliased response from the filter [6]. Here we have considered a 5-level decomposition as a reasonable compromise for the mitigation of the interference signal while simultaneously constraining the processing burden.

Step 2: Detection

The detection phase involves the comparison of the wavelet coefficients within each packet to corresponding threshold values, representing coefficients of the interference-free signal. These threshold values are determined empirically before the detection process, wherein the standard deviation is computed for each scale. The distribution of coefficients (as an interquartile range) of the interference-free signal is illustrated in Figure 4.24, with a threshold (represented by a black line) indicating the 3-sigma value of that particular

scale. The presence of the interference signal is identified when the coefficient value exceeds the threshold value, this will be detailed in the results section.

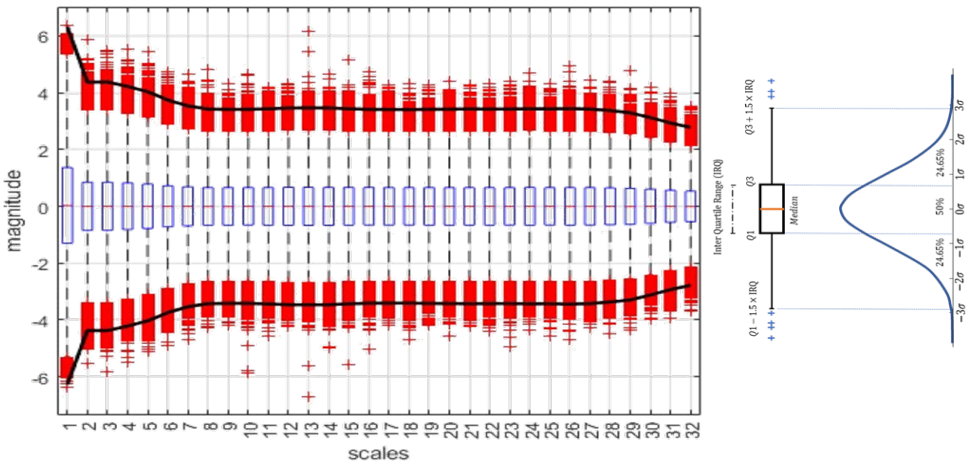

Figure 4.24: Wavelet coefficient distribution in interference-free conditions

Step 3: Mitigation

Once the interference components have been identified, the next step involves the removal of the interference components. This is accomplished through the coefficient blanking process, whereby the interference components are suppressed by assigning zero to the coefficient value when the detection flag is raised. Consequently, the elimination of all the coefficient values exceeding the detection threshold would remove all additional energy induced by the interfering signal.

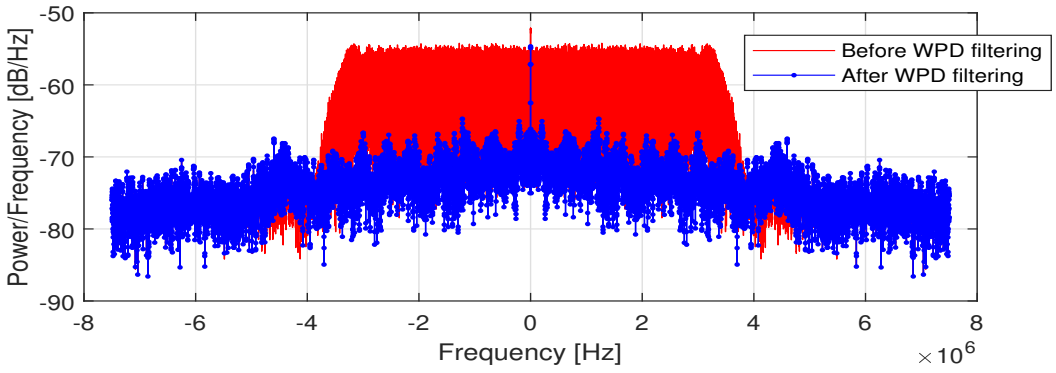

Figure 4.25: Spectrum of the signal before and after mitigation of chirp interference with WPD filtering

Step 4: Reconstruction

Finally, the signal is reconstructed using the inverse wavelet transform by passing the decomposed signal through reconstruction filters and followed by up sampling process. The spectrum, as shown in Figure 4.25, illustrates the presence of a chirp signal (depicted in red), covering a wide frequency range and the frequency spectrum following the implementation of WPD filtering (depicted in blue).

4.5.2 Adaptive Notch Filter (ANF)

Adaptive Notch Filter (ANF) is a widely investigated technique against Frequency Modulated Continuous Wave (FMCW), also referred to as chirp signal. The ANF can be

seen as an extension of the classical Notch Filter with an additional integrated adaptive module. Its main purpose is to continuously track and attenuate the frequency of the unwanted signal, which may change over time. The transfer function of a single pole IIR notch filter can be written as:

$$H(z) = \frac{1 - z_0[n]z^{-1}}{1 - k_\alpha z_0[n]z^{-1}} \tag{4.6}$$

where k_α represents the pole contraction factor that controls the notch bandwidth, and $z_0[n]$ is the filter zero that determines the position of the notch in the complex plane. The transfer function in (Eq. 4.6) can be written separately into two components: the numerator signifies the Moving Average (MA) function and the denominator signifies the Auto-Regressive (AR) function. The resulting output from the MA and AR block can be written as:

$$y[n] = x_r[n] - z_0[n-1]x_r[n-1] \tag{4.7}$$

The value of z_0 is constrained to move on the unit circle of the complex plane and the relation between notch frequency and the transfer function zero is given as:

$$z_0[n] = a_0 e^{j2\pi \widehat{f}_0 T_s} \tag{4.8}$$

where $\widehat{f}_0$ is the instantaneous frequency of the filter, a_0 is the magnitude of the complex estimate $z_0[n]$ that defines the depth of the notch and $T_s = \frac{1}{f_s}$ is the sampling interval. The 3-dB bandwidth in terms of pole contraction factor can be estimated as:

$$B_{3\text{dB}} \approx (1 - k_\alpha) f_s \frac{\pi}{10} \tag{4.9}$$

The notch bandwidth is typically kept narrow to target a very specific portion of the spectrum to preserve at most the useful content of the signal. The ensure stable operation, the pole contraction factor is typically selected in the range between 0 and 1. Eq. 4.9 indicates that the width of the notch gets increasingly narrower as k_α approaches 1. The adaptive block drives the position of the notch, moving z_0 in the complex plane until it converges to the interference frequency. This convergence is achieved using a Least Mean Square (LMS) based gradient descent algorithm, which minimizes the cost function to estimate the value of z_0 at each sample instance.

$$z_0[n] = z_0[n-1] - \mu[n] g\left(J[n]\right) \tag{4.10}$$

where $g(.)$ represents the stochastic gradient of the cost function $J[n]$ and $\mu[n]$ is the normalized algorithm step. The cost function can be minimized by either minimizing energy at the output of the notch filter (or the moving average block) or by minimizing energy at the output of the auto-regressive block. There are numerous adaptation approaches presented in the literature [82][115][116]. We have adopted the adaptation approach proposed in [82]. This approach involves the minimization of instantaneous energy at the filter output $y[n]$. The stochastic gradient of the cost function can thus be expressed as:

$$g(J[n]) = \frac{\partial[|y[n]|^2]}{\partial z_0} \tag{4.11}$$

By solving the partial derivative with respect to complex pole z_0, the Eq 4.11 can be written as:

$$g\left(J[n]\right) = y[n] \cdot x_r^*[n-1] \tag{4.12}$$

where (*) denotes the complex conjugate. The normalized step can be written as:

$$\mu[n] = \frac{\delta}{E|x_r[n]|^2} \tag{4.13}$$

where $\{E|x_r[n]|^2\}$ is the power at the output of the Auto-Regressive block and δ represents the adaptation step of LMS algorithm that controls the algorithm convergence.

Now that the two techniques have been presented, Section 4.5.3 will present their application on a combination of real GNSS signals with simulated interference for performance evaluation.

4.5.3 Results and Analysis

In this particular section, we will present a comprehensive discussion of our investigation findings for the scenarios previously presented in Section 4.2. It involves a thorough evaluation of performance across multiple signal-processing stages. Note that these results are generated after processing the signal IQs using an open-source software receiver [117], which will ultimately lead to the assessment of positioning Key Performance Indicators (KPIs) using the Stanford diagram.

- ***Interference Identification and Mitigation***

Figure 4.26 shows the frequency estimated by the adaptive notch filter in the presence of frequency hopping (left) and chirp (right) signals. As mentioned earlier, ANF is a parametric technique, and its performance depends on the proper selection of the filter parameters. In this case, an adaptation step of 0.05 and a pole contraction factor of 0.8 are used for both signals, within the recommended range. Using these parameters, ANF appears to closely track the interference frequencies in comparison to the scenarios represented in Figure 4.10. Nevertheless, the adaptation step appears to be the cause of oscillations around the slowly varying interference frequency in the case of frequency hopping.

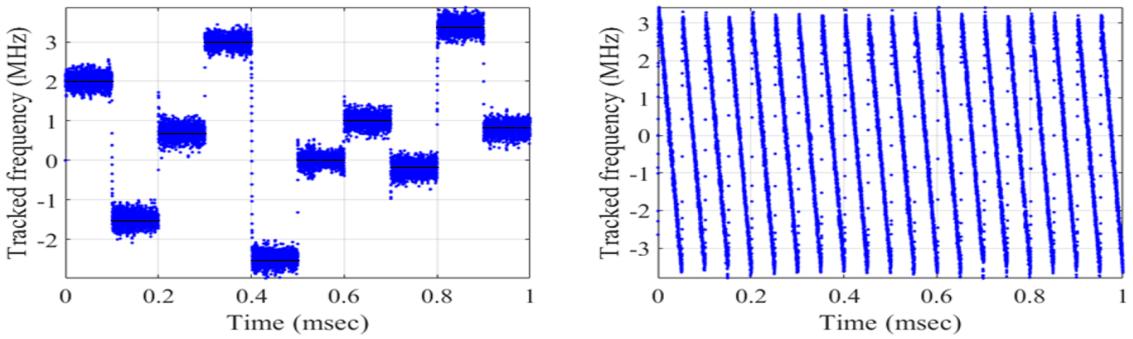

Figure 4.26: Interference Frequency Tracked by Adaptive Notch Filter (Adaptation Step =0.05 and Pole Contraction Factor =0.8) In Case of Frequency Hopping (Left) and Chirp Signal (Right)

Figure 4.27 illustrates interference localization with the wavelet packet decomposition method represented in the time-scale domain. A 5-level decomposition is realized using the 'Symlet' wavelet function, resulting in 32 wavelet packets, each representing a specific portion of the frequency band. In the calibration phase, a threshold mask is estimated with the individual calibration of the wavelet scales. The threshold is determined by setting the 3-sigma value for each scale in interference-free conditions. By observing the wavelet coefficients, it is possible to identify instances where the coefficients exceed the

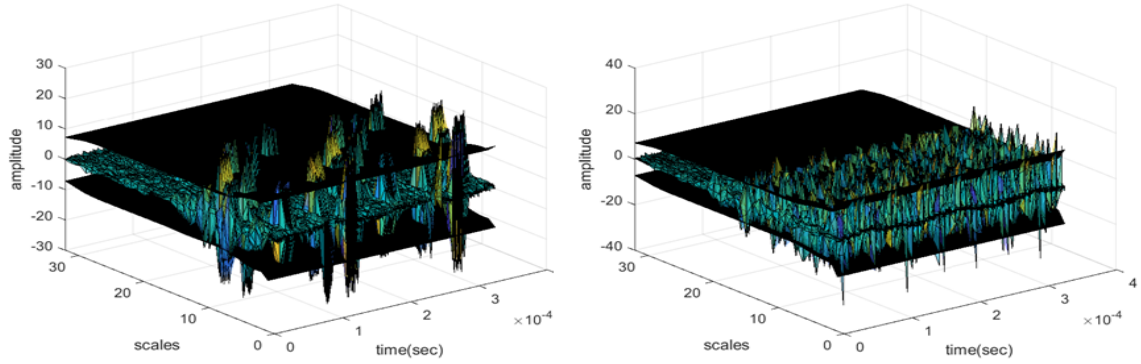

Figure 4.27: Time-Scale Representation with 5-Level Decomposition of GPS L1 Signal Interfered with Frequency Hopping (Left) and Chirp Signal (Right).

threshold value due to an increase in energy concentration, thereby indicating the presence of an interference signal. Notably, the energy of the signal is primarily concentrated in the lower scales, with almost no activity at higher scales, as the interference signal only covers 40% of the recorded frequency bandwidth. Following the detection process, the wavelet coefficients that represent the interference signal (i.e., those with higher coefficient values) are suppressed by replacing them with null values, which is commonly referred to as the coefficient blanking method.

- ***Acquisition***

The acquisition is the primary block in the receiver processing chain. The acquisition process involves searching for the satellite signal in the signal search space. Once the satellite presence is confirmed by the correlation peak, the code delay and the doppler frequency are estimated to facilitate the tracking of the satellite signals. The signal search space, as shown in Figure 4.28 for GPS PRN #02, is obtained after performing signal correlation for 1 ms (coherent accumulation) and subsequently averaging it with 7 ms of incoherent accumulations. Figure 4.28(a) shows a very distinct correlation peak emerging from the noise floor in the absence of interference. However, in the presence of a frequency hopping signal, as depicted in Figure 4.28(b), the jamming signal completely overpowers the satellite signal, increasing the noise level, and the peak is no longer visible. As an interference countermeasure, both WPD and ANF techniques are employed. The acquisition of search spaces after mitigation with these techniques is shown in Figures 4.28(c) and (d). The results show that the satellite peak resurfaced with the suppression of the interference signal, leading to a decrease in the noise level. However, WPD seems to perform much better than the ANF in the suppression of the interfering signal, as evidenced by the significant reduction of the noise level.

A similar trend is visible in the presence of a linear chirp jammer, as shown in Figure 4.29. In this case, the jamming signal introduced a substantial amount of noise, completely masking the signal underneath and thereby rendering signal acquisition impossible. Nevertheless, the satellite signal is recovered after filtering interference with both WPD and ANF techniques, as shown in Figure 4.29(c) and (d). Additionally, in this case, it can be observed that ANF filtering tends to be noisier in comparison to WPD-based mitigation.

- ***Tracking***

The subsequent step in the receiver involves the process of signal tracking, which is aimed at refining and continuously tracking the initial code and carrier estimates provided by the acquisition stage. The tracking process is carried out through two closed loops

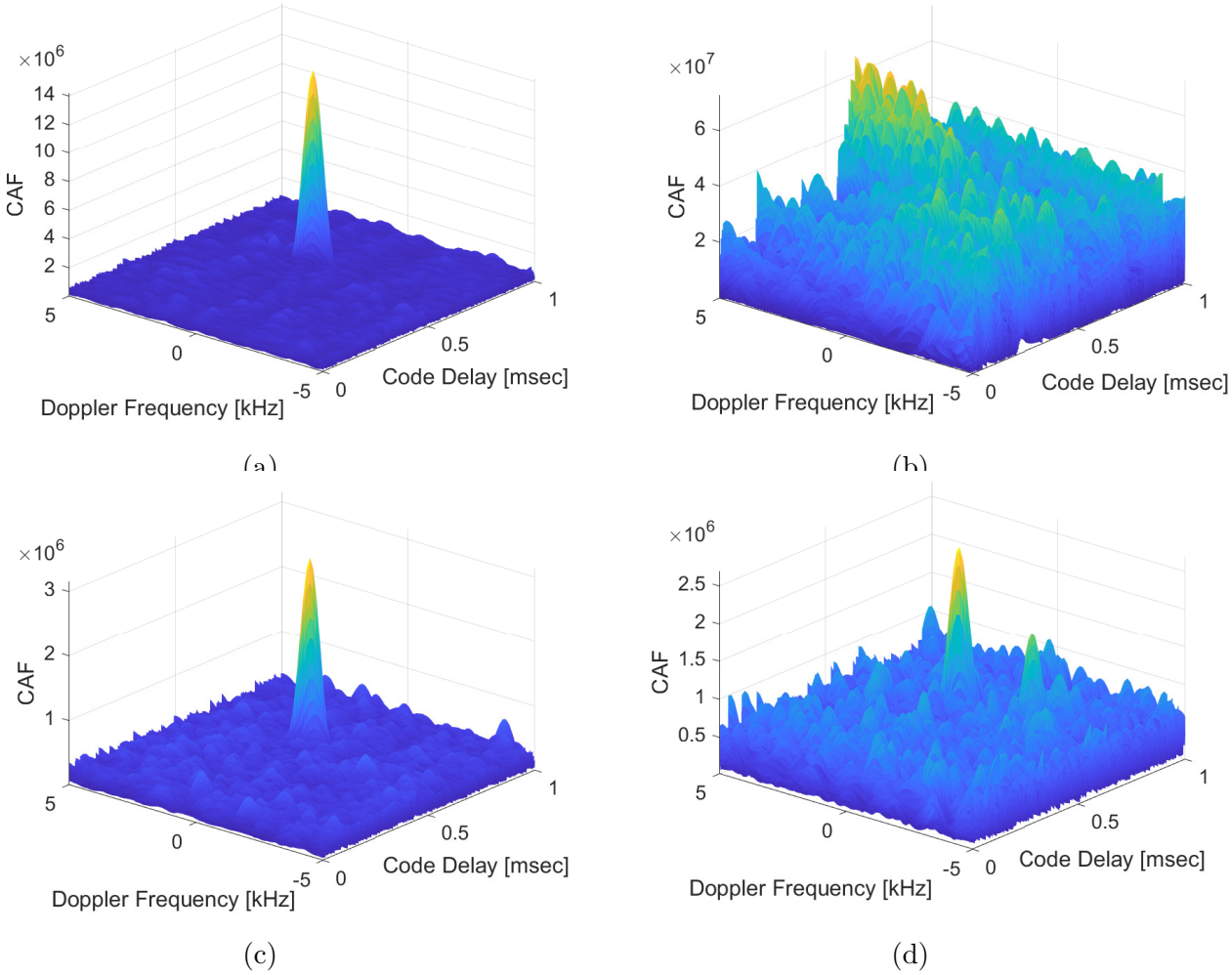

Figure 4.28: GPS L1 C/A signal search space of Sat#02 a) in the absence of jamming signal, b) in the presence of frequency hopping jammer, c) after applying WPD-based mitigation, and d) after ANF-based mitigation.

within the tracking channel namely the Delay Lock Loop (DLL) and Phase Lock Loop (PLL). This section will provide results related to signal tracking, particularly presenting the filtered output of the discriminator and (), which is a metric for assessing the tracking quality of the signal.

The tracking behavior, as illustrated in Figure 4.30, seems to be consistent with the acquisition results. The unmitigated interference (as depicted in red) has a significant impact on tracking, highlighting the importance of a mitigation technique to properly track the satellite signal. It can be observed in both scenarios that the impact of interference started at approximately 58 seconds, causing the receiver to diverge. At this instant, the receiver completely loses the tracking of the satellite signal and instead locks on to the interference signal, which is considerably stronger than the GNSS signal. In this case, both mitigation methods exhibit comparable performance at the tracking level, enabling the receiver to continue tracking the satellite signal. Moreover, in the case of frequency hopping (left), the WPD (as depicted in green) appears to significantly minimize the tracking noise in comparison to the ANF filtering (as depicted in blue). This effect could be attributed to a mismatch between the filter dynamics and relatively slow frequency variations of the interfering signal, as previously observed in the frequency hopping case depicted in Figure 4.26.

A similar trend can be observed in the Carrier-to-Noise ratio (CNO) estimation, which represents the tracking quality of the signal. As shown in Figure 4.31, when no mitigation technique is applied, the CNO value shows “abnormal” fluctuations as the jamming signal

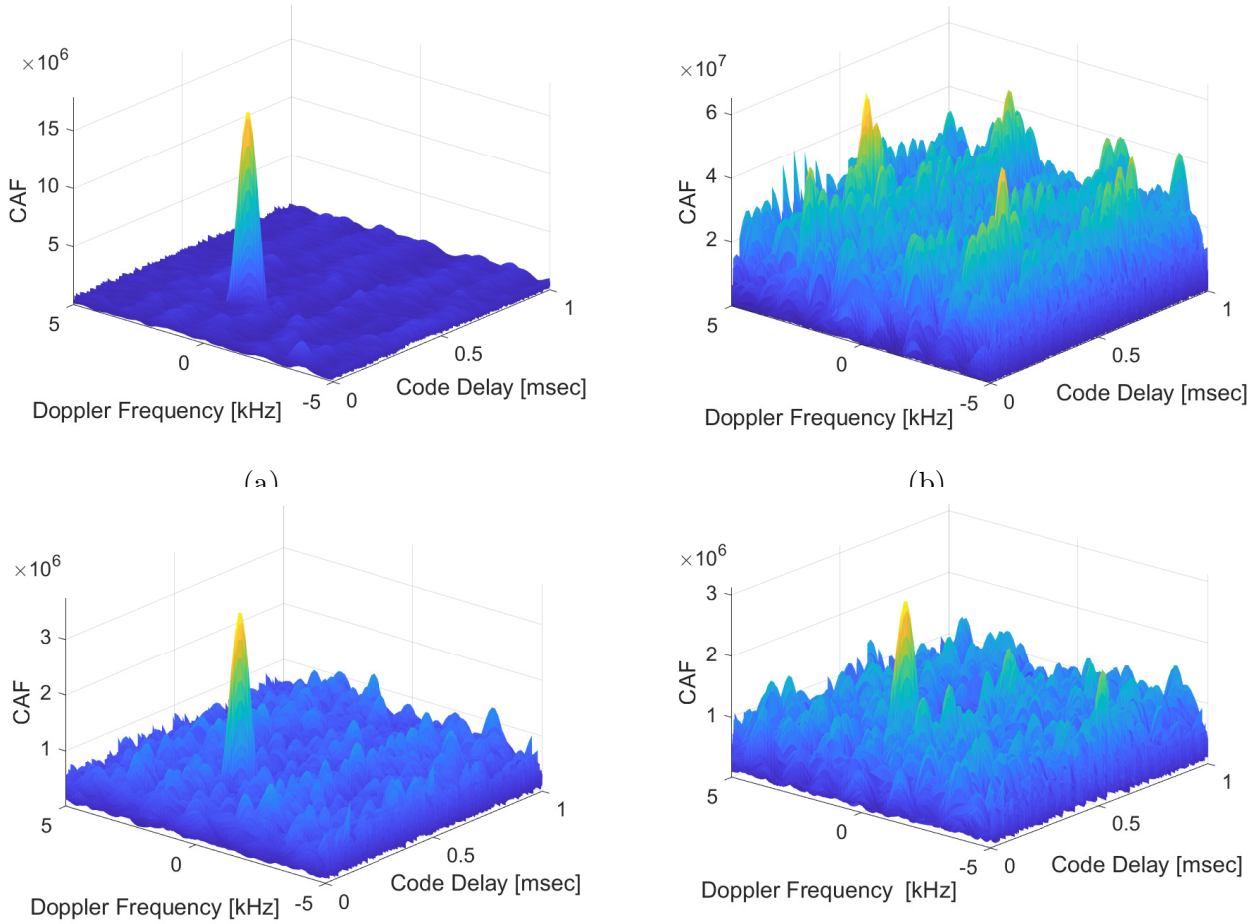

Figure 4.29: GPS L1 C/A signal search space of Sat#02 a) in the absence of jamming signal, b) in the presence of chirp jammer, c) after applying WPD-based mitigation, and d) after ANF-based mitigation.

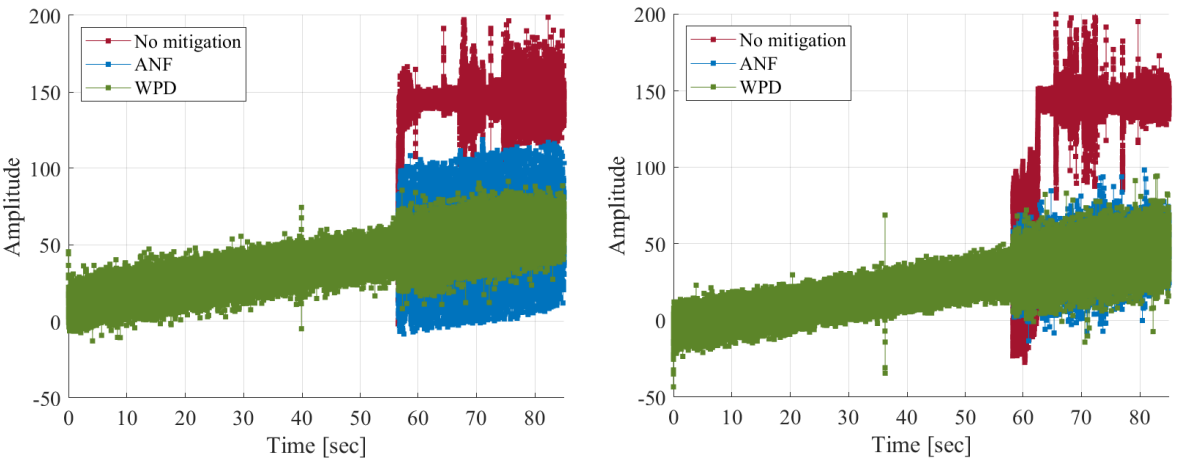

Figure 4.30: Satellite (PRN 02) Tracking State a) in The Presence of Frequency Hopping (Left) and b) Chirp (Right) Interference; No Mitigation (Red), ANF (Blue) And WPD (Green).

completely overpowers the GNSS signal. However, CNO has improved in both interference scenarios with the implementation of mitigation techniques. However, as expected, the CNO dropped by a few dB as the mitigation technique not only suppresses the interference signal but also removes some portion of the useful signal. Both mitigation techniques show similar performance in the case of the chirp scenario. Nevertheless, WPD (as depicted

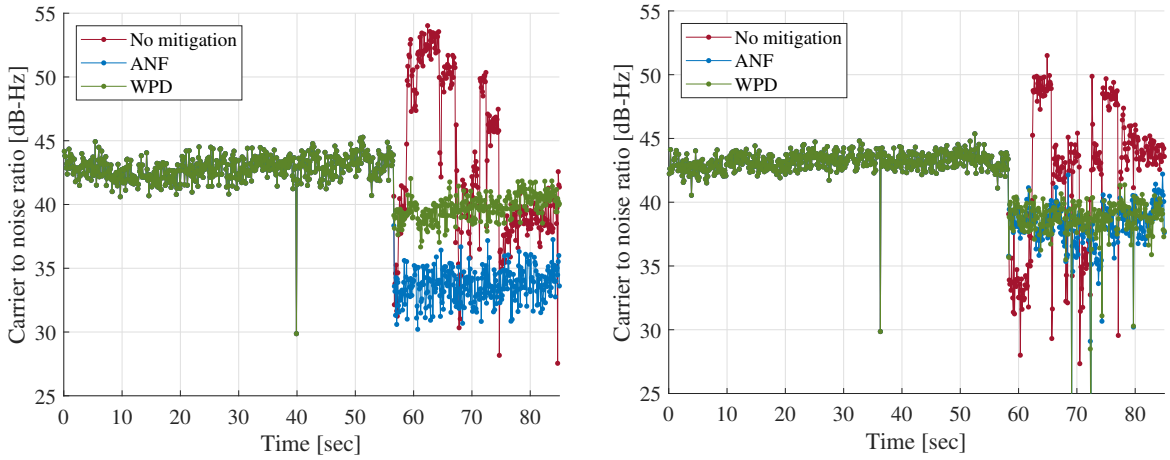

Figure 4.31: Carrier-to-Noise Ratio (CNO) Estimated After the Satellite Tracking Stage for PRN 02 a) In the Presence of Frequency Hopping (Left) and b) Chirp (Right) Interference, With No Mitigation (Red), After Applying ANF (Blue) And WPD (Green).

in green) performed better than ANF (as depicted in blue) in the frequency hopping scenario, resulting in reduced tracking noise and gaining approximately 6 dB more after filtering the interfering signal.

- ***Positioning***

The final stage of the receiver processing chain allows the receiver to estimate its position. We have used the Weighted Least Square (WLS) algorithm to estimate the position where elevation, CNO, and hybrid models are used to construct the weighting matrix. Furthermore, the weighting functions are also used to estimate the positioning protection level. A detailed description of the WLS positioning algorithm and protection level is provided in Chapter 2. To evaluate the position performance, the Stanford diagram is presented to analyze accuracy, availability, and safety from the localization function point of view. This diagram simplifies the analysis by allowing the assessment of multiple performance parameters in a single representation by comparing HPL, HPE, and AL that we have purposely set AL to 30 m, though it can be adjusted to meet requirements specific to certain applications. Firstly, we present results in the nominal conditions, which include all the instances (epochs) where the position is estimated in the absence of interference and is referred to as a 'reference case'. It provides a way to generalize the achievable performance from these measurements, which are processed with a particular receiver configuration to assess the impact of interference and the effectiveness of the mitigation techniques.

In the absence of interference, no significant difference in positioning accuracy is observed for each weighting model, as seen in Figure 4.32 with three different models. Typically, the average value and the standard deviation of position error are approximately 4.5 m and 2.5 m, respectively. In terms of safety considerations, each model provides nearly 99% of normal operations. This constitutes system availability, which is indicated by instances where positioning errors are well-bounded by the estimated protection level. Generally, the elevation weighting model appears to bound the errors better (left plot), with only 4 MIs representing unbounded but safe (HPL <HPE <AL) instances than CNO and a hybrid model with 32 and 11 instances, respectively. The hybrid model, since it is the product of elevation and CNO-based models, tends to be more conservative in the estimation of the PL.

Figure 4.33 represents positioning performance in the presence of interference and without

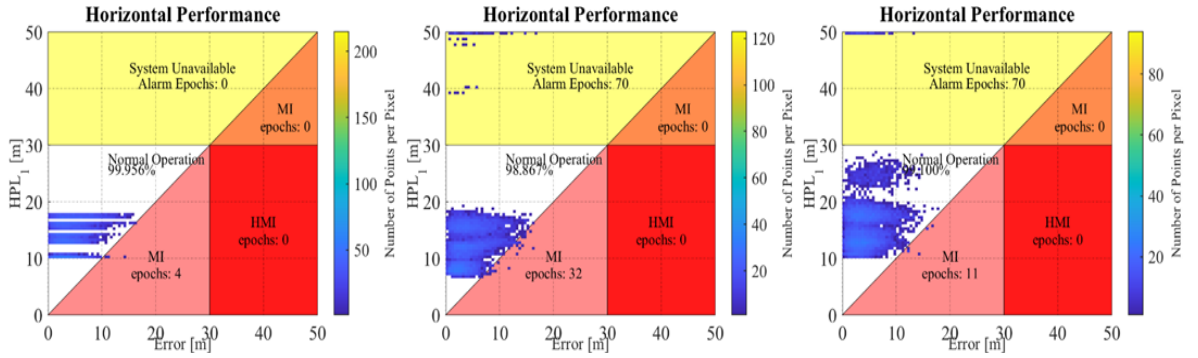

Figure 4.32: Stanford Diagram Representing Performance in Nominal Condition Using Different Weighting Schemes; Elevation (Left), CNO (Middle), And Hybrid (Right).

any mitigation strategy. It is worth noting that approximately 65% of the instances correspond to normal operations, which are interference-free epochs. The remaining 35% of the instances indicate the presence of interference. The two interference scenarios considered in this analysis displayed a similar impact on the positioning performance. It is evident from the user perspective that interference has an adverse impact on positioning accuracy, as indicated by a higher concentration of points in HMI (> 50 m error). The CNO and hybrid models, in contrast to the elevation-based weighting model, appear to play a role in managing the effects of interference by increasing the protection level. By enlarging the protection level, it is possible to compensate some of the HMI with unavailability, which is nevertheless not sufficient to completely isolate positioning points affected by interference. The results obtained at the positioning level are very much aligned with the behavior of CNO and the tracking, as previously observed for the interference scenarios. Particularly, Figure 4.30 illustrated that the receiver, instead of tracking the satellite signal (red curve), locked onto the interference signal, resulting in errors of more than tens of km. This also caused an 'abnormal' increase of the CNO as shown in Figure 4.31 when compared with the nominal situation. Considering the CNO-based model appears to have a negative impact, which provides a protection level that underestimates the true error, leading to an increased number of points in the MI and HMI zone.

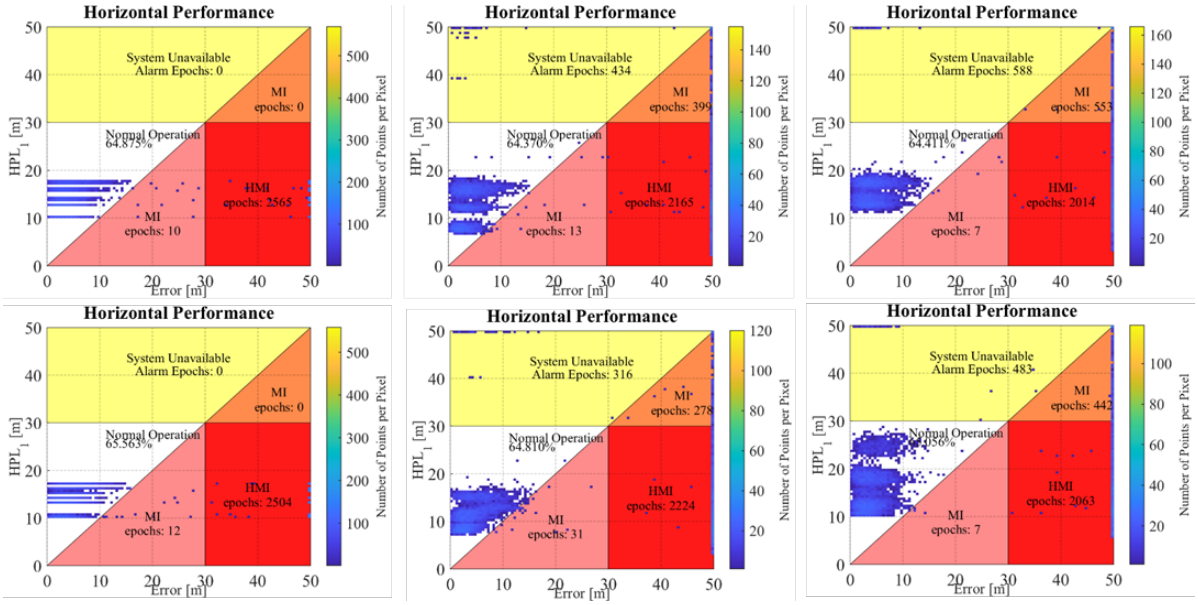

Figure 4.33: Stanford Diagram Representing Performance in The Presence of Interference; Chirp (Upper Panel) And Frequency Hopping (Lower Panel) Before Mitigation, Using Weighting Schemes; Elevation (Left), CNO (Middle) And Hybrid (Right)

Moving forward, we present the results of ANF and WPD mitigation for the two interference scenarios namely chirp and frequency hopping. Initially, we analyze the mitigation performance of the two techniques in suppressing the effects induced by the chirp signal. As depicted in Figure 4.34, the performance of ANF (upper panel) and WPD (lower panel) at the position level, considerably increased the normal operations. The elevation model seems to maximize the normal operation (white) to more than 96%, but in certain instances, it could not adequately bound the true error, thus resulting in some data points in the MI (pink) region. Conversely, the CNO and Hybrid model appears to be excessively over-protective, resulting in additional undue unavailability (yellow), which is particularly evident in the case of the hybrid model. It seems that the drop in CNO (as seen in Figure 4.31) could potentially be the cause of this overprotection. Since each satellite measurement experienced somehow similar drop, it tends to significantly enlarge the overall uncertainty bound.

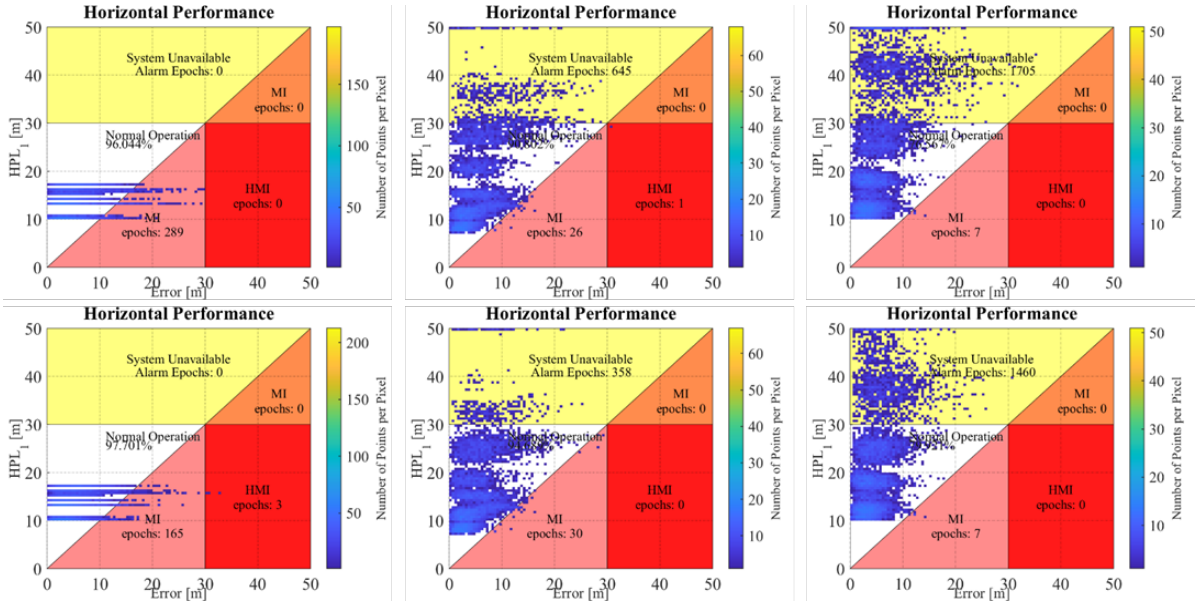

Figure 4.34: Stanford Diagram Representing Performance After Mitigation of Chirp Signal by ANF (Upper Panel) And WPD (Lower Panel), Using Weighting Schemes; Elevation (Left), CNO (Middle) And Hybrid (Right)

Figure 4.35 presents the performance of ANF (upper panel) based mitigation at the position level in the presence of a Frequency Hopping signal. Following the mitigation process, it is evident that HMIs are significantly reduced, however, there remain some instances where the error exceeds 30 m. Moreover, it can also be observed that in comparison to the previously presented chirp scenario, ANF completely underperformed in the frequency hopping case. Notably, the elevation-based model remains the most unsafe, with 865 MIs (pink) and 49 HMIs (red). Additionally, it can also be observed that CNO and the hybrid model managed to remove the HMI but significantly increased the system unavailability.

The results obtained demonstrate that WPD (lower panel) outperformed ANF (upper panel) in suppressing the distortions induced by the frequency hopping signal. Particularly, in this case, WPD nearly retrieved the same performance as the reference scenario (see reference case in Figure 4.32). It can be seen that after filtering, normal operations (white) experienced a significant increase ($> 99\%$) and with no HMI (red) instances. It is important to note that, as previously demonstrated (see Figure 4.31), the signal quality improved significantly after applying WPD mitigation in the frequency hopping case. This improvement directly leads to an increase in the positioning accuracy (mean error 4.5m and standard deviation 2.8m) and, more importantly, ensures completely safe instances.

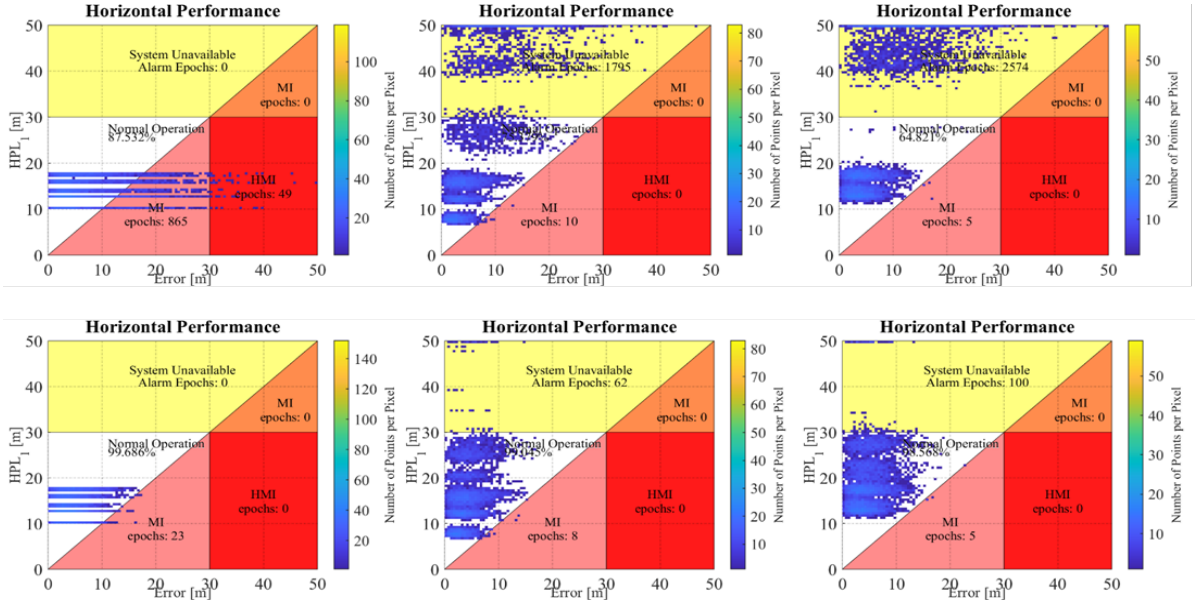

Figure 4.35: Stanford Diagram Representing Performance After Mitigation of Frequency Hopping Signal by ANF (Upper Panel) And WPD (Lower Panel), Using Weighting Schemes; Elevation (Left), CNO (Middle) And Hybrid (Right)

4.5.4 Conclusion on Notch Filtering versus Wavelet Transform

We previously presented a comparative study on the two interference countermeasures, namely Adaptive Notch Filter (ANF) and Wavelet Packet Decomposition (WPD). A comprehensive analysis has been conducted to evaluate the performance of these methods against the frequency hopping and chirp signals. The impact of interference and effectiveness of the mitigation methods have been assessed at multiple stages of receiver processing, including satellite acquisition, tracking, and position level. In addition, as a primary objective, we have also provided a comprehensive assessment of positioning Key Performance Indicators (KPIs): availability, accuracy, and safety concerns, for each of the presented cases.

The interference scenarios investigated in this study have demonstrated that the jamming signal completely overpowered the satellite signals. It has been observed that signal acquisition becomes impossible in the presence of interference. This is mainly due to the increase in the noise power level, which leads to a complete submersion of satellite signal peak in the noise, as observed in the signal search space. Consequently, the interference also hindered the satellite tracking process. With the emergence of interference, it became impossible for the receiver to keep tracking the satellite signal, instead, the tracking loop started to follow the interfering signal. This behavior resulted in fluctuations in the Carrier-to-Noise ratio (CNO) with an occasional increase in the CNO value beyond the nominal level. Furthermore, as expected, interference if not mitigated, completely jeopardizes the safety of the positioning system, as seen by a significant increase in Hazardous Misleading Information (HMI) instances.

Our investigation has shown that ANF and WPD are very effective in suppressing the interference signal. Upon mitigation, a clear and distinct correlation peak reappeared in the signal search space. Similarly, mitigation made it possible for the receiver to keep tracking satellite signals. Moreover, the mitigation results have demonstrated that the detection and mitigation layer in the localization function is essential in effectively dealing with the interference signal, whereas an inadequate strategy can also lead to hazardous consequences endangering the safety of the system, which can lead to a fatal accident. In most of the studied cases, mitigation of interference led to a significant reduction in HMIs.

However, this came at the cost of increased unavailability, thus compromising availability for system safety.

The main concern that arises regarding the choice of parameters for the mitigation techniques. Even though the two signals, frequency hopping, and chirp, have completely different signal dynamics, we deliberately applied identical parameters to highlight the importance of the appropriate parameter selection. The results showed that ANF performed relatively better for the chirp signal than in the frequency hopping case. However, the mitigation performance could have been much better with proper tuning of the filter. On the other hand, WPD performed exceptionally well for the frequency hopping case and almost retrieved a similar performance as in the case of nominal conditions. However, it was unable to provide similar performance against chirp interference. Perhaps a different wavelet function, increasing the filter length, or the decomposition stage could help in achieving better performance. The other prospect regarding the use of classical weighting models, which could also be recalibrated to reduce unnecessary unavailability, implies the conditions where the HPE $<$ AL $<$ HPL.

4.6 Summary and Conclusions

The investigations that are presented in this chapter have been conducted in several stages. In each of these phases, the same experimental protocol has been consistently followed throughout the research, which is: i) to assess the impact of interference and ii) to determine the effectiveness of the employed mitigation techniques. Our study aims to evaluate the preparedness and capability of the existing technology (or techniques) in managing the issue of radio frequency interference concerning safety-critical applications. To evaluate this, we presented three scenarios: the reference case - in the absence of an interference signal, the interference case - without any mitigation, and the mitigated case - applying a mitigation strategy to filter the interfering signal. Our analysis incorporated two non-stationary signals, namely frequency hopping and linear chirp. The characteristics of these signals differ in the way the frequency is gradually varied over time. Furthermore, we have investigated the behavior of the classical weighting schemes including elevation, carrier-to-noise ratio, and hybrid (that combines elevation and carrier-to-noise ratio) model.

Our research findings have confirmed that unmitigated interference can have a significant impact on the availability of the localization system and more importantly, it can also have potentially serious implications for the safety of the system. Furthermore, we have observed that the weighting models behave differently in the presence of interference signals. The weighting model solely based on elevation is the least effective in bounding the positioning uncertainty, as it does not consider the impact of interference. As a result, the elevation-based model is not considered a predominant criterion in this case. On the other hand, the weighting model that involves CNO has shown the ability to reduce (and in some cases eliminate) HMI instances at the expense of increased unavailability.

In the initial phase, we conducted a preliminary investigation analyzing the effectiveness of mitigation solutions that are available in the Commercial Off-The-Shelf (COTS) receiver. During this investigation, the COTS module, which is an integrated mitigation solution provided by the Septentrio receiver has been employed to effectively filter out the interference signals. Our findings provide compelling evidence regarding the receiver's resilience and robustness following the implementation of these mitigation solutions, particularly for the presented interference scenarios. Note that we have considered the receiver's entire processing stages as a closed system, which probably involved several complementary actions that contributed to a highly accurate positioning solution. Upon evaluating

these findings on the Stanford diagram, it has been observed that after the mitigation the HMI instances are eliminated, resulting in an exceedingly accurate positioning solution. Nevertheless, it still could not manage to bring the performance to an acceptable level as in many instances the positioning points are considered operationally unavailable as indicated by a higher number of unavailable instances in the Stanford diagram.

The findings in the aforementioned study have motivated further investigation into existing mitigation solutions found in the literature. Our primary objective remains unchanged, as we aim to maximize the operational availability of the localization system while prioritizing the safety concerns associated with it. To achieve this objective, three interference mitigation techniques have been implemented namely Karhunen Loéve Transform (KLT), Wavelet Packet Decomposition (WPD), and Adaptive Notch Filter (ANF). The findings show that, for the frequency hopping scenario, these mitigation techniques particularly Karhunen Loéve Transform (KLT) and Wavelet Packet Decomposition (WPD) have proven to be very effective in retrieving back performance to a level very close to the nominal case. However, when dealing with the chirp scenario, these techniques could not deliver similar performance as in the previous case to meet the performance requirements. In general, the mitigation process successfully eliminated HMI instances, however, it also resulted in a considerable number of unavailable points on the Stanford diagram. The Karhunen Loéve Transform (KLT) study suggested that the effectiveness of the mitigation countermeasure is conditioned on the parameter choices, and fine-tuning the threshold leads to a near-optimal performance. We expect a similar approach could be applied to each of the techniques against the chirp signal, to meet the performance requirement. This matter will be further addressed in the upcoming chapter.

Chapter 5

Contribution to the parameterization of single pole adaptive notch filter against a wide range of linear chirp interference

5.1 Introduction

In Chapter 4, we thoroughly discussed the implementation of three state-of-the-art interference mitigation techniques: Adaptive Notch Filter (ANF), Wavelet Packet Decomposition (WPD), and Karhunen Loéve Transform (KLT). Our primary objective was to evaluate their performance against frequency hopping and linear chirp signals. We conducted a thorough analysis across different receiver processing stages, emphasizing particularly Key Performance Indicators (KPIs) related to safety-critical applications. In the following, we will go through the summary of each technique, explore their limitations, and discuss the outcome of our investigation.

- Starting with KLT, its computation involves solving the eigenvalues problem and analyzing them to identify and isolate the principal components associated with the interference signal. Due to substantial computational demands, it is primarily considered for post-processing analysis. Furthermore, its realization can be quite cumbersome, depending on the characteristics of the interfering signal. In our implementation, the KLT analysis showed highly promising results in the frequency hopping case, particularly in the retrieval of positioning KPIs identical to the nominal conditions. However, for the chirp scenario characterized by a broad spectrum of signal components affected by interference, the computational cost is particularly constraining. Thus it required a higher-level decomposition, thereby increasing the number of observation samples. The calibration of the threshold adds further complexity to the process, limiting the effective recovery of the GNSS signal. In this case, finding a representative Stanford diagram to demonstrate the effectiveness of the technique became unfeasible for this specific case. Consequently, after numerous trials, we decided to halt our investigation, deferring it for future study.

- The WPD decomposes the signal into various frequency sub-bands, allowing localization of the signal in the time-frequency domain. This method relies on the choice of the wavelet function and the number of decomposition stages. Increasing the decomposition level generates sub-bands, which subsequently increase the computational demands. Furthermore, the appropriate selection of a wavelet kernel matching

the characteristic features of the interference signal is crucial but requires exhaustive trials. Our findings showed exceptional performance of WPD-based mitigation for the frequency hopping case similar to the KLT outcome. However, it could not perform similarly in the case of a chirp signal. Despite a significant improvement in positioning accuracy, HMI instances were predominantly replaced by unavailable instances.

- Lastly, the ANF offers a simple and easy-to-implement solution involving real-time adaptation to changing signal conditions. It effectively eliminates specific frequency components of the signal by dynamically positioning the notch around the unwanted content while preserving the other components. However, the effectiveness of the filter relies on the selected values of the adaptation step and pole contraction factor. In the presented scenarios, ANF fell short of meeting the desired performance level, and the filter tuned with parameters selected from the interval recommended in various studies proved to be inappropriate. In both cases, mitigation effectively improved positioning accuracy with no HMI but most instances remained unavailable in the Stanford plot.

Given the aforementioned points, we have selected ANF for further investigation. The motivation behind this reason mainly lies in its implementation simplicity, widespread usage in receivers, and abundance of research interest as a countermeasure strategy against interference signals. Our current emphasis is on ANF, and our efforts will be directed towards addressing the observed limitation related to the selection of filter parameters, specifically tailored for chirp signals. The main goal is to enhance the performance of ANF, enabling it to effectively handle the challenges posed by linear chirp signals. It is anticipated that an optimally tuned ANF filter can recover the useful signal effectively, leading to a global improvement in the KPIs.

This chapter is structured in different sections. Section 5.2 presents the problem statement related to ANF characteristic parameters. Section 5.3 unfolds the initial approach for the filter parameterization. This involves a detailed breakdown of the process, including data preparation, labeling, and application of Multivariate Polynomial Regression (MPR) for modeling the parameters. It subsequently presents the results and analysis, including comparisons with other signal-level metrics. In Section 5.4, an improved approach is introduced incorporating acquisition-level labeling, regression using the Neural Network method, and a subsequent discussion on performance. Finally, Section 5.5 concludes by summarizing the outcomes of these investigations.

5.2 Problem Statement: Exploring Adaptive Notch Filter (ANF) Characteristic Parameters

The existing literature underscores the necessity of appropriate parameterization for optimizing the performance of ANF, emphasizing that inappropriate selection not only reduces effectiveness but also introduces distortions in the useful signal [5]. Despite these insights, a notable gap persists in the literature regarding a well-defined methodology for ANF parameterization. To address this deficiency, this chapter introduces a novel perspective by investigating and proposing a comprehensive methodology tailored to the distinct attributes of chirp signals. Before presenting this methodology, let's examine the characteristic parameters of ANF including the pole contraction factor, which defines the notch bandwidth, the notch depth, and the adaptation step.

In an ideal situation, the notch bandwidth is kept narrow to target a very specific portion of the spectrum to preserve the useful content of the signal at maximum. To ensure the stability of the filter, the pole contraction value is typically selected within the range $k_\alpha \in [0, 1]$. Figure 5.1 (a) shows the magnitude response of $H(z)$ for different pole contraction factor values, and with a unit amplitude ($a_0 = 1$), the notch bandwidth becomes increasingly narrower as $k_\alpha \to 1$.

The second important parameter is the notch depth which represents the magnitude of the complex estimate that controls the attenuation level applied to the signal. Figure 5.1 (b) shows the magnitude response of $H(z)$ for different values of amplitude with a constant pole contraction factor ($k_\alpha = 0.9$). The notch filter functions as an all-pass filter when the amplitude is zero ($a_0 = 0$) and applies spectral null around the central frequency when the amplitude is a non-zero value ($a_0 = 1$).

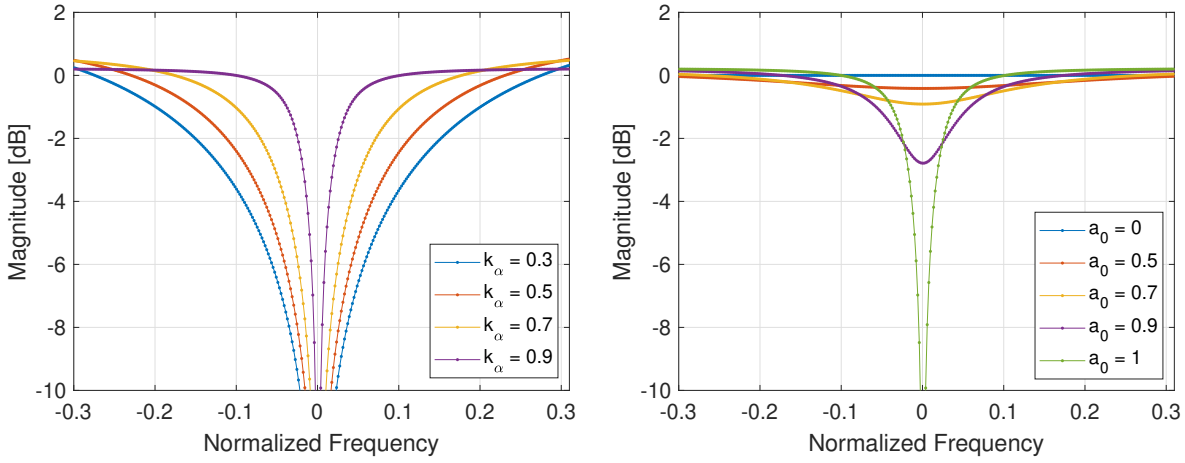

(a) (b)

Figure 5.1: Magnitude response of the transfer function H(z) against a) different values of pole factor (k_α) with unit amplitude (left) and b) different values of complex amplitude (a_0) with $k_\alpha = 0.9$.

The third parameter is the adaptation step, which determines the speed of the adaptation algorithm. In Figure 5.2, the notch frequency estimation for different adaptation step values is illustrated, for a constant value of the pole contraction factor ($k_\alpha = 0.8$). To highlight the influence of the adaptation step, a specific scenario involving the GPS L1 signal sampled at 15 MHz, subjected to chirp interference with a 5 MHz bandwidth, a 50 µs sweep rate, and a relative jamming to noise power ratio of 15 dB. The smaller adaptation step ($\delta = 0.01$) leads to relatively lower oscillations in the ramp region while tracking the frequency variations, but increases the convergence time during the transition period. Conversely, a larger value of the adaptation step ($\delta = 0.1$) results in relatively more noise, but it quickly converges to the interference frequency.

Given that the nature of interference is often ambiguous and constantly evolving, it becomes very important to proficiently suppress the induced distortions. The adaptive nature of the interference, whether coming from an unintentional source or an intentional source, necessitates an equally adaptive and sophisticated mitigation strategy. The exploration of ANF becomes crucial in achieving optimal mitigation, given its ability to dynamically adjust its response based on the specific characteristics of the interference signal. However, the effective implementation of ANF requires proper selection of the aforementioned parameters, which demands a thorough understanding of interference signal characteristics. In this context, Figure 5.3 presents general processes at the precorrelation level contributing to an interference management solution where this approach could be integrated. This solution encompasses various processes, including signal interference detection, classification, characterization, mitigation, and filter parameter tuning.

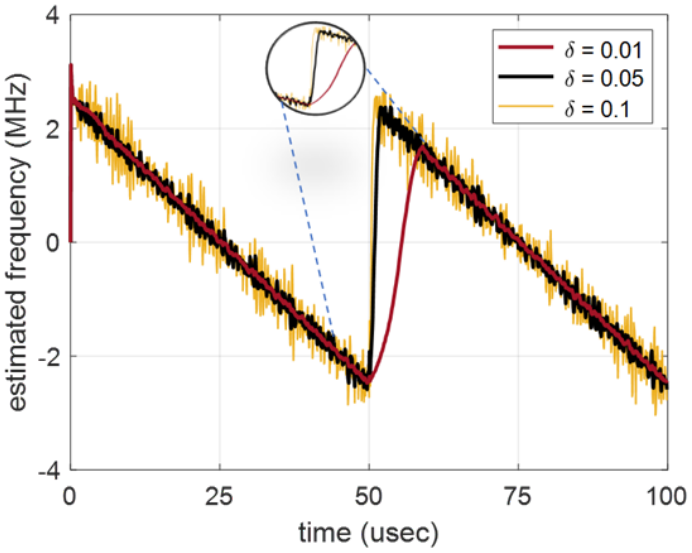

Figure 5.2: Interference tracking performance for different values of adaptation step (δ) with $k_\alpha = 0.8$ against chirp interference (Bandwidth = 5MHz, repetition rate = 50 µs and JNR = 15 dB)

Following up on the discussion, we will review various processes involved in this solution.

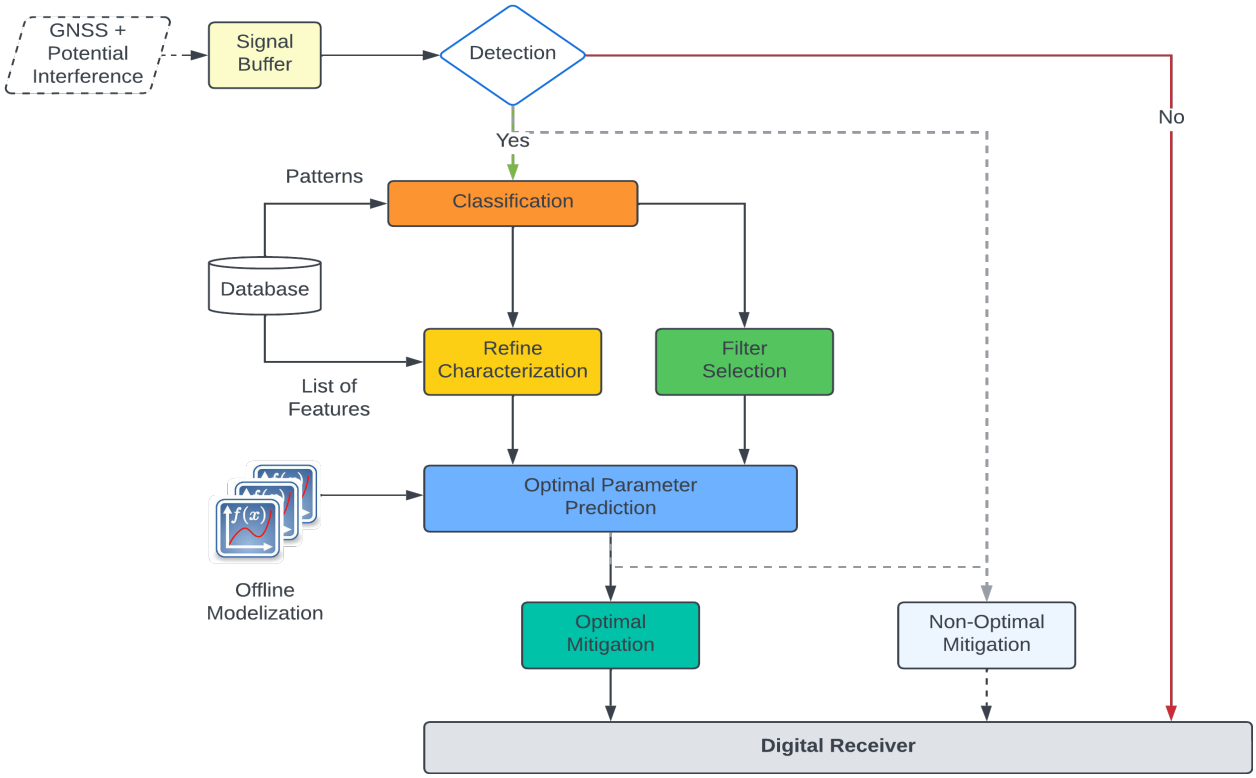

Figure 5.3: GNSS Interference Mitigation Management Solution with precorrelation level processing.

- **Detection**

The first crucial step in interference management at the precorrelation level involves the detection of undesirable signals. Various signal processing algorithms, both traditional and advanced, including machine learning techniques, are employed to analyze samples for a certain duration and identify the presence of interference.

- **Classification**

Once interference is detected, the subsequent classification stage categorizes the nature of the interfering signal, whether unintentional or intentional. The classification step would be essential for the activation of targeted countermeasures against a particular type of interference. In literature, machine learning algorithms are predominately employed to distinguish between various interference types as presented in Section 3.3.1.9. The classification stage could allow the system to adapt to different interference scenarios.

- **Characterization**

Following detection and classification, interference characterization involves a detailed analysis of the interference properties, including modulation characteristics, frequency distributions, and spatial attributes. This profound understanding of signal attributes helps in the subsequent stages, aiding in the selection of the filter and tailoring it for specific interference types.

- **Filter Selection and Optimal Parameter Tuning:**

With well-characterized interference attributes, the next step involves selecting appropriate countermeasures, followed by a fine-tuning of the mitigation filter through the selection of optimal parameters, which will be the primary emphasis of this chapter. Adaptive filtering techniques permit dynamic adjustment of the parameter in response to changes in the interference conditions. The main goal remains to isolate the interference signal while preserving the useful signal. The following discussions will delve into this stage and present the modeling approaches for ANF parameterization.

5.3 Filter Parameterization with Signal Level Labeling (Initial attempt)

In this section, we will present our initial approach, which involves the application of Multivariate Polynomial Regression (MPR) to model previously discussed ANF parameters. The comprehensive methodology depicted in Figure 5.4 encompasses a four-step process:

- Initially, in the first step, a diverse database of chirp signals with varying characteristics is created, incorporating variations in bandwidth, sweep rate, and power level.
- The second step involves a labeling process, where optimal ANF configurations for each scenario are determined using a RMSE criterion.
- Subsequently, the third step involves a 2-step regression process. Initially, a 3rd order MPR is applied considering two input features: sweep rate and bandwidth. Then, a 3rd-order mono-variable polynomial regression is applied to MPR coefficients to generalize power level variations.
- Finally, in the fourth step, the Generalized Multivariate Polynomial Regression (GMPR) model represented by polynomial functions is obtained and utilized for predicting the adaptation step and pole contraction factor values.

In this investigation, diverse scenarios with low, moderate and fast-varying chirp signals with different power levels are chosen. Now, we will further delve into a detailed discussion on each of these steps in the following:

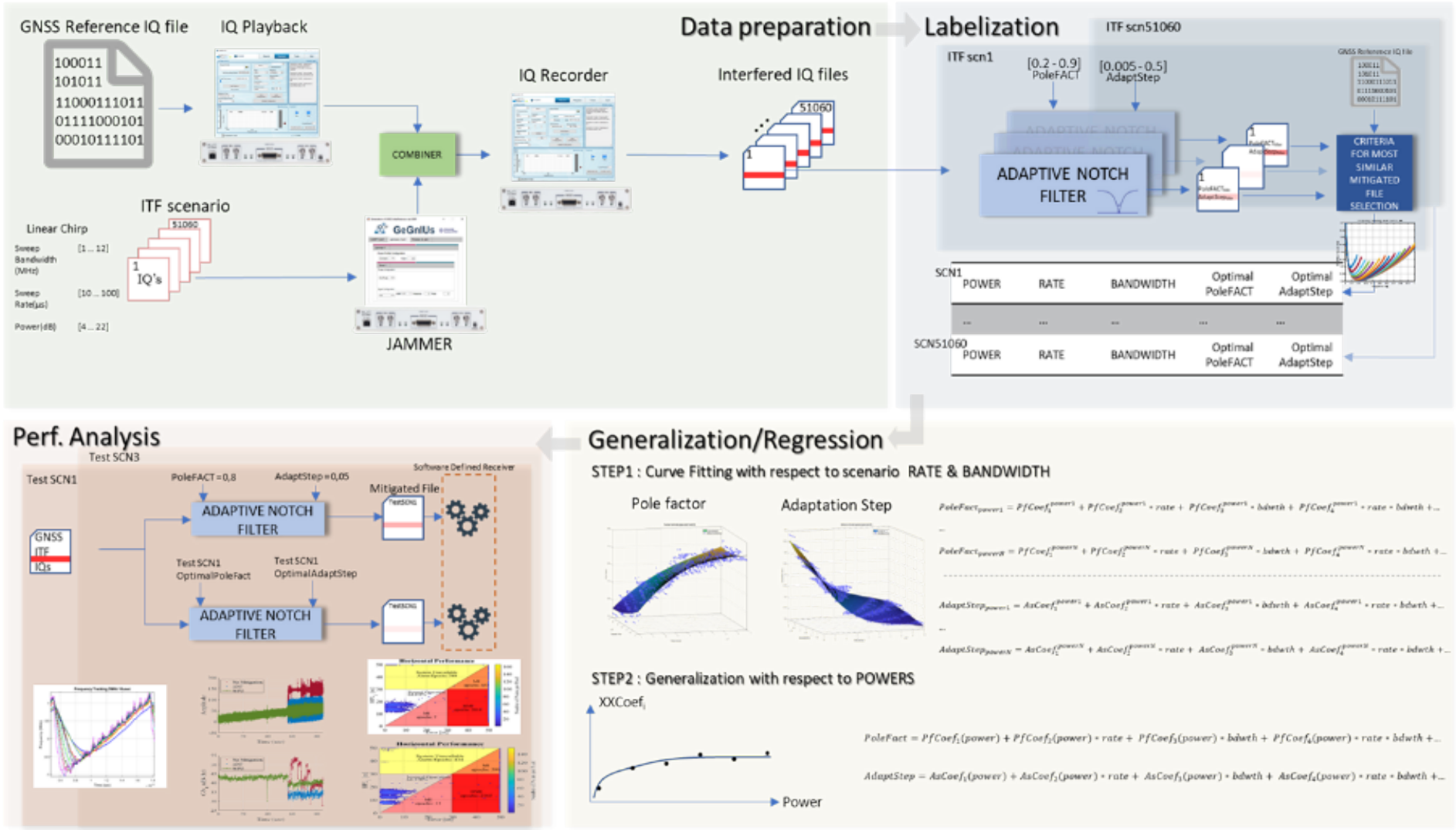

Figure 5.4: The complete processes involved in modelization of ANF parameters

5.3.1 Data preparation

The initial step in our approach involves the creation of interference scenarios characterized by diverse chirp signal attributes. To achieve this, we systematically vary signal parameters such as power, bandwidth, and repetition rate within realistic ranges. We considered 46 sweep rate values between 10 and 100 microseconds, 111 bandwidth values spanning 1 to 12 MHz, and 10 power levels, adjusting the Jammer-to-Signal Ratio (JSR) between 4 and 22 dB to simulate the proximity of the jammer source.

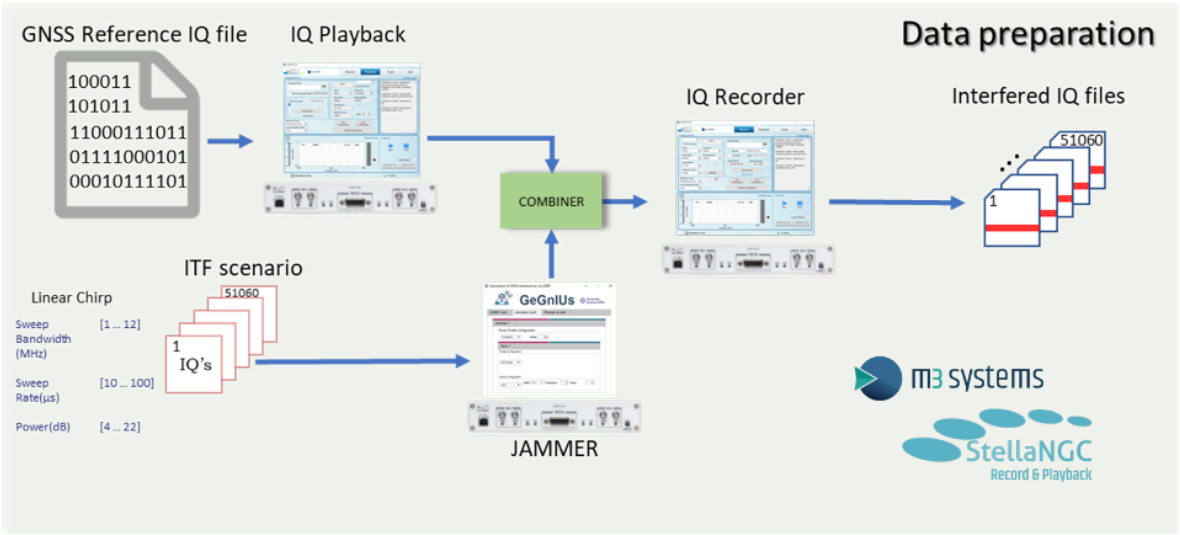

Figure 5.5: Database creation with record and playback system

The complete procedure involving the creation of the database is shown in Figure 5.5. In each iteration, a new interfered scenario is recorded by combining pre-recorded GNSS and interference signals, with a sampling rate of 15 MHz. Thanks to the Stella IQ record and playback system provided by M3systems, we created a database with more than fifty thousand scenarios.

5.3.2 Labeling

In the labeling process, the goal is to attribute meaningful tags or labels to the input features, which in our case are the jammer signal characteristic parameters. This step requires first the identification of suitable Adaptive Notch Filter (ANF) parameters tailored for each interference scenario. An exhaustive parametric sweep has been performed to search for the optimal parameters for each scenario, as illustrated in Figure 5.6.

It involves systematically adjusting the filter parameters within a specified range where pole factor values are varied between 0.2 to 0.9 and adaptation step values are changed between 0.005 and 0.5. For the selection of the optimal parameter, a Root Mean Square Error (RMSE) criterion has been applied, which is given as the difference between the reference and the filtered signal samples. The labels are then assigned to the corresponding scenario based on minimizing the RMSE, ensuring the closest match between the reference and the filtered signal

The RMSE is calculated using the formula:

$$\text{RMSE} = \sqrt{\frac{1}{N}\sum_{n=1}^{N}\left(|x-\widehat{x}|\right)^2} \tag{5.1}$$

Here, x represents the reference GNSS signal, $\widehat{x}$ is the recovered signal after applying the mitigation process, and N is the number of observation samples. The pursuit of a

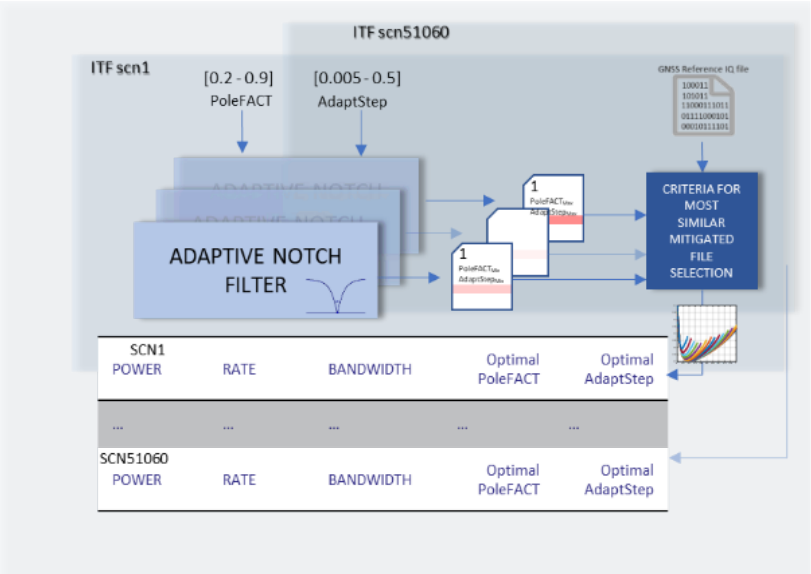

Figure 5.6: labeling process within database creation

single optimal combination drives the search for the appropriate ANF configuration that demonstrates the best performance in terms of GNSS signal retrieval. Figure 5.7 shows the parameter search grid of two distinct cases taken from the database, with the adaptation step and pole contraction factor on the x-axis and y-axis, respectively, while RMSE is on the z-axis. The two curves manifest a clear global minimum, indicating a relatively lower value for the given combinations. Additionally, when comparing Figures 5.7 (a) and (b), it is evident that the point of minimum moves for scenarios with a different bandwidth and sweep rate. The parameter combination exhibiting the lowest RMSE value is selected as the optimal ANF parameter choice. Similarly, each of the scenarios in the database is tagged with the optimal output combination consisting of the pole factor and adaptation step. Figure 5.8 shows the selected values of the pole contraction factor and adaptation step, where the RMSE value is found to be minimum against a wide range of scenarios with three different power levels.

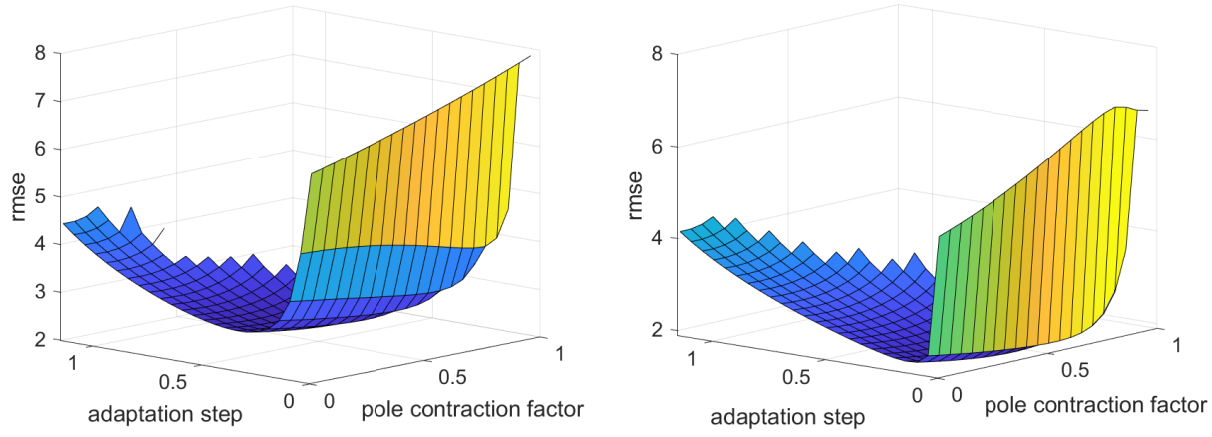

Figure 5.7: RMSE across the search grid to determine the optimal combination for two distinct cases.

5.3.3 Multivariate polynomial regression (MPR)

Regression analysis serves as a statistical tool to model and quantify relationships within the dataset, finding applications in diverse scenarios for forecasting and variable analysis.

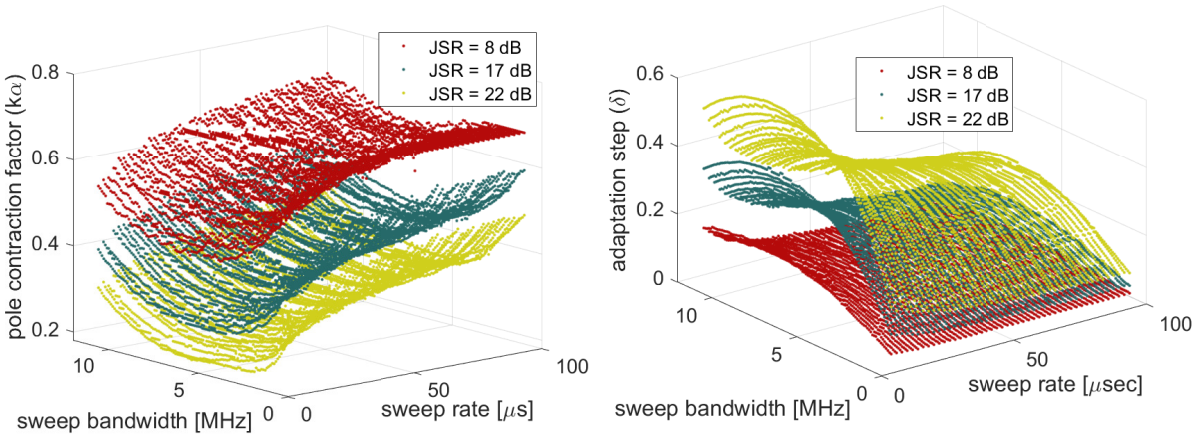

Figure 5.8: Optimal values of a) pole factor and b) adaptation step for different chirp scenarios with changing bandwidth, sweep rate and power level

The process involves identifying dependent and independent variables, determining the form of the relationship, computing the regression equation and conducting a thorough analysis of residuals. Polynomial regression is an extension of linear regression with an additional polynomial term to describe the nonlinear relationship between the input and the output variables. This can be applied to a single regressor variable to achieve simple polynomial regression or to multiple regressor variables in the form of MPR. A n-order polynomial regression for a signal variable can be expressed as:

$$y = \ p_0 + \ p_1 x + \ p_2 x^2 + \ldots + p_n x^n \tag{5.2}$$

Here, x represents the input variable, y is the output variable, and p_n is the coefficient of the nth-order term. A polynomial regression applied to two or more regressor variables is considered as MPR. A second-order MPR with two variables x_1 and x_2 can be expressed as:

$$y = \ p_{00} + \ p_{10} x_1 + \ p_{01} x_2 + p_{20} x_1^2 + p_{02} x_2^2 + \ p_{11} x_1 x_2 \tag{5.3}$$

Here, p_{10} p_{01} are called linear effect parameters. p_{10} p_{01} are called quadratic effect parameters. p_{12} is called quadratic effect parameters. The simplified form of MPR is:

$$y = \sum_{i=0}^{n} \sum_{j=0}^{n-i} p_{\mathrm{ij}} \ x_1 x_2 \tag{5.4}$$

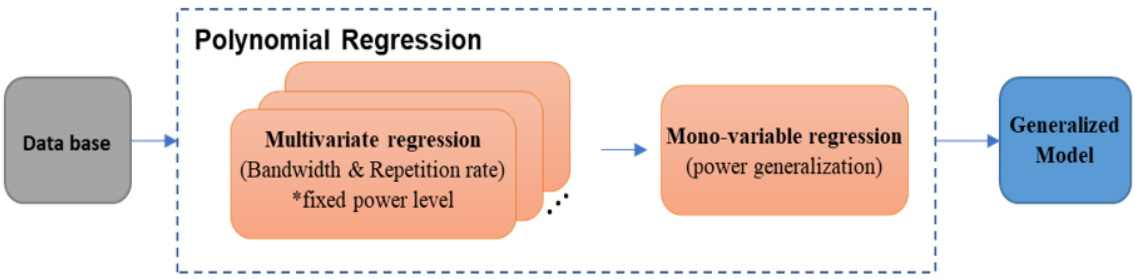

Figure 5.9: Modeling ANF parameters with a 2-level regression approach.

Figure 5.8 provides a visual representation, revealing a distinct pattern depicting the underlying relationship between the input signal features (sweep bandwidth, sweep rate,

and power) and the resulting values of the pole contraction factor (k_α) and adaptation step (δ). Here, the sweep bandwidth and sweep rate generally describe the shape of the curves, and the power level emerges to shift the curve upward or downward. Figure 5.9 presents a two-level regression approach employed for the modeling, resulting in the formation of a generalized model represented by two distinct functions.

In the first level of regression, a multivariate third-order polynomial regression is applied to model the variations of the adaptation step and the pole contraction factor. The initial regression incorporates the sweep bandwidth and sweep rate as the two input variables while keeping a constant power level. Figure 5.10 illustrates the regression curve for the adaptation step and the pole contraction factor approximating variations in the sweep bandwidth and sweep rate for a constant power level of 22 dB.

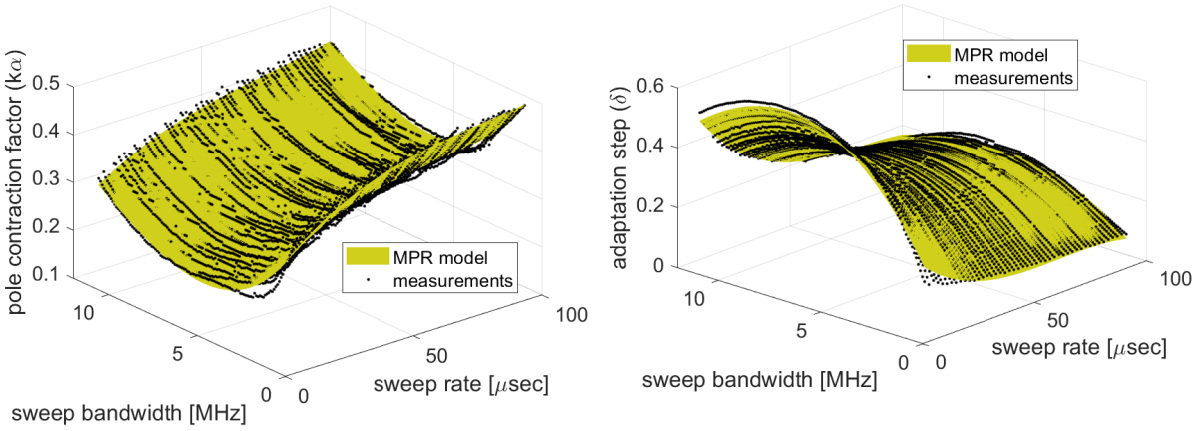

(a) (b)

Figure 5.10: Multivariate regression curves a) pole contraction factor and b) adaptation step, for a complete range of bandwidth and sweep rate with constant power level (JSR = 22dB).

Moving to the second level, a subsequent third-order regression, as illustrated in Figure 5.11, is applied to the coefficients derived from the initial regression, generalizing the variations introduced by different power levels. The resultant generalized regression models are then approximated, which consider three parameters (sweep rate, bandwidth, and power) as input features for predicting the two output variables (adaptation step and pole contraction factor).

Considering the generalized model, Figure 5.12 displays the approximated regression curves generated for complete grid points for three different power levels. To evaluate the mitigation performance, three distinct scenarios are selected, initializing ANF with the predicted values, this will be presented in the following section.

5.3.4 Results and Analysis

In this section, we aim to conduct a detailed analysis comparing the performance of ANF tuned differently using two different combinations of pole contraction factor k_α and adaptation step δ. The first set of parameters is based on the values predicted by the model earlier, while the second set is an arbitrary choice selected from the interval presented by most of the studies [118][119]. The performance includes various signal processing levels, including frequency estimation by the filter, tracking, and Carrier-to-Noise ratio level. Moreover, Key Performance Indicators (KPIs) such as accuracy, availability, and safety are also discussed to provide a positioning-level perspective. To create the chirp database, we utilized the record and playback functionality. The prerecorded IQs acquired on February 8, 2023, with GPS L1 (1575.42MHz) as the central frequency and a 15MHz

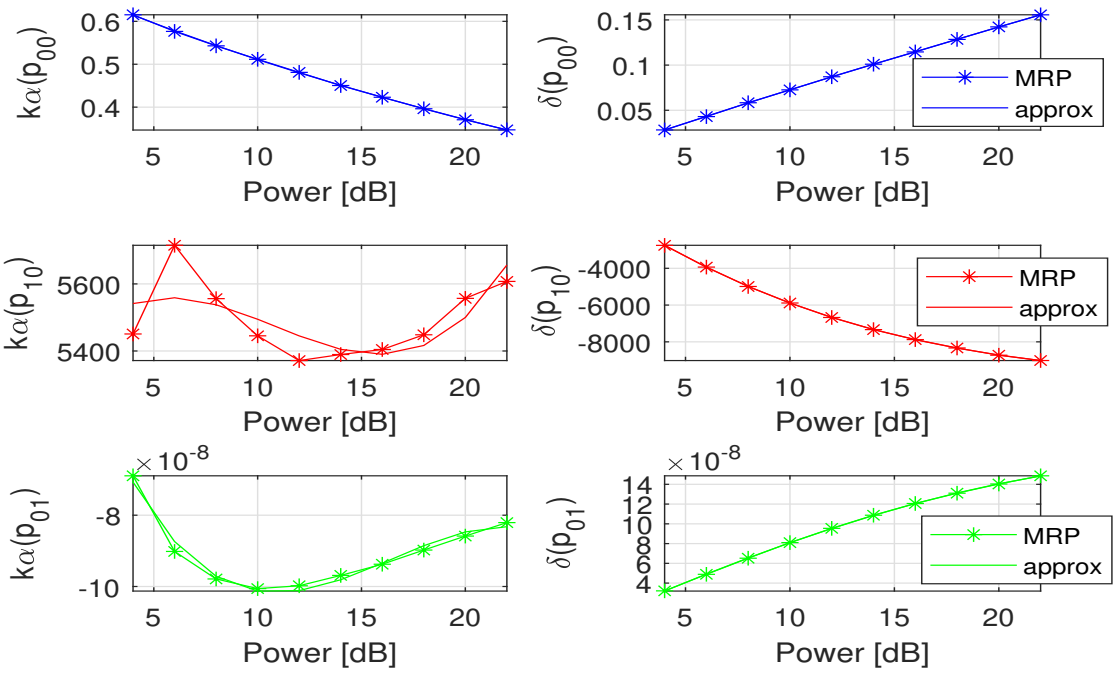

Figure 5.11: P00, P10 and P01 coefficients of pole factor and adaptation step approximated from the MRP coefficients to generalize power levels in the regression model.

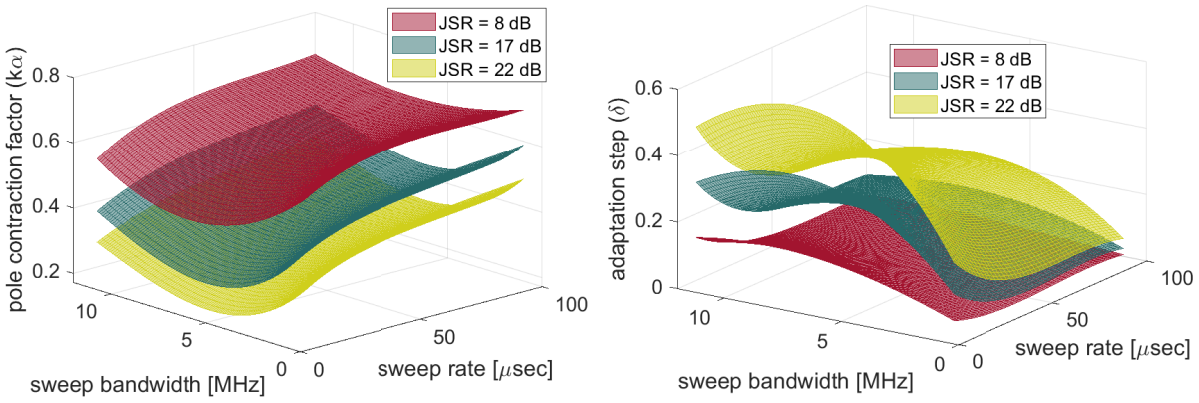

(a) (b)

Figure 5.12: Approximated curves with a) pole contraction factor and b) adaptation step from the generalized regression model for different values of sweep bandwidth and sweep rate for 3 different power levels.

sampling rate, are played back. A radio signal recorder (NI-USRP 2954R) is connected to a roof antenna, installed in a relatively open sky condition. An interference signal of 30 seconds duration is introduced at around 50 seconds to ensure normal signal tracking at the start and complete IQs are recorded back with the same system. Three chirp scenarios with slow, moderated, and fast rates along with different power levels are prepared. Table 5.1 outlines the scenarios with the predicted values of ANF parameters. For clarity, we will denote 'Set A' as the predicted combination and 'Set B' as the arbitrary parameter choice with $\delta = 0.05$ and $k_\alpha = 0.8$.

In the following, we will now analyze the impact of the parameter choice across different levels: notch frequency estimation, signal tracking, carrier-to-noise ratio and, more

Scenario	Category	Linear Chirp Parameters			Predicted parameters (Set A)	
		Bandwidth [Mhz]	Repitition rate [usec]	JSR [dB]	Pole Cont. Factor ($\widehat{k}_\alpha$)	Adapt. Step ($\widehat{\delta}$)
1	Slow	1	90	17	0.61	0.03
2	Moderate	5	50	9	0.55	0.06
3	Fast	7.5	10	14	0.32	0.26

Table 5.1: Predicted combination for three chirp scenarios under investigation.

importantly, the user KPIs.

- ***Interference frequency estimation***

  Figure 5.13 shows the notch frequency estimated by the ANF, offering a performance comparison for tracking the interference signal with Set A and Set B, for the three distinct chirp scenarios. In all the cases, Set A (depicted in a blue curve) appears to be the optimal choice for ANF. It allows the filter to closely track the interference frequency and simultaneously reduce the noise in the frequency estimation. In scenario 3, Figure 5.13 (c) demonstrates that ANF tuned with Set B (depicted in a purple curve) is less reactive to rapid variations in the fast chirp signal, taking approximately 2µs longer to reconverge to the interference frequency.

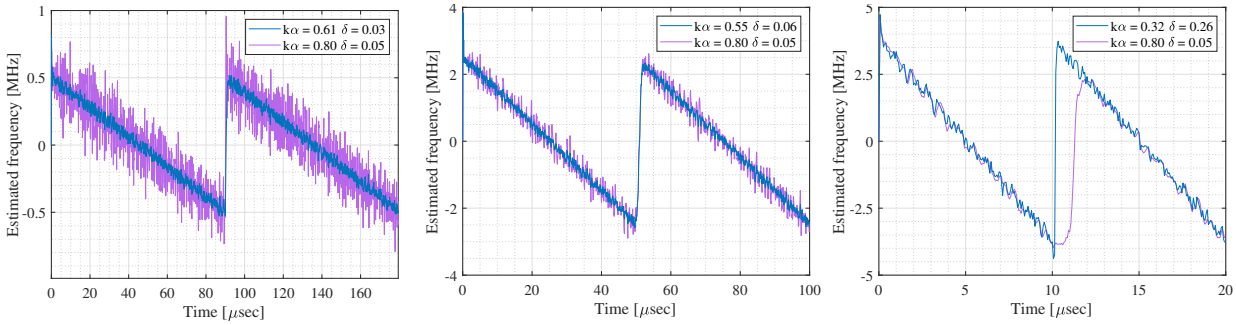

(a) (b) (c)

Figure 5.13: Notch frequency estimated by the ANF for the three scenarios with a) slow (Left), b) moderate (middle) and c) fast (right) chirp with predicted (Blue) and fixed (Purple) values of ANF parameters.

- ***Satellite signal tracking***

  Moving to satellite signal tracking, as depicted in Figure 5.14, for the three chirp scenarios, with the green curve representing tracking under nominal conditions. In each interfered case, with the emergence of the interference signal, the tracking loop shows divergence at around 50 seconds after losing the lock. Simultaneously, it starts tracking the interference signal, unreasonably increasing the CNO level to somehow similar levels as in the nominal conditions, as shown in Figure 5.15 (b) and (c). Scenario 3, featuring a fast chirp, proves to be more challenging, displaying greater deviation as it accumulates larger tracking errors.

However, applying the filtering operation using Set A (depicted in a blue curve), the tracking loop retrieves back the satellite signal with relatively less tracking noise, improving the CNO estimation in scenario 1. In the same case, Set B (depicted in a purple curve) exhibits larger fluctuations during the tracking phase, which is also visible in the CNO estimation. For scenario 2, both Set A and Set B show very similar performance in tracking and CNO level, as shown in Figure 5.14 (b) and Figure 5.15 (b) (red curves). Surprisingly, in scenario 3 with a fast-varying chirp, Set A appears to be an inadequate choice for finding a reasonable compromise for interference removal. As observed previously, a wide notch ($k_\alpha = 0.32$) with large steps ($\delta = 0.26$) seems to be better at tracking the interference frequency but fails to sufficiently suppress the interference content, probably due to the wider notch. As a result, it introduces relatively more noise in tracking the satellite signal and results in a low CNO level compared to Set B, as shown in Figure 5.14 (c) and Figure 5.15 (c).

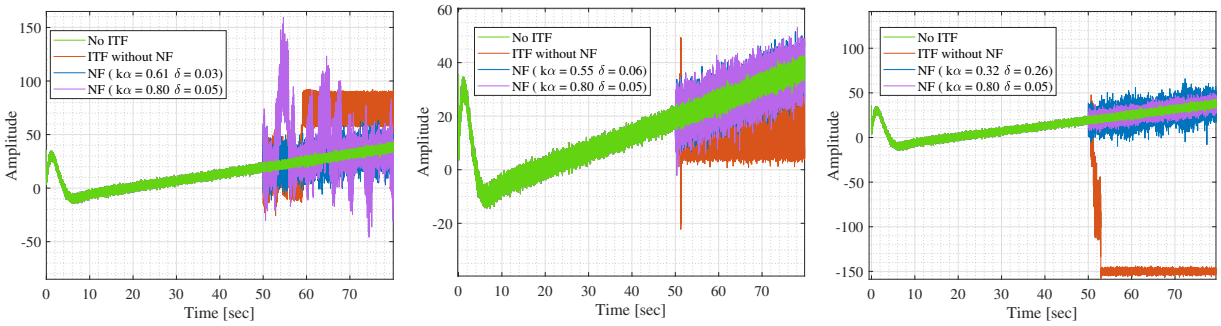

(a) (b) (c)

Figure 5.14: Tracking performance (PRN 32) in the three scenarios with a) slow (left), b) moderate (middle) and c) fast (right) chirp; reference - without interference (green), interference without mitigation (red), mitigation with ANF using predicted parameters (blue) and fixed parameters (purple).

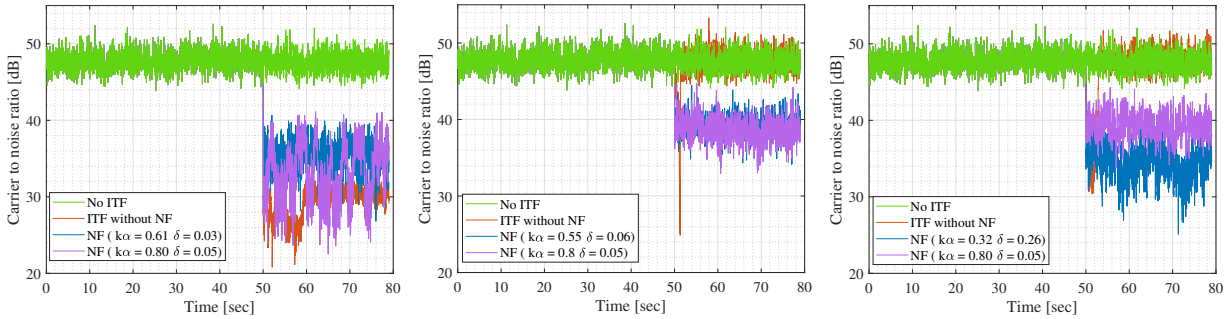

(a) (b) (c)

Figure 5.15: Estimated carrier-to-noise ratio of satellite (PRN 32) for the three scenarios with a) slow (left), b) moderate (middle) and c) fast (right) chirp; reference - without interference (green), interference without mitigation (red), mitigation with ANF using Set A (blue) and Set B (purple).

- ***Positioning level***

Now we evaluate the results at the position level, presenting the impact of interference and the effectiveness of mitigation on KPIs such as accuracy, availability, and safety. As a reminder, we utilize the Stanford diagram for a comprehensive evaluation of KPIs, employing the Weighted Least Square (WLS) algorithm with a hybrid weighting model (product of Carrier-to-Noise ratio and sine-elevation model), as

detailed in Chapter 2, to compute the positioning solution and the error bound, or the protection level.

In Figure 5.16, the Stanford diagram presents positioning performance under nominal conditions, excluding the interference instances from the recorded data. This diagram serves as a reference for comparison, indicating the maximum achievable performance expected from the same receiver configuration under nominal conditions. In nominal conditions, all the points appear in normal operation (white), with zero instances of unavailability (yellow) and HMI (red). Figure 5.17 shows the impact of interference in the three cases with slow, moderate, and fast chirps. Here, 62.25 % of points in the normal operation (white) represent interference-free instances, while the remaining 37.5 % represent 30 seconds of interference duration. In all cases, interference adversely impacts KPIs, significantly reducing positioning accuracy with HPE $> 50m$. Furthermore, unbounded errors, represented by HMI (red), completely expose the positioning system vulnerability, necessitating a mitigation strategy for positioning safety.

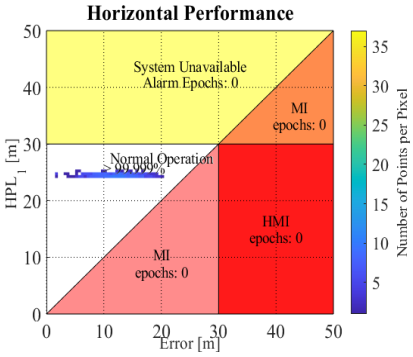

Figure 5.16: Stanford diagram representing positioning performance in nominal conditions

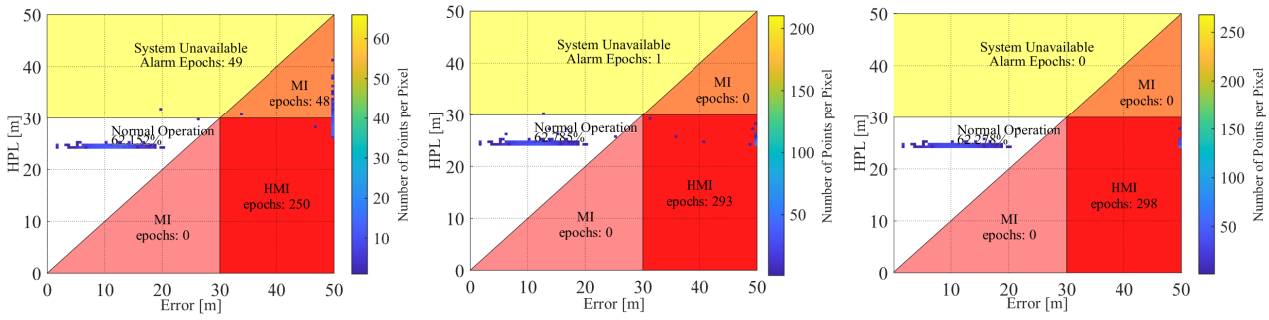

(a) (b) (c)

Figure 5.17: Stanford diagram representing positioning performance for the three cases with a) slow, b) moderate and c) fast chirp before mitigation.

Moving to Figure 5.18 depicts the positioning performance of scenario 1 (bandwidth = 1 MHz, repetition rate = 70 μ sec, and JSR = 17 dB) after applying ANF mitigation with Set A (left) and Set B (right) parameters. Mitigation using Set A parameters appears to significantly improve positioning performance compared to Set B parameters. It reduces positioning error (HPE <28 m) and increases normal operation (white) to approximately 83%, with 130 instances of unavailability (yellow) and 1 MI (pink). However, Set B does not retrieve the same level of performance, exhibiting relatively lower positioning accuracy, with many instances of HPE exceeding 50 m. Additionally, it fails to ensure complete positioning safety with 135 HMI (red), 143 unavailability, and 112 MI (pink & orange) instances.

In scenario 2, as shown in Figure 5.19, both parameter combinations Set A and Set B demonstrated similar performance. Nevertheless, Set A still exhibits relatively better performance with around 96% of points in normal operation (white), 30 unavailable, and 0 HMI instances, while Set B has approximately 93% points in normal operation with 49 unavailability, 1 MI, and 3 HMI instances.

Figure 5.20 illustrates the positioning performance in the third scenario with ANF mitigation using Set A and Set B. In this case, Set A parameters could not improve as much as in the previous scenarios, with around 75 % normal operation (white), 127 unavailable (yellow), 50 MI (pink & orange), and 60 HMI instances, respectively. However, Set B performs better with approximately 95% normal operation (white), 25 unavailable (yellow), 11 MI (pink & orange), and 9 HMI instances.

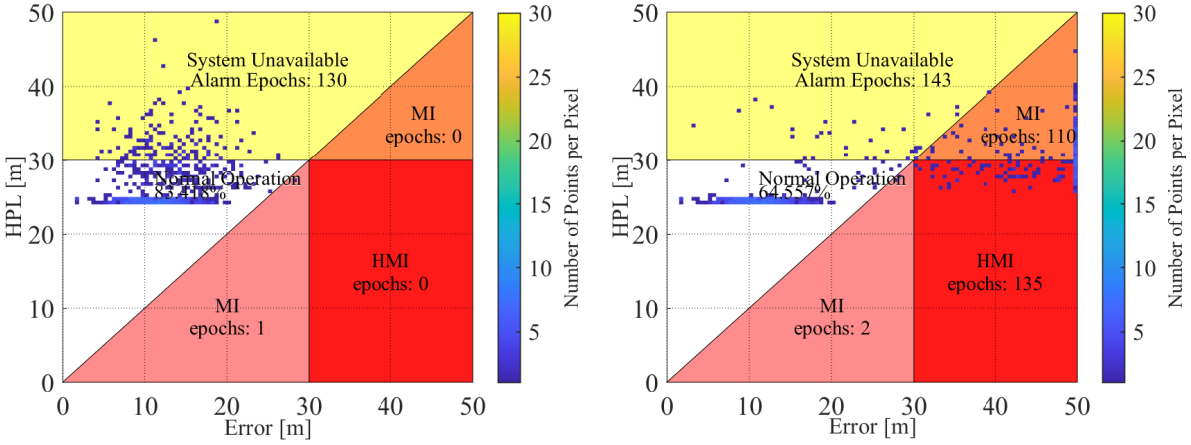

Figure 5.18: Stanford diagram representing performance after applying mitigation in the first scenario with slow varying chirp (bandwidth = 1MHz, repetition rate = 90us and JSR = 17dB) using ANF a) Set A ($\delta = 0.03$ and $k_\alpha = 0.61$) and b) Set B ($\delta = 0.05$ and $k_\alpha = 0.8$).

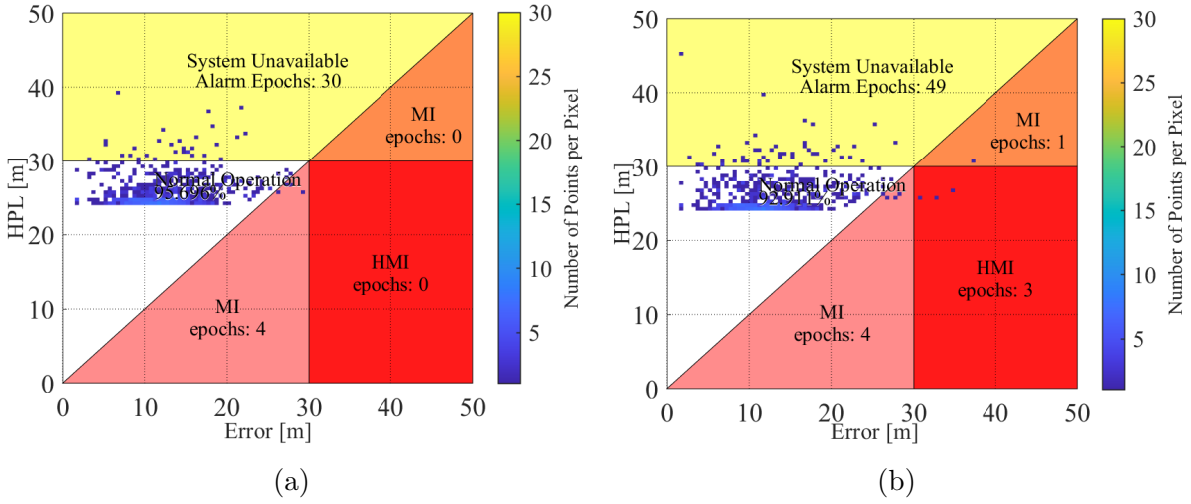

Figure 5.19: Stanford diagram representing performance after applying mitigation in scenario 2 with moderate chirp (bandwidth = 5MHz, repetition rate = 50us and JSR = 9dB) using ANF a) Set A ($\delta = 0.06$ and $k_\alpha = 0.55$) and b) Set B ($\delta = 0.05$ and $k_\alpha = 0.8$)

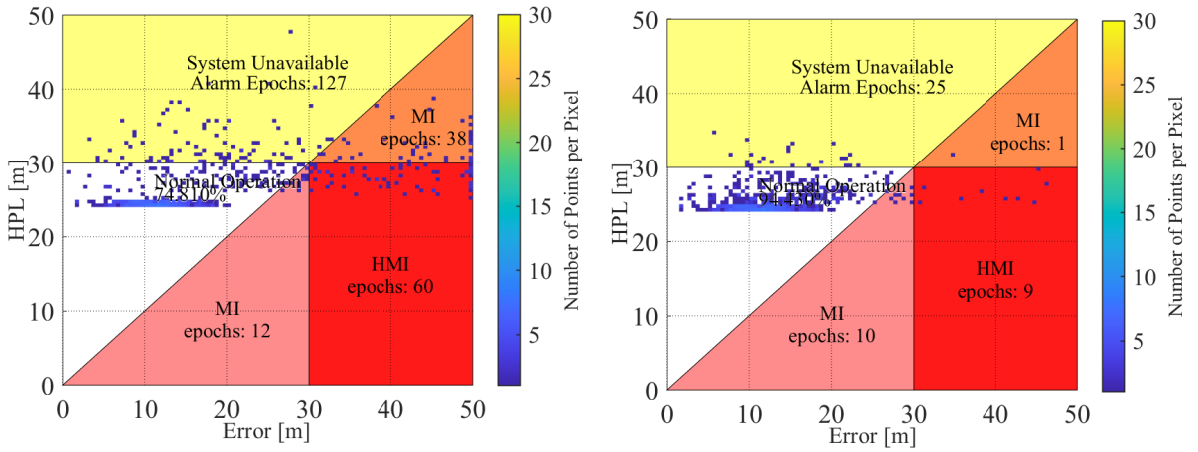

Figure 5.20: Stanford diagram representing performance after applying mitigation in the third scenario with fast varying chirp (bandwidth = 7.5 MHz, repetition rate = 10 μ sec and JSR = 14 dB) using ANF combination a) Set A ($\delta = 0.26$and $k_\alpha = 0.32$) and b) Set B ($\delta = 0.05$ and $k_\alpha = 0.8$)

5.3.5 Summary of results with other signal-level (precorrelation) metrics

The proposed precorrelation level approach, although it requires a substantial number of simulations to create models for selecting ANF tunable parameters, proved to be very effective in the suppression of interference in scenarios 1 and 2. It successfully eliminated all instances of HMI events and reduced unavailability compared to naively selected values of the pole contraction factor ($k\alpha = 0.8$) and adaptation step ($\delta = 0.05$). However, it underperformed for scenario 3, which involved a fast-varying chirp and resulted in a significant number of HMI instances. A further investigation revealed that RMSE, despite covering the complete interference bandwidth, could not find a needed compromise in removing necessary unwanted content from the signal. On the other hand, with a naively chosen combination, the ANF took longer to converge but efficiently removed the unwanted content with a narrow notch. This seems to be a compromise, leaving some interference residue on the far end and precisely targeting interference close to the central frequency, which proved to be very effective.

Similarly, our investigation encompassed various other metrics for suitable labeling. These metrics include Cross-Power Spectral Density (CPSD), Peak Signal-to-Noise Ratio (PSNR), and Mean Absolute Deviation (MAD). The description of each of these metrics is as follows:

Cross-correlation spectral density:

The Cross-Power Spectral Density (CPSD) serves as a statistical measure that characterizes the frequency domain relationship between two signals. It specifically describes how the power of the reference signal is correlated with the filtered signal. Mathematically, it is represented as the Fourier transform of the cross-correlation function between two signals. The cross-correlation function is given as:

$$R_{\mathrm{XY}}[m] = \sum_{n=0}^{N-1} X[n]Y^*[n-m] \tag{5.5}$$

Here, m denotes the time shift, X is the reference signal and Y^* is the complex conjugate of the filtered signal. The discrete Fourier transform of R_{XY} also referred to as

CPSD, is given as:

$$S_{\mathrm{XY}}[k] = \sum_{m=0}^{N-1} R_{\mathrm{XY}}[m] \cdot e^{-j\omega_k m} \tag{5.6}$$

Here, S_{XY} represents the cross-correlation correlation spectral density, and ω_k corresponds to the digital frequency of the signal.

Peak Signal-to-Noise Ratio (PSNR):

The term Peak Signal-to-Noise Ratio (PSNR) is the metric that quantifies the relationship between the maximum amplitude of the signal and the mean squared error of the time series signal. The PSNR is expressed as:

$$PSNR = 10.\ log\ (\frac{V_{p-p}^2}{\mathrm{MSE}}) \tag{5.7}$$

where the mean squared error (MSE) is given as:

$$MSE = \frac{1}{N} \sum_{n=1}^{N} (X[n] - Y[n])^2 \tag{5.8}$$

Here, MSE represents the mean squared error, V_{P-P} the peak-to-peak amplitude, X is the reference signal and y is the filtered signal.

Mean Absolute Deviation (MAD):

The Mean Absolute Deviation (MAD) serves as a statistical metric that quantifies the average absolute difference between each sample within the given dataset as the mathematical mean of the entire signal. The MAD can be expressed as:

$$MAD = \frac{1}{N} \sum_{n=1}^{N} |X[n] - mean(X[n])| \tag{5.9}$$

Here, $X[n]$ represents each sample and N is the total number of samples in the dataset.

These three metrics are chosen to determine the optimal combination and selection based on finding the closest match to the reference signal by comparing the metric values of the reference and the filtered signals. A total of nine distinct chirp scenarios are selected from the database, each with the same power level (JSR = 10 dB). In figure 5.21, the scenarios are numbered in the bandwidth versus sweep rate matrix. The process outlined in Section 5.3.2 is then repeated to determine a single matrix that unanimously provides the optimal solution among others. The chosen parameter combinations are applied to fine-tune the notch filter for the specific scenario during the mitigation process, and then the navigation solution is estimated using a GPS software receiver. Figure 5.21 summarizes the outcome from these metrics, presenting the position errors metric after processing a filtered signal of 10 seconds. Notably, it becomes evident that there is not a single metric that can be universally considered as the optimal candidate across all scenarios. This observation suggests that achieving optimal combination selection using a criterion at the precorrelation level is at least a highly challenging task, prompting exploration of ANF parameters at alternative levels, which will be presented in the subsequent section.

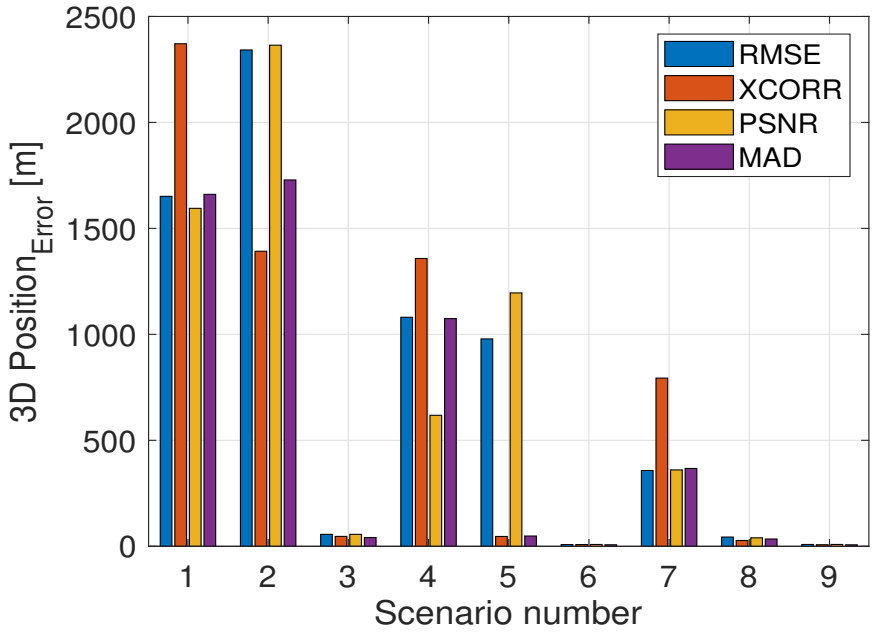

Figure 5.21: 3D positioning accuracy of different signal level criterion

5.4 Filter Parameterization with Acquisition Level Labeling in Final Trail

In the earlier investigations, labeling at the precorrelation level did not emerge as a suitable choice, leading to a reevaluation of our approach. In this section, we will explore the potential of acquisition-level parameter selection for data labeling. To achieve this, we introduced two major modifications to the previously presented approach, as detailed in Section 5.3. Firstly, the conventional RMSE criterion will be replaced with a more tailored acquisition-level criterion, as depicted in Figure 5.22. This modification aims to construct the labeling process with an acquisition-level approach, indicating the revival of the satellite acquisition following interference mitigation with the chosen ANF parameters. Secondly, a novel dimension is introduced to our methodology by incorporating a machine learning approach for modeling the selected acquisition-level parameters. Leveraging machine learning facilitates the integration of this solution into a cascaded system with prerequisite steps, including interference detection, classification, and characterization, drawing upon numerous ML-based approaches that have already been explored in the literature.

5.4.1 Acquisition Level labeling

In Chapter 3, we have discussed signal acquisition, a process that employs a correlation function to align the received signal with a locally generated replica. This method helps in determining the signal parameters, such as code and carrier offset, of the visible satellites. It is mainly realized by identifying an emerging correlation peak in the signal search space, as observed in previous investigations. However, interference can introduce ambiguities, making it challenging to accurately identify the correct correlation peak, which may become less distinct or may even disappear, as some of the examples are shown in Figure 5.23. In our context, we aim to establish an acquisition level criterion to determine the optimal ANF combination. The selection aims to obtain a relatively cleaner acquisition search space with a distinct correlation peak. Here, using simple metrics such

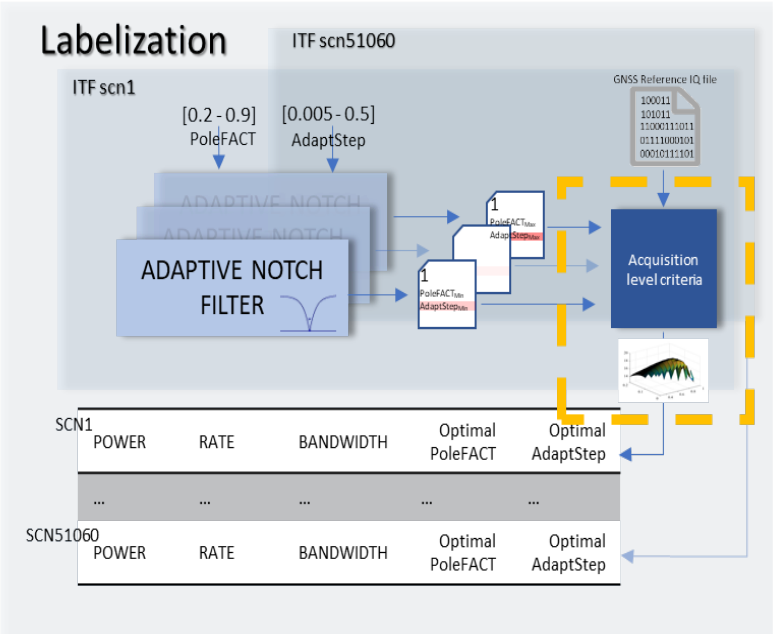

Figure 5.22: labeling process with acquisition level criterion.

as *alpha-mean* (which is the ratio of correlation peak value and the noise floor) can be deceptive, particularly because interference may introduce additional energy into the signal search space. A correlation function is computed, processing a 10 ms filtered signal with a particular parameter combination. The following rules are applied to remove any possibility of ambiguities in the signal search space.

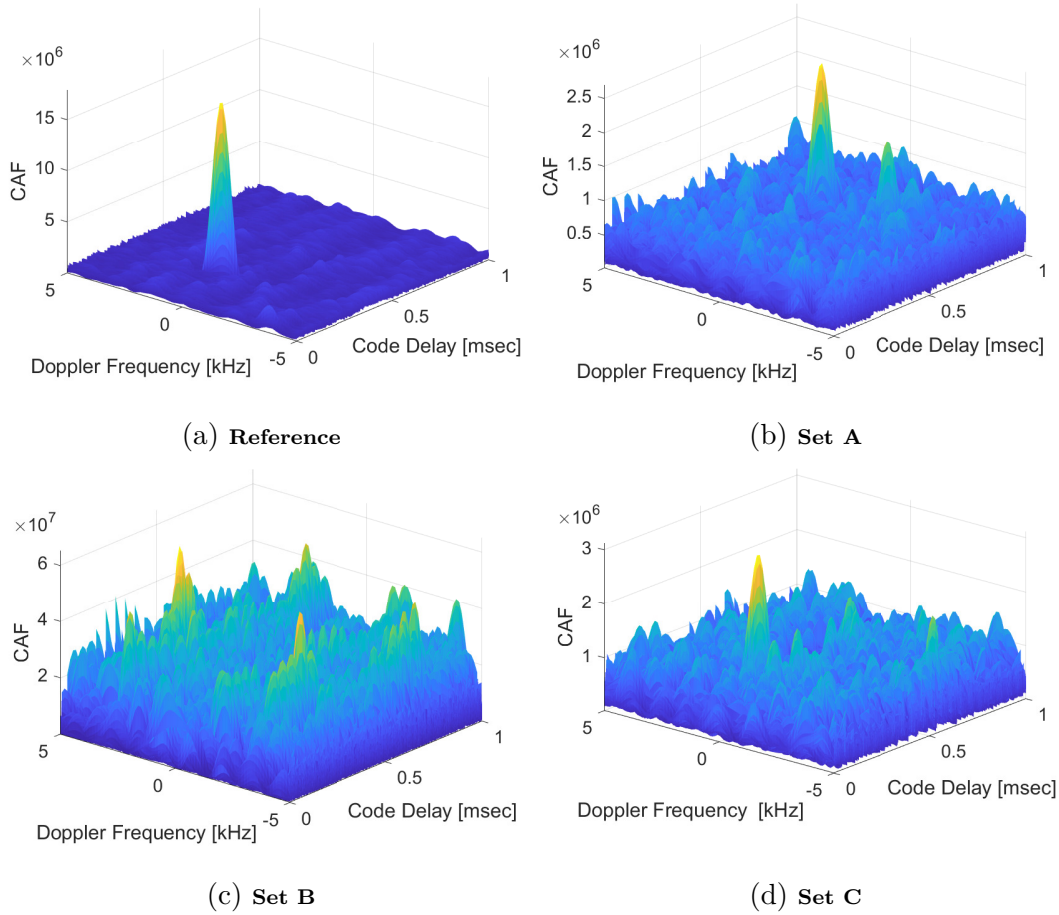

(a) **Reference** (b) **Set A**

(c) **Set B** (d) **Set C**

Figure 5.23: Some examples of signal search space with different sets of parameter combinations.

- **Rule A: Peak location determination**

In the initial stage, the process involves determining the peak position, or equivalently, the cell location, following the implementation of ANF with a specific parameter combination. Subsequently, given that the peak location under interference-free conditions is known, the distance between the reference cell and the newly estimated cell is calculated, as illustrated in Figure 5.24. Ideally, it is expected for a peak to emerge in the same cell and the resulting distance to remain zero. However, a margin is maintained, and consideration is given to a certain number of nearby cells where the peak could potentially emerge after the mitigation process.

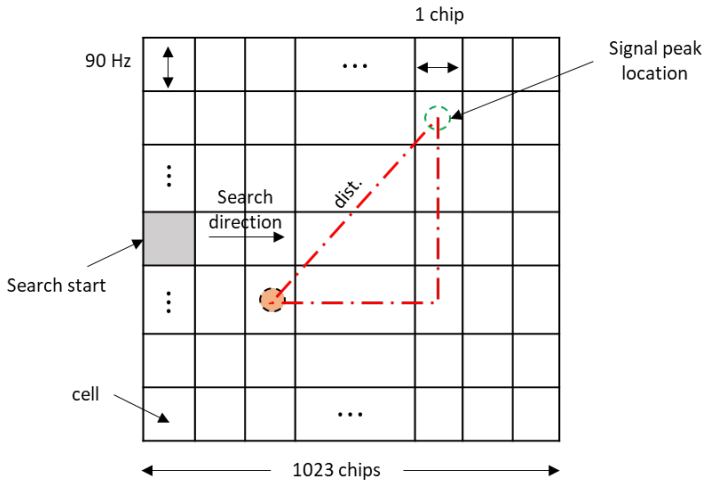

Figure 5.24: Signal search grid with distance estimation between the cells

- **Rule B: Relative peak separation**

Following the peak position rule, the next step is to determine the peak metric by dividing the maximum correlation value across the entire signal search space by the second-highest peak value. The ratio serves as a measure indicating the relative difference in magnitude between the highest obtained value and the other correlation components.

- **Rule C: Alpha-mean computation**

In the subsequent step, the alpha-mean metric is computed, representing the ratio between the peak value and the average noise floor in the signal search space, as depicted in Figure 5.25. The alpha-mean can be expressed as:

$$\alpha_{\text{mean}} = 20\ log\left(\frac{X_p}{E}\right) \tag{5.10}$$

Here, X_p represents the correlation peak value and E represents the average of the signal search space noise floor.

- **Rule D: Parameter Selection, Maximum average peak metric**

In the final step, the alpha-mean values of the satellites for which the peak metric (Rule B) exceeds the threshold are considered. The average value is then computed and the combination providing the highest value is considered to select the optimal parameter for tuning ANF, thereby effectively suppressing the given interference scenario. Figure 5.26 shows the outcome of the acquisition-level criterion presented previously for a given

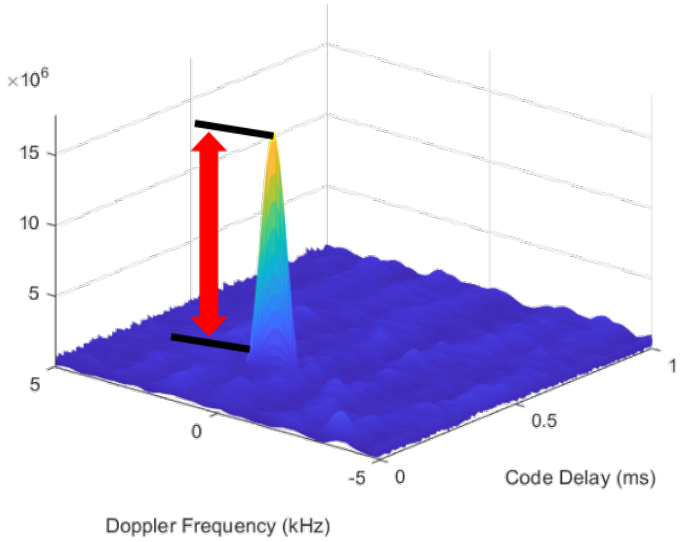

Figure 5.25: alpha-mean metric, an estimate of the peak-to-noise floor ratio

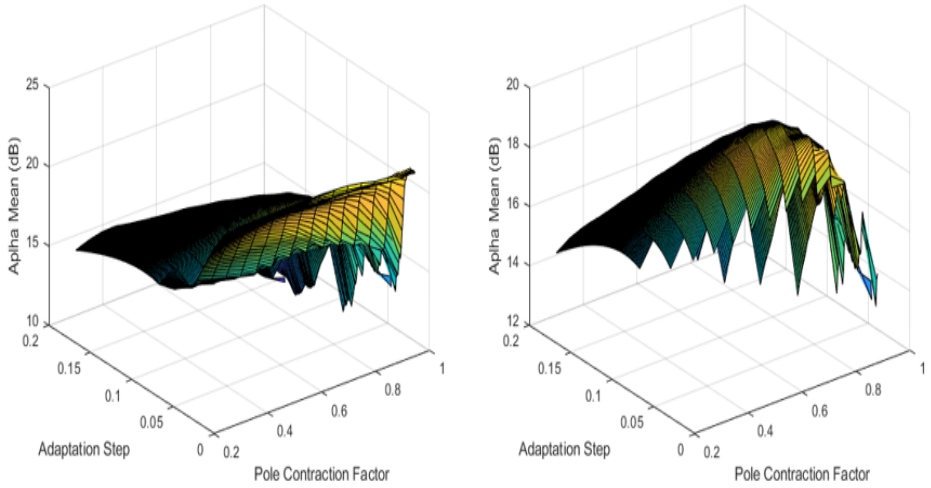

Figure 5.26: Parameter search grid of a given scenario with a classical alpha mean metric (left) and constrained logic following the defined rules (right)

interference scenario. The parameter search grid is depicted with a simple alpha-mean metric on the left and constrained logic following Rule A to Rule D on the right. With the application of constrained rules, a distinct global maximum emerges, indicating the optimal parameter combination with the highest average alpha-mean value for the given scenario. Similarly, the same approach is repeated for the remaining cases to determine the adaptive step and pole contraction factor to label the database.

5.4.2 Regression with Neural Network (NN) Technique

The application of Machine Learning (ML) algorithms is becoming increasingly popular in numerous fields, including GNSS, with a primary aim to enhance the resilience of location-based services. ML algorithms are predominantly used for classification, clustering, forecasting, and anomaly detection to overcome the challenges inherent in traditional GNSS systems [74][75][76]. By exploring hidden dependencies in the data or pattern, ML models are developed to make predictions and decisions. Numerous ML approaches exist,

designed for specific tasks and datasets. These techniques include ***supervised learning***, where the algorithm is trained on labeled data; ***unsupervised learning***, which does not require data labels and is employed for pattern identification; ***semi-supervised learning***, which combines both supervised and unsupervised learning; ***reinforcement learning***, where algorithm training also involves interaction with an environment and network feedback; and ***deep learning*** involves complex neural networks to extract complicated features from the data.

Regression is a type of supervised learning that is used to predict a continuous output variable based on one or more predictor variables. Here, this is accomplished through the Neural Network (NN) approach, where Multilayer Perceptron (MLP) forms the fundamental basis. It consists of components such as an input layer, hidden layers, an output layer, activation functions, and a collection of weights and biases.

- **Input layer**

The primary layer in ML architecture is the input layer. It consists of neurons corresponding to the number of input features in the data, where each neuron represents a distinct feature.

- **Hidden layer**

The intermediate layers positioned between the input and output layers are referred to as hidden layers. These layers are responsible for extracting and learning complex patterns and relationships within the data. The neurons of each layer are interconnected with the neurons of the other layers. The selection of the number of neurons and hidden layers serving as hyperparameters is selected depending on the complexity of the problem and is typically determined during the model design phase.

- **Output layer**

The output layer contains neurons matching the number of output parameters. This layer provides predictions based on the learned patterns and relationships within the data.

- **Activation function**

Activation functions are the mathematical operations that determine the output of a given node or neuron. Basically, the neuron computes the weighted sum of its inputs, adds bias and then feeds the outcome to the activation function to yield the final output, a process illustrated in Figure 5.27 while the activation functions, including Sigmoid, Hyperbolic tangent, ReLU, and SoftMax are illustrated in Figure 5.28. Other hyperparameters, like learning rate, batch size, epochs, and loss function, also influence the Neural Network's performance.

The learning rate controls the optimization algorithm step size, affecting the speed and stability. The batch size indicates the number of training samples in each iteration. The number of epochs specifies the number of iterations to completely process the training dataset, and the loss function measures the difference between the model predictions and the actual values. In network design, hyperparameter tuning has a significant impact on performance. Therefore, during the training process, several combinations are tested while changing the number of neurons, number of layers, and activation functions, as presented in Table 5.2. In our realization, we used the Keras library in Python to design the neural network model.

Figure 5.29 illustrates the loss function for different hyperparameter configurations tested for training the model along with the settling time given by the epoch. Among

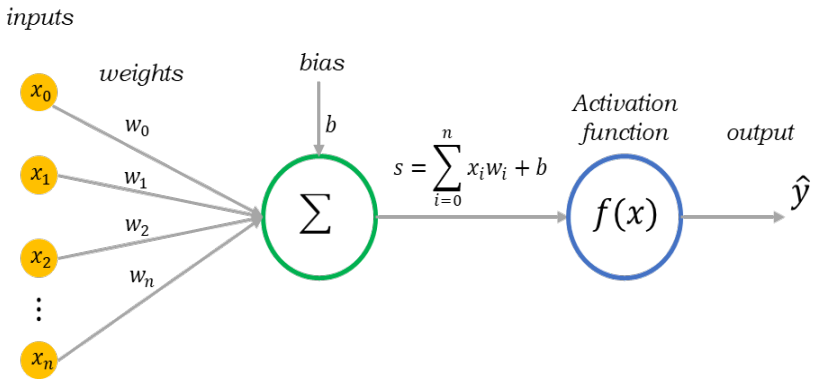

Figure 5.27: An illustration of the node output.

Sigmoid	**Tanh**	**ReLU**	**SoftMax**
$g(z) = \frac{1}{1+e^{-z}}$	$g(z) = \frac{e^{z}-e^{-z}}{e^{z}+e^{-z}}$	$g(z) = max(0,z)$	$\frac{e^{z_i}}{\sum_{j=1}^{K} e^{z_j}}$
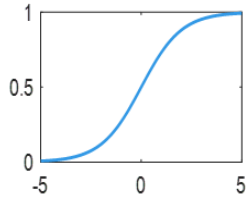	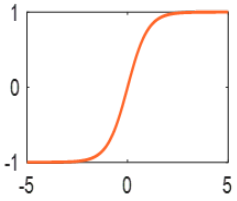	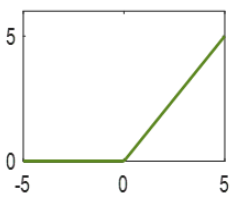	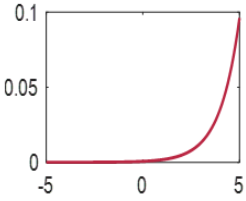

Figure 5.28: Activation functions, Sigmoid, Tanh, ReLU and SoftMax.

Table 5.2: Hyperparameters used for the training process.

Hyper-parameter	Learning Rate	0.001
	Number of Layers	[2, 3, 4, 5, 6]
	Number of Neurons	[24, 48, 64, 128, 256]
	Activation Functions	ReLU, Sigmoid and SoftMax
	Batch Size and Number of Epochs	10 (batch size) 50 (epochs)
Evaluation Metric	Loss Function	Mean Absolute Error (MAE)

the various combinations explored, both the Sigmoid and Rectified Linear Unit (ReLU) activation functions demonstrate effectiveness in minimizing the training loss and appear to be a suitable choice for the neural network architecture. However, the SoftMax function displayed an unstable trend loss function while changing the number of layers and number of neurons per layer. This led to a rationale for excluding SoftMax during the network design phase. After careful consideration, we selected the ReLU activation function, consisting of 4 hidden layers with 64 neurons per layer, a neural network architecture shown in Figure 5.30. Subsequently, 80% of the database samples are trained on this network, and the trained model is later employed for the prediction tasks.

Now, the trained Multilayer Perceptron model is prepared to provide predictions related to the choice of Adaptive Notch Filter (ANF) parameters which will be used for the suppression of the interference signal. The mitigation performance will be analyzed in the following section.

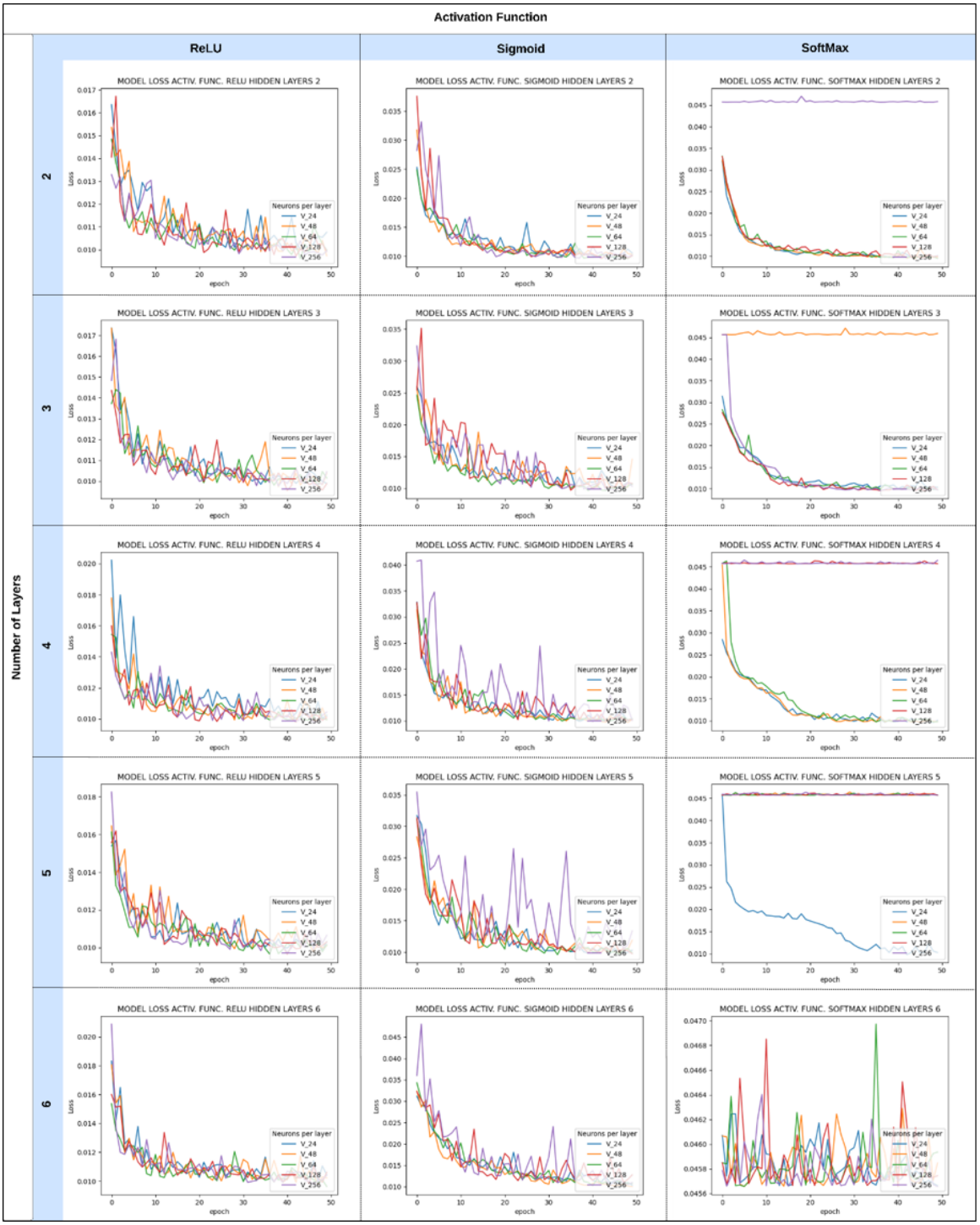

Figure 5.29: Loss functions for hyperparameter tuning.

5.4.3 Performance Analysis

This section presents the performance of acquisition-level parameter selection by comparing the results obtained from the parametric search at the position level. Notably, in the position-level selection, a similar approach has been adopted as presented in Section 5.3.2 and Section 5.4.1. The only distinction being made is that this time the parametric sweep is exclusively carried out for the three scenarios under investigation and in case the optimal parameter is chosen based on the resultant 3D positioning error. Although labeling the complete database in this manner would have been a preferable choice, however, it proved to be excessively time-consuming and it was therefore not adopted. In the result analysis, the position-level results are intuitively considered as the reference for the

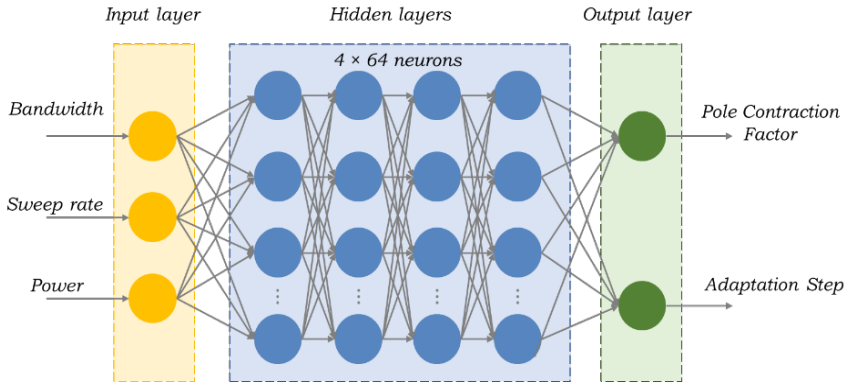

Figure 5.30: Neural Network architecture for regression.

performance comparison. Following this, the signal filtered using the parameter predicted from the acquisition-level approach is then processed with a GNSS software receiver and these results will be presented in the following discussion. The position-level parameters, along with acquisition-level predictions from the presented model are listed in Table 5.3. From now onwards, the position level parameter combination will be referred to as 'Set A' and acquisition level predictions indicated by 'Set B'.

Table 5.3: Parameter choices at the position and acquisition level for different types of chirp signals

Scenario	Category	Linear Chirp Parameters			Position-level Selection (Set A)		Acquisition-level Prediction (Set B)	
		Bandwidth [MHz]	Repitition rate [µsec]	JSR [dB]	Pole Cont. Factor ($\widehat{k}_\alpha$)	Adapt. Step ($\widehat{\delta}$)	Pole Cont. Factor ($\widehat{k}_\alpha$)	Adapt. Step ($\widehat{\delta}$)
1	Slow	1	90	17	0.65	0.03	0.7	0.028
2	Moderate	5	50	9	0.75	0.02	0.8	0.009
3	Fast	7.5	10	14	0.8	0.05	0.7	0.060

Now, we will assess the effectiveness of the predicted parameter combination across different levels of the receiver processing chain. This analysis includes evaluating ANF signal tracking capability, as well as examining satellite signal tracking and Carrier-to-Noise ratio and ultimately positioning Key Performance Indicators (KPIs) using the Stanford diagram.

- Interference Signal Tracking

Figure 5.31 depicts the notch frequency estimation for the three scenarios with slow, moderate and fast chirp signals. In Scenario 1, characterized by a slow chirp, both parameter choices Set A and Set B exhibit very similar performance in tracking the interference frequency. In Scenario 2, for a moderate chirp, both combinations appear to be relatively slow in following the interference frequency, with Set B notably 5 µsec slower compared to Set A. Similarly, in Scenario 3 with a fast chirp, both parameter choices show a very similar trend, making notch filter less reactive to the rapid variations during the transition period.

- Satellite Signal Tracking

Figure 5.32 depicts the signal tracking performance for the three chirp scenarios, with the green curve representing the reference trend under nominal conditions. In each scenario, the satellite signal is overpowered by interference, leading to the divergence of the

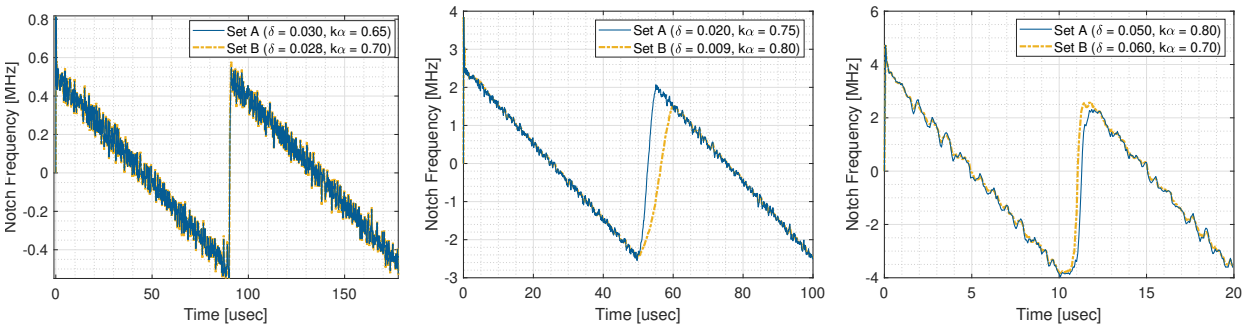

(a) (b) (c)

Figure 5.31: Notch frequency estimated by the ANF for the three scenarios with a) slow (Left), b) moderate (middle), and c) fast (right) chirp with Set A (selection - position level) and Set B (prediction-acquisition level) values of ANF parameters.

tracking loop at around 50 seconds with the introduction of the jamming signal. Consequently, the receiver starts following the interference signal after losing the lock, resulting in an unusual increase in CNO level after a brief drop, reaching an equivalent level as in the normal condition, as shown in Figure 5.33 (b) and (c).

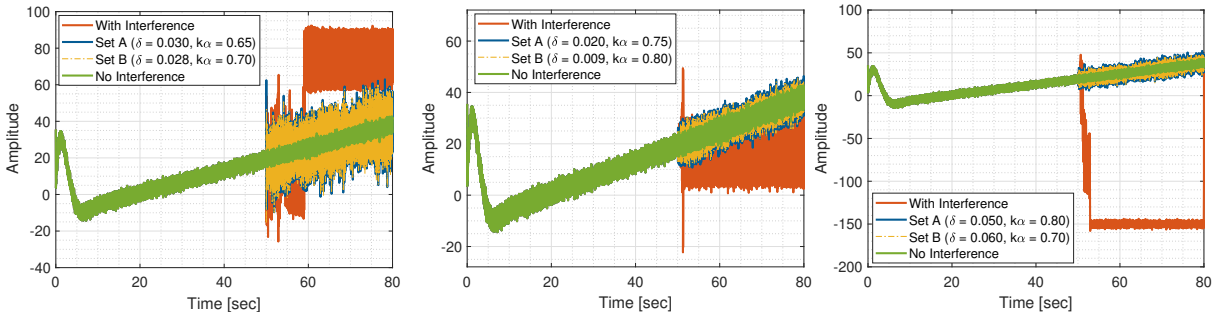

(a) (b) (c)

Figure 5.32: Tracking performance (PRN 32) in the three scenarios with a) slow (left), b) moderate (middle), and c) fast (right) chirp; reference – no interference (green), interference without mitigation (orange), after suppression with ANF using 'Set A' parameters (selection - position level) and 'Set B' (prediction acquisition level) parameter.

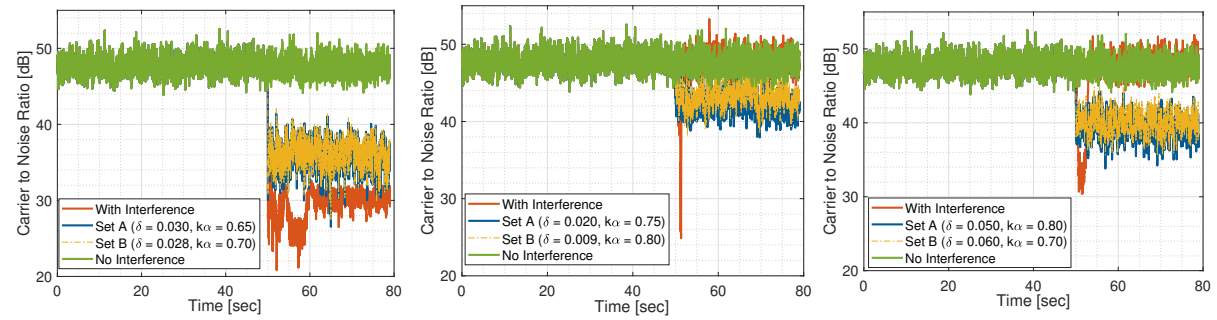

(a) (b) (c)

Figure 5.33: Estimated carrier-to-noise ratio of satellite (PRN 32) for the three scenarios with a) slow (left), b) moderate (middle), and c) fast (right) chirp; reference - no interference (green), interference without mitigation (orange), after suppression with ANF, using 'Set A' parameters (selection - position level) and 'Set B' (prediction acquisition level) parameter.

Following the application of the ANF filter, in each scenario, 'Set B' shows slightly better performance compared to 'Set A'. In both cases, the mitigation process allows the

receiver to continuously track the satellite signal with some noise. In Scenario 1, featuring a slow chirp, there is relatively higher tracking noise, as shown in Figure 5.32 (a), resulting in an average CNO of 36 dB, as depicted in Figure 5.33 (a). In Scenarios 2 and 3, the signal tracking is performed with a slight increase in the tracking noise as shown in Figure 5.32 (b) and (c), leading to further improvement in the average CNO, as shown in Figure 5.33 (b) and (c),

Now we evaluate the results at the positioning level, presenting the impact of interference and the effectiveness of the mitigation on the KPIs such as accuracy, availability, and safety. As a reminder, we utilize the Stanford diagram for the comprehensive evaluation of KPIs, employing the WLS algorithm with a hybrid model (product of CNO and elevation model) to compute the positioning solution and its associated error bound or protection level.

In Figure 5.34, the Stanford diagram reminds the positioning performance under nominal conditions, considering only the interference-free instances. This diagram serves as a reference, indicating the maximal achievable performance expected from the receiver with the given configuration under nominal conditions. In normal conditions, all the points appear in the normal operation (white), with zero instances of unavailability (yellow) and HMI (red).

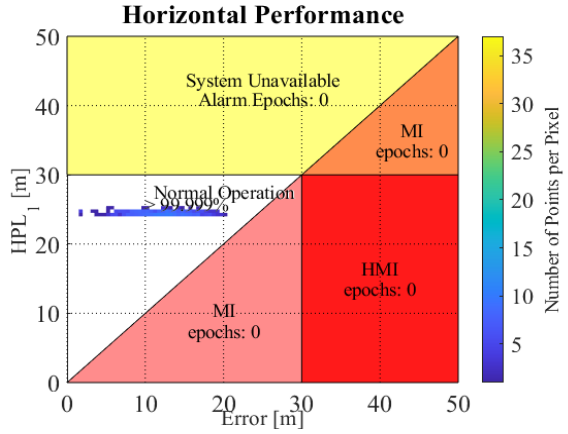

Figure 5.34: Stanford diagram representing positioning performance in nominal conditions.

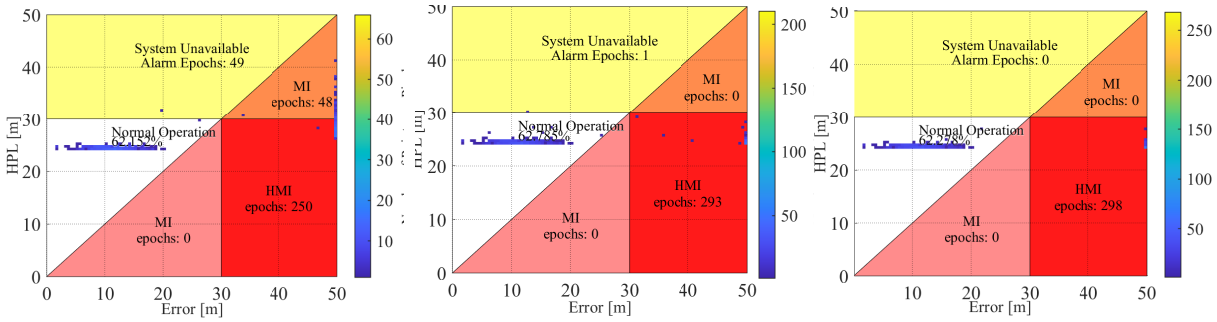

(a) (b) (c)

Figure 5.35: Stanford diagram representing positioning performance for the three cases with a) slow, b) moderate, and c) fast chirp before mitigation.

Figure 5.35 shows the impact of interference in the three cases with slow, moderate and fast chirps. Here, 62.25% of the points in the normal operation (white) represent interference-free instances, while the remaining 37.75% represent 30 seconds of interference duration. In all cases, interference adversely impacts KPIs, significantly reducing positioning accuracy with HPE >50m. Furthermore, unbounded errors, represented by

HMI (red), indicate the positioning system vulnerability and require a mitigation strategy for safe positioning.

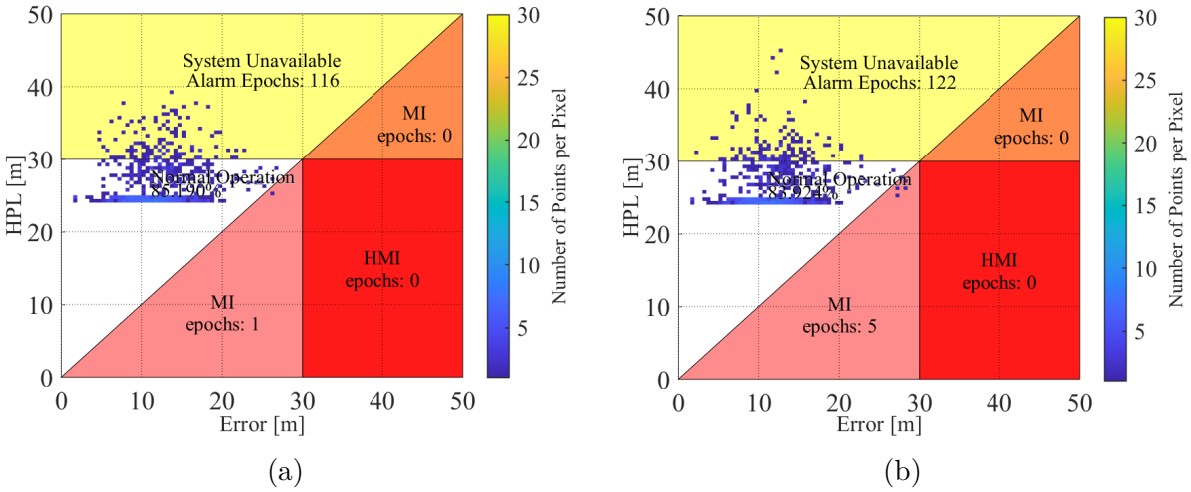

Figure 5.36: Stanford diagram representing performance after applying mitigation for Scenario 1 (Slow chirp) using ANF a) Set A – Position Level Selection and b) Set B – Acquisition Level Prediction.

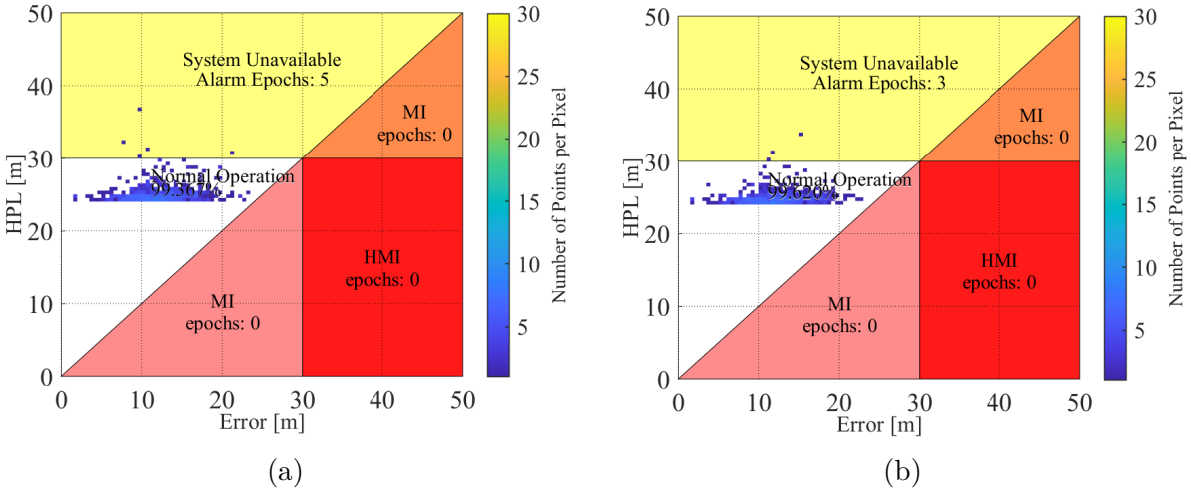

Figure 5.37: Stanford diagram representing performance after applying mitigation for Scenario 2 (Moderate chirp) using ANF a) Set A – Position Level Selection and b) Set B – Acquisition Level Prediction.

Moving to Figures 5.36, 5.37 and 5.38, we can observe positioning performance following the mitigation process for the three scenarios with a slow, moderate and fast varying chirp respectively. In each scenario, the two-parameter combinations, Set A and Set B, demonstrated very similar performance, resulting in an increase in normal operations and the complete removal of HMIs except for the last scenario. In Scenario 1 (bandwidth = 1 MHz, repetition rate = 70 us, and JSR = 17 dB), both combinations lead to a reduction in positioning error (HPE $<$ 30). The noticeable decrease in CNO, as shown in Figure 5.33, contributes to an increase in the protection level, leading to some unavailable instances. Set B parameter results in a significant increase in the normal operation (white) to more than 83%, with 122 instances of unavailability, 5 MI (pink), and 0 HMI. In comparison, Set A parameters provide approximately 86% normal operation with 116 instances of unavailability, 1 MI (pink) and 0 HMI.

In Scenario 2 (bandwidth = 5 MHz, repetition rate = 50 us, and JSR = 9 dB), the two combinations exhibit performance closely resembling the nominal case, as presented in Figure 5.34 with nearly all points in the normal operations and most importantly with

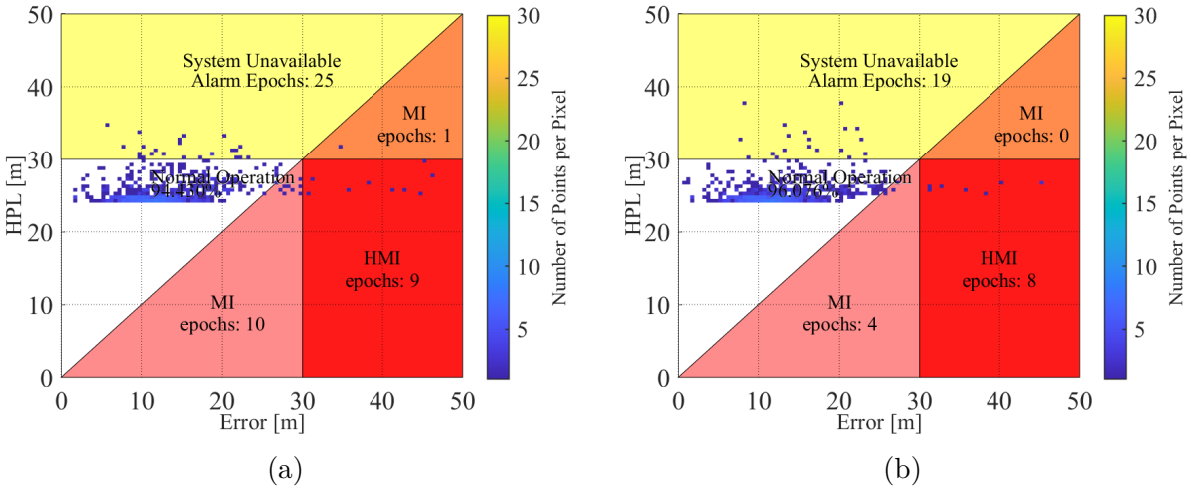

Figure 5.38: Stanford diagram representing performance after applying mitigation for Scenario 3 (Fast chirp) using ANF a) Set A – Position Level Selection and b) Set B – Acquisition Level Prediction.

zero HMIs. Very few unavailable instances give evidence of a significant improvement in CNO, as depicted in Figure 5.33. Nevertheless, Set B seems to offer slightly better performance with more than 99% normal operations, 3 instances of unavailability, and 0 HMI compared to Set A combination with more than 99% normal operations, with 5 instances of unavailability and 0 HMIs.

In Scenario 3 (bandwidth = 7.5 MHz, repetition rate = 10 us and JSR = 14 dB), the performance of both parameter combinations, Set A and Set B, has not reached the same level, especially considering the complete removal of HMIs, which represent unbounded position errors, as in the previous cases. Here, Set B, to some extent, appears to be better with 97% normal operations, including 19 instances of unavailability, 4 MI and 8 HMIs. In comparison, the Set A combination achieves 95% normal operations, 25 instances of unavailability, 11 MI (pink & orange) and 9 HMIs.

The results from the three investigated scenarios indicate that selecting ANF parameters using the acquisition level criterion is sufficient to achieve performance equivalent to the position level selection. This approach not only highlights the effectiveness of the acquisition level parameter selection but also avoids the exhaustive time constraint associated with position-level labelization in database creation. With these parameter settings, the mitigation effectiveness of ANF has significantly increased, resulting in a higher number of normal operations and the successful removal of 'Hazardous Misleading Information (HMI). As far as Scenario 3 is concerned, the acquisition level combination appears to exhibit slightly better performance than the position level. This performance is attributed to two key reasons: 1) Position-level selection is based on average accuracy and is not specifically designed to consider the best Stanford representation. This necessitates finding a balanced compromise to replace HMI with the normal operations at maximum rather than making these instances unavailable, and 2) the tested combinations at the position level are conducted with much broader steps to expedite the process. Due to these two reasons, we consider that the parameter selected by such an approach offers not a true optimal but rather a near-optimal solution.

5.5 Summary and Conclusions

In conclusion, this chapter significantly contributes to the modeling of ANF parameters for the effective suppression of interference signals, validating that a properly tuned Adaptive Notch Filter (ANF) improves the suppression of chirp-like interference signals. This is

crucial for meeting the performance metrics concerning safety-critical applications where positioning availability is not solely determined by the accessibility of the positioning solution with a certain level of accuracy. It also necessitates ensuring that the positioning error is well-constrained and remains below the alarm limit.

As discussed in Chapter 4, ANF can eliminate Hazardous Misleading Information (HMI) events, ensuring safe localization depending on the selection of appropriate parameters. However, it resulted in the substitution of most HMIs with unavailable (PE $<$ AL $<$ PL) instances, especially when considering Carrier-to-Noise ratio (CNO) measurements in the weighting model. In such situations, two complementary actions could enhance availability: 1) an optimal choice of ANF parameters and 2) a specific calibration of the weighting model, possibly adopting a less conservative approach following the mitigation process. However, the acceptability of recalibration raises important concerns at the certification level, and it is considered out of the scope of this study.

This study assumes that rapid and accurate characterization of the interference signal is possible, providing valuable information for adapting mitigation filter parameters to enhance performance. In this regard, two modeling approaches have been explored to determine the appropriate ANF parameters, specifically the pole contraction factor and adaptation step. The initial approach involved modeling the parameter using Multivariate Polynomial Regression (MPR) at the precorrelation level. A parametric sweep was conducted to filter the signal, while the Root Mean Square Error (RMSE) criteria was chosen for the optimal parameter selection.

Our investigation involved three scenarios with distinct chirp signal characteristics, varying the bandwidth, sweep rate, and power level. The finding revealed ANF effectiveness with the predicted parameters for 2 out of 3 scenarios when compared to the naively selected values of the pole contraction factor ($k_\alpha = 0.8$) and adaptation step ($\delta = 0.05$). In Scenario 1 and Scenario 2, with slow and moderate chirps, respectively, all HMIs were removed successfully, resulting in an increase in normal operations with some instances of unavailability. However, in Scenario 3, involving fast chirp, the ANF failed to deliver similar performance, leading to a significant number of HMIs. While these results are promising, they underscore the fact that the RMSE criterion cannot be considered a universal choice for different chirp scenarios. Similarly, other precorrelation level criteria such as Cross-Power Spectral Density (CPSD), Peak Signal-to-Noise Ratio (PSNR) and Mean Absolute Deviation (MAD) were also considered, however, none of them yielded satisfactory outcomes. These considerations suggest that achieving optimal selection using criterion at the precorrelation level is highly challenging, prompting exploration of ANF parameters at alternative levels.

In the final endeavor, a post-correlation (acquisition level) criterion was tailored to determine optimal ANF parameters. This involved computing a Cross Ambiguity Function (CAF) for each of the tested ANF combinations. Four rules were applied in succession to avoid ambiguities caused by the interference residue or distortions introduced by the filtering process. Additionally, the conventional regression approach is replaced by Neural Network (NN) based regression for modeling purposes. A Multilayer Perceptron (MLP) comprising 4 hidden layers, each layer composed of 64 neurons, and the ReLU activation function was employed as an alternative for the network training.

A comparative analysis is presented to evaluate the effectiveness of the ANF-based mitigation, which was fine-tuned with the predicted parameters provided by the trained model, in contrast to position-level selection. The results indicated that with the predicted parameters, ANF performed equally well compared to position-level selection. In Scenario 1 and Scenario 2, ANF completely removed all HMIs with the predicted parameters and increased the normal operation with very few unavailable instances. However, Scenario 3 presented challenges even after applying near-optimal parameters, resulting in fewer

HMI instances suggesting the need for supplementary actions such as the utilization of sequential filter to further enhance the performance.

Chapter 6

Conclusions and Perspectives

6.1 Summary and Conclusions

This chapter serves as a reflective overview of the extensive discussions and insights presented in the preceding sections, offering a comprehensive summary of key findings and avenues for future work. Throughout the preceding chapters, an in-depth exploration of the jamming issue and mitigation solutions in the Global Navigation Satellite System (GNSS) has been undertaken concerning its utilization in safety-critical land transportation systems.

Chapter 2 laid the groundwork by providing an overview of the fundamental principles of GNSS, encompassing theoretical discussions, core concepts and key definitions to establish foundations for subsequent discourse. Chapter 3 exclusively concentrated on the pervasive issue of jamming in GNSS, exploring state-of-the-art countermeasures for the detection and mitigation of interference signals. The main objectives were to enhance understanding of the subject, emphasize the significance of addressing interference concerns, present existing solutions and resources required, and acknowledge the inherent limitations of these mitigation strategies.

Furthermore, Chapter 4 conducted a detailed examination of three distinct techniques, including Adaptive Notch Filter (ANF), Wavelet Packet Decomposition (WPD) and Karhunen Loéve Transform (KLT). These techniques, belonging to different categories and featuring diverse computational requirements, were chosen to address the jamming issue. Our investigations focused on two specific types of interference signals: frequency hopping and chirp interference. These signals possess unique characteristics in terms of how frequency varies over time and are expected to challenge the mitigation filters differently. The conventional approaches presented in the literature often assessed mitigation effectiveness at intermediate processing levels. We have chosen to investigate a further step and also consider the evaluation of positioning Key Performance Indicators (KPIs) with a specific focus on safety-critical applications, representing a novel consideration in the analysis. The outcomes of these investigations are outlined as follows:

- The KLT method demonstrated promising results in the frequency hopping case, which successfully retrieved the positioning KPIs identical to the nominal conditions. However, the challenge remains the substantial computational demands, especially for the chirp case. The higher-level decomposition requirement for this scenario, along with the calibration complexity, leads us to suspend the investigation for future work.

- Similarly, the WPD technique showed exceptional performance in mitigating the frequency hopping interference. However, in the case of the chirp signal, there was a notable improvement in the positioning accuracy and complete removal of

HMI though they were mostly replaced by unavailable instances. Our exploration specifically employed the 'Symlet' wavelet function with 5 decomposition levels, providing a somewhat limited perspective on the full potential of WPD. To gain a more comprehensive understanding, future research could explore different wavelet functions and various levels of decomposition to optimize mitigation performance.

- Lastly, the ANF offers a simple, real-time adaptable solution to eliminate specific frequency components of the signal. However, its effectiveness relies on the proper selection of parameters, including the pole contraction factor and adaptation step value. In the presented scenarios, ANF fell short of achieving the desired performance level, as the filter tuned with the parameter values taken from recommended intervals proved to be inappropriate. Although mitigation effectively improved positioning accuracy in both cases, predominately replaced HMI by unavailable instances.

Consequently, based on these findings, we selected ANF for further investigation, and Chapter 5 made a significant contribution by focusing on the modeling of ANF parameters. The primary objective was to address the existing gap in the literature by exploring the optimal parameterization of ANF against linear chirp interference. This extensive study incorporated a diverse range of signals, varying the bandwidth, sweep rate and power level. The initial approach involved modeling the parameters using Multivariate Polynomial Regression (MPR) at the pre-correlation level. A parametric sweep was executed to filter the interference signal with the Root Mean Square Error (RMSE) criteria chosen for the optimal parameter selection.

In this investigation, three distinct interference signals were included featuring slow, moderate and fast chirp. The ANF configured with the values derived from the generalized model proved highly effective in enhancing normal operations and eliminating the HMI instances for two out of three scenarios. However, in the third scenario featuring fast chirp, ANF failed to provide similar performance and resulted in a considerable number of HMI instances. These results were even promising, but it became evident that RMSE cannot be a universal choice for different types of chirp signals. Similarly, the exploration of alternate pre-correlation level criterion also did not yield satisfactory outcomes.

The ultimate approach involved exploration at the acquisition level, leveraging the Cross Ambiguity Function (CAF) for the parameterization task. Furthermore, a neural network-based regression approach using Multilayer Perceptron (MLP) architecture was introduced to train the model. Our observation demonstrated that ANF configured with the predicted values performed exceptionally well, particularly for Scenario 1 and Scenario 2, and retrieved similar performance as in the reference case. However, Scenario 3 remained somehow challenging, resulting in very few instances of HMI. This highlights that for some cases, even fine-tuning ANF with optimal or near-optimal parameters could not guarantee HMI-free operations, thereby necessitating supplementary actions, including the implementation of a sequential filter for performance enhancement.

6.2 Perspectives

Moving forward, the research outlined in Chapter 5 sets the stage for several promising avenues for future work that could be conducted in several phases for the refinement and expansion of the proposed methodology. In the initial stage of enhancement to the methodology, the following improvements could be applied:

- The presented methodology, which is centered on linear chirp features, proficiently identifies near-optimal parameters for ANF. This resulted in achieving a position-

level performance for the given scenarios through acquisition-level parameterization. However, there is a potential for further improvement in the labeling process of the methodology such as by exploiting satellite tracking information. This exploration could involve a comprehensive performance comparison across a broader range of scenarios, including those not initially considered in the investigations.

- To optimize the filtering performance of ANF, a refinement could be introduced, such as incorporating a switching mechanism to regulate the filter's ON/OFF state and inclusion of another parameter for adjusting the notch depth. These customization options would further tailor the ANF response to a desired level, effectively preventing potential distortions induced by the filter.

- The developed methodology used readily available information about the chirp signal characteristics, serving as inputs for the constructed models to predict optimal parameters. In the real-world scenario, the signal features are unknown and have to be estimated in the signal-processing stage. This layer could be integrated alongside the developed approach in future work where classification and characterization blocks will be implemented leading to a comprehensive adaptive interference management system.

- Another prospect for future work could involve exploring the dependency of front-end characteristics and GNSS software receiver configuration during the parameterization process. This direction could contribute to a more profound understanding of the adaptability of ANF to various receiver setups. Leveraging this knowledge could facilitate fine-tuning of the filter and optimizing its performance for a specific receiver configuration.

- We introduced a couple of approaches: initially presenting a set of third-order polynomial functions and secondly, employing a neural network to train the model by learning the dependencies between the input chirp features and near-optimal ANF parameterization. Future research activities may involve investigating the possibilities of finding symbolic functions for the ANF parameterization. Formulating such symbolic functions has the potential to provide a deeper insight into the underlying mathematical principles governing ANF adaptation. This approach offers a practical and versatile solution, allowing a simple calibration of functions to enhance the adaptability of ANF for specific configurations, as discussed previously.

Similarly, broadening the scope of this research, the next phase could involve:

- Exploring alternative forms of chirp signals, such as quadratic and algorithmic chirps, provides an opportunity to customize ANF for a wide range of chirp-like signals. This would allow testing the versatility and applicability of the ANF for different types of chirp jammers.

- Furthermore, the research could delve into jammers belonging to other classes, initiating a comprehensive examination of various mitigation solutions to address a wider array of potential jamming threats.

- Additionally, the introduction of advanced machine-learning models into interference countermeasures involves the exploration of deep learning approaches such as Convolution Neural Network (CNN) or Recurrent Neural Network (RNN). These approaches could enhance the capability of mitigation solutions by recognizing complex interference patterns and dynamically adapting the mitigation strategies accordingly.

Finally, in the last phase, the overall system's capability could be significantly enhanced by the implementation of complementary actions at different levels. This enhancement involves exploiting vector tracking, incorporating multi-array antenna architecture and integrating multi-constellation and multi-frequency solutions. Furthermore, the system's resilience to jamming could be further bolstered by leveraging external aiding from the sensors such as inertial measurement unit (IMU) and odometer that remain unaffected by jamming influences. The synergies between these diverse technologies and sensors create a comprehensive defense mechanism, empowering the system to address sophisticated scenarios involving multiple jammers of various classes and including instances where jammers interfere at different times or simultaneously, as well as scenarios incorporating dynamic situations with moving jammers and/or receiver.

These aforementioned points collectively could pave the way in setting the foundation for developing a demonstrator with built-in intelligence, showcasing an adaptive interference mitigation management system.

Bibliography

Bibliography

[1] Daniele Borio et al. "Time-frequency excision for GNSS applications". In: *IEEE Systems Journal* 2.1 (2008), pp. 27–37.

[2] J Rossouw Van Der Merwe et al. "Adaptive notch filtering against complex interference scenarios". In: *2020 European Navigation Conference (ENC)*. IEEE. 2020, pp. 1–10.

[3] Luciano Musumeci and Fabio Dovis. "Use of the Wavelet Transform for Interference Detection and Mitigation in Global Navigation Satellite Systems." In: *International Journal of Navigation & Observation* (2014).

[4] J Merwe et al. "Exotic FMCW waveform mitigation with an advanced multi-parameter adaptive notch filter (MPANF)". In: *Proceedings of the 35th International Technical Meeting of the Satellite Division of The Institute of Navigation (ION GNSS+ 2022)*. 2022, pp. 3783–3819.

[5] Wenjian Qin et al. "An assessment of impact of adaptive notch filters for interference removal on the signal processing stages of a GNSS receiver". In: *IEEE Transactions on Aerospace and Electronic Systems* 56.5 (2020), pp. 4067–4082.

[6] Luciano Musumeci, James T Curran, and Fabio Dovis. "A comparative analysis of adaptive notch filtering and wavelet mitigation against jammers interference". In: *Navigation: Journal of The Institute of Navigation* 63.4 (2016), pp. 533–550.

[7] Daniele Borio and Ciro Gioia. "Robust interference mitigation: a measurement and position domain assessment". In: *Proceedings of the 2020 International Technical Meeting of The Institute of Navigation*. 2020, pp. 274–288.

[8] John A Klobuchar. "Ionospheric time-delay algorithm for single-frequency GPS users". In: *IEEE Transactions on aerospace and electronic systems* 3 (1987), pp. 325–331.

[9] G Di Giovanni and SM Radicella. "An analytical model of the electron density profile in the ionosphere". In: *Advances in Space Research* 10.11 (1990), pp. 27–30.

[10] J Saastamoinen. "Contributions to the theory of atmospheric refraction". In: *Bulletin Géodésique (1946-1975)* 105.1 (1972), pp. 279–298.

[11] Helen S Hopfield. "Tropospheric effect on electromagnetically measured range: Prediction from surface weather data". In: *Radio science* 6.3 (1971), pp. 357–367.

[12] Okuary Osechas et al. "Detecting multipath errors in terrestrial GNSS applications". In: *Proceedings of the 2015 International Technical Meeting of The Institute of Navigation*. 2015, pp. 465–474.

[13] Michael S Braasch. ", Multipath Effects". In: *Global Positioning System: Theory and Aplications* (1996).

[14] Mohammad Hatef Keshvadi, Ali Broumandan, and Gérard Lachapelle. “Analysis of GNSS beamforming and angle of arrival estimation in multipath environments”. In: *Proceedings of the 2011 International Technical Meeting of The Institute of Navigation*. 2011, pp. 427–435.

[15] Lionel Garin, Frank van Diggelen, and Jean-Michel Rousseau. “Strobe & edge correlator multipath mitigation for code”. In: *Proceedings of the 9th International Technical Meeting of the Satellite Division of the Institute of Navigation (ION GPS 1996)*. 1996, pp. 657–664.

[16] AJ Van Dierendonck, Pat Fenton, and Tom Ford. “Theory and performance of narrow correlator spacing in a GPS receiver”. In: *Navigation* 39.3 (1992), pp. 265–283.

[17] Paul D Groves and Ziyi Jiang. “Height aiding, C/N0 weighting and consistency checking for GNSS NLOS and multipath mitigation in urban areas”. In: *The Journal of Navigation* 66.5 (2013), pp. 653–669.

[18] Andreas Wieser and Fritz K Brunner. “An extended weight model for GPS phase observations”. In: *Earth, planets and space* 52.10 (2000), pp. 777–782.

[19] C O’Driscoll, G Lachapelle, and ME Tamazin. “Investigation of the benefits of combined GPS/GLONASS receivers in urban environments”. In: *Proceeding on RIN NAV10 Conference on Position, Location, Timing: Everyone, Everything, Everywhere*. 2010.

[20] Shaojun Feng, Shenghai Wang, and Washington Ochieng. “A Core Constellation Based Multiple-GNSS Positioning and Integrity Monitoring Algorithm”. In: *Proceedings of the 27th International Technical Meeting of the Satellite Division of the Institute of Navigation (ION GNSS+ 2014)*. 2014, pp. 307–314.

[21] Syed Ali Kazim, Nourdine Aıt Tmazirte, and Juliette Marais. “Realistic position error models for GNSS simulation in railway environments”. In: *2020 European Navigation Conference (ENC)*. IEEE. 2020, pp. 1–9.

[22] Syed Ali Kazim, Nourdine Aıt Tmazirte, and Juliette Marais. “On the impact of temporal variation on GNSS position error models”. In: *Proceedings of the 2021 International Technical Meeting of The Institute of Navigation*. 2021, pp. 728–737.

[23] Sébastien Peyraud et al. “About non-line-of-sight satellite detection and exclusion in a 3D map-aided localization algorithm”. In: *Sensors* 13.1 (2013), pp. 829–847.

[24] Li-Ta Hsu, Yanlei Gu, and Shunsuke Kamijo. “NLOS correction/exclusion for GNSS measurement using RAIM and city building models”. In: *Sensors* 15.7 (2015), pp. 17329–17349.

[25] Mounir Adjrad and Paul D Groves. “Enhancing conventional GNSS positioning with 3D mapping without accurate prior knowledge”. In: *Proceedings of the 28th International Technical Meeting of the Satellite Division of the Institute of Navigation (ION GNSS+ 2015)*. 2015, pp. 2397–2409.

[26] Xin Han et al. “GNSS/IMU tightly coupled scheme with weighting and FDE for rail applications”. In: *Proceedings of the 2020 International Technical Meeting of The Institute of Navigation*. 2020, pp. 570–583.

[27] Juliette Marais et al. “Multipath and NLOS detection based on the combination of CN0 values and a fish-eye camera”. In: *2020 European Navigation Conference (ENC)*. IEEE. 2020, pp. 1–13.

[28] Li-Ta Hsu, Yanlei Gu, and Shunsuke Kamijo. “3D building model-based pedestrian positioning method using GPS/GLONASS/QZSS and its reliability calculation”. In: *GPS solutions* 20 (2016), pp. 413–428.

[29] Rakesh Kumar and Mark G Petovello. “A novel GNSS positioning technique for improved accuracy in urban canyon scenarios using 3D city model”. In: *Proceedings of the 27th International Technical Meeting of the Satellite Division of the Institute of Navigation (ION GNSS+ 2014)*. 2014, pp. 2139–2148.

[30] Ziyi Jiang et al. “Multi-constellation GNSS multipath mitigation using consistency checking”. In: *Proceedings of the 24th International Technical Meeting of The Satellite Division of the Institute of Navigation (ION GNSS 2011)*. 2011, pp. 3889–3902.

[31] Hiroshi Isshiki. “A New Method for Detection, Identification and Mitigation of Outliers in Receiver Autonomous Integrity Monitoring (RAIM)”. In: *Proceedings of the 21st International Technical Meeting of the Satellite Division of The Institute of Navigation (ION GNSS 2008)*. 2008, pp. 151–158.

[32] Mathieu St-Pierre and Denis Gingras. “Comparison between the unscented Kalman filter and the extended Kalman filter for the position estimation module of an integrated navigation information system”. In: *IEEE Intelligent Vehicles Symposium, 2004*. IEEE. 2004, pp. 831–835.

[33] Chunbo Luo et al. “UAV position estimation and collision avoidance using the extended Kalman filter”. In: *IEEE Transactions on vehicular technology* 62.6 (2013), pp. 2749–2762.

[34] Federico Grasso Toro et al. “Particle Filter technique for position estimation in GNSS-based localisation systems”. In: *2015 International Association of Institutes of Navigation World Congress (IAIN)*. IEEE. 2015, pp. 1–8.

[35] Fredrik Gustafsson. “Particle filter theory and practice with positioning applications”. In: *IEEE Aerospace and Electronic Systems Magazine* 25.7 (2010), pp. 53–82.

[36] Liyan Li, Jie Zhong, and Minjian Zhao. “Doppler-aided GNSS position estimation with weighted least squares”. In: *IEEE transactions on vehicular technology* 60.8 (2011), pp. 3615–3624.

[37] M Vermeer. “The precision of geodetic GPS and one way of improving it”. In: *Journal of Geodesy* 71 (1997), pp. 240–245.

[38] M Rothacher et al. “Processing strategies for regional GPS networks”. In: *Advances in Positioning and Reference Frames: IAG Scientific Assembly Rio de Janeiro, Brazil, September 3–9, 1997*. Springer. 1998, pp. 93–100.

[39] N Talbot. “Optimal weighting of GPS carrier phase observations based on the signal-to-noise ratio”. In: *Proceedings of the international symposia on global positioning systems*. 1988, pp. V–4.

[40] Horst Hartinger and Fritz K Brunner. “Variances of GPS phase observations: the SIGMA- model”. In: *GPS solutions* 2 (1999), pp. 35–43.

[41] FK Brunner, H Hartinger, and L Troyer. “GPS signal diffraction modelling: the stochastic SIGMA-Δ model”. In: *journal of Geodesy* 73 (1999), pp. 259–267.

[42] Sarab Tay and Juliette Marais. “Weighting models for GPS Pseudorange observations for land transportation in urban canyons”. In: *6th European workshop on GNSS signals and signal processing*. 2013, 4p.

[43] Pieter Bastiaan Ober. “Integrity prediction and monitoring of navigation systems.” In: (2004).

[44] Young C Lee. "Analysis of range and position comparison methods as a means to provide GPS integrity in the user receiver". In: *Proceedings of the 42nd Annual Meeting of The Institute of Navigation (1986)*. 1986, pp. 1–4.

[45] Juan Blanch, Todd Walter, and Per Enge. "Optimal positioning for advanced RAIM". In: *Navigation: Journal of the Institute of Navigation* 60.4 (2013), pp. 279–289.

[46] Qian Meng et al. "Improved ARAIM fault modes determination scheme based on feedback structure with probability accumulation". In: *GPS Solutions* 23 (2019), pp. 1–11.

[47] Young C Lee. "A position domain relative RAIM method". In: *IEEE Transactions on Aerospace and Electronic Systems* 47.1 (2011), pp. 85–97.

[48] Livio Gratton, Mathieu Joerger, and Boris Pervan. "Carrier phase relative RAIM algorithms and protection level derivation". In: *The Journal of Navigation* 63.2 (2010), pp. 215–231.

[49] Washington Y Ochieng et al. "User level integrity monitoring and quality control for seamless positioning in all conditions and environments". In: *Proceedings of the 20th International Technical Meeting of the Satellite Division of The Institute of Navigation (ION GNSS 2007)*. 2007, pp. 2573–2583.

[50] Steve Hewitson and Jinling Wang. "Extended receiver autonomous integrity monitoring (e raim) for gnss/ins integration". In: *Journal of Surveying Engineering* 136.1 (2010), pp. 13–22.

[51] Ni Zhu. "GNSS propagation channel modeling in constrained environments: Contribution to the improvement of the geolocation service quality". PhD thesis. Université de Lille, 2018.

[52] Felipe A Costa de Oliveira, Frank Sill Torres, and Alberto García-Ortiz. "Recent advances in sensor integrity monitoring methods—A review". In: *IEEE Sensors Journal* 22.11 (2022), pp. 10256–10279.

[53] Ryan SY Young, Gary A McGraw, and Brian T Driscoll. "Investigation and comparison of horizontal protection level and horizontal uncertainty level in FDE algorithms". In: *Proceedings of the 9th International Technical Meeting of the Satellite Division of The Institute of Navigation (ION GPS 1996)*. 1996, pp. 1607–1614.

[54] R Grover Brown. *GPS RAIM: Calculation of thresholds and protection radius using chi-square methods; A geometric approach*. Radio Technical Commission for Aeronautics, 1994.

[55] RTCA SC. "Minimum Operational Performance Standards for Global Positioning System/Wide Area Augmentation System Airborne Equipment". In: *RTCA DO-229* (1996).

[56] James V Carroll. "Vulnerability assessment of the US transportation infrastructure that relies on the global positioning system". In: *The Journal of Navigation* 56.2 (2003), pp. 185–193.

[57] E Backer, D Van Willigen, and R Rawlings. "Technical and operational assessment of the suitability of GPS to meet the BRNAV requirements". In: *Delft University of Technology, Telecommunications and Traffic Control Systems Group* (1997).

[58] Grace Xingxin Gao et al. "Protecting GNSS receivers from jamming and interference". In: *Proceedings of the IEEE* 104.6 (2016), pp. 1327–1338.

[59] Ruben Morales-Ferre et al. “A survey on coping with intentional interference in satellite navigation for manned and unmanned aircraft”. In: *IEEE Communications Surveys & Tutorials* 22.1 (2019), pp. 249–291.

[60] Daniele Borio et al. “Impact and detection of GNSS jammers on consumer grade satellite navigation receivers”. In: *Proceedings of the IEEE* 104.6 (2016), pp. 1233–1245.

[61] Thomas Kraus, Roland Bauernfeind, and Bernd Eissfeller. “Survey of in-car jammers-analysis and modeling of the RF signals and IF samples (suitable for active signal cancelation)”. In: *Proceedings of the 24th International Technical Meeting of The Satellite Division of the Institute of Navigation (ION GNSS 2011)*. 2011, pp. 430–435.

[62] Frederic Bastide et al. “Automatic gain control (AGC) as an interference assessment tool”. In: *Proceedings of the 16th International Technical Meeting of the Satellite Division of The Institute of Navigation (ION GPS/GNSS 2003)*. 2003, pp. 2042–2053.

[63] Asghar Tabatabaei Balaei, Beatrice Motella, Andrew G Dempster, et al. “GPS interference detected in Sydney-Australia”. In: *Proceedings of the IGNSS Conference*. 2007, pp. 74–76.

[64] Beatrice Motella, Marco Pini, and Fabio Dovis. “Investigation on the effect of strong out-of-band signals on global navigation satellite systems receivers”. In: *GPS Solutions* 12 (2008), pp. 77–86.

[65] Andrea Tani and Romano Fantacci. “Performance evaluation of a precorrelation interference detection algorithm for the GNSS based on nonparametrical spectral estimation”. In: *IEEE Systems Journal* 2.1 (2008), pp. 20–26.

[66] Beatrice Motella and Letizia Lo Presti. “Methods of goodness of fit for GNSS interference detection”. In: *IEEE Transactions on Aerospace and Electronic Systems* 50.3 (2014), pp. 1690–1700.

[67] Fernando D Nunes and Fernando MG Sousa. “GNSS blind interference detection based on fourth-order autocumulants”. In: *IEEE Transactions on Aerospace and Electronic Systems* 52.5 (2016), pp. 2574–2586.

[68] Roberto Calcagno et al. “An interference detection algorithm for COTS GNSS receivers”. In: *2010 5th ESA Workshop on Satellite Navigation Technologies and European Workshop on GNSS Signals and Signal Processing (NAVITEC)*. IEEE. 2010, pp. 1–8.

[69] Sascha Bartl, Philipp Berglez, and Bernhard Hofmann-Wellenhof. “GNSS interference detection, classification and localization using Software-Defined Radio”. In: *2017 European Navigation Conference (ENC)*. IEEE. 2017, pp. 159–169.

[70] Daniele Borio and Ciro Gioia. “Real-time jamming detection using the sum-of-squares paradigm”. In: *2015 International Conference on Localization and GNSS (ICL-GNSS)*. IEEE. 2015, pp. 1–6.

[71] EL Valles, C Yu, and R Elasmar. “Interference detection algorithms for GNSS-enabled android devices”. In: *Proceedings of the 28th International Technical Meeting of the Satellite Division of The Institute of Navigation (ION GNSS+ 2015)*. 2015, pp. 317–324.

[72] Frederic Bastide, Eric Chatre, and Christophe Macabiau. “GPS interference detection and identification using multicorrelator receivers”. In: *Proceedings of the 14th International Technical Meeting of the Satellite Division of the Institute of Navigation (ION GPS 2001)*. 2001, pp. 872–881.

[73] Christophe Ouzeau et al. “Performance assessment of multi correlators interference detection and repair algorithms for civil aviation”. In: *ENC-GNSS 2008, Conférence Européenne de la Navigation*. 2008.

[74] Ruben Morales Ferre, Alberto de la Fuente, and Elena Simona Lohan. “Jammer classification in GNSS bands via machine learning algorithms”. In: *Sensors* 19.22 (2019), p. 4841.

[75] Wutao Li et al. “A real-time interference monitoring technique for GNSS based on a twin support vector machine method”. In: *Sensors* 16.3 (2016), p. 329.

[76] Wenjian Qin and Fabio Dovis. “Situational awareness of chirp jamming threats to GNSS based on supervised machine learning”. In: *IEEE Transactions on Aerospace and Electronic Systems* 58.3 (2021), pp. 1707–1720.

[77] Saiful Islam et al. “Combating Single-Frequency Jamming through a Multi-Frequency, Multi-Constellation Software Receiver: A Case Study for Maritime Navigation in the Gulf of Finland”. In: *Sensors* 22.6 (2022), p. 2294.

[78] Paul D Groves and Daniel C Long. “Combating GNSS interference with advanced inertial integration”. In: *The Journal of Navigation* 58.3 (2005), pp. 419–432.

[79] Bradfrod W Parkinson. “Global Positioningb System: Theory and applications”. In: *Progress in Astronautics and Aeronautics Series* (1996), pp. 547–568.

[80] Christopher Hegarty et al. “Suppression of pulsed interference through blanking”. In: *Proceedings of the IAIN World Congress and the 56th Annual Meeting of The Institute of Navigation (2000)*. 2000, pp. 399–408.

[81] Luciano Musumeci, Jaron Samson, and Fabio Dovis. “Performance assessment of pulse blanking mitigation in presence of multiple distance measuring equipment/tactical air navigation interference on global navigation satellite systems signals”. In: *IET Radar, Sonar & Navigation* 8.6 (2014), pp. 647–657.

[82] Daniele Borio, Laura Camoriano, and Letizia Lo Presti. “Two-pole and multi-pole notch filters: A computationally effective solution for GNSS interference detection and mitigation”. In: *IEEE Systems Journal* 2.1 (2008), pp. 38–47.

[83] Micaela Troglia Gamba et al. “FPGA implementation issues of a two-pole adaptive notch filter for GPS/Galileo receivers”. In: *Proceedings of the 25th International Technical Meeting of The Satellite Division of the Institute of Navigation (ION GNSS 2012)*. 2012, pp. 3549–3557.

[84] J Wendel et al. “Limits of narrowband interference mitigation using adaptive notch filters”. In: *Proceedings of the 29th International Technical Meeting of The Satellite Division of the Institute of Navigation (ION GNSS+ 2016)*. 2016, pp. 286–294.

[85] Daniele Borio. “Loop analysis of adaptive notch filters”. In: *IET Signal Processing* 10.6 (2016), pp. 659–669.

[86] Micaela Troglia Gamba and Emanuela Falletti. “Performance analysis of FLL schemes to track swept jammers in an adaptive notch filter”. In: *2018 9th ESA Workshop on Satellite NavigationTechnologies and European Workshop on GNSS Signals and Signal Processing (NAVITEC)*. IEEE. 2018, pp. 1–8.

[87] Micaela Troglia Gamba and Emanuela Falletti. “Performance comparison of FLL adaptive notch filters to counter GNSS jamming”. In: *2019 International Conference on Localization and GNSS (ICL-GNSS)*. IEEE. 2019, pp. 1–6.

[88] Syed Waqas Arif, Adem Coskun, and Izzet Kale. “A Fully Adaptive Lattice-based Notch Filter for Mitigation of Interference in GPS”. In: *2019 15th Conference on Ph.D Research in Microelectronics and Electronics (PRIME)*. 2019, pp. 217–220. DOI: 10.1109/PRIME.2019.8787822.

[89] Wann-Jiun Ma, Wei-Lung Mao, and Fan-Ren Chang. “Design of adaptive all-pass based notch filter for narrowband anti-jamming GPS system”. In: *2005 International Symposium on Intelligent Signal Processing and Communication Systems*. IEEE. 2005, pp. 305–308.

[90] J. Rossouw van der Merwe et al. “Adaptive notch filtering against complex interference scenarios”. In: *2020 European Navigation Conference (ENC)*. 2020, pp. 1–10. DOI: 10.23919/ENC48637.2020.9317518.

[91] Neeraj Varshney and RC Jain. “An adaptive notch filter for narrow band interference removal”. In: *2013 National Conference on Communications (NCC)*. IEEE. 2013, pp. 1–5.

[92] Jont B Allen and Lawrence R Rabiner. “A unified approach to short-time Fourier analysis and synthesis”. In: *Proceedings of the IEEE* 65.11 (1977), pp. 1558–1564.

[93] Moeness G Amin, Chenshu Wang, and Alan R Lindsey. “Optimum interference excision in spread spectrum communications using open-loop adaptive filters”. In: *IEEE Transactions on Signal Processing* 47.7 (1999), pp. 1966–1976.

[94] TACM Claasen and W Mecklenbräuker. “Time-frequency signal analysis”. In: *Philips Journal of Research* 35.6 (1980), pp. 372–389.

[95] Boualem Boashash and Peter Black. “An efficient real-time implementation of the Wigner-Ville distribution”. In: *IEEE transactions on acoustics, speech, and signal processing* 35.11 (1987), pp. 1611–1618.

[96] SJ Loutridis. “Instantaneous energy density as a feature for gear fault detection”. In: *Mechanical systems and signal processing* 20.5 (2006), pp. 1239–1253.

[97] AA Chanerley and NA Alexander. “Correcting data from an unknown accelerometer using recursive least squares and wavelet de-noising”. In: *Computers & structures* 85.21-22 (2007), pp. 1679–1692.

[98] Ioannis Delakis, Omer Hammad, and Richard I Kitney. “Wavelet-based de-noising algorithm for images acquired with parallel magnetic resonance imaging (MRI)”. In: *Physics in Medicine & Biology* 52.13 (2007), p. 3741.

[99] J Rafiee et al. “A novel technique for selecting mother wavelet function using an intelli gent fault diagnosis system”. In: *Expert Systems with Applications* 36.3 (2009), pp. 4862–4875.

[100] Fabio Dovis and Luciano Musumeci. “Use of wavelet transforms for interference mitigation”. In: *2011 International Conference on Localization and GNSS (ICL-GNSS)*. IEEE. 2011, pp. 116–121.

[101] Luciano Musumeci and Fabio Dovis. “Performance assessment of wavelet based techniques in mitigating narrow-band interference”. In: *2013 International Conference on Localization and GNSS (ICL-GNSS)*. IEEE. 2013, pp. 1–6.

[102] Bo-Seok Seo, Kwi-Woo Park, and Chansik Park. “Performance of Interference Mitigation with Different Wavelets in Global Positioning Systems”. In: *Journal of Positioning, Navigation, and Timing* 8.4 (2019), pp. 165–173.

[103] Claudio Maccone. “The KLT (Karhunen–Loève Transform) to extend SETI searches to broad-band and extremely feeble signals”. In: *Acta Astronautica* 67.11-12 (2010), pp. 1427–1439.

[104] Luciano Musumeci and Fabio Dovis. “A comparison of transformed-domain techniques for pulsed interference removal on GNSS signals”. In: *2012 International Conference on Localization and GNSS*. IEEE. 2012, pp. 1–6.

[105] Fabio Dovis and Luciano Musumeci. “Use of the Karhunen–Loève transform for interference detection and mitigation in GNSS”. In: *ICT Express* 2.1 (2016), pp. 33–36.

[106] Andriy Konovaltsev et al. “Mitigation of continuous and pulsed radio interference with GNSS antenna arrays”. In: *Proceedings of the 21st International Technical Meeting of the Satellite Division of The Institute of Navigation (ION GNSS 2008)*. 2008, pp. 2786–2795.

[107] Shunxiao Wu et al. “A GNSS Space-Time Anti-jamming Algorithm Based on Convex Optimization”. In: *China Satellite Navigation Conference (CSNC) 2014 Proceedings: Volume I*. Springer. 2014, pp. 725–738.

[108] Yaohui Chen et al. “An Improved Approach of SFAP Algorithm for Suppressing Concurrent Narrowband and Wideband Interference”. In: *China Satellite Navigation Conference (CSNC) 2016 Proceedings: Volume II*. 2016, pp. 69–80.

[109] Inder J. Gupta, Ira M. Weiss, and Allen W. Morrison. “Desired Features of Adaptive Antenna Arrays for GNSS Receivers”. In: *Proceedings of the IEEE* 104.6 (2016), pp. 1195–1206. DOI: 10.1109/JPROC.2016.2524416.

[110] M.G. Amin, Liang Zhao, and A.R. Lindsey. “Subspace array processing for the suppression of FM jamming in GPS receivers”. In: *IEEE Transactions on Aerospace and Electronic Systems* 40.1 (2004), pp. 80–92. DOI: 10.1109/TAES.2004.1292144.

[111] Saeed Daneshmand et al. “GNSS Space-Time Interference Mitigation and Attitude Determination in the Presence of Interference Signals”. In: *Sensors* 15.6 (2015), pp. 12180–12204. DOI: 10.3390/s150612180.

[112] Eugenio Realini and Mirko Reguzzoni. “goGPS: open source software for enhancing the accuracy of low-cost receivers by single-frequency relative kinematic positioning”. In: *Measurement Science and Technology* 24.11 (2013), p. 115010. DOI: 10.1088/0957-0233/24/11/115010.

[113] Omid Sharifi-Tehrani, Mohamad Farzan Sabahi, and Meysam Raees Danaee. “Efficient GNSS Jamming Mitigation Using the Marcenko Pastur Law and Karhunen–Loeve Decomposition”. In: *IEEE Transactions on Aerospace and Electronic Systems* 58.3 (2021), pp. 2291–2303.

[114] Peter Yusuf Dibal et al. “Application of wavelet transform in spectrum sensing for cognitive radio: A survey”. In: *Physical Communication* 28 (2018), pp. 45–57.

[115] Vincent Calmettes, Frédéric Pradeilles, and Michel Bousquet. “Study and comparison of interference mitigation techniques for GPS receiver”. In: *Proceedings of the 14th International Technical Meeting of the Satellite Division of The Institute of Navigation (ION GPS 2001)*. 2001, pp. 957–968.

[116] Petre Stoica and Arye Nehorai. “Performance analysis of an adaptive notch filter with constrained poles and zeros”. In: *IEEE Transactions on Acoustics, Speech, and Signal Processing* 36.6 (1988), pp. 911–919.

[117] Joan Bernabeu et al. “A collection of SDRs for global navigation satellite systems (GNSS)”. In: *Proceedings of the 2022 International Technical Meeting of The Institute of Navigation*. 2022, pp. 906–919.

[118] Daniele Borio and Ciro Gioia. “GNSS interference mitigation: A measurement and position domain assessment”. In: *NAVIGATION: Journal of the Institute of Navigation* 68.1 (2021), pp. 93–114.

[119] Syed Ali Kazim, Juliette Marais, and Nourdine Ait Tmazirte. “Interferences in Safety Critical Land Transport Application: Notch Filtering vs Wavelet Transform, an Experimental Analysis”. In: *Proceedings of the 35th International Technical Meeting of the Satellite Division of The Institute of Navigation (ION GNSS+ 2022)*. 2022, pp. 3743–3757.